UQAC
Université du Québec à Chicoutimi

ESTIMATION OF SOME PARAMETERS INFLUENCING THE FLANKING AIRBORNE SOUND TRANSMISSION IN LIGHTWEIGHT BUILDINGS

WITH A FOCUS ON THE BUILDING HEIGHT IN CLT BUILDINGS, THE BEARING DIRECTION OF CLT ELEMENTS, AND VENTILATION DUCTS WITH AND WITHOUT EXTERNAL LAGGING OF STONE WOOL

BY

ERIK NILSSON

Direction:

Sylvain Ménard, ing., Ph.D. - Professor, Department of applied sciences, UQAC

Codirection:

Delphine Bard, Dr. ès Sc. - Researcher, KU Leuven, Belgium

THESIS PRESENTED TO THE UNIVERSITY OF QUEBEC AT CHICOUTIMI FOR THE DEGREE OF PHILOSOPHIAE DOCTOR (PhD) IN CIVIL ENGINEERING

Defended 24th **May, 2024**

Jury Members

Jean Perron	Professor	University of Québec at Chicoutimi	Jury President
Örjan Johansson	Professor	Luleå University of Technology	External member
Joonhee Lee	Associate Professor	Concordia University	External member
Sylvain Ménard	Professor	University of Québec at Chicoutimi	Research director
Delphine Bard	Researcher	KU Leuven, Belgium	Research co-director

Québec, Canada
© Erik Nilsson, Summer 2024

RÉSUMÉ

Ce projet de recherche vise à développer des estimations de plusieurs paramètres qui influencent les transmission latérales du bruit aérien dans les bâtiments légers en se basant sur des données de mesure en laboratoire et sur le terrain. Étant donné que de nombreux paramètres influencent les transmission latérales du bruit aérien, nous nous concentrerons sur certains d'entre eux specifiquement.

Le premier paramètre étudié est l'affaiblissement acoustique des conduits de ventilation, en particulier la diminution de l'isolation acoustique lorsque les conduits sont montés à travers un mur léger. Trois murs et trois conduits de ventilation (deux circulaires et un rectangulaire) ont été mesurés en laboratoire. Une analyse comparative est effectuée entre les théories existantes et les mesures avec un modèle de transmission du son proposé. En raison des différences apparentes entre la théorie existante et les mesures expérimentales, le cadre théorique est révisé. Le modèle de transmission proposé, qui incorpore les théories existantes modifiées et les théories nouvellement développées, s'aligne étroitement sur les données de mesure, démontrant une différence de 0 à 1 dB dans l'indice de réduction sonore pondéré pour les différentes configurations.

Le deuxième paramètre pris en compte est le traitement acoustique des conduits de ventilation, en particulier le calorifugeage externe en laine de roche autour du périmètre extérieur des conduits. Alors que les recherches précédentes se sont concentrées sur les silencieux et le revêtement intérieur, il est peu expliqué comment le calorifugeage extérieur, en particulier avec de la laine de roche, affecte la réduction globale du bruit. Sur la base de mesures effectuées en laboratoire, des estimations ont été élaborées par le biais d'un processus itératif pour des conduits de ventilation circulaires et rectangulaires. Les résultats montrent que le calorifugeage extérieur avec de la laine de roche réduit efficacement la transmission des bruits aériens latéraux, et que les estimations développées correspondent bien aux données de mesure. L'étude souligne l'importance d'appliquer les traitements au plus près du mur et que le calorifugeage extérieur est une solution pratique pour minimiser la transmission des bruits aériens lorsqu'une grande gaine de ventilation traverse un mur aux valeurs d'isolation acoustique élevées.

Le troisième paramètre examiné est la direction d'appui des éléments en bois lamellé-croisé (CLT). Étant donné que les éléments CLT sont conçus avec plusieurs couches orientées dans des directions différentes, les vibrations peuvent diminuer différemment d'un élément à l'autre. De plus, par rapport à une jonction, les éléments CLT peuvent être orientés parallèlement ou perpendiculairement. Les niveaux de vitesse sur un mur en CLT et l'indice de réduction des vibrations des jonctions sont mesurés dans un bâtiment. Les mesures sur le terrain suggèrent une corrélation entre l'augmentation des lamelles dans la couche extérieure et la diminution des niveaux de vibration dans les éléments CLT. L'étude conclut également que la direction

des appuis influence l'indice de réduction des vibrations des jonctions en CLT, une orientation parallèle étant considérée comme la plus favorable.

Le quatrième paramètre étudié est la hauteur des bâtiments en CLT et l'effet de l'augmentation de la charge en bas des bâtiments. 58 mesures verticales de l'isolation contre les bruits aériens dans quatre bâtiments avec différents systèmes et couches intermédiaires révèlent une diminution de l'isolation contre les bruits aériens plus bas dans le bâtiment. En outre, 12 mesures de l'indice de réduction des vibrations des jonctions dans quatre bâtiments avec différents détails de jonction révèlent également une diminution de l'indice de réduction des vibrations plus bas dans les bâtiments, en particulier pour la voie mur-mur, indépendamment des couches intermédiaires résilientes dans la jonction. La diminution de l'isolation des bruits aériens est d'environ 0,5 dB par étage, en fonction de l'influence des voies latérales par rapport aux autres voies de transmission. Ces résultats soulignent l'importance de prendre en compte l'effet de la hauteur du bâtiment dans la phase de conception, car il peut influencer de manière significative l'isolation acoustique dans les immeubles de grande hauteur en bois avec de multiples chemins d'accès entre les appartements.

ABSTRACT

This research project aims to develop estimations of some parameters that influence the flanking airborne sound insulation in lightweight buildings, based on laboratory and field measurement data. Since numerous parameters affect flanking sound transmission in lightweight buildings, some of them will be focused on.

The first parameter explored is the sound reduction of ventilation ducts, specifically the decreased sound insulation when the ducts are mounted through a lightweight wall. Three walls and three ventilation ducts (two circular and one rectangular) were measured in a laboratory setting. Comparative analysis is conducted between existing theories and the measurements with a proposed sound transmission model. Due to the apparent differences between the existing theory and the experimental measurements, the theoretical framework is revised. The proposed transmission model, incorporating modified existing and newly developed theories, aligns closely with measurement data, demonstrating a difference of 0-1 dB in the weighted sound reduction index across the various configurations.

The second parameter considered is acoustical treatments on ventilation ducts, specifically external lagging of stone wool around the outer perimeter of ducts. While previous research has focused on silencers and internal lining, there is limited understanding of how external lagging, particularly with stone wool, affects the overall sound reduction. Based on existing measurements in a laboratory, estimations are developed through an iterative process for circular and rectangular ventilation ducts. Results show that external lagging with stone wool effectively reduces the flanking airborne sound transmission, and the developed estimations fit well with measurement data. The study emphasizes the importance of applying treatments closest to the wall and that external lagging is a practical solution to minimize airborne sound transmission when a large ventilation duct passes through a wall with high sound insulation values.

The third parameter examined is the bearing direction of cross-laminated timber (CLT) elements. Given the design of CLT elements with several layers oriented in different directions, vibrations can decrease differently over the elements. Moreover, in relation to a junction, CLT elements can be oriented parallel or perpendicular. Velocity levels over a CLT wall and the vibration reduction index of junctions are measured in a building. Field measurements suggest a correlation between increased lamellas in the outer layer and decreased vibration levels in CLT elements. The study also concludes that bearing direction influences the vibration reduction index of CLT junctions, with a parallel orientation being deemed most favorable.

The fourth parameter investigated is the building height of CLT buildings and the effect of increasing load lower down the buildings. 58 vertical airborne sound insulation measurements in four buildings with varying systems and interlayers reveal a decrease in sound insulation lower down the buildings. Furthermore, 12 vibration reduction index measurements of

junctions in four buildings with varying junction details also reveal a decrease in the vibration reduction index lower down the buildings, especially for the Wall-Wall path, regardless of resilient interlayers in the junction. The decrease in airborne sound insulation is found to be approximately 0.5 dB per story, depending on the influence of flanking paths compared to other transmission paths. These findings underscore the importance of considering the building height effect in the design phase, as it can significantly influence the sound insulation in high-rise wooden buildings with multiple flanking paths between apartments.

TABLE OF CONTENTS

LIST OF FIGURES

LIST OF TABLES

LIST OF ABBREVIATIONS

ANN	Artificial Neural Networks
ASHRAE	American Society of Heating, Refrigerating and Air-Conditioning Engineers
ASTM	American Society for Testing and Materials
BEM	Boundary Element Method
CLT	Cross-Laminated Timber
FE	Finite Element
FEM	Finite Element Method
Glulam	Glued-laminated timber
HVAC	Heating, Ventilation, and Air Conditioning
ISO	International Organization for Standardization
LVL	Laminated veneer lumber
ML	Machine Learning
RME	Root Mean Square
RMSE	Root Mean Square Error
SD	Standard Deviation
SEA	Statistical Energy Analysis
Std Dev	Standard Deviation

LIST OF DISCRIPTORS

Symbol	Description	SI-unit
A	Absorption area	m^2
A_0	Surface area factor	m^2
A_i	Cross-section area factor	m^2
A_R	Room constant	m^2
ATL	Apparent transmission loss	dB
a	Longest dimension of rectangular duct's cross section	m
a_i	Absorption length for element i	m
a_j	Absorption length for element j	m
b	Shortest dimension of rectangular duct's cross section	m
C	Sound attenuation factor	dB
C_0	Correction factor for duct type	Constant
c_0	Speed of sound in air	m/s
c_L	Speed of sound in solid mediums	m/s
CAC	Ceiling attenuation class	dB
D_{nT}	Standardized level difference	dB
$D_{n,c,w}$	Weighted normalized sound level difference for ceilings	dB
D_{pr}	Sound pressure insulation (reciprocity method)	dB
$D_{v,ij}$	Velocity level difference, element i excited	dB
$D_{v,ji}$	Velocity level difference, element j excited	dB
$\overline{D_{v,ij}}$	Direction-averaged velocity level difference	dB
d	Diameter	m
E	Modulus of elasticity	Pa
f	Frequency	Hz
f_0	Resonance frequency	Hz
f_1	Cut-off frequency	Hz
f_c	Critical frequency	Hz
f_d	Cross-over frequency, double leaf construction	Hz
f_e	Cut-off frequency factor	Hz
f_L	Cross-over frequency, rectangular ventilation duct	Hz
f_R	Ring frequency	Hz
f_{ref}	Reference frequency	Hz
K_{ij}	Vibration reduction index	dB

Symbol	Description	SI-unit
L	Length of the duct	m
L_{p1}	Sound level in the sending room	dB
L_{p2}	Sound level in the receiving room	dB
L_v	Velocity level	dB
L_{wrap}	Length of the external lagging coverage	m
M_{duct}	Surface area of the duct	m^2
M_{wrap}	Surface area of the duct that is wrapped	m^2
NR	Noise reduction	dB
NNR	Normalized noise reduction	dB
P	Perimeter of the duct	m
PWL_i	Sound power level inside a duct, sending room side	dB
PWL_{out}	Breakout sound power level radiated by a duct	dB
PWL_{in}	Sound power level in a duct where it leaves the room	dB
PWL_{inc}	Sound power level on the outside of a duct	dB
Q	Directivity factor	Constant
q_0	Mass per unit area of the duct	kg/m^2
q_{wrap}	Mass per unit area of the external lagging	kg/m^2
r	Distance from the line source to the receiver	m
R & R'	Sound reduction	dB
R_{duct}	Sound reduction of the ventilation duct	dB
R_w & R'_w	Weighted sound reduction	dB
R_{wall}	Sound reduction of the separating construction	dB
R_{wrap}	Sound reduction of the external lagging	dB
S	Cross-section area of the duct	m^2
S_{tot}	Total area of several combined subareas	m^2
S_{wall}	Separating area of the wall	m^2
STC	Sound transmission class	dB
T	Reverberation time	s
T_0	Reference reverberation time	s
T_s	Structural reverberation time	s
TL	Sound transmission loss	dB
TL_{out}	Transmission loss for break out	dB
TL_{in}	Transmission loss for break in	dB
t	Thickness of the duct material	m
ρ	Density	kg/m^3
ω	Radian frequency	degree/s
ΔL_1	Sound attenuation per unit length	dB
τ	Transmission factor	Constant

ACKNOWLEDGEMENTS

SCIENTIFIC PUBLICATIONS

Peer-reviewed journal articles

Nilsson, E.; Ménard, S.; Bard, D.; Hagberg, K. Effects of building height on the sound transmission in cross-laminated timber buildings – Vibration reduction index. Buildings 2023, 13(12). DOI: 10.3390/buildings13122943.

Nilsson, E.; Ménard, S.; Bard, D.; Hagberg, K. Effects of building height on the sound transmission in cross-laminated timber buildings – Airborne sound insulation. Building and Environment 2023, 229. DOI: 10.1016/j.buildenv.2023.109985.

Nilsson, E.; Ménard, S.; Bard Hagberg, D.; Vardaxis, N.-G. Acoustical Treatments on Ventilation Ducts through Walls: Experimental Results and Novel Models. Acoustics 2022, 4, 276-296. DOI: 10.3390/acoustics4010017.

Nilsson, E.; Vardaxis, N.-G.; Ménard, S.; Bard Hagberg, D. Sound Reduction of Ventilation Ducts through Walls: Experimental Results and Updated Models. Acoustics 2021, 3, 695-716. DOI: 10.3390/acoustics3040044.

Conference papers

Nilsson, E.; Ménard, S.; Bard, D. Airborne Sound Transmission in Cross-Laminated Timber Buildings: The Influence of Building Height. In proceedings of Acoustics Week in Canada 2023, September 2023. Available from: jcaa.caa-aca.ca/index.php/jcaa/issue /view/302 (accessed 2024-02-10).

Nilsson, E.; Ménard, S.; Bard, D.; Hagberg, K. Effect of Bearing Direction and Mounting Techniques on Cross-Laminated Timber Elements in the Field. In proceedings of the 51st International Congress and Exposition on Noise Control Engineering (Inter-Noise), 21-24 August 2022. DOI: 10.3397/IN_2022_0274.

CHAPTER 1

INTRODUCTION

1.1 Overview

Acoustics in sustainable building design significantly influences various aspects of human life, affecting productivity in workplaces and the quality of sleep in residential buildings. It covers a range of different sectors, including building acoustics. Basically, building acoustics is about controlling the noise in buildings, ensuring that the sound transmission between spaces is minimized within the limits set for the building [1].

Buildings in the future need a shift towards more sustainable materials to reduce the carbon emission impact from the building industry, which contributes to around 38 % of global energy-related CO_2 emissions [2]. Choosing environmentally friendly building materials is an effective strategy to reduce energy consumption. Since wood stands out among other building materials for its environmental advantages, wood plays an important role in future buildings [3–8]. Moreover, wooden buildings and specifically buildings with Cross-Laminated Timber (CLT) is increasing in interest in many countries [9]. CLT is an important wooden load-bearing product to analyze in more depth. To additionally reduce the carbon emissions from the building industry, it is necessary to optimize the buildings with appropriate solutions. This is a reason why estimations for various scenarios are essential.

Several sound transmission paths must be considered to estimate the sound insulation between two spaces (for example between rooms in two apartments). The path that usually comes first in mind is the direct path, which is the path that is directly between two spaces,

usually a wall or a floor. The sound insulation should not be confused with sound absorption. Sound absorption is related to the sound energy transformed to heat in some material, and a good absorber is typically porous and light. Sound insulation reduces sound energy when sound is transmitted through a wall or a floor, and constructions with good sound insulation are typically airtight and heavy [10]. In addition to the direct sound transmission, additional sound is transmitted between two spaces in typical buildings via flanking transmission paths. Flanking transmission takes place when sound indirectly travels from one space to another through connected components of the building structure. A typical flanking path in a multi-family apartment building is a continuous floor or continuous wall between two apartments. Other common flanking paths are via cavity walls, suspended ceilings, pipe work, and ducting [1]. Some typical flanking paths are shown in Figure 1.1.
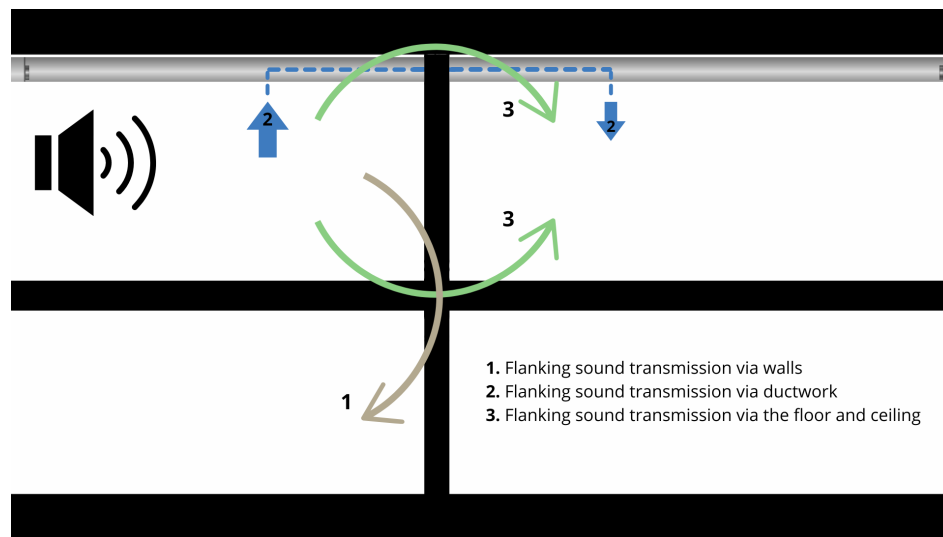
Figure 1.1: Illustration of some flanking transmission paths between rooms.

1.2   Statement of the problem

The flanking sound transmission in lightweight buildings often constitutes limitations for the building structure, and many lightweight buildings are complex to model [11]. Moreover, the final evaluation of a lightweight building can reveal significant variations in sound insulation measurements between rooms with similar construction details [12]. Parameters affecting

sound transmission in lightweight buildings include the room volume, the surface dividing area between apartments, the bearing direction of the structural elements, the static load on the junctions, the workmanship, the ventilation ducts, and more.

Consequently, a part of this thesis directs attention to sound propagation via the surface area of ventilation ducts. Firstly, sound can propagate via the material and the air inside a ventilation duct that passes through two rooms, reducing the sound insulation. The radiated sound from the surface area of ventilation ducts depends on several parameters, including the sound that breaks into and out of the ventilation duct [13]. It is described as a flanking sound transmission problem because of two structural elements with a common junction. The problem is narrower in dwellings but much broader in schools, hospitals, and offices where larger ventilation ducts are used. One way to reduce the sound transmission via the ventilation duct is to apply external lagging along the surface area of the ventilation duct. This acoustic treatment is a common application to solve an existing breakout noise problem [1, 14], but it can also be a part of the early design when a building is planned.

Secondly, sound can propagate between two spaces via the structure-bearing building elements. The radiated sound from structure-bearing building elements depends on the sound reduction of the elements and the junction's acoustic performance. According to Forssén et al. [11], prediction models need to be developed to account for flanking sound transmission in lightweight buildings. Bader Eddin et al. [15] developed an ANN (Artificial Neural Networks) model to predict airborne and impact sound insulation in the field of CLT buildings where parameters like the volume of the room and the surface dividing area were discussed in the sensitivity analysis. The increasing static load on junctions down the building, caused by an increasing number of stories, is suggested to affect the sound transmission by Bard, Davidsson, and Wernberg [16]. The effect is observed in several studies with a few measurements [16–19], here called the building height effect. With increasing building heights in high-rise CLT buildings, there is a need to quantify the acoustic effect of static load on the junctions properly with measurements of various junction details in different buildings.

1.3   Aims and objectives

The scope of the research project is to develop estimations of some parameters that influence the flanking airborne sound insulation in lightweight buildings, based on laboratory and field measurement data. Since numerous parameters affect flanking sound transmission in lightweight buildings, some of them will be focused on.

First, the aim is to develop estimations for the contribution of different ventilation ducts (dimension and shape) to the total sound transmission of a separating lightweight structure when the duct goes through the structure.

Second, the objective is to formulate estimations to calculate the proper acoustic treatments needed if the ducts are covered with external lagging of stone wool.

Third, the aim is to investigate if different static load and bearing direction variations affect the flanking airborne sound transmission in erected CLT buildings.

Fourth, the goal is to develop estimations of the bearing direction and building height effect, if they influence the sound transmission, to account for them in the design stage.

1.4   The originality of the research

In recent years, there has been a growing focus on studying sound transmission in lightweight buildings. Despite this, acousticians struggle to develop practical prediction tools for calculating the sound insulation of lightweight buildings in real-world scenarios. The thesis seeks to address several areas where there is a lack of accurate estimations to account for various parameters influencing flanking airborne sound transmission, particularly in lightweight buildings.

A review of existing literature, as highlighted in an article by Caniato et al. [20], mentions limited attention given to duct-borne sound in prior research on acoustics in lightweight buildings. While existing models describe the sound transmission of ventilation ducts for

different paths [13, 21–34], few studies explore how sound propagates between rooms via the surface area of a ventilation duct. E Nilsson [35] provides equations to calculate the flanking sound transmission through ventilation ducts but lacks accurate application and theoretical development. As a result, this thesis will clarify and develop existing theory to describe how sound propagate via the surface area of ventilation ducts between two rooms.

Several authors investigated the external lagging effect on ventilation ducts with different prediction models [14, 36, 37]. However, they are primarily focused on rectangular ventilation ducts, and only when the whole ventilation duct is covered. In this thesis, estimations are addressing both rectangular and circular ventilation ducts when they are completely and also partly covered, which is not previously described in the literature with equations.

Previous studies have not investigated if the bearing direction of CLT elements affects the vibration reduction index, but a few studies investigated if the number of stories, or the static load, affects the sound transmission between stories. While the results from Refs. [16–19] do not agree completely, the majority found a corresponding difference, and it is suggested that the result could be caused by the difference in load over the junctions [16]. The effect is not sufficiently covered in previous studies since only a few junctions or measurements are evaluated, and it is not enough for estimations. Therefore, more contributions to the literature are made in this thesis to estimate the building height and the bearing direction effect in CLT buildings.

Through estimations to account for various parameters affecting the flanking airborne sound insulation, this thesis seeks to enhance our understanding of sound transmission in lightweight buildings and contribute valuable insights to the field of acoustics.

1.5   Thesis outline and chapters organization

This thesis includes eight chapters, and the majority of the content is centered around four peer-reviewed articles produced during the research project to attain a Doctorate of Philosophy

in Engineering. It starts with a summary in English and French (resumé) summarizing the main findings and is followed by scientific publications (peer-reviewed and conference papers).

Chapter 1 discusses the overview and the statement of the problem of the thesis. Moreover, the aims of the thesis and the objectives are presented, which are to develop estimations of some parameters that influence the flanking airborne sound insulation in lightweight buildings. In addition, the originality of the research is discussed.

Chapter 2 first examines the basics of acoustics, starting with the propagation through different mediums. It deals with the physics of sound insulation and the corresponding frequency regions. Then, sound transmission paths in buildings are reviewed, including the direct path, the flanking paths, and components mounted in the separating element. Next follows procedures for airborne sound insulation and vibration reduction index measurements, with a comparison between the two most commonly used standards worldwide (ISO and ASTM). Lastly, flanking sound transmission in CLT buildings and the sound reduction of ventilation ducts are examined more thoroughly.

Chapter 3 covers the method and results for measurements and theoretical estimations of existing theory [13, 33, 34] with a proposed transmission path model to describe the sound reduction of ventilation ducts through walls. It demonstrates the strengths and the weaknesses of existing theory, along with modifications of existing theory or the development of new equations. Both circular and rectangular ventilation ducts are covered through several types of walls.

Chapter 4 depicts the various acoustic treatments available on ventilation ducts. Moreover, equations to estimate the acoustic effect of treatments with external lagging of stone wool are analyzed and developed for partial and complete covering of circular and rectangular ducts. In addition, suspended ceilings and their positive effects are discussed and compared with measurement results.

Chapter 5 focuses on airborne sound insulation measurements regarding the building height effect in CLT buildings. Vertical airborne sound insulation measurements in four

CLT buildings with various building systems and with some number of stories in between measurements are thoroughly investigated and compared. An initial estimation curve for the decrease in sound insulation per story is presented. Lastly, measurement uncertainties are discussed, and more accurate estimations are presented to account for the building height effect during the design phase of a building.

Chapter 6 discusses the difference between beeswax and double-sided tape as mounting techniques for attaching accelerometers to CLT elements. Additionally, the bearing direction effect of CLT elements is discussed, and results are presented on how it influences the vibration reduction index of junctions.

Chapter 7 examines the building height effect with vibration reduction index measurements, which is a more detailed analysis of the acoustic performance in the junctions compared to Chapter 5. Again, four CLT buildings with different junction details are measured and compared. Two initial estimation curves for the decrease in vibration reduction index per story are presented, one for T-junctions and one for X-junctions. Lastly, measurement uncertainties and the differences between vibration reduction index measurements in the field and a laboratory are discussed.

In the concluding chapter, Chapter 8 summarizes the primary discoveries and scientific contributions made throughout the thesis. Additionally, it offers insights into the potential research applications in shaping the design of upcoming lightweight buildings.

CHAPTER 2

LITERATURE REVIEW

2.1 Basics of acoustics

2.1.1 Sound levels and the decibel scale

Sound is an audible vibration from the air, in liquids or solid materials [10], and sound can be expressed with several quantities. The sound from industrial equipment are typically described with the emitted sound power, while the sound in a room is usually described with the sound pressure. Both the sound power and the sound pressure can be expressed in decibels. Decibel is a unit that represents ten times the logarithmic ratio of two quantities, the measured value and a reference value [1]. The sound pressure level is described with Equation 2.1:

$$L_p = 10 \cdot \log_{10}\left(\frac{p^2}{p_{\text{ref}}^2}\right), \tag{2.1}$$

where the measured value is sound pressure, p, and it is based on a reference sound pressure, p_{ref}, of 20 μPa [10]. The measured value for the sound power level is sound power, P_w, and the reference value is $P_{\text{ref}} = 1$ pW [10]. The decibel scale is used in all building acoustic applications to describe sound insulation. Human ears can typically hear frequencies between 20 Hz to 20 000 Hz, and the human ear interprets sound from the pressure variations in an incoming sound wave [1, 10, 38].

2.1.2 Propagation of sound in air

Sound in air is caused by compressions and rarefractions of the air particles during wave propagation. Longitudinal waves are formed when the air particles move back and forth in the direction of the propagation, see Figure 2.1. The movement causes temporal variation in sound pressure [38].
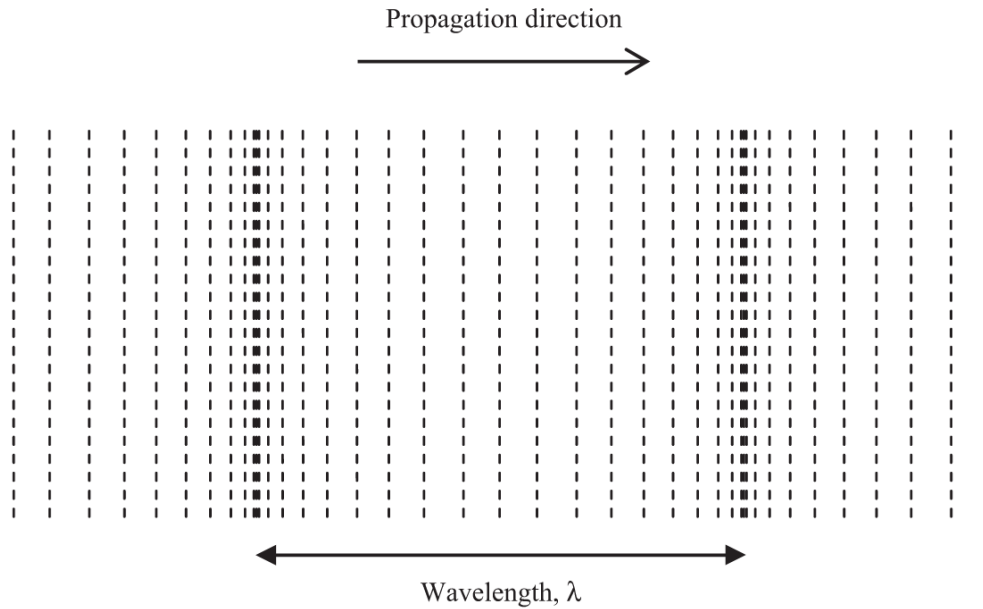
Figure 2.1: Illustration of compressions and rarefractions for a longitudinal wave. Figure from Hopkins [38].

Two types of waves in the air are mainly described in the literature. One of them is plane waves, which can be realized in a long hollow cylinder with rigid walls. The sound pressure for plane waves propagating in the positive direction of x, y, and z can be described with Equation 2.2:

$$p(x,y,z,t) = \hat{p}e^{-ik_x x}e^{-ik_y y}e^{-ik_z z}e^{i\omega t}, \tag{2.2}$$

where $\hat{p}$ is an arbitrary constant for the peak value and k_x, k_y, k_z are the constants related to the wavenumber [38]. Moreover, ω is the angular frequency, calculated with Equation 2.3:

$$\omega = 2\pi f = \frac{2\pi}{T_1}, \tag{2.3}$$

where T_1 is the duration of a period and f is the frequency [10].

Another commonly described wave in the air is a spherical wave, and a loudspeaker can, for example, be modeled as a point source that generates spherical waves [38]. The sound pressure for spherical waves propagating across a space is described with Equation 2.4:

$$p(r,t) = \frac{\hat{p}}{r} e^{-ikr} e^{i\omega t}, \tag{2.4}$$

where r is the distance between a spherical wavefront and the sound source [38]. The wavenumber, k, is dependent on the angular frequency and the speed of sound, presented in Equation 2.5:

$$k = \frac{\omega}{c_0} = \frac{2\pi}{\lambda}, \tag{2.5}$$

where λ is the wavelength, illustrated in Figure 2.1. The speed of sound, c_0, is temperature dependent and calculated to 343 m/s at 20 degrees Celsius [38].

2.1.3 Propagation of sound in solid mediums

A solid medium, for example, a plate, differs from fluids in terms of acoustics since it can resist shear forces. Apart from the longitudinal wave typical in both solid mediums and air, solid mediums will also have shear waves and combinations of the two. The most important combination of the two waves is the bending wave [10]. Both wave types, longitudinal and shear, follow the wave equation. Equation 2.6 describes the wave equation for a plane wave propagating in the x-direction:

$$\frac{\partial^2 u}{\partial x^2} = \frac{1}{c^2} \cdot \frac{\partial^2 u}{\partial t^2}, \tag{2.6}$$

where u is the particle velocity. The magnitude of the wave speed, c, will change depending on the type of wave. Figure 2.2 shows different waves in solid mediums from Rindel [10], and combined waves, like the bending wave, can not be described with the wave equation [10].
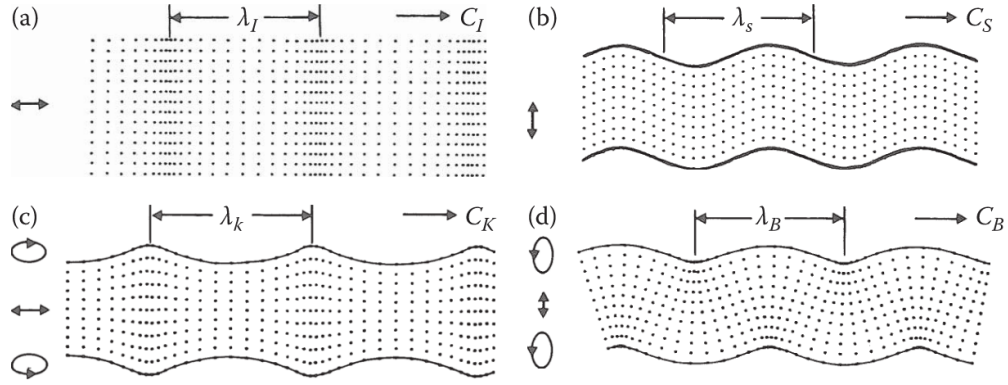
Figure 2.2: Different type of waves in solid mediums. (a) Longitudinal; (b) quasilongitudinal; (c) shear; (d) bending. Figure from Rindel [10].

The speed of sound for longitudinal waves, c_L, is for the simplest case calculated with Equation 2.7 where E is Young's modulus and ρ_m is the density of the solid material:

$$c_L = \sqrt{\frac{E}{\rho_m}}. \qquad (2.7)$$

In a plate or an extended solid medium, the Poisson's ratio, μ, tends to increase the bulk ratio, and, thus, the speed of sound [10].

Bending waves occur perpendicular to both the propagation and the surface of an element, and the motion causes sound to radiate to the surrounding air. The bending wave equation for the x-direction is described with Equation 2.8 [10]:

$$B \cdot \frac{\partial^4 v}{\partial x^4} + m \cdot \frac{\partial^2 v}{\partial t^2} = 0, \qquad (2.8)$$

where v is the vibration velocity perpendicular to the plate and m is the mass per unit area of the plate. The speed of sound for bending waves, c_B, is frequency-dependent and determined with Equation 2.9 [10]:

$$c_B = \sqrt{2\pi f} \cdot \sqrt[4]{\frac{Eh^2}{12\rho_m(1-\mu^2)}}, \qquad (2.9)$$

where h is the plate thickness.

2.1.4 Sound insulation of walls

An incident sound wave that encounters an infinite single-leaf wall can be reflected back to the space, absorbed by the single-leaf wall, and transmitted through the single-leaf wall if there is sufficient energy in the sound waves [1, 38]. Figure 2.3 from Hopkins [38] illustrates an incident sound wave with the reflected and transmitted wave, without the absorption. Absorption is described as the loss or dissipation of sound energy by friction to heat energy.
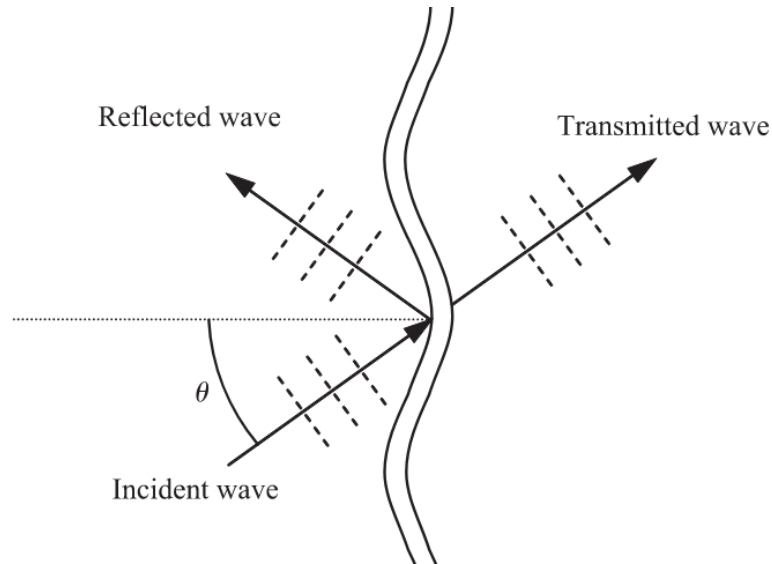
Figure 2.3: Incident plane wave encountering an infinite single-leaf wall. Figure from Ref. [38].

The passage of sound through a wall is described with the term *sound transmission*, and the sound transmitted is determined by the sound insulation of the separating element [1, 10]. The sound transmission coefficient, τ, is the transmitted and incident sound power ratio. Sound insulation is commonly described with the sound reduction index, R, which is determined by the sound transmission coefficient according to Equation 2.10 [10, 39]:

$$R = 10 \cdot \log_{10}\left(\frac{1}{\tau}\right). \qquad (2.10)$$

The sound reduction of a single-leaf wall can be described with three different regions following Figure 2.4 from [1]. The first is the stiffness-controlled region, which occurs for frequencies below the lowest resonance frequency of the single-leaf. The single-leaf can be considered very thin and vibrate as a whole element. The sound transmission through the single-leaf in the stiffness-controlled region is not so dependent on the mass or the damping but the stiffness of the single-leaf [1].
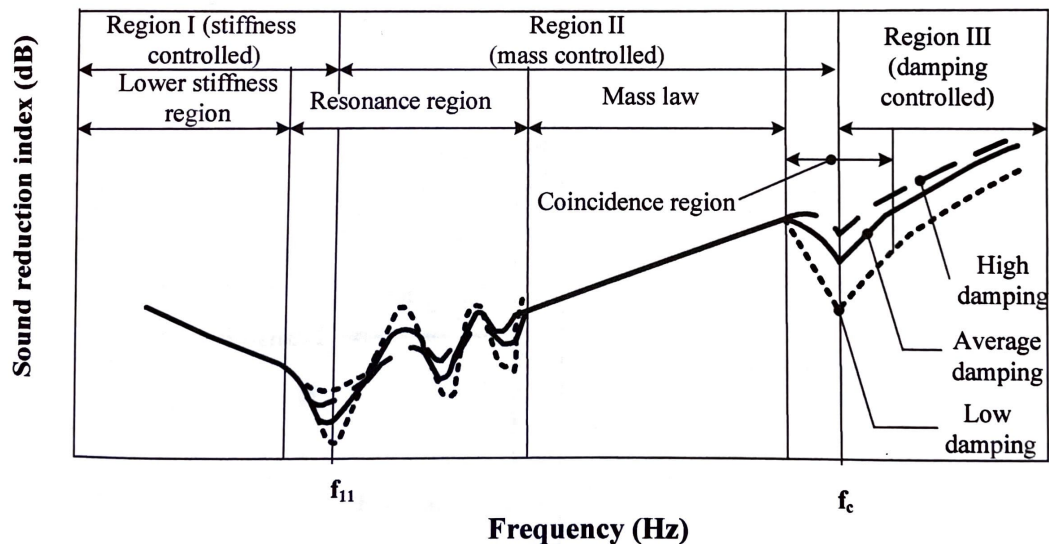
Figure 2.4: Typical sketch from Hassan [1] for the sound reduction of a single-leaf partition with different frequency regions.

The second region is controlled by the mass, which is usually in the mid-frequency range above the resonance frequency and below the critical frequency of the single-leaf. The sound transmission depends on the mass, and part of the region can be described with the mass law, which is a linear increase of the sound reduction in decibels. However, the mass law only applies to limp (low bending stiffness) and non-rigid partitions, which do not apply to common building materials. Therefore, it should be used mainly as an approximate guide [1].

The third region is the damping region, and it is found above the critical frequency where

coincidence causes a dip in sound reduction. The sound transmission in this region is affected by damping, surface density, and stiffness [1].

Two single-leaves separated by an air space, called a double-leaf wall, is more cost-effective to reduce the sound compared to an equivalent weight single wall [1]. A common behavior of a lightweight double-leaf wall is shown in Figure 2.5 from Rindel [10] with the different frequency regions marked out.
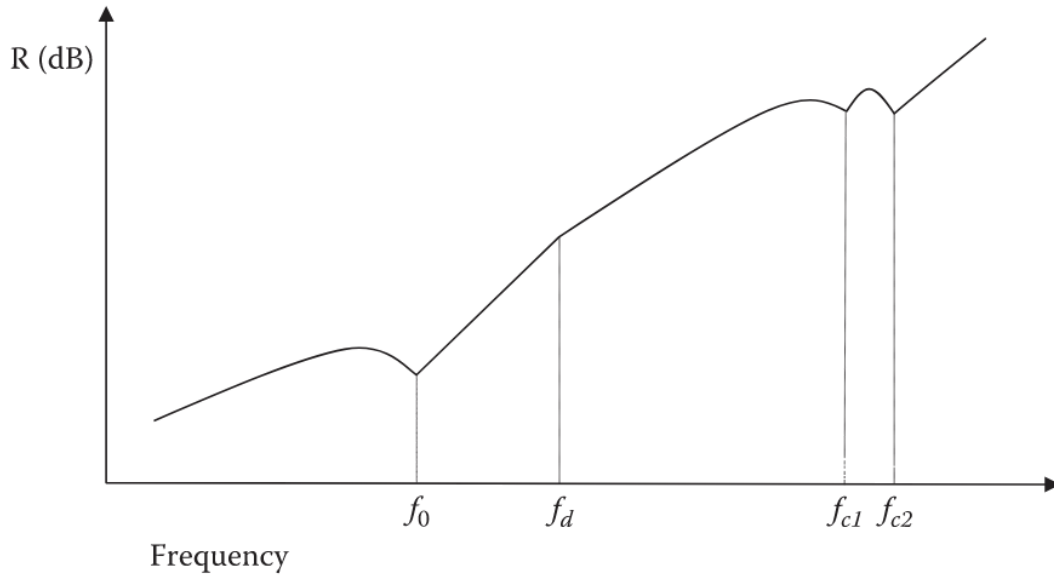
Figure 2.5: Typical sketch from Rindel [10] for the sound reduction of a double leaf wall with different frequency regions. If the leaves on each side of the cavity have the same properties, then $f_{c1} = f_{c2}$.

The critical frequency is defined as when the speed of bending waves for a single-leaf equals the speed of sound in air. The sound insulation tends to drop at the critical frequency and is calculated for a homogeneous single-leaf with Equation 2.11 according to Hopkins [38]:

$$f_c = \frac{c_0^2}{2\pi} \sqrt{\frac{\rho_s}{B_p}} = \frac{c_0^2}{\pi} \cdot \sqrt{\frac{3\rho_s(1-\mu^2)}{Eh^3}}, \tag{2.11}$$

where ρ_s is the surface density (kg/m^2) and B_p is the bending stiffness per unit width for a single-leaf (Nm). An orthotropic single-leaf has two critical frequencies in x- and y-direction

respectively caused by the bending stiffness in the different directions following Equation 2.12:

$$f_{c,x} = \frac{c_0^2}{2\pi} \sqrt{\frac{\rho_s}{B_x}},$$

(2.12)

$$f_{c,y} = \frac{c_0^2}{2\pi} \sqrt{\frac{\rho_s}{B_y}},$$

where B_x and B_y is the bending stiffness in the x- and y-directions [40]. A simplified critical frequency for an orthotropic single-leaf, the effective critical frequency $f_{c,\text{eff}}$, is calculated following Equation 2.13 from Ref. [38]:

$$f_{c,\text{eff}} = \sqrt{f_{c,x} \cdot f_{c,y}},$$

(2.13)

Resonance in a system is according to Rindel [10] defined as a state in which any change in excitation frequency results in a decreased response. One common resonance is the mass-spring-mass resonance, f_0, and it is the result of the spring effect of the gas in the cavity. It is commonly found in double-leaf walls and is calculated following Equation 2.14:

$$f_0 \cong \frac{c_0}{2\pi} \cdot \sqrt{\frac{\rho}{d} \left(\frac{1}{m_1} + \frac{1}{m_2} \right)},$$

(2.14)

where d is the depth of the cavity and m_1 and m_2 is the surface mass of the single-leaves on each side of the cavity [10]. The resonance frequency is usually in lower frequencies, and the shift from low- to high-frequency behavior of the air cavity is defined with the cross-over frequency, f_d, following Equation 2.15 from Rindel [10]:

$$f_d = \frac{c}{2\pi d}.$$

(2.15)

The air cavity's behavior shifts from resembling a simple spring below the cross-over frequency to that of a transmission channel at higher frequencies [10].

2.2 Sound transmission paths

The sound produced in a room by a loudspeaker or another source can propagate to adjacent rooms through more transmission paths than just the separating structure. The apparent sound reduction index, R' (see also Section 2.3.1.3), is dependent on the total sound transmission between rooms, τ', following Equation 2.16 [39]. The total sound transmission can be divided into transmission factors, τ_d, τ_f, τ_e, τ_s, that describe all the transmission paths related to the system according to Equation 2.17 from ISO 12354-1 [39]:

$$R' = -(10 \cdot \log_{10}(\tau')), \text{where} \tag{2.16}$$

$$\tau' = \tau_d + \sum_{f=1}^{n} \tau_f + \sum_{e=1}^{m} \tau_e + \sum_{s=1}^{k} \tau_s. \tag{2.17}$$

The indices d, f, e, and s in Equation 2.17 refer to the different transmission paths between rooms according to Figure 2.6.
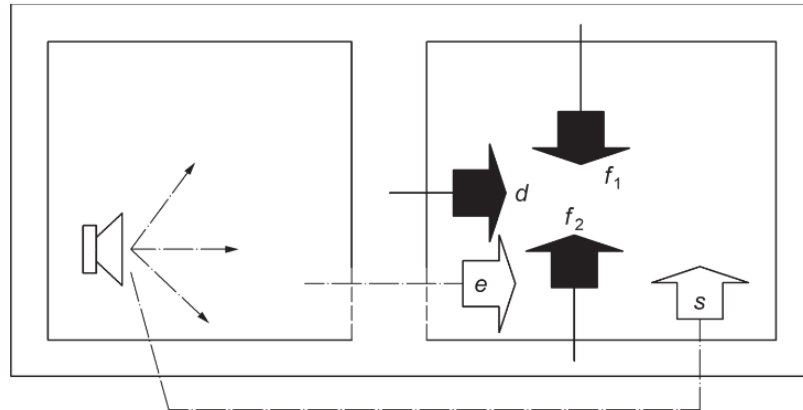
Figure 2.6: Illustration of transmission paths between two rooms. Figure from Ref. [39].

Index d is related to the direct sound transmission, e.g. the separating element (typically a floor or a wall). Index f is related to the flanking sound transmission, e.g. walls, floors, and ceilings that are connected to the separating element. Index e is related to sound transmission from elements mounted in the separating structure, e.g. doors and windows. Index s is related

to the indirect airborne transmission paths, e.g. corridors, double facades, and ventilation system that is not mounted through the separating wall). The minimum number of transmission paths between typical rooms is 13 paths, including 1 direct and 12 flanking transmission paths [1].

2.2.1 Direct sound transmission

Direct sound transmission is the sound that propagates through the separating element between two spaces, for example, a wall that separates two rooms described in Section 2.1.4. The sound transmission through lightweight walls is covered in many studies with various models, including SEA, FEM, and ML approaches.

Craik and Smith [41] developed two theories for the structural coupling between the leaves of a lightweight double-leaf partition. One is based on a wave theory where the frame forms a line connection, and one is based on the connection being at independent points. According to the authors, the result agrees with measured data, and the models can be used in a SEA model. In another paper, Craik and Smith [42] showed that a SEA model can predict sound transmission through a lightweight wall, where different models are used depending on the frequency range. In a later paper by Craik [43], a SEA model is shown, which can be used to improve predictions compared with measurement data for a double leaf wall with different cavity thicknesses.

Shen et al. [44] developed a theoretical model for a sandwich structure with a corrugated core to predict sound transmission. They found, among other things, that structural links reduce sound insulation. Wang et al. [45] present theoretical models of sound transmission for double-leaf partitions, a periodic and a smeared model. When compared with measurement data, the periodic model follows the same trend as the measurement. However, the model is undulating.

Vibroacoustic characteristics of CLT panels were studied in Y Yang et al. [46] with a wave and finite element method. According to the authors, the model makes it possible to

predict the vibroacoustic characteristics of CLT panels. Qian et al. [47] at UQAC used a stochastic process in an FE model to quantify uncertainties generated by material properties. They found that the simulated dynamic response under 100 Hz correlated better with the measured dynamic response of CLT and that a stochastic method can be applied to a FE model to quantify uncertainties.

Guigou-Carter and Villot [48] formulated an analytical model for a single and double plate with stiffeners. When the separation meets a junction, the vibrational flanking path at the boundaries is considered with a SEA model. The results show good agreement between measured and predicted data. Furthermore, prediction with increasing spacing between the stiffeners shows improved transmission loss in the mid-frequency range with little effect in low frequency for a single plate. For a double plate, predictions show a clear difference with and without stiffeners.

A master thesis by Zimmermann [49] at UQAC summarized several prediction models and developed a mathematical program to calculate the airborne sound insulation of lightweight walls. The program works well when compared with measurements of a single plate but deviates more from other predictions of a double-leaf wall.

Recently, a neural network approach to predict the direct sound insulation of both lightweight floors and facades was developed by Bader-Eddin et al. at UQAC in two articles [50, 51] with satisfactory results. Moreover, a neural network approach was also developed for field measurements to predict the sound insulation in buildings with CLT as the primary bearing structure [15].

Several other papers have studied different parameters and models to predict or understand sound transmission through a lightweight element [52–68]. Various models mentioned previously can be used to predict direct sound transmission. One method to predict the sound transmission is to divide the model into different sequences depending on the frequency regions. This approach is used in many building acoustic applications. Davy et al. [69] combined several models to predict the sound insulation of double-leaf cavity stud building

elements with stiffer studs. Models from different authors and articles are used at different frequency regions, which are compared with experimental results. However, the theory is deviating from measurements for certain frequencies.

2.2.2 Components mounted in the separating element

The transmission factor for components mounted in the separating element, τ_e, is according to ISO 12354-1 [39] related to the element normalized level difference, $D_{n,e}$, and presented in Equation 2.18:

$$\tau_e = \frac{A_o}{S_S} + 10^{-D_{n,e}/10},\qquad(2.18)$$

where S_S is the area of the separating element and A_o is the reference equivalent sound absorption area (usually 10 m^2) [39]. A typical example of elements mounted in the separating construction is a door or a window. The sound reduction is, in this case, a combination of the sound insulation of the wall and the door or window mounted in it. With the assumption that there is a diffuse sound field, the sound reduction of the combined elements can be determined according to Equation 2.19:

$$R_{\text{combined}} = 10 \cdot \log_{10}\left(\frac{S_{\text{tot}}}{\sum_n S_n \cdot 10^{-R_n/10}}\right),\qquad(2.19)$$

where S_n is the area of each element in the separating partition [70]. Moreover, Equation 2.19 is built up so that the sum of each subarea, S_n, shall be equal to the total area, S_{tot}.

2.2.3 Flanking sound transmission

Flanking transmission occurs when sound indirectly travels from one space to another through connected components of the building structure. Typical flanking paths in multi-family apartment buildings are continuous floors between two apartments or via cavity walls, suspended ceilings, pipe work, and ducting [1]. Twelve first-order flanking paths are usually present for

rectangular rooms directly above each other [71]. First-order flanking paths are described in this thesis as paths that include one junction, one source surface, and one receiving surface. Three of these flanking paths, together with the direct sound transmission path (Dd), are illustrated in Figure 2.7 from the standard ISO 12354-1 [39]. Indices F and D describe the flanking and separating element in the sending room, and indices f and d describe the flanking and separating element in the receiving room.

By following the paths in Figure 2.7, it is apparent that the transmission factor for the separating element, τ_d, is affected by contributions from other flanking paths, and not just the airborne direct sound transmission, described with Equation 2.20 [39]:

$$\tau_d = \tau_{Dd} + \sum_{F=1}^{n} \tau_{Fd}.$$ (2.20)

The transmission factor, τ_f, for various flanking elements consists of contributions from mainly two types of flanking transmission paths as illustrated in Figure 2.7 according to Equation 2.21:

$$\tau_f = \tau_{Df} + \tau_{Ff}.$$ (2.21)

The transmission factors in Equation 2.21 are related to the sound reduction index described further in ISO 12354-1 [39].
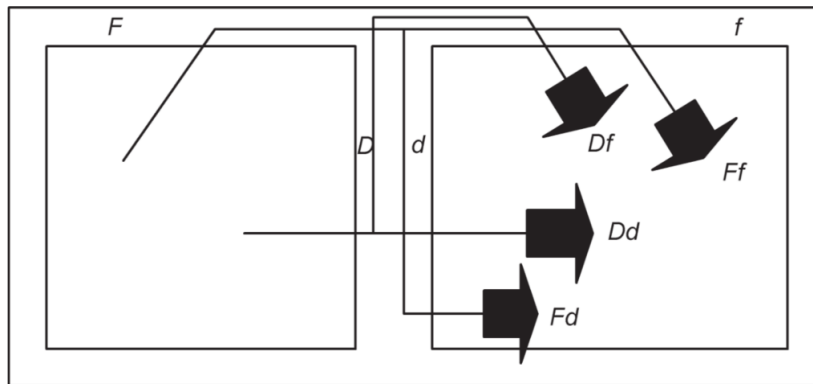
Figure 2.7: Illustration of some flanking transmission paths between two rooms. Figure from Ref. [39].

Flanking sound transmission paths can be estimated using the standard ISO 12354-1 [39]. The standard works well in calculating the sound transmission through various flanking paths, assuming that the velocity level difference is measured and used in calculations. However, estimated values found in the standard do not always yield satisfactory results, as shown by Galbrun [72]. A similar statement is mentioned by Poblet-Puig [73], who indicate that the flanking transmission model in ISO 12354 [39] can underestimate the sound reduction index of flanking paths for lightweight structures. In Galbrun [72], a SEA model is compared with measurements, which also does not yield satisfactory results. Schoenwald [71] studied flanking sound transmission through lightweight constructions using SEA, and the model is, according to the author, in good agreement with measurement results. However, Schoenwald [71] mentions that the model works best for the case considered in the thesis.

In Ref. [74], a BEM prediction model calculates a lightweight structure's flanking sound transmission. Predictions are compared with the simplified method in ISO 12354-1 and not actual measurements. In Bard, Sonnerup, and Sandberg [75], a lightweight structure was modeled using FEM, and flanking sound transmission was calculated and compared with measurements. The authors in Ref. [75] state that predictions correlate sufficiently well with measurements.

Other studies have also modeled the flanking sound transmission of lightweight structures [76–81]. In J Davy et al. [82], a prediction method named CSTB is recommended, and it takes into account the airborne and resonant radiation efficiencies. However, they mention that the model needs more measurement data to be improved.

2.3 Measurement parameters of sound insulation

2.3.1 Airborne sound insulation parameters

Airborne sound insulation is a measure of how much the sound is reduced between two spaces. This sound level difference, D according to ISO 16283-1 [83] or NR according to ASTM E336

[84], is a difference of the energy-averaged sound pressure level between the sending room, L_{p1}, and the receiving room, L_{p2}, according to Equation 2.22 from ISO 16283-1 [83]:

$$D = L_{p1} - L_{p2}.$$ (2.22)

The airborne sound insulation is frequency dependent and it is typically corrected with the reverberation time or the absorption area in the receiving room. Moreover, different standards for measuring the sound insulation apply depending on the country and if measurements occur in a laboratory or the field.

2.3.1.1 Reverberation time

The reverberation time, T, in a room is defined as the time it takes for the sound pressure level to decay to one-millionth of the initial value, i.e., a 60 dB decay, typically denoted T_{60}. Figure 2.8 illustrates an example of a measured decay curve.
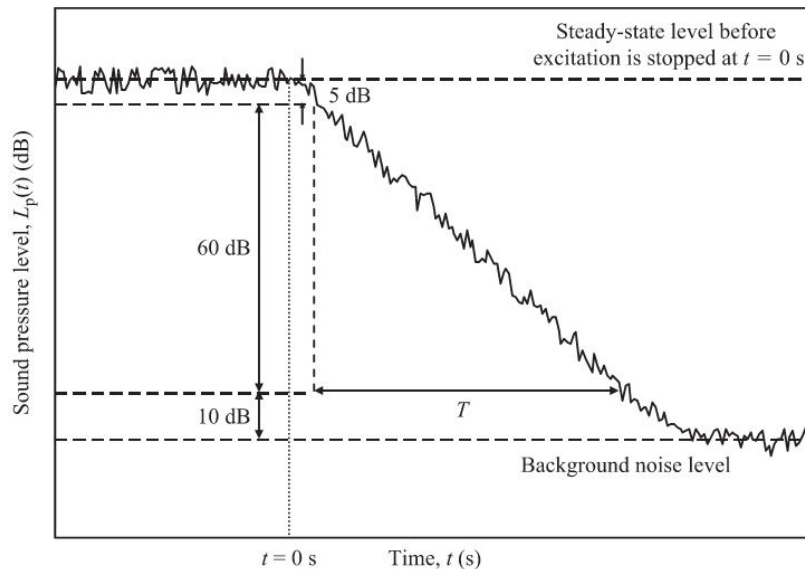
Figure 2.8: Example of a measured decay curve in a room. Figure from Hopkins [38].

Generally, a decrease of 60 dB is seldom reached for the whole frequency range. Hence, a shorter reverberation time, T_{20} or T_{30}, is used [10]. The measured time it takes for a decrease of 20 or 30 dB is multiplied by three respectively two, to reach T_{60}. The reverberation time

depends on the measured room's volume and absorption area. For a normal rectangular room with the sound absorption equally distributed on the surfaces, Sabine's formula can be used to calculate the reverberation time following Equation 2.23 [10]:

$$T = \frac{55.3 \cdot V}{c_0 \cdot A}.$$
(2.23)

2.3.1.2   In a laboratory

The airborne sound insulation is in a laboratory mainly dependent on the direct sound transmission through the separating element since laboratories are designed to suppress flanking paths [85], similar to the ones presented in section 2.2.3.

Airborne sound insulation measurements in a laboratory for floors and walls are evaluated with the sound reduction index from ISO, R, or transmission loss from ASTM, TL [86, 87]. The principle is to account for the absorption area in the receiving room, which affects the measured receiving sound pressure level. In Equation 2.24, the sound pressure level difference is corrected with the absorption area and the separating partition area, S [86].

$$R = L_{p1} - L_{p2} - 10 \cdot \log_{10}\left(\frac{A}{S}\right).$$
(2.24)

2.3.1.3   In the field

Airborne sound insulation measurements are evaluated in the field with usually one of two physical quantities. One is the apparent sound reduction index from ISO, R', or the apparent transmission loss from ASTM, ATL [83, 84]. The one from ISO is presented in Equation 2.24, but for the field, the physical quantity is presented with an apostrophe to mark that the index is for field measurement. The other physical quantity is the standardized level difference from ISO, $D_{\mathrm{n}T}$, or the normalized noise reduction from ASTM, NNR [83, 84]. The difference in sound pressure level is instead corrected with the measured reverberation time, T, and a reference reverberation time, T_0, according to Equation 2.25 from ISO [83]:

$$D_{\mathrm{n}T} = L_{p1} - L_{p2} + 10 \cdot \log_{10}\left(\frac{T}{T_0}\right). \tag{2.25}$$

2.3.2 Vibration reduction index parameters

Measurements of the vibration reduction index in the laboratory should be performed according to ISO 10848-1 [88]. Vibrations can be measured with both acceleration and velocity. However, the standard suggests that the acceleration level is used when measuring the structural reverberation time to avoid that signal processing could affect the decay curve. For the vibration level difference, acceleration or velocity can be used. The averaged velocity level is calculated according to Equation 2.26:

$$L_{\mathrm{v}} = 10\log_{10}\left(\frac{\frac{1}{T_{\mathrm{m}}} \cdot \int_0^{T_{\mathrm{m}}} v^2(t)\,dt}{v_0^2}\right), \tag{2.26}$$

where v is the velocity level over time and v_0 is the reference velocity level [88]. The vibration reduction index is calculated according to Equation 2.27:

$$K_{\mathrm{ij}} = \overline{D_{\mathrm{v,ij}}} + 10\log_{10}\left(\frac{l_{\mathrm{ij}}}{\sqrt{a_{\mathrm{i}} \cdot a_{\mathrm{j}}}}\right), \tag{2.27}$$

where $\overline{D_{\mathrm{v,ij}}}$ is the direction-averaged velocity level difference, calculated according to Equation 2.28:

$$\overline{D_{\mathrm{v,ij}}} = \frac{1}{2} \cdot \left(D_{\mathrm{v,ij}} + D_{\mathrm{v,ji}}\right). \tag{2.28}$$

In Equation 2.28, $D_{\mathrm{v,ij}}$ is the velocity level difference when element i is excited, and $D_{\mathrm{v,ji}}$ is instead when element j is excited. The vibration reduction index in Equation 2.27 is also dependent on the common junction length l_{ij} and the equivalent sound absorption length for each element, a_{i} and a_{j}, calculated according to Equation 2.29:

$$a_\mathrm{j} = \frac{2.2 \cdot \pi^2 \cdot S_\mathrm{j}}{T_\mathrm{s,j} \cdot c_0 \cdot \sqrt{\frac{f}{f_\mathrm{ref}}}},\qquad(2.29)$$

where S_j is the surface area of the element, $T_\mathrm{s,j}$ is the structural reverberation time of the element, c_0 is the speed of sound in air, and f_ref is the reference frequency [88].

2.3.3 Acoustic measurement standards – ISO and ASTM

Measurements of acoustic parameters generally follow international standards published by ASTM or ISO. ASTM standards are commonly used in the United States and Canada, while ISO standards are used in, for example, Europe. Table 2.1 illustrates a comparison between ISO and ASTM acoustic standards.

Table 2.1: Comparison of ISO and ASTM acoustic measurement standards.

ISO	Year	Title	ASTM equivalent
ISO 717-1	2020	Rating of sound insulation in buildings and of building elements. Part 1: Airborne sound insulation	ASTM E413
ISO 10140-2	2021	Laboratory measurement of sound insulation of building elements. Part 2: Measurement of airborne sound insulation	ASTM E90
ISO 10848-1	2017	Laboratory and field measurement of flanking transmission for airborne, impact and building service equipment sound between adjoining rooms. Part 1: Frame document	No equivalent
ISO 3382-2	2008	Measurement of room acoustic parameters. Part 2: Reverberation time in ordinary rooms	ASTM E2235
ISO 16283-1	2014	Field measurement of sound insulation in buildings and of building elements. Part 1: Airborne sound insulation	ASTM E336

The comparison focuses on the names without considering the specific differences within each standard. Overall, the equations in the standards are similar, but the measurement

procedures can vary more. In some cases, ASTM standards refer to ISO standards when an ASTM standard is not developed, for example, measurements of the vibration reduction index (ISO 10848-1). One big difference between ISO and ASTM standards is that ISO uses correction factors for variations in the frequency spectra along with weighted single-number values, while ASTM considers this when the weighted single-number values are determined.

2.4 Airborne sound transmission of CLT elements

2.4.1 Cross-Laminated Timber

Wooden buildings in general and specifically buildings with Cross-Laminated Timber (CLT) are increasing in interest in many countries [9]. CLT is an engineered wood product made with several layers of lumber boards that are stacked in alternating directions of 90 degrees. CLT often consists of an odd number of layers (usually 3-7) [89]. The panels are prefabricated before they are mounted and used in the field, and holes for doors and windows can be cut out with CNC routers [90]. CLT is suitable for several applications, including walls, floors, and roofs since it is a stable, strong, and stiff product [9]. CLT also has good seismic and thermal performance [91]. Wood has a radial and an axial system, and because of this, wood can be observed in three main perspectives that yield more information about the wood. The perspectives are the transverse, radial, and tangential plane of section [92]. Wood, and thereby lumber boards, has three different moduli of elasticity depending on orientation. Therefore, CLT panels will also have different moduli of elasticity depending on the global axis since the boards in each layer alternate.

In terms of acoustics, a low bending stiffness or a heavy mass often results in a good acoustic performance of a structure [93]. Because CLT is lightweight, it cannot fulfill different acoustic requirements alone. Additionally, due to different modulus of elasticity of a CLT panel's major and minor axis, it is suggested that CLT has two critical frequencies [94] and the sound insulation is generally worse around the critical frequency [93]. Moreover, it is

suggested that the two critical frequencies of a CLT panel result in not just a dip in one specific third-octave band but instead a dip between these two frequencies as a range of third-octave bands [94]. According to Refs. [93, 95], the critical frequency of CLT elements is between 100 Hz and 500 Hz. Therefore, the mid-frequency area around 500 Hz is interesting to investigate as well, in contrast to the low-frequency region, which is often highlighted as an important frequency for lightweight buildings [20, 96, 97].

CLT panels have different bearing directions and, in relation to a junction, the moduli of elasticity for CLT is different depending on the bearing direction [98]. Furthermore, CLT panels usually have the boards on the outer layers parallel to the strongest load-bearing direction [90], illustrated in Figure 2.9.
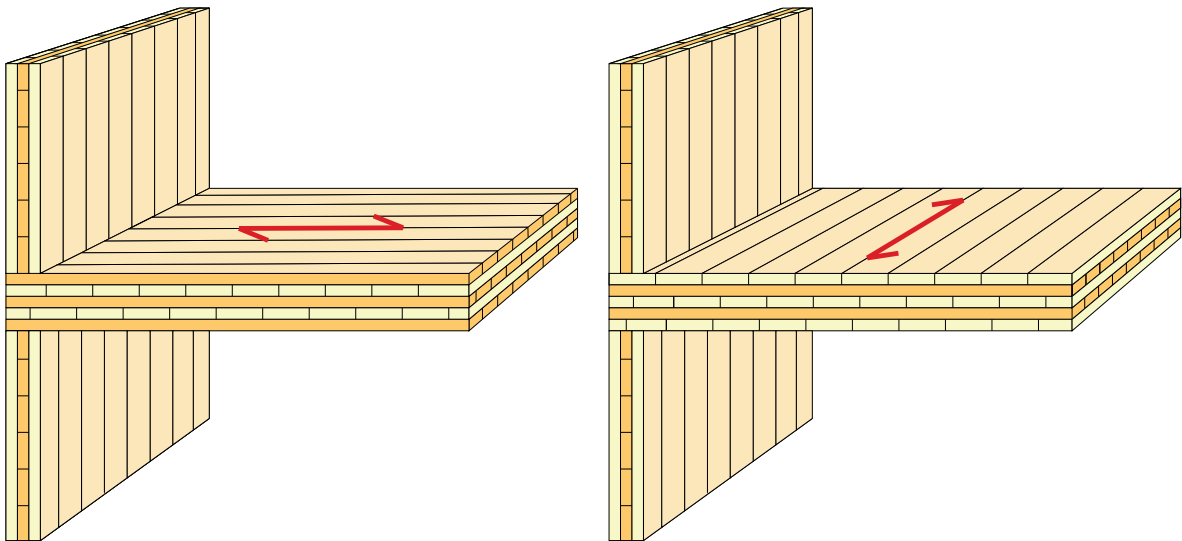
Figure 2.9: T-junctions of CLT elements with the bearing direction perpendicular (left) and parallel (right) in relation to the junction [98].

Two junction types, here called X- and T-junctions, are typically used for CLT buildings illustrated in Figure 2.10 without resilient interlayers.

(a) X-junction   (b) T-junction
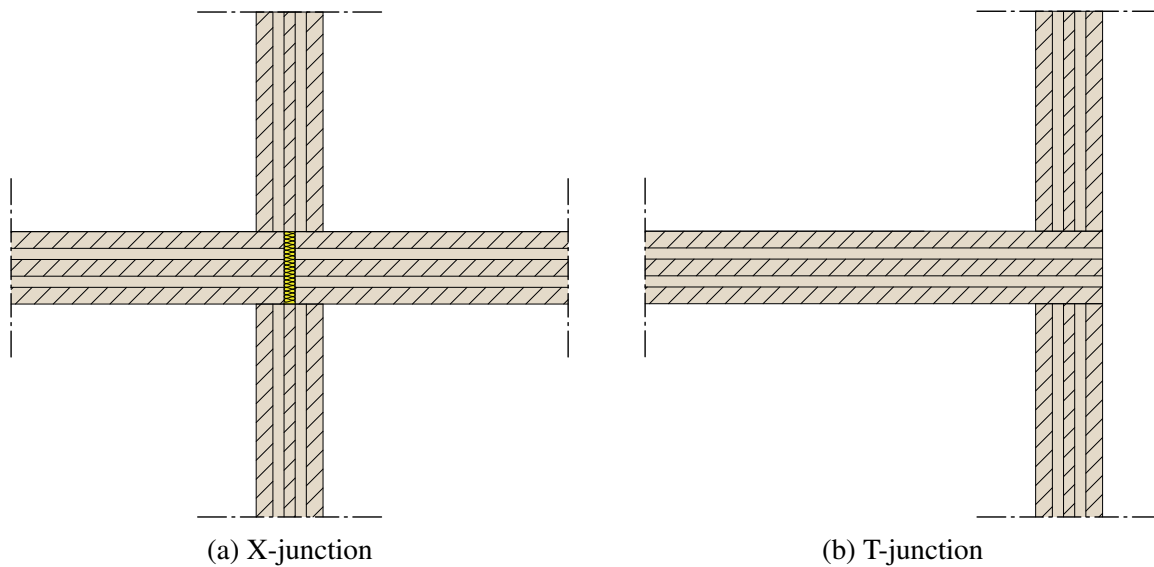
Figure 2.10: Two common principle junction types for CLT elements in buildings.

2.4.2 Resilient interlayer

Resilient interlayers are often required in wooden buildings to fulfill different acoustic requirements, and they are usually placed between load-bearing walls and floors to limit the flanking sound transmission [11]. A type of resilient interlayer is a viscoelastic interlayer commonly used in wooden buildings. Viscoelastic materials exhibit properties between a viscous liquid and an elastic solid [99–101], and the behavior is frequency dependent [102]. A viscoelastic interlayer can be modeled as a spring with a certain stiffness, and the stiffness is selected based on a calculated load [101, 103–105]. Figure 2.11 shows several types of viscoelastic interlayers from various manufacturers, and the colors represent a specific stiffness from each manufacturer.

Craik and AG Osipov [106] found that a junction with an elastic interlayer has a frequency-dependent transmission loss, unlike rigid junctions without interlayers where the transmission loss is nearly independent with frequency. Measurements in Kim et al. [107] showed that the dynamic stiffness decreases with increasing thickness of the resilient materials in a floating floor construction. Furthermore, lower vibration-damping properties could occur if resilient interlayers are not utilized or selected for the right load interval, according to Ref. [108]. On

the other hand, measurements by Jarnerö et al. [109] found that stiff interlayers that are not selected for the right load still contribute to floor vibration.

Figure 2.11: Various types of viscoelastic interlayers commonly used in wooden buildings.

Different laboratories have measured the difference with and without resilient interlayers and Ref. [18, 110–114] show that the vibration reduction index increases with a resilient interlayer. However, one should observe that a resilient interlayer changes the distribution of sound energy in the structure. Thus, they can be implemented to reduce the flanking sound transmission in a specific direction only since they do not change the total energy in the system [106, 115]. A junction's vibration reduction index is dependent on various factors. This includes not just the presence of resilient interlayers but also the type of screws and connectors used to hold a junction's elements together. Several configurations with connectors and screws were tested in laboratories by several papers [18, 116, 117]. A few examples of different usages of resilient interlayers are displayed in Figure 2.12.

(a) Resilient interlayers between bearing elements and under bracket.

(b) CLT-junctions in a staircase with resilient interlayers.

Figure 2.12: Different usage of resilient interlayers in CLT buildings.

2.4.3 Previous measurements of CLT structures

Various authors studied flanking sound transmission measurements of CLT panels in several laboratories. Schoenwald et al. [117, 118] measured the vibration reduction index of a CLT junction and found that a continuous floor path is a more important flanking path than vertical wall-wall paths. Moreover, it was found that either an additional floor and ceiling treatment or a structural break is necessary to improve the sound insulation.

Di bella et al. [113] compared vibration reduction index measurements of different mounting conditions. They found that increasing the number of panels increases the attenuation for each transmission path because of the re-distribution of energy. Moreover, they found that a resilient layer improves most of the transmission paths, but not all of them. Consequently, resilient interlayers should be implemented to reduce the flanking sound transmission in a specific direction only since they do not change the total energy in the system [106, 115], mentioned under Section 2.4.2 and illustrated in Figure 2.13.
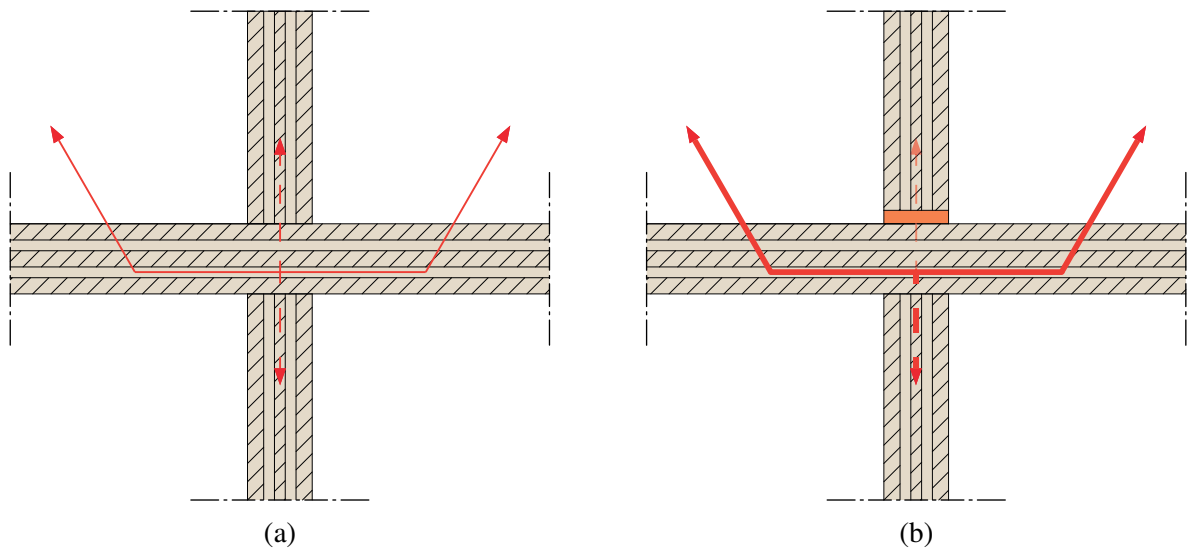
Figure 2.13: Simplified sketch of the distribution of sound energy without (a) and with (b) an elastomer, based on Refs. [106, 113, 115].

Morandi et al. [116] analyzed measurements of the vibration reduction index made in a laboratory. They found that energy transmitted through a junction strongly relates to the metallic connectors that hold the CLT panels in place. Moreover, a comparison between measurements and values presented in ISO 12354-1 shows great differences for frequencies in the higher and lower regions.

Hörnmark [19] measured the vibration reduction index in the field of a CLT building and concluded that Annex E in ISO 12354-1 is not applicable to predict the vibration reduction index for CLT constructions.

Jarnerö et al. [119, 120] measured floor vibration properties in both a laboratory and in situ. They found that the in situ conditions influence the floor damping and the natural frequencies to a higher degree. This is likely partly caused by the integration of the floor into the building and the interaction between them. Several other authors have measured and analyzed the vibration reduction index of various CLT junctions [97, 111, 112, 121–123].

2.5   Airborne sound reduction of ventilation ducts

Sound can propagate via the material and the air inside a ventilation duct that goes from one room to another through a separating element, and the path can be rather complex to model. The sound radiating in the receiving room depends on the sound that breaks into and out from the ventilation duct [13]. A model similar to the ones presented in Refs. [124, 125], and the one presented in Refs. [126, 127] is illustrated according to Figure 2.14 to describe the transmission of sound via the ventilation duct when it goes through a separating element. The model can be described as a flanking sound transmission problem since two structural elements with a common junction are present.
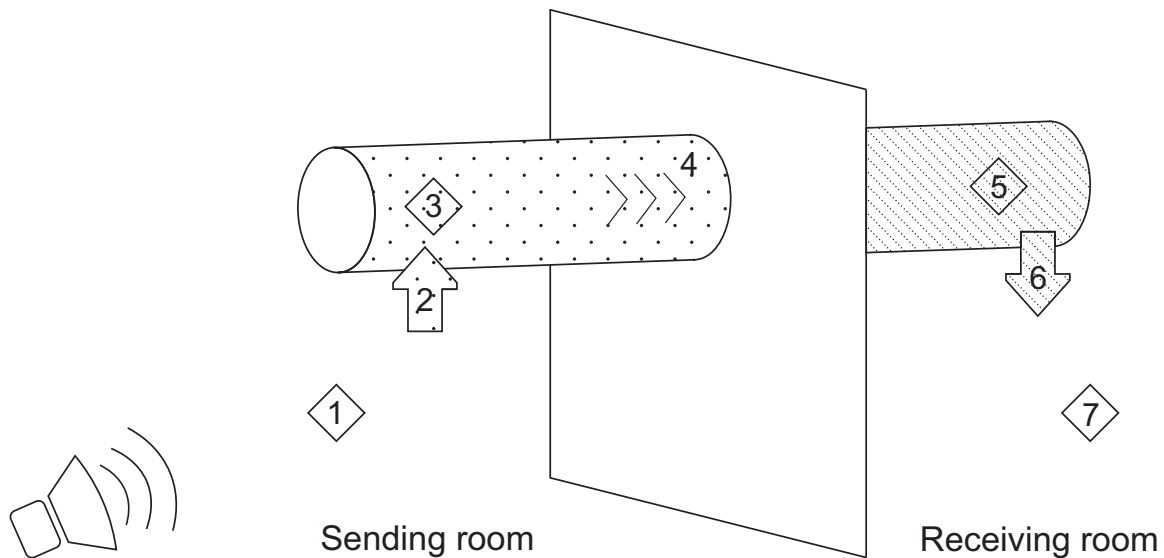
Figure 2.14: Illustration of transmission paths between two rooms with a ventilation duct through the separation [127].

In Figure 2.14, Segment 1 is described as the sound power in the sending room. Segment 2 is the transmission loss when sound breaks into the ventilation duct. Segment 3 is the sound power inside the ventilation duct in the sending room. Segment 4 is the transmission loss inside the ventilation duct. Segment 5 is the sound power inside the ventilation duct in the receiving room. Segment 6 is the transmission loss when sound breaks out from the ventilation duct in the receiving room. Finally, Segment 7 is the sound power in the receiving room. The

seven segments describe the whole system of the transmission path model. Segments 1-3 describe the breakin of the system, while Segments 5-7 describe the breakout of the system.

Although the model in Figure 2.14 can be described as a flanking sound transmission problem, the ventilation duct is still mounted through the separating element. Thus, Equation 2.19 can be used based on the principles presented under Section 2.2.2, which forms Equations 2.30 and 2.31, where M_{duct} is the surface area of the duct:

$$S_{\text{tot}} = S_{\text{wall}} + M_{\text{duct}} \tag{2.30}$$

$$R_{\text{combined}} = 10 \cdot \log_{10} \left(\frac{S_{\text{wall}} + M_{\text{duct}}}{S_{\text{wall}} \cdot 10^{-R_{\text{wall}}/10} + M_{\text{duct}} \cdot 10^{-R_{\text{duct}}/10}} \right). \tag{2.31}$$

Cummings, partly together with Astley, investigated the sound transmission of ventilation ducts in many publications with a focus on rectangular ventilation ducts and the performance in low frequency [21–28]. Cummings [22] presents a theory to predict the breakout transmission loss of rectangular ventilation ducts. Furthermore, Cummings, partly together with Chang, investigated the sound transmission of circular ventilation ducts, but not to the same extent as rectangular ducts [29–32]. In Cummings and Chang [29] and Cummings, Chang, and Astley [30], theoretical models are presented to predict the transmission loss for breakout (TL-breakout) for circular ducts. In one more recent article, Cummings [14] presents a popular equation to predict the transmission loss when sound breaks into a ventilation duct.

Vér [13] has in a report presented methods to predict the sound transmission of a system similar to Figure 2.14, including the transmission loss for breakin and breakout for both rectangular and circular ventilation ducts. The breakout transmission loss for rectangular ducts is based on Cummings [22] and for circular ducts, it is based on a design scheme from Heckl and Müller [128].

Reynolds [33] presents similar equations as Cummings and Vér for the transmission loss when sound breaks in and out from a duct, but some equations are described differently, and

some have minor changes.

Long [34] presents similar equations based on theories from Vér and Reynolds. However, one equation is presented to translate the sound pressure to the sound power level in the sending room, which the other theories do not present.

The theories mentioned above mainly use feet, inches and pounds to describe different parameters. However, Cummings uses SI units such as meters instead, which is important to keep track of when using the equations. The theories mentioned above can be used to describe the model in Figure 2.14, which is presented in Sections 2.5.2, 2.5.3, 2.5.4, 2.5.5 and 2.5.6. The theories are also primarily based on frequencies in octave bands, while Refs. [126, 127] (Chapters 3 and 4) uses them in third-octave bands.

2.5.1   Introduction equations

There are a few acoustic properties that theoretical models should consider for ventilation ducts. Both rectangular and circular ventilation ducts have different cross modes depending on the dimensions of the cross-section, and the lowest of these modes occur around the so-called cutoff frequency, f_1, for breakin [33]. Only plane wave modes exist below the cutoff frequency, and the duct can be described as a pulsating cylinder. Above the cutoff frequency, higher order modes become proportional [13].

The transmission loss when sound breaks in is dependent on the cutoff frequency, f_1, and it is calculated with Equation 2.32 and with SI-units [129]:

$$f_1 = \frac{0.586 \cdot c_0}{d}, \tag{2.32}$$

where d is the diameter of the circular ventilation duct. The cutoff frequency is described as the frequency for the lowest acoustic cross-mode [33], illustrated in Figure 2.15 from Vér [13], where α_{10} in Figure 2.15 is more precisely specified in Equation 2.32 following ASHRAE [129].
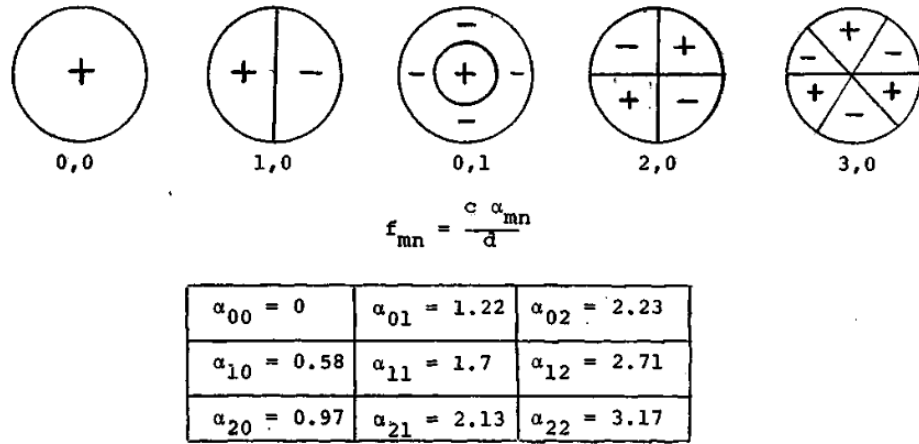
Figure 2.15: Different acoustic modes in a round duct presented in Ref. [13].

Furthermore, the cutoff frequency for a rectangular duct is calculated following Equation 2.33 from Ref. ASHRAE [129] with SI-units:

$$f_1 = \frac{0.5 \cdot c_0}{a}, \tag{2.33}$$

where a is the larger dimension of the cross-section.

According to Vigran [130], high sound radiation will occur around the ring frequency, f_R, where the circumference of the ventilation duct, P, and the longitudinal wavelength of the material of the ventilation duct, c_L, correlates. The ring frequency is also mentioned by Vér [13], and he describes it as the frequency where the internal longitudinal sound waves most easily form periodic volume changes. The volume change can, for a circular duct, be described as the wall of the duct stretching out. The ring frequency is calculated according to Equation 2.34 with SI-units:

$$f_R = \frac{c_L}{P}. \tag{2.34}$$

Similar to circular ventilation ducts, one more frequency is important to consider when describing the breakout transmission loss for rectangular ducts, which is the crossover frequency, f_L. It describes the separation between two areas for the transmission loss and is calculated

with Equation 2.35 from Reynolds [33]:

$$f_L = \frac{24134}{\sqrt{a \cdot b}},$$ (2.35)

where b is the shortest dimension of the cross-section (a and b in inches). In the first area, below f_L, plane waves are dominant and above f_L, plane waves are no longer dominant. Instead, multi-modes dominate the transmission loss over the crossover frequency, f_L.

2.5.2 Theory according to Vér [13]

The theories presented under Section 2.5 use different units and variables, and Table A1 displays the units used in the theory adapted from Vér [13].

2.5.2.1 Breakout for a system

According to Vér [13], sound that breaks out from a ventilation duct to a receiving room is described with Equation 2.36:

$$PWL_{\text{out}} = PWL_{\text{i}} - TL_{\text{out}} + 10 \cdot \log_{10}\left(\frac{PL}{S}\right) + C,$$ (2.36)

where PWL_{i} is the sound power level inside the ventilation duct on the sending room side, PWL_{out} is the breakout sound power radiated by the ventilation duct and TL_{out} is the sound transmission loss when sound breaks out from the ventilation duct. Furthermore, S is the cross area, and C accounts for the decrease in the intensity of the internal sound field in the ventilation duct with increasing axial distance due to both dissipation and sound radiation [13]. C is defined according to Equation 2.37 and may be negligible for short unlined unlagged ventilation ducts [13]:

$$C = 10 \cdot \log_{10}\left(\frac{1 - e^{-(\tau+\beta)\cdot L}}{(\tau+\beta)\cdot L}\right), \text{ where}$$

$$\beta = \frac{\Delta L_1}{4.34} \tag{2.37}$$

$$\tau = \frac{P}{S} \cdot 10^{-TL_{\text{out}}/10}.$$

Equation 2.37 is used throughout the presented theories and is not presented again. ΔL_1 is the sound attenuation per unit length, presented in Section 2.5.7.

2.5.2.2 Sound transmission loss for breakout - circular ducts

The sound transmission loss when sound breaks out from circular ventilation ducts is calculated according to a prediction scheme in Vér [13] based on the work by Heckl and Müller [128]. The prediction scheme is built on a graph, presented in Figure 2.16.
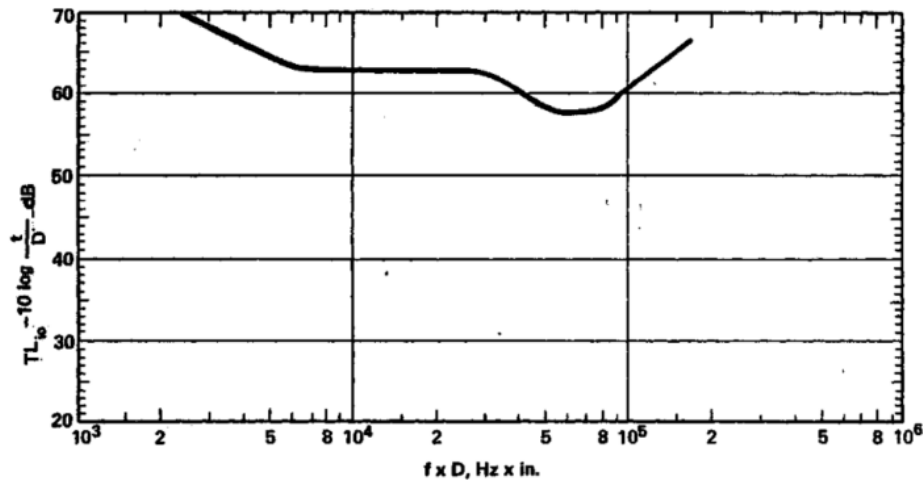
Figure 2.16: Prediction scheme, transmission loss for breakout for circular ventilation ducts adopted from Heckl and Müller [128] presented in Vér [13].

The horizontal axis in Figure 2.16 is a scale based on the duct's frequency and diameter. The vertical axis is the transmission loss for breakout with corrections depending on the thickness of the material of the ventilation duct, t, and the diameter (D in Figure 2.16 and d in the thesis). The prediction scheme is according to Vér [13] divided into the following steps:

Step 1

First, the downward vertical shift of the normalized curve in Figure 2.16 is determined with Equation 2.38:

$$\Delta \text{dB} = 10 \cdot \log_{10}\left(\frac{t}{d}\right),\qquad(2.38)$$

where t and d are in inches.

Step 2

Next, the side-way horizontal shift of the normalized curve in Figure 2.16 is determined with Equation 2.39:

$$(fd)_{1000\ \text{Hz}} = 1000 \cdot d.\qquad(2.39)$$

Step 3

Now, shift the curve in Figure 2.16 vertically according to Equation 2.38, and shift the horizontal scale to the right so that the number calculated in Equation 2.39 corresponds to 1000 Hz. For example, if Equation 2.39 is calculated to $2 \cdot 10^4$, the scale is moved from 10^3 to $2 \cdot 10^4$.

Step 4

Lastly, the shifted curve corresponds to the transmission loss when sound breaks out from a circular ventilation duct. Moreover, the straight curve at both ends can be extended to cover lower and higher frequencies. However, the transmission loss value at high frequencies should be limited to 45 dB.

2.5.2.3 Sound transmission loss for breakout - rectangular ducts

The sound transmission loss when sound breaks out from rectangular ventilation ducts is calculated according to a prediction scheme in Vér [13] based on Cummings [22], which is based on the following steps:

Step 1

First, calculate the crossover frequency, f_L, with Equation 2.35.

Step 2

Next, calculate the transmission loss for when the frequency is lower than the crossover frequency, f_L, according to Equation 2.40:

$$TL_{\text{out}} = 49 - 10 \cdot \log_{10}(a+b) + 20 \cdot \log_{10}(t) + 10 \cdot \log_{10}(f). \qquad (2.40)$$

Step 3

Next, calculate the duct wall resonance frequency, f_0, following Equation 2.41:

$$f_0 = 1.83 \cdot 10^4 \cdot \frac{(\gamma a)^2}{a^2} \cdot t, \qquad (2.41)$$

where γ describes the fundamental resonance frequency of four edge-coupled duct walls, and it is determined with Figure 2.17.
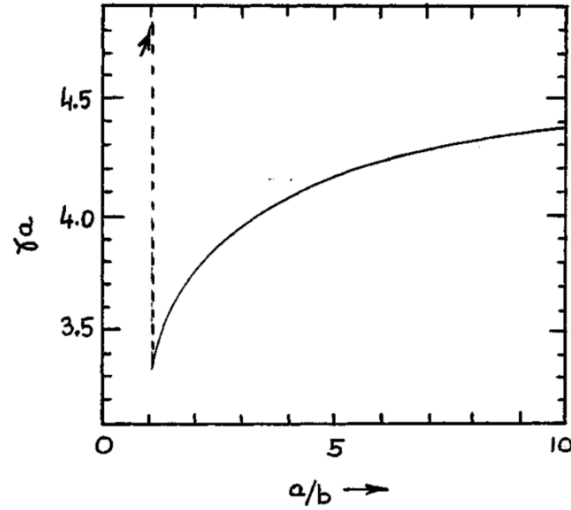
Figure 2.17: Curve for γ in Equation 2.41 presented in Ref. [13] by Cummings [27].

Step 4

Now, reduce the octave band for TL_{out} that contains f_0 by 5 dB, to account for duct wall resonances.

Step 5

Lastly, for frequencies above f_L, calculate the transmission loss with Equation 2.42:

$$TL_{\text{out}} = 1 + 20 \cdot \log_{10}(t) + 20 \cdot \log_{10}(f), \tag{2.42}$$

where the maximum value of the transmission loss is set to 45 dB.

2.5.2.4 Sound power to sound pressure level in the receiving room

The sound power level can be rewritten to sound pressure level in the receiving room according to Equation 2.43, which is a simplified prediction scheme from Ref. [13]:

$$L_{p2} = PWL_{\text{i}} + 10 + 10 \cdot \log_{10}(n) - TL_{\text{out}} + C + 10 \cdot \log_{10}\left(\frac{P}{S}\right)$$
$$+ 10 \cdot \log_{10}\left(\frac{1}{2\pi r} + \frac{4L}{A}\right). \tag{2.43}$$

In Equation 2.43, n takes into account the placement of the ventilation duct in the room according to Equation 2.44. Moreover, r is the distance from the line source (ventilation duct) to the receiver, and A is the total absorption area in the receiving room.

$$
n = \begin{cases} 1 \text{ if the ventilation duct is not close to any surfaces,} \\ 2 \text{ if the ventilation duct is close to a parallel surface, like the roof,} \\ 4 \text{ if the ventilation duct is close to two surfaces, like a corner.} \end{cases} \tag{2.44}
$$

2.5.2.5 Breakin for a system

The system in a sending room, when sound breaks into a ventilation duct, is described with Equation 2.45:

$$
PWL_{\text{in}} = PWL_{\text{inc}} - TL_{\text{in}} - 3 + C, \tag{2.45}
$$

where TL_{in} is the sound transmission loss when sound breaks into the ventilation duct, PWL_{inc} is the sound power level on the outside of the ventilation duct, and PWL_{in} is the sound power level in the ventilation duct where the ventilation duct leaves the room.

2.5.2.6 Sound transmission loss for breakin - circular ducts

The equations describing the sound transmission loss for sound that breaks into a circular ventilation duct are divided depending on the cutoff frequency.

When $f \leq f_1$, Equation 2.46 applies:

$$
TL_{\text{in}} = \text{ the larger of } \begin{cases} TL_{\text{out}} - 4 + 20 \cdot \log_{10}\left(\frac{f}{f_1}\right) \\ 10 \cdot \log_{10}\left(\frac{PL}{2S}\right). \end{cases} \tag{2.46}
$$

When $f > f_1$, Equation 2.47 applies and it is based on the principle of reciprocity:

$$TL_{\text{in}} = TL_{\text{out}} - 3.\tag{2.47}$$

2.5.2.7 Sound transmission loss for breakin - rectangular ducts

The equations describing the sound transmission loss for sound that breaks into a rectangular ventilation duct are divided depending on the cutoff frequency.

When $f \leq f_1$, Equation 2.48 applies:

$$TL_{\text{in}} = \text{ the larger of } \begin{cases} TL_{\text{out}} - 4 - 10 \cdot \log_{10}\left(\frac{a}{b}\right) + 20 \cdot \log_{10}\left(\frac{f}{f_1}\right) \\ 10 \cdot \log_{10}\left(\frac{PL}{2S}\right). \end{cases}\tag{2.48}$$

When $f > f_1$, Equation 2.49 applies:

$$TL_{\text{in}} = TL_{\text{out}} - 3.\tag{2.49}$$

2.5.2.8 Sound power to sound pressure level in the sending room

The following theory is not from Vér [13] since no equation is presented in the report. Therefore, an equation from Long [34] is used instead; see Equation 2.51.

According to Long [34]

The sound power level is described as sound pressure level in the sending room with Equation 2.50:

$$L_{p1} = PWL_{\text{inc}} - 10 \cdot \log_{10}(PL) + 14.5.\tag{2.50}$$

However, it is concluded that Equation 2.50 should be written as Equation 2.51 based on both Long [34] and Reynolds [33]:

$$L_{p1} = PWL_{\text{inc}} - 10 \cdot \log_{10}(A_0) + 14.5.\tag{2.51}$$

where Long [34] mentions that the dimensions should be in feet. For circular ventilation ducts, A_0 is calculated with Equation 2.52:

$$A_{0,ver} = 12\pi \cdot d_{\text{feet}} \cdot L, \tag{2.52}$$

where L and d_{feet} is in feet. For rectangular ventilation ducts, A_0 is calculated following Equation 2.53:

$$A_{0,\text{ver}} = 2L \cdot (a_{\text{feet}} + b_{\text{feet}}), \tag{2.53}$$

where L, a_{feet}, and b_{feet} is in feet.

If PWL_{inc} from Equation 2.45 is entered into Equation 2.51, a more detailed relationship in the sending room is obtained following Equation 2.54 for Vér [13]:

$$L_{p1} = PWL_{\text{in}} + TL_{\text{in}} - C - 10 \cdot \log_{10}(A_{0,\text{ver}}) + 17.5. \tag{2.54}$$

2.5.2.9   Rewriting to sound reduction

If we assume that $PWL_{\text{i}} = PWL_{\text{in}}$, and if we enter both Equation 2.43 and 2.54 into Equation 2.24, Equation 2.55 is formed. Equation 2.55 can be used to compare calculations with airborne sound insulation measurements:

$$
\begin{aligned}
R_{\text{duct,Ver}} = {} & TL_{\text{out}} + TL_{\text{in}} - 10 \cdot \log_{10}(n) - 10 \cdot \log_{10}\left(\frac{1}{2\pi r} + \frac{4L}{A}\right) \\
& -10 \cdot \log_{10}\left(\frac{P}{S}\right) - 10 \cdot \log_{10}(A_{0,\text{ver}}) + 7.5 - 2C - 10 \cdot \log_{10}\left(\frac{A}{M_{\text{duct}}}\right).
\end{aligned}
\tag{2.55}
$$

2.5.3   Theory according to Reynolds [33]

Table A2 displays the units used in the theory adapted from Reynolds [33].

2.5.3.1 Breakout for a system

According to Reynolds [33], sound that breaks out from a ventilation duct to a receiving room is described with Equation 2.56:

$$PWL_{\text{out}} = PWL_{\text{i}} - TL_{\text{out}} + 10 \cdot \log_{10}\left(\frac{A_{0,\text{rey}}}{A_{i,\text{rey}}}\right). \tag{2.56}$$

For circular ventilation ducts, $A_{0,\text{rey}}$ and $A_{i,\text{rey}}$ are calculated following Equation 2.57:

$$A_{0,\text{rey}} = 12\pi \cdot d \cdot L,$$
$$A_{i,\text{rey}} = \frac{\pi \cdot d^2}{4}, \tag{2.57}$$

where L is in feet and d is in inches. For rectangular ventilation ducts, $A_{0,\text{rey}}$ and $A_{i,\text{rey}}$ are calculated following Equation 2.58:

$$A_{0,\text{rey}} = 24L \cdot (a+b),$$
$$A_{i,\text{rey}} = a \cdot b, \tag{2.58}$$

where L is in feet, a is in inches, and b is in inches.

Contrary to Vér [13], Reynolds [33] does not include the factor C in Equation 2.56. However, PWL_{i} in Reynolds [33] is defined as the sound power level inside the ventilation duct where the sound is expected to break out, which is different compared to Vér [13]. Therefore, C is included later to form the model presented in Figure 2.14.

2.5.3.2 Sound transmission loss for breakout - circular ducts

The sound transmission loss when sound breaks out from a circular ventilation duct is approximated linearly with Equation 2.59:

$$TL_{\text{out}} = \text{the larger of} \begin{cases} 17.6 \cdot \log_{10}(q_0) - 49.8 \cdot \log_{10}(f) - 55.3 \cdot \log_{10}(d) + C_0, \\ 17.6 \cdot \log_{10}(q_0) - 6.6 \cdot \log_{10}(f) - 36.9 \cdot \log_{10}(d) + 97.4, \end{cases} \quad (2.59)$$

where q_0 is the mass/unit area (lb/ft^2) of the duct. However, the maximum value of TL_{out} in Equation 2.59 shall be set to 50 dB. C_0 is a correction factor depending on the properties of the circular ventilation duct with Equation 2.60:

$$C_0 = 230.4 \text{ for long seam ducts,}$$
$$C_0 = 232.9 \text{ for spiral wound ducts.} \quad (2.60)$$

Moreover, when the diameter of the ventilation duct is equal to or larger than 26 inches, the transmission loss for breakout is defined according to Equation 2.61 when the 1/1 octave band center frequency is equal to 4000 Hz:

$$TL_{\text{out,4000}} = 17.6 \cdot \log_{10}(q_0) - 36.9 \cdot \log_{10}(d) + 90.6. \quad (2.61)$$

2.5.3.3 Sound transmission loss for breakout - rectangular ducts

The equations describing the sound transmission loss for sound that breaks out from a rectangular ventilation duct are divided depending on the crossover frequency.

When $f < f_L$, Equation 2.62 applies:

$$TL_{\text{out}} = 10 \cdot \log_{10} \left(\frac{f \cdot q_0^2}{a+b} \right) + 17. \quad (2.62)$$

When $f \geq f_L$, Equation 2.63 applies, and the maximum value is set to 45 dB. Observe that the equation in Reynolds [33] is written wrong and that the best estimated guess based on the description to that equation in Reynolds [33] is presented in Equation 2.63:

$$TL_{\text{out}} = 20 \cdot \log_{10}(f \cdot q_0) - 31. \tag{2.63}$$

Moreover, TL_{out} has a minimum value following Equation 2.64:

$$TL_{\text{out,min}} = 10 \cdot \log_{10}\left(24 \cdot L \cdot \left(\frac{1}{a} + \frac{1}{b}\right)\right). \tag{2.64}$$

2.5.3.4 Sound power to sound pressure level in the receiving room

The sound power level is rewritten to sound pressure level in the receiving room with Equation 2.65, where the ventilation duct is approximated to a line source [33]:

$$L_{p2} = PWL_{\text{out}} + 10 \cdot \log_{10}\left(\frac{Q}{4\pi rL} + \frac{4}{A_R}\right) + 10.5, \tag{2.65}$$

and where A_R is the room constant. The room constant is determined with Equation 2.66:

$$A_R = \frac{A}{1 - \alpha}, \tag{2.66}$$

where α is the average room absorption coefficient [33, 129]. Q in Equation 2.65 is a constant that describes the relationship between the sound source and the room, determined with Equation 2.67:

$$Q = \begin{cases} 1 \text{ for a whole space,} \\ 2 \text{ for a half space,} \\ 4 \text{ for a quarter space,} \\ 8 \text{ for an eighth space.} \end{cases} \tag{2.67}$$

To compare Equation 2.65 from Reynolds [33] with Equation 2.43 from Vér [13], PWL_{out} from Equation 2.56 is entered in Equation 2.65 to form Equation 2.68:

46

$$L_{p2} = PWL_{\mathrm{i}} + 10.5 - TL_{\mathrm{out}} + C + 10 \cdot \log_{10}\left(\frac{A_{0,\mathrm{rey}}}{A_{i,\mathrm{rey}}}\right) + 10 \cdot \log_{10}\left(\frac{Q}{4\pi rL} + \frac{4}{A_R}\right). \quad (2.68)$$

Note in Equation 2.68 that C is included with the argument from Section 2.5.3.1.

2.5.3.5 Breakin for a system

The system in a sending room when sound breaks into a ventilation duct is described with Equation 2.69:

$$PWL_{\mathrm{in}} = PWL_{\mathrm{inc}} - TL_{\mathrm{in}} - 3. \quad (2.69)$$

With the same argument as in Section 2.5.3.1, factor C will be included later.

2.5.3.6 Sound transmission loss for breakin - circular ducts

The equations describing the sound transmission loss for sound that breaks into a circular ventilation duct are divided depending on the cutoff frequency.

When $f \leq f_1$, Equation 2.70 applies:

$$TL_{\mathrm{in}} = \text{ the larger of } \begin{cases} TL_{\mathrm{out}} - 4 + 20 \cdot \log_{10}\left(\frac{f}{f_1}\right), \\[2mm] 10 \cdot \log_{10}\left(\frac{2L}{d}\right). \end{cases} \quad (2.70)$$

When $f > f_1$, Equation 2.71 applies:

$$TL_{\mathrm{in}} = TL_{\mathrm{out}} - 3. \quad (2.71)$$

2.5.3.7 Sound transmission loss for breakin - rectangular ducts

The equations describing the sound transmission loss for sound that breaks into a rectangular ventilation duct are divided depending on the cutoff frequency.

When $f \leq f_1$, Equation 2.72 applies:

$$TL_{\text{in}} = \text{the larger of} \begin{cases} TL_{\text{out}} - 4 - 10 \cdot \log_{10}\left(\frac{a}{b}\right) + 20 \cdot \log_{10}\left(\frac{f}{f_1}\right), \\ 10 \cdot \log_{10}\left(12L \cdot \left(\frac{1}{a} + \frac{1}{b}\right)\right). \end{cases} \quad (2.72)$$

When $f > f_1$, Equation 2.73 applies:

$$TL_{\text{in}} = TL_{\text{out}} - 3. \quad (2.73)$$

2.5.3.8   Sound power to sound pressure level in the sending room

The following theory is not from Reynolds [33] since no equation is present in the chapter. Therefore, an equation from Long [34] is used instead following Equation 2.74:

According to Long [34]

$$L_{p1} = PWL_{\text{inc}} - 10 \cdot \log_{10}(A_0) + 14.5. \quad (2.74)$$

where Reynolds [33] uses different units than Long [34] to determine A_0 following Equations 2.57 and 2.58. Thus, $A_{0,\text{rey}}$ is used to follow the adapted theory from Reynolds [33] moving forward.

If PWL_{inc} from Equation 2.69 is entered into Equation 2.74, a more detailed relationship in the sending room is obtained following Equation 2.75:

$$L_{p1} = PWL_{\text{in}} + TL_{\text{in}} - C - 10 \cdot \log_{10}(A_{0,\text{rey}}) + 17.5. \quad (2.75)$$

Note in Equation 2.75 that C is included with the argument from Section 2.5.3.1.

2.5.3.9 Rewriting to sound reduction

If we assume that $PWL_i = PWL_{in}$, and if we enter both Equation 2.68 and 2.75 into Equation 2.24, Equation 2.76 is formed. Equation 2.76 can be used to compare calculations with airborne sound insulation measurements:

$$
\begin{aligned}
R_{\text{duct,Reynolds}} = TL_{\text{out}} + TL_{\text{in}} - 10 \cdot \log_{10} \left(\frac{Q}{4\pi rL} + \frac{4}{A_R} \right) - 10 \cdot \log_{10} \left(\frac{A_{0,\text{rey}}}{A_{i,\text{rey}}} \right) \\
- 10 \cdot \log_{10} \left(A_{0,\text{rey}} \right) + 7 - 2C - 10 \cdot \log_{10} \left(\frac{A}{M_{\text{duct}}} \right).
\end{aligned}
\tag{2.76}
$$

2.5.4 Theory according to Long [34]

Table A3 displays the units used in the theory adapted from Long [34].

2.5.4.1 Breakout for a system

According to Long [34], sound that breaks out from a ventilation duct to a receiving room is described with Equation 2.77:

$$
PWL_{\text{out}} = PWL_i - TL_{\text{out}} + 10 \cdot \log_{10} \left(\frac{A_{0,\text{long}}}{A_{i,\text{long}}} \right) + C
\tag{2.77}
$$

For circular ventilation ducts, $A_{0,\text{long}}$ and $A_{i,\text{long}}$ are calculated following Equation 2.78:

$$
\begin{aligned}
A_{0,\text{long}} &= 12\pi \cdot d \cdot L, \\
A_{i,\text{long}} &= \frac{\pi \cdot d^2}{4},
\end{aligned}
\tag{2.78}
$$

where L and d are in feet. The theory from Long [34] mixes between feet and inches for A_0 and A_i. For consistency, feet are chosen. For rectangular ventilation ducts, $A_{0,\text{long}}$ and $A_{i,\text{long}}$ are calculated following Equation 2.79:

$$A_{0,\text{long}} = 2L \cdot (a + b),$$

$$A_{i,\text{long}} = a \cdot b,$$

(2.79)

where L, a and b are in feet.

2.5.4.2 Sound transmission loss for breakout - circular ducts

Same equations as Reynolds [33] are used, see Section 2.5.3.2, where d is in inches.

2.5.4.3 Sound transmission loss for breakout - rectangular ducts

The equations describing the sound transmission loss for sound that breaks out from a rectangular ventilation duct are divided depending on the crossover frequency.

When $f \leq f_L$, Equation 2.62 applies from Reynolds [33], where a and b are in inches.

When $f > f_L$, Equation 2.80 applies from Long [34]:

$$TL_{\text{out}} = 20 \cdot \log_{10}(f \cdot q_0) - K_{TL},$$

(2.80)

where K_{TL} is 33.5 in FP units and 47.3 in SI units.

2.5.4.4 Sound power to sound pressure level in the receiving room

The sound power level can be rewritten to sound pressure level in the receiving room for a line source with Equation 2.81:

$$L_{p2} = PWL_{\text{out}} + 10 \cdot \log_{10} \left(\frac{Q}{2\pi rL} + \frac{4}{A_R} \right) + K,$$

(2.81)

where K is 10.5 in FP units and 0.1 in SI units.

To compare Equation 2.81 from Long [34] with Equation 2.43 from Vér [13], PWL_{out} from Equation 2.77 is entered in Equation 2.81 to form Equation 2.82:

$$L_{p2} = PWL_i + 10.5 - TL_{\text{out}} + C + 10 \cdot \log_{10} \left(\frac{A_{0,\text{long}}}{A_{i,\text{long}}} \right) + 10 \cdot \log_{10} \left(\frac{Q}{2\pi rL} + \frac{4}{A_R} \right) \quad (2.82)$$

2.5.4.5 Breakin for a system

Same equation as Vér [13] is used, see Section 2.5.2.5.

2.5.4.6 Sound transmission loss for breakin - circular ducts

The equations describing the sound transmission loss for sound that breaks into a circular ventilation duct are divided depending on the cutoff frequency.

When $f \leq f_1$, Equation 2.83 applies:

$$TL_{\text{in}} = \text{ the larger of } \begin{cases} TL_{\text{out}} - 4 + 20 \cdot \log_{10} \left(\frac{f}{f_1} \right), \\ 10 \cdot \log_{10} \left(\frac{A_{0,\text{long}}}{2 \cdot A_{i,\text{long}}} \right). \end{cases} \quad (2.83)$$

When $f > f_1$, Equation 2.84 applies:

$$TL_{\text{in}} = TL_{\text{out}} - 3. \quad (2.84)$$

2.5.4.7 Sound transmission loss for breakin - rectangular ducts

The same equations and units as Vér [13] are used, see Section 2.5.2.7.

2.5.4.8 Sound power to sound pressure level in the sending room

The sound power level in the sending room can, according to Long [34], be rewritten to the sound pressure level with Equation 2.85:

$$L_{p1} = PWL_{\text{inc}} - 10 \cdot \log_{10} \left(A_{0,\text{long}} \right) + 14.5. \quad (2.85)$$

If PWL_{inc} from Equation 2.45 is entered into Equation 2.85, a more detailed relationship in the sending room is obtained following Equation 2.86:

$$L_{p1} = PWL_{\text{in}} + TL_{\text{in}} - C - 10 \cdot \log_{10}\left(A_{0,\text{long}}\right) + 17.5. \tag{2.86}$$

2.5.4.9 Rewriting to sound reduction

If we assume that $PWL_{\text{i}} = PWL_{\text{in}}$, and if we enter both Equation 2.81 and 2.85 into Equation 2.24, Equation 2.87 is formed. Equation 2.87 can be used to compare calculations with airborne sound insulation measurements:

$$
\begin{aligned}
R_{\text{duct,Long}} = TL_{\text{out}} + TL_{\text{in}} - 10 \cdot \log_{10}\left(\frac{Q}{2\pi rL} + \frac{4}{A_R}\right) - 10 \cdot \log_{10}\left(\frac{A_{0,\text{long}}}{A_{i,\text{long}}}\right) \\
- 10 \cdot \log_{10}\left(A_{0,\text{long}}\right) + 7 - 10 \cdot \log_{10}\left(\frac{A}{M_{\text{duct}}}\right) - 2 \cdot C.
\end{aligned}
\tag{2.87}
$$

2.5.5 Theory according to Cummings [14]

The theory presented here is primarily based on equations presented in Section 2.5.2 from Vér [13]. However, the transmission loss when sound breaks in is primarily used from Cummings [14] for both rectangular and circular ventilation ducts, presented in Equation 2.88 with SI-units:

$$TL_{\text{in}} = TL_{\text{out}} + 10 \cdot \log_{10} \cdot \left(\frac{S^2 \cdot k^2}{4 \cdot \pi \cdot P \cdot L}\right). \tag{2.88}$$

Equation 2.88 is formed if the axial attenuation rate is small and if we assume that the phase speed of the fundamental mode in the duct is equal to the sound speed. The minimum value of Equation 2.88 and Equation 2.47 is used in the model presented in Figure 2.14. Equation 2.47 mainly affects values at high frequencies in this model.

Moreover, the transmission loss when sound breaks out for rectangular ducts is used from

Cummings [22] following Equations 2.89 and 2.90 with SI-units:

When $f < f_L$, Equation 2.89 applies:

$$TL_{\text{out}} = 10 \cdot \log_{10} \left(\frac{4\omega q_0^2}{\rho_{\text{air}}^2 c_0 (a+b)} \right), \tag{2.89}$$

When $f \geq f_L$, Equation 2.90 applies:

$$TL_{\text{out}} = 10 \cdot \log_{10} \left(\frac{q_0^2 \omega^2}{7 \cdot 5 \cdot \rho_{\text{air}}^2 c_0^2} \right). \tag{2.90}$$

2.5.6 Theory according to Vér [13] and Reynolds [33]

The theory presented here is a mix between Vér [13] and Reynolds [33], presented in Sections 2.5.2 and 2.5.3.

The transmission loss when sound breaks out and breaks in, TL_{out} and TL_{in}, are calculated according to Vér [13] for both circular and rectangular ducts.

The other equations are instead used mainly from Reynolds [33], for example equations describing breakout and breakin for a system. However, the factor in $A_{0,\text{ver\&rey}}$ for the rectangular duct is a mix between A_{ver} and A_{rey}, while the circular follows Reynolds [33] according to Equation 2.91 where $A_{0,\text{ver\&rey}}$ has the same unit as $A_{0,\text{rey}}$ in Table A2:

$$\text{Rectangular duct: } A_{0,\text{ver\&rey}} = 14L \cdot (a+b),$$
$$\text{Circular duct: } A_{0,\text{ver\&rey}} = 12\pi \cdot d \cdot L. \tag{2.91}$$

For the combined theory with Vér [13] and Reynolds [33], Equation 2.92 is used for the model presented in Figure 2.14.

$$R_{\text{duct,ver\&rey}} = TL_{\text{out}} + TL_{\text{in}} - 10 \cdot \log_{10} \left(\frac{Q}{4\pi rL} + \frac{4}{A_R} \right) - 10 \cdot \log_{10} \left(\frac{A_{0,\text{ver\&rey}}}{A_{i,\text{rey}}} \right)$$
$$- 10 \cdot \log_{10}(A_{0,\text{ver\&rey}}) + 7 - 2 \cdot C - 10 \cdot \log_{10} \left(\frac{A}{M_{\text{duct}}} \right). \tag{2.92}$$

2.5.7 Sound attenuation in ventilation ducts

The sound attenuation per unit length in a ventilation duct is in this paper described as ΔL_1, used in Equation 2.37, and its value is different depending on the frequency, the shape of the ventilation duct and the present of internal lining or not. The impact on the sound attenuation with or without internal lining is investigated in several studies [131–137].

The sound attenuation in circular ducts is much smaller compared to rectangular ducts, about 1/10 [34], and they are described with Figure 2.18 from Ref. [138]. The same figure is used for sound attenuation of rectangular ducts, where the difference in sound attenuation between circular and rectangular ventilation ducts is visible.
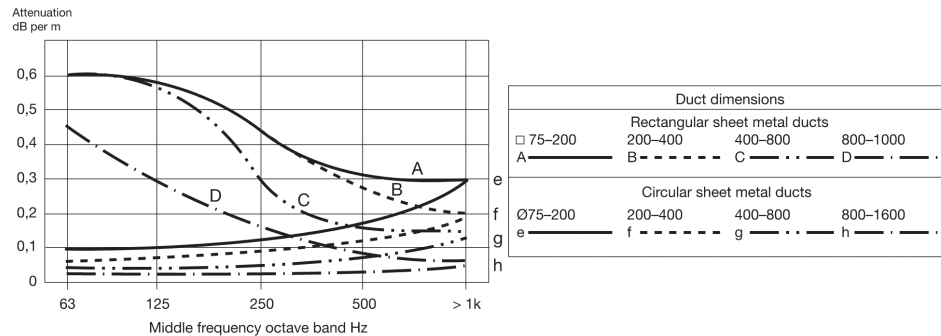
Figure 2.18: Sound attenuation in straight sheet metal ducts (1 mm sheet metal thickness) from Lindab [138].

2.5.8 Acoustic treatments on ventilation ducts

As mentioned before in Section 2.5, sound can propagate via the material and the air inside of a ventilation duct that goes from one room to another through a separating element. The sound can thereby break in and out from the ventilation duct, and the sound reduction is described thoroughly in Section 2.5.

One way to reduce the sound transmission via the ventilation duct is to apply external lagging along the surface area of the ventilation duct. This acoustic treatment is a common application to solve an already existing breakout noise problem [1, 14]. However, it can also be a part of the early design when a building is planned. External lagging of ventilation duct

includes gypsum boards and wrapping with fibrous materials such as glass fiber or stone wool [1, 14]. Several authors have investigated the effect of external lagging on ventilation ducts with different prediction models [14, 36, 37]. However, they are primarily focused on rectangular ventilation ducts and only when the whole ventilation duct is covered.

A more realistic model, similar to the ones presented in Figure 2.14, is shown in Figure 2.19, where sound can propagate via air diffusers. In Figure 2.19, Segments 2a and 6a are described as transmission losses via the air diffusers in the sending and receiving room. The term cross-talk describes the path between Segments 2a and 6a. Internal lagging primarily affects path number 4, and thus, it improves scenarios presented in both Figures 2.14 and 2.19.
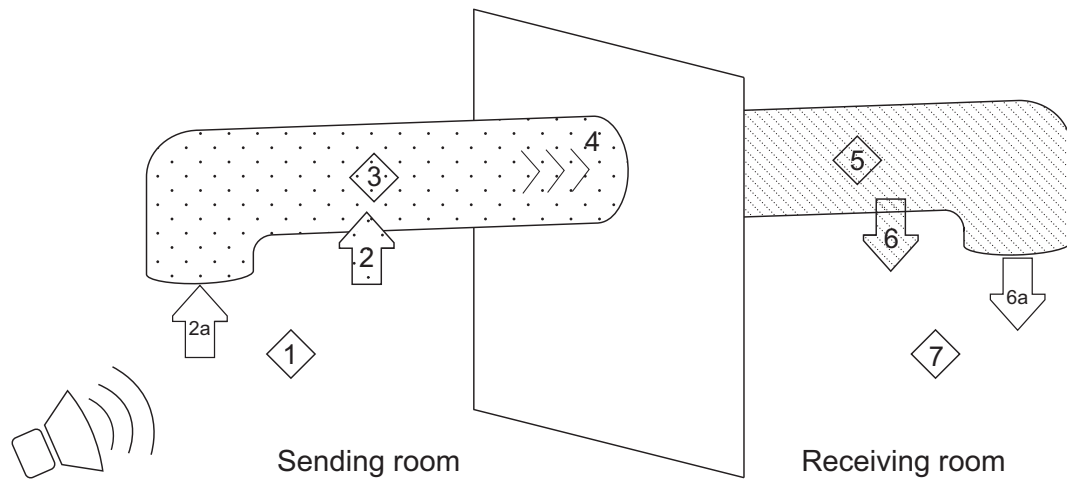
Figure 2.19: Illustration of transmission paths between two rooms with air diffusers [127].

A silencer is a unit mounted along the path of the duct system, increasing the sound attenuation and thereby decreasing the sound transmission. According to ASHRAE [139], three types of HVAC duct silencers are used called: active, reactive, and dissipative. Active duct silencers send out a sound wave that is inverse to the sound wave of the unwanted noise and is typically used for low frequencies. Reactive duct silencers have tuned chamber voids with fibrous material covered with a tuned perforated metal. Dissipative silencers have an acoustic grade fiberglass covered with a perforated material. Prediction models are presented in Refs. [140–145] to calculate the transmission or insertion loss in silencers. However, ASHRAE [139] states that transmission or insertion loss data should be used

from measurements (following the standard ASTM E477 [146]) rather than calculations for dissipative and reactive silencers.

The paths affected by a silencer depend on where the silencer is placed, illustrated in Figure 2.20. If a silencer is placed in position a, marked with a blue color, then the silencer will mainly affect the sound attenuation between paths 2a and 6a. Sound can still break in on the section between the silencer and the wall, thus passing by the silencer without affecting the sound transmission over that path. However, if the silencer is placed in position b, marked with a green color, more segments and paths are affected, and the silencer works more efficiently. Therefore, the placement of a silencer can be crucial, depending on the effect the designer wants to achieve. With similar principles, the placement of silencers can be adapted to the case with external lagging with the best effect closest to the duct. However, external lagging mainly affects segments 2 and 6, presented in Figure 2.20.
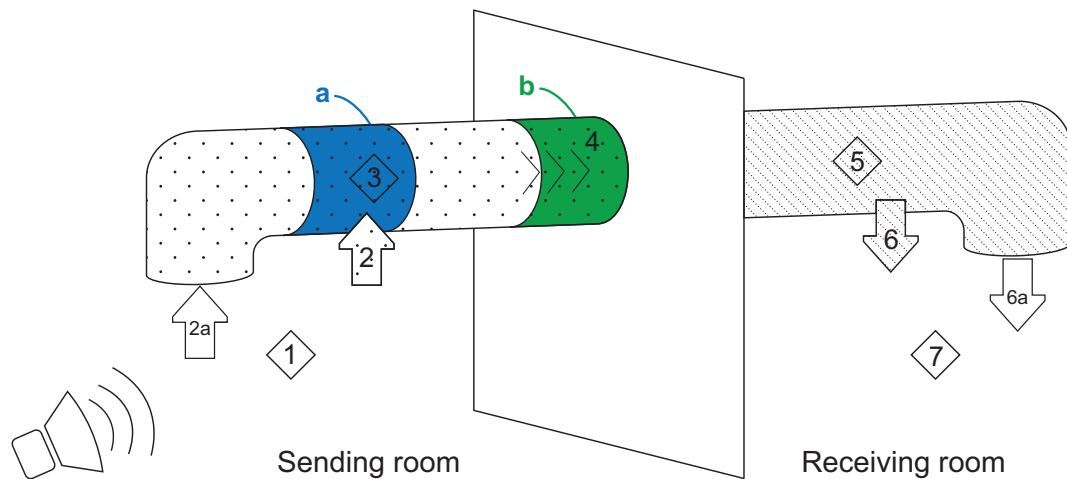
Figure 2.20: Illustration of transmission paths between two rooms with air diffusers from Ref. [127]. The colored areas represent different treatment locations.

The mentioned treatments, including internal lining with absorption material, external lagging of boards or fibrous materials, and silencers, are the commonly used solutions to treat building acoustic problems of ventilation ducts, together with vibration isolating the duct from the structures [139].

CHAPTER 3

SOUND REDUCTION OF VENTILATION DUCTS THROUGH WALLS: EXPERIMENTAL RESULTS AND UPDATED MODELS

Résumé

Les conduits de ventilation peuvent avoir un effet défavorable sur l'indice d'affaiblissement acoustique entre deux pièces s'ils traversent la structure de séparation sans traitement. L'affaiblissement acoustique global d'une gaine de ventilation dépend de plusieurs facteurs, dont la perte de transmission lorsque le son entre et sort de la gaine. Cette étude vise à modéliser l'affaiblissement acoustique d'un système combiné comprenant un mur de séparation et un conduit de ventilation qui le traverse. Trois murs, caractérisés selon la norme ISO 717-1, sont combinés avec trois conduits de ventilation différents, deux circulaires et un rectangulaire de dimensions différentes. Les données de mesure en laboratoire sont utilisées pour déterminer la réduction sonore des différentes configurations et le type de traitement nécessaire pour chaque configuration. Un modèle proposé selon la théorie existante pour décrire les pertes de transmission du son des conduits de ventilation circulaires et rectangulaires prédit la forme des données de mesure pour de nombreuses bandes de fréquence. Une nouvelle partie théorique est développée à travers un processus itératif pour les conduits circulaires. Elle est basée sur des mesures avec des méthodes et des études antérieures comme guide puisque que le schéma de prédiction existant est quelque peu déroutant. Pour les conduits rectangulaires, la théorie existante a été mise à jour pour mieux correspondre aux données de mesure. L'application de

la théorie et du modèle proposé dans cet article donne des résultats similaires aux mesures. La différence d'indice de réduction du bruit pondéré entre les théories développées et les données de mesure est de 0 à 1 dB pour chaque configuration.

Mots clés: gaine de ventilation, transmission du son, paroi de gaine, breakout, breakin, réduction du son

Abstract

Ventilation ducts can have a negative effect on the sound reduction index between two rooms if they pass through the dividing structure without treatments. The overall sound reduction of a ventilation duct is dependent on several factors including the transmission loss when sound is breaking in and out from the duct. This study aims to model the sound reduction of a combined system with a separating wall and a ventilation duct through it. Three walls, characterized according to ISO 717-1, are combined with three different ventilation ducts, two circular and one rectangular with different dimensions. Laboratory measurement data are used to determine the sound reduction of the different configurations and the type of treatments needed for each configuration. A proposed model with existing theory for describing sound transmission losses of circular and rectangular ventilation ducts predicts the shape of the measurement data for many frequency bands. A new theory part is developed through an iterative process for circular ducts, which is based on measurements with previous methods and studies as a guide because the existing prediction scheme is somewhat perplexing. For rectangular ducts, the existing theory has been updated to better match measurement data. The application of the proposed theory and model in this article shows similar results when compared to measurements. The difference in weighted sound reduction index between developed theories and measurement data is 0–1 dB for every configuration.

Keywords: ventilation duct, sound transmission, duct wall, breakout, breakin, sound reduction

3.1 Introduction

This chapter, except Section 3.8, is a copy of a journal article published in MDPI Acoustics in 2021 [126].

The sound that is produced in one room can propagate to adjacent rooms by several paths. The first common path is through the separating wall itself, but sound can take several indirect paths. For instance, sound can travel via slits or small holes in walls that occur during the construction phase, which has a considerable effect on the sound reduction of the separating wall [147]. Other more complex paths are flanking paths which arise when different elements are connected such as the walls and the floor [124]. However, the indirect construction paths are not considered in this article.

Another complexed path is via the ventilation duct when, for example, the duct goes from one room to another through a separating wall [124, 125]. With this configuration, sound can propagate via the material of the ventilation duct and via the air inside. For pipes and smaller ventilation ducts, it is often sufficient to apply a sealant as a treatment between the tube and the wall for the pipe (or duct) to not affect the sound reduction of the separated wall [148]. For bigger dimensions which mostly concern ventilation ducts, there is no easy solution to calculate the proper treatment. Larger ventilation ducts are mostly used in offices, schools and hospitals whereas smaller ducts are used in dwellings. There are some theories to calculate how much the ventilation duct will affect the sound reduction of the separated wall, which depends on if the sound breaks in or out from the duct [13].

The purpose of this article is to model the sound reduction of a combined system with a separating wall and a ventilation duct through it. This study mainly covers how the surface area of ducts affects the sound reduction and not how the sound is spread via air diffusers. It is to some extent a summary of a master thesis [35] (in Swedish) by the first author (a deeper understanding of the derivation and measurement setup can be seen in Ref. [35]). This article investigates further the important modified or developed theories that can be used in practice

with new modifications.

Alan Cummings, partly together with Jeremy Astley, has approached the problem regarding the sound transmission of ventilation ducts in many publications with a focus on rectangular ducts and specifically on how the low-frequency area is affected [21–28]. Cummings has also investigated circular and flat-oval ducts, but not to the same extent, together with Chang [29–32]. In one of Cummings' latest articles [14], the most popular equation to predict transmission loss (TL) is described when sound breaks into a ventilation duct, TL-breakin. A theory to predict TL-breakout (transmission loss when sound breaks out from a ventilation duct) is also presented for rectangular ducts according to Ref. [22]. Cummings also describes how to predict TL-breakout for circular ducts in [29, 30] together with Chang, in which the theory is very comprehensive and not investigated further. Istvan L. Vér has developed simple equations based on Ref. [22] to calculate TL-breakout for rectangular ducts. Vér [13] has also developed methods to calculate TL-breakin based on the principle of reciprocity and presents equations that describe breakout for a system for both rectangular and circular shapes. Furthermore, Vér presents a prediction scheme for TL-breakout for circular ducts based on Heck and Mueller [128]. Douglas D. Reynolds [33] describes similar equations as Vér and Cummings for rectangular ducts with a few tweaks and a different shifting factor. Reynolds presents different equations to describe TL-breakout for circular ducts. The last-mentioned theory is by Marshall Long [34] that uses theories from Vér and Reynolds with an equation to translate sound pressure to power in the source room. Other studies and articles have also investigated TL-breakout [37, 149] but not with the same purpose as this study.

The presented theories above complement each other to model and calculate the sound reduction of a ventilation duct between different rooms by describing the different parameters. However, none of the mentioned theories compile the detailed model and validate it to measurement data. A simplified model is described by the authors of Ref. [125] but it lacks some important parameters that the authors of refs. [13, 33, 34] highlight. Another study presents a SEA model to determine the noise reduction of a duct between two rooms which is

not investigated in this article [150].

A short theoretical description is presented to describe the acoustic properties of ducts which depends on if the sound breaks in or out from the duct [13]. The measurement setup is presented thereafter, followed by measurement results compared to existing, proposed and adapting theories. Treatments are also presented to prevent the ventilation ducts from affecting the sound reduction of the combined system.

3.2 Theory

The sound waves emitted from a sound source in a room with ventilation can propagate via the material of the duct to other connected rooms. The air inside the ventilation duct is also affected, which drives noise transferring to adjacent rooms. A simplified model is described in Ref. [125], while this article presents models based on the theory in Refs. [13, 33, 34].

Sound propagating from a source in a room with a ventilation duct transmits into the duct, which is described as a breakin for a system. It is a relationship between the sound power in the source room (Figure 3.1, element 1), the transmission loss when sound breaks into the ventilation duct (element 2, TL-breakin) and the sound power in the duct (element 3) [33]. The opposite effect is described as a breakout for a system; the sound that propagates inside a ventilation duct transmits out to the surrounding environment. The term can be described as a relationship between the sound power inside the duct (element 5), the transmission loss when sound breaks out to the surrounding room (element 6, TL-breakout) and the sound power in that room (element 7) [33]. The transmission loss when sound breaks in and breaks out from the ventilation duct is dependent on several factors including shape, mass and frequency. The sound attenuation inside the duct should be considered when describing a whole system (element 4) since the sound is, to some extent, absorbed inside the ventilation duct (mainly if there is an inner lining) and the air [34]. Several studies have investigated this phenomenon for lined and unlined ducts [131–137].
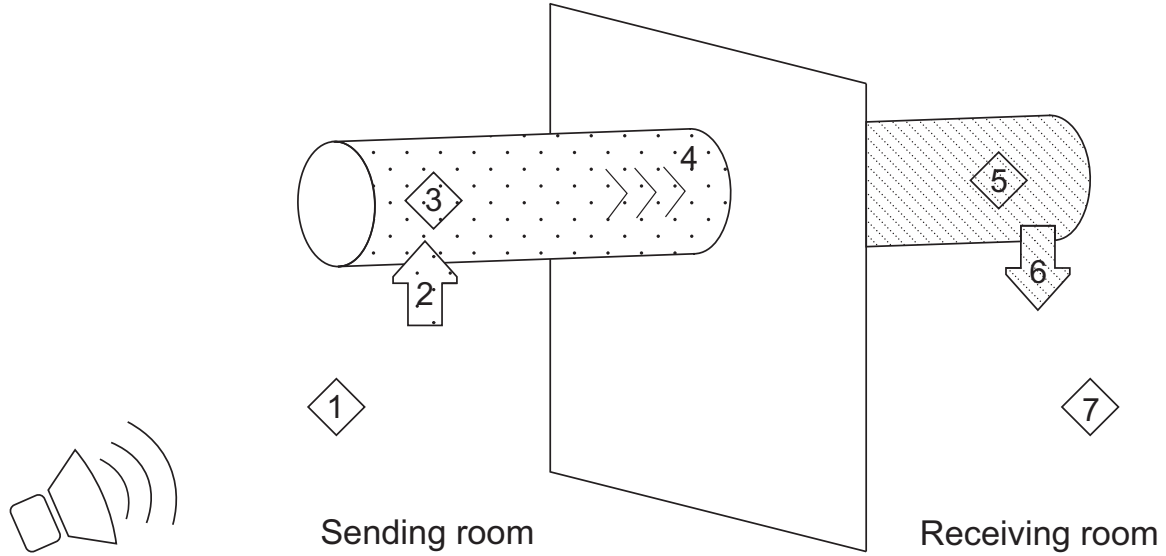
Figure 3.1: Factors affecting the whole system of a ventilation duct through a wall. Element 1 is the sound power in the source room. Element 2 is the transmission loss for breakin (TL-breakin). Element 3 is the sound power in the ventilation duct on the source room side. Element 4 describes the sound attenuation when the sound propagates inside the ventilation duct. Element 5 is the sound power in the ventilation duct on the receiving room side. Element 6 is the transmission loss for breakout (TL-breakout). Element 7 is the sound power in the receiving room.

In practice, it is easier to use the sound pressure level instead of the generic sound power (elements 1 and 7) when describing a system. Previous studies [13, 33, 34] describe equations to translate sound power into sound pressure in both the sending, L_{p1}, and receiving room, L_{p2}. To compare the existing theories with the proposed model against measurements, the sound pressure level in the receiving room is subtracted from the sound pressure level in the sending room. In addition, the absorption area also needs to be considered in the receiving room. The effects of breakin and breakout for a ventilation duct can now be described as a whole system with the sound reduction index, R_{duct}, according to Equation 3.1 from Ref. [35]:

$$R_{\text{duct}} = L_{p1} - L_{p2} - 10 \cdot \log_{10} \left(\frac{A}{M_{\text{duct}}} \right). \tag{3.1}$$

A is the absorption area in the receiving room and M_{duct} is the surface area of the ventilation duct. The sound pressure in both rooms can be described as the earlier mentioned relationships

according to Equations 3.2 and 3.3 [35]:

$$L_{p1} = TL_{\text{in}} + 17.5 - C - 10 \cdot \log_{10}(A_0),\qquad(3.2)$$

$$L_{p2} = -TL_{\text{out}} + 10.5 + C + 10 \cdot \log_{10}\left(\frac{A_0}{A_i}\right) + 10 \cdot \log_{10}\left(\frac{Q}{4\pi rL} + \frac{4}{A_R}\right).\qquad(3.3)$$

TL_{in} is the transmission loss when sound is traveling from the sending room into the ventilation duct, earlier described as TL-breakin. TL_{out} is the transmission loss when sound is traveling from the ventilation duct to the receiving room, earlier described as TL-breakout [13]. C is the transmission loss inside the ventilation duct for the room that the ventilation duct is situated in. A_i is the cross area and A_0 is the surface area multiplied by a factor that is dependent on the shape of the duct and the theory applied [13, 33, 34]. Q is a constant that describes the relationship between the sound source in the receiving room and the room's properties known as the directivity factor. Q equals 1, 2, 4 or 8 depending on if the room is considered a whole, half, quarter or eighth sphere space compared to the source. Then, r is the distance between the source and the receiver, L is the length of the line source (in this case, the ventilation duct) and A_R is the room constant [33].

Four different theories are investigated against measurement data for each configuration. Most of the presented theories below cannot alone be used to describe the system in Figure 3.1, they need to use some equations from each other. This is described briefly below and in more detail in Ref. [35].

Cummings' articles are primarily the foundation for the equations describing TL-breakout of rectangular ducts. For circular ducts, two different equations are used to describe TL-breakout: one from Heckl and Müller [128] (presented in Vér [13]) and one from Reynolds [33] (also presented in Long [34]). Vér is presenting the equation for TL-breakin above the cutoff frequency based on reciprocity, which is used in Vér, Reynolds and Long for both shapes. Cumming presents a different equation in reference [14]. Vér also presents an equation

64

for TL-breakin below the cutoff frequency that is used in the other theories as well [13]. Vér, Reynolds and Long present different equations to describe breakout for a system, the decisive difference is the shifting factor used in Reynolds [33]. The theory in Long [34] is the only one that presents an equation for translating sound pressure to sound power in the source room which is used in all methods.

Vér's theory (named Ver (1983)) is missing some equations to describe the model in Figure 3.1 and therefore, some equations are used from Reynolds [33], Cummings [22] and Long [34]. For Reynolds's theory (named Reynolds (1990)), some equations are used from Refs. [13, 22, 34] to make the model in Figure 3.1 complete. The theory presented in Long [34] (named (Long 2006)) can be used directly from the book.

The last presented variant is named Cummings (2001). For the rectangular and circular ducts, TL-breakin is calculated according to Ref. [14]. The other equations are based on the theory according to Vér [13] with the earlier described additions.

The sound reduction index in Equation 3.1 is only for the ventilation duct which must be weighted with the sound reduction index of the wall. The surface area in one room is used for the ventilation duct and the area of the wall is used as the whole area of the wall minus the cross area of the ventilation duct according to Equation 3.4 from Ref. [1].

$$R_{\text{combined}} = 10 \cdot \log_{10} \left(\frac{S_{\text{wall}} + M_{\text{duct}}}{S_{\text{wall}} \cdot 10^{-R_{\text{wall}}/10} + M_{\text{duct}} \cdot 10^{-R_{\text{duct}}/10}} \right). \qquad (3.4)$$

3.3   Method

The experimental part was performed in the sound transmission lab at Lund University, LTH, Faculty of Engineering, Division of Acoustics. Two similar rooms were separated by a wall with a section where a 10 m^2 mock-up wall can be constructed (Figure 3.2). Three different types of walls were tested during the experiment from Gyproc with the sound reduction indices (in field, R'_{w}) 35, 44 and 52 dB. Lab measurements yield R_{w} of 35, 46 and 54 dB. The setups

included the same steel frame, which is named Gyproc XR 95/95 (450 c/c). The differences between the walls were the number of gypsum boards and the presence of insulation in the wall or not. Sealant was applied around the edges on all sides of the test wall structures.

(a)   (b)

Figure 3.2: Pictures from the measurements of the separating reference wall: (a) The finished mounted wall; (b) The inside of the wall with a sound reduction index of R_w: 54 dB.

For the ventilation duct setup, two circular dimensions with diameters of 315 and 630 mm were used; they were from the Swedish manufacturer Lindab. In addition, a rectangular duct was tested with the dimension 700×250 mm, also from Lindab. The circular duct element components come in lengths of 3 m and the rectangular elements come in lengths of 1 m. To simulate the worst case for the circular duct, the 3-m-long duct was mounted in the wall so that it protruded 1.5 m on each side. Then, one other circular duct element was cut in half and connected on each side to the duct through the wall with a coupling connector with rubber lining from Lindab named NPU [151] (Figure 3.3d) making the whole section 3 m long in each room. With this setup, a homogeneous ventilation duct went through the wall instead of mounting a coupling connector in the middle. This has been previously described as a worse case since the sound can propagate via the material directly to the other room without going through a connector with rubber lining, which acts as a dampener [35]. For the rectangular duct, five connections were required to obtain the same length where a different coupling connector was used, also with a soft foam lining (Figure 3.3c). The circular ducts were instead

using two connections each (Figure 3.3d). To only measure the sound transmission between the rooms via the surface area, both ends were plugged with a metal plate with two gypsum boards on the inside of each plate together with sealant around the edges, see Figure 3.3a and 3.3b. The metal plate also had rubber or foam lining on the outer surface making the connection airtight for both circular and rectangular ducts.

(a)

(b)

(c)

(d)
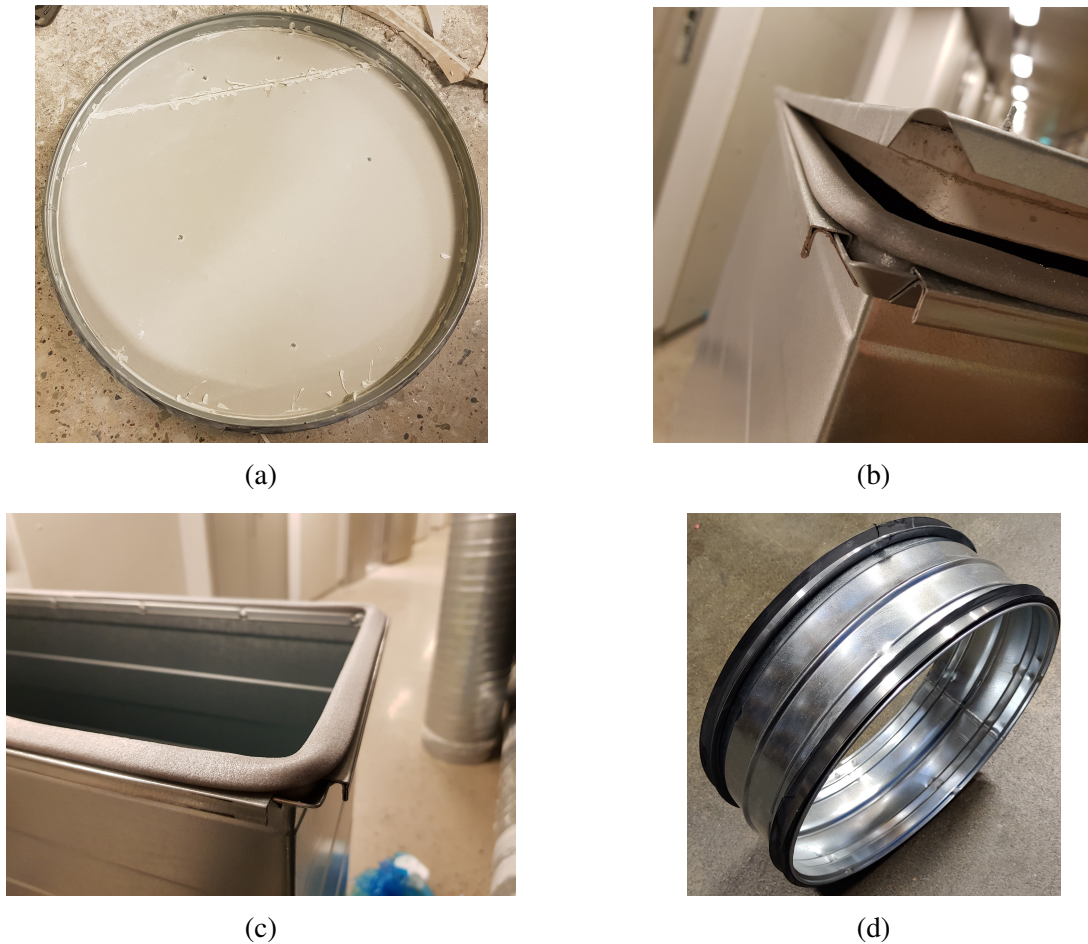
Figure 3.3: Pictures from the measurements: (a) Cover cap for the circular duct: rubber lining, gypsum boards and sealant around the border; (b) Cover cap for the rectangular duct: foam lining and gypsum boards; (c) Foam lining for rectangular duct; (d) Rubber lining connector for circular duct, NPU [151].

To quantify the impact of the ventilation ducts on the test walls, a measurement was made on the wall with no holes in it, see Figure 3.2. This represented a reference value that can be used in Equation 3.4 to compare the experimental results with the theory. The duct was then mounted through the wall where several treatments were applied on the duct according to the

cases below:

1. No treatment.

2. Applying sealant between the ventilation duct and the wall.

3. Case 2 + applying insulation in the wall around the ventilation duct.

4. Case 2 + wrapping the duct with 50 mm stone wool with a density of 100 kg/m3 from ISOVER.

5. The same as number 4 above but with 100 mm stone wool instead, same manufacturer and density.

The theory in Section 3.5 was developed for case 2 to describe how different ventilation ducts affect the sound reduction of the separating wall without any heavy treatments.

Pictures from the measurement setup are displayed in Figure 3.4 where different treatments for different configurations are applied according to cases 1–5 presented before. For cases 4 and 5, a length of 600 mm on each side was added in stages for each measurement, starting closest to the wall. The reverberation time was measured for every new arrangement according to the standards ISO 10140-4 and ISO 3382-2 [152, 153] for measuring reverberation time in the lab.

The sound pressure levels in each room were measured with five fixed positions according to the standard ISO 10140-2 [86]. Two loudspeakers were used in the sending room to create a stable sound field and with this setup, the sound pressure level only needed to be measured one time (with five positions) in each room according to the standard ISO 10140-5 [85]. Each loudspeaker was connected to an amplifier with constant level settings (Brüel & Kjær Type 2734) emitting pink noise.
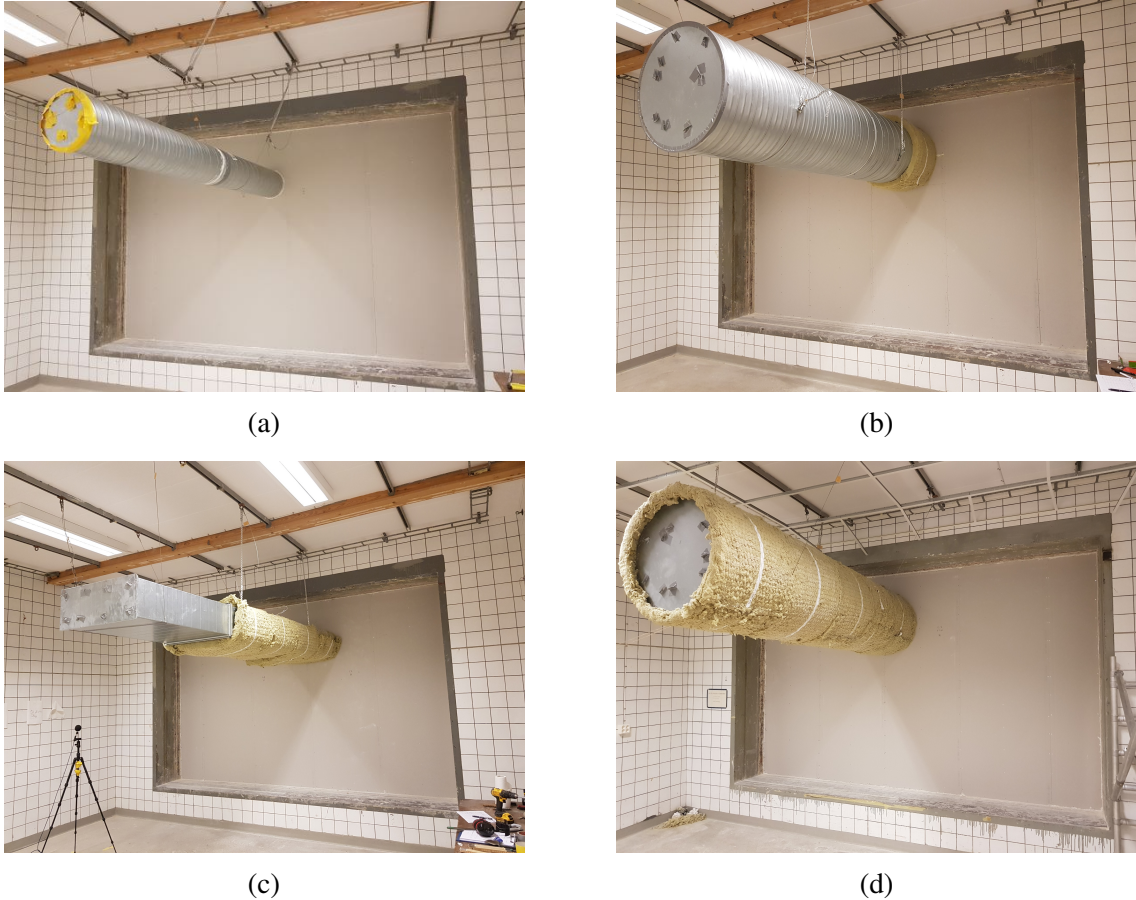
Figure 3.4: Pictures from the measurements in one of the rooms: (a) Circular 315 mm duct, treatment as case 2; (b) Circular 630 mm duct, treatment according to case 4, stone wool at a length of 600 mm; (c) Rectangular duct, 700×250 mm, treatment according to case 4, stone wool at a length of 1800 mm; (d) Circular 630 mm duct, treatment according to case 4, stone wool at a full length of 3000 mm.

3.4   Measurement Results

Three walls were measured together with three different ventilation ducts which adds up to nine combinations. One wall and three ventilation ducts are described as one sequence. The walls were initially measured for each sequence without the ducts. The initial measurement was used as a reference value. The ducts were mounted through the wall where different treatments, according to case 1–5, were applied. Case 2 was primarily used to compare current theories or to develop new theories for the sound reduction of ventilation ducts. Cases 3–5

were used to investigate which treatments are required for the ventilation duct to not reduce the sound reduction index of the separated wall compared to the reference wall. The treatment fulfilling this condition for each sequence is described as sufficient.

3.4.1 For Wall A, with a Measured Sound Reduction Index of 35 dB

Simple treatments were required for all three ventilation ducts. For the rectangular duct, a sealant was sufficient. For the small circular 315 mm duct, 50 mm stone wool (density: 100 kg/m^3) was needed to cover the surface area closest to the wall on each side by 600 mm. For the larger circular duct, 630 mm, the wrapping length must be 1200 mm instead.

3.4.2 For Wall B, with a Measured Sound Reduction Index of 46 dB

The ventilation ducts through the second wall required different treatments. For the circular 315 mm duct, 50 mm stone wool (density: 100 kg/m^3) was needed to cover the surface area closest to the wall on each side by 1800 mm. For the rectangular and the larger circular duct, the whole length needed to be covered with stone wool (density: 100 kg/m^3), 50 mm in thickness on both sides of the wall. Unlike wall A, the two last-mentioned ducts required the same treatments for wall B.

3.4.3 For Wall C, with a Measured Sound Reduction Index of 54 dB

The ventilation ducts through the third wall required the most treatment. The circular 315 mm duct needed to be covered completely with 50 mm stone wool (density: 100 kg/m^3) in both rooms. This treatment was not sufficient for the other ducts. Both the rectangular and the larger circular duct, 630 mm, needed to be covered with 100 mm stone wool at a length of 1800 mm closest to the wall. For the rest of the surface area, 50 mm stone wool was sufficient, both with a density of 100 kg/m^3.

3.4.4 Existing Theory Compared to Measurement Result for Case 2

Measurement results from case 2 are presented in Figure 3.5, Figure 3.6 and Figure 3.7 for wall C since the difference between the theories is most visible for those configurations. The existing theory, described in Section 3.2 and Ref. [35], is presented with the measurements. Measurement data compared with the existing theory for the other walls are displayed in Figure B1, Figure B2, Figure B3, Figure B4, Figure B5 and Figure B6.
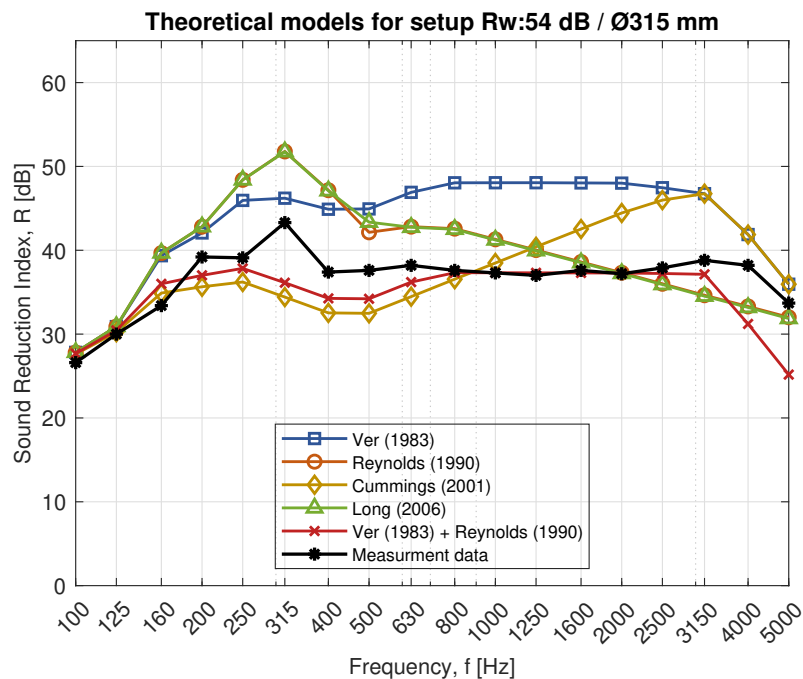
Figure 3.5: Theoretical sound reduction index according to different theories compared to measurements for the configuration with a circular ventilation duct, diameter 315 mm, through wall C, with a measured weighted sound reduction index of R_w 54 dB.
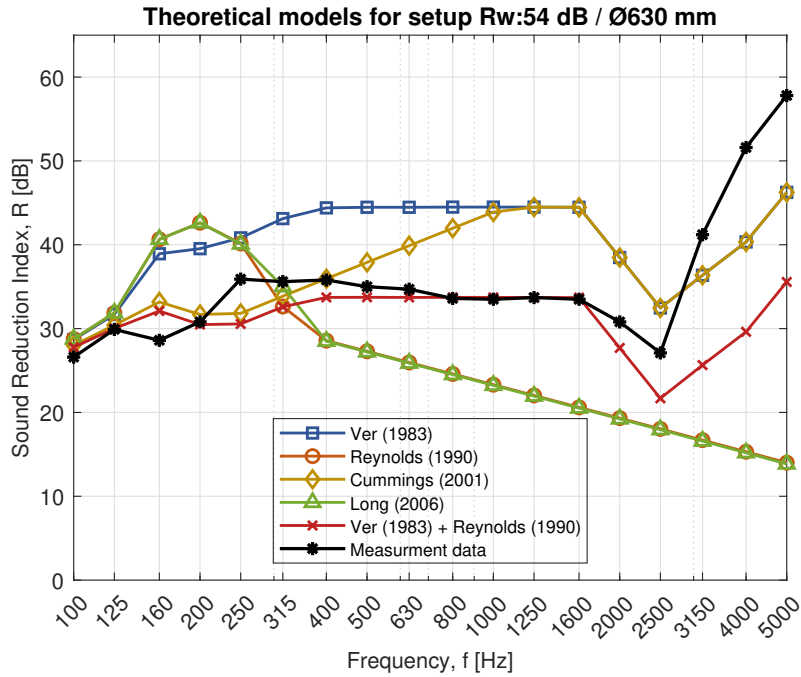
Figure 3.6: Theoretical sound reduction index according to different theories compared to measurements for the configuration with a circular ventilation duct, diameter 630 mm, through wall C, with a measured weighted sound reduction index of R_w 54 dB.
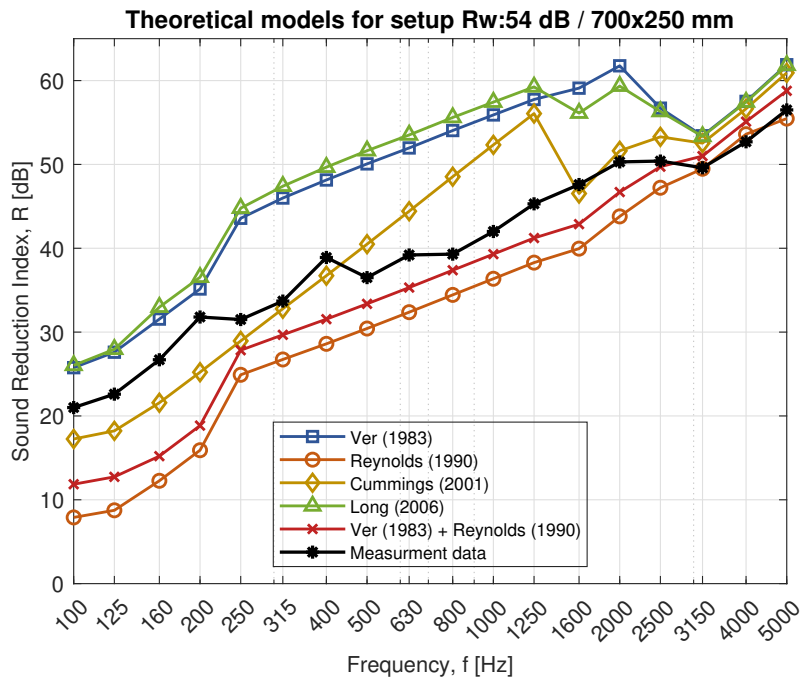
Figure 3.7: Theoretical sound reduction index according to different theories compared to measurements for the configuration with a rectangular ventilation duct, 700×250 mm, through wall C, with a measured weighted sound reduction index of R_w 54 dB.

3.5 Theoretical Analysis

Comparing the existing theory to measurement data in Figure 3.5, Figure 3.6 and Figure 3.7, several discrepancies can be observed. Some predicted curves for the circular ducts do not match the measurement data in either value or shape, as shown in Figure 3.5 and Figure 3.6 and Figure B1, Figure B2, Figure B3 and Figure B4. The theories are either overestimating or underestimating the sound reduction and the shape of the theoretical curves is inconsistent with the measurement data. However, by combining the theory regarding TL-breakout and TL-breakin according to Vér with the equations describing breakin and breakout for a system according to Reynolds, consistency between measurement data and theory is fulfilled. Similar results can be observed for the rectangular duct through the different walls in Figure 3.7, Figure B5 and Figure B6.

Only the theory according to Refs. [13, 128] considers the ring frequency, f_R. The latter term refers to the frequency at which the longitudinal sound waves arrive just in phase after they have circulated an entire lap along the inner circumference of the duct which causes resonance effects [13].

This study also considers theory from Cummings [14] for both the rectangular and the circular ducts with different inputs. When the transmission loss for breakin from Cummings [14] is added to Vér's theory [13] for circular ducts, the sound reduction curve increases with the frequency over the cut-off frequency, f_1, which is visually described in Figure 3.6 (yellow line). The cut-off frequency denotes the frequency at which the lowest acoustic cross-mode occurs for a ventilation duct [33]. Cross-modes are modes that excite standing waves inside the duct that oscillate in a direction perpendicular to the main flow velocity and the cylinder axis [154]. The theoretical shape with the proposed model (yellow lines in Figure 3.5 and Figure 3.6) does not match the measurement data.

If the transmission loss for breakin from Cummings [14] is combined with Vér's theory [13] for rectangular ducts, the sound reduction decreases (compared to only Vér's theory) with

a better match to the measurement data, specifically below 500 Hz (see Cummings (2001) in Figure 3.7). However, these changes are not enough to describe the sound reduction index of ventilation ducts with adequate accuracy for all three configurations.

The current theories regarding sound transmission via circular ventilation ducts are, to some extent, insufficient when compared to measurement data. Thus, improvements are needed to better and easier describe the sound reduction for the ventilation duct. TL-breakout is calculated according to a prediction scheme from Ref. [128] in Ref. [13] that is not easily adapted. Instead, by studying the shape of the curves on both the theory and the measurement data, conclusions were made to decide the shape of the sound reduction curve for the ventilation duct. Further studies are required to deeper understand how the ventilation ducts behave acoustically for the circular ducts.

For measurement data of the circular ducts in Figure 3.5 and Figure 3.6, when only the sealant is applied, the sound reduction index tends to increase with the frequency up until the cut-off frequency, f_1. The increase is divided into two sections, one below the cut-off frequency divided by 1.9, named f_e and one above. Afterward, the sound reduction index seems to be constant with increased frequency until 5000 Hz in Figure 3.5 or 2500 Hz in Figure 3.6. Here, one can notice a significant linear drop over two-third of the octave bands followed by an increase of the sound reduction index once more. From measurement data, it was concluded that the drop is related to the ring frequency, f_R, of the ventilation duct. This is described by Refs. [13, 30] for the transmission loss when sound breaks out and is confirmed for measurement data in the study [35], as well when measuring the sound reduction index. The ring frequency can be calculated with the circumference, P, and the speed of longitudinal waves in the duct wall material, c_L, according to Equation 3.6, which depends on the density and modulus of elasticity of the material [13, 130]. The ring frequency for the circular ducts, 315 and 630 mm, is calculated to 5100 and 2550 Hz. The identified points where a significant drop occurred were for the frequencies 5000 Hz (duct with Ø315 mm) and 2500 Hz (duct with Ø630 mm), which is close to the ring frequency for each dimension.

For the rectangular duct, the theory according to Reynolds [33], which includes theory from Refs. [13, 22, 34], is adapted since it best describes the measurements with few deviations. The adaptation is described in more detail in Ref. [35] where the theory is originally calculated according to the Imperial system. Modifications have been made between the theory in Ref. [35] and this article.

Theories are developed, with the conclusions above, through an iterative process with the final result as the equations in Section 3.5.1 and Section 3.5.2 for circular and rectangular ducts which describe the sound reduction index for the ducts only. The newly developed equations for circular ducts have been evaluated together with the theory named Ver (1983) + Reynolds (1990) to test the impact of the different inputs that have not been tested in the laboratory. Changes have been made during the iteration process to make sure that the following equations suit a large number of different combinations.

3.5.1 Sound Reduction for Circular Ducts Based on the Proposed Theory

The International System of Units should be used with the equations in this section. Physical quantities and units are displayed in Table B1. Before calculating the sound reduction for circular ducts, the cut-off frequency and the ring frequency need to be determined according to Equations 3.5 and 3.6 from Refs. [13, 21]:

$$f_1 = \frac{0.58 \cdot c_0}{d}, \tag{3.5}$$

$$f_R = \frac{c_L}{P}. \tag{3.6}$$

$$f_e = \frac{f_1}{1.9}. \tag{3.7}$$

where c_0 is the speed of sound in air, d is the diameter of the duct, c_L is as mentioned before and P is the perimeter of the ventilation duct. The sound reduction of the ventilation duct can be calculated according to the proposed theory in Equations 3.8-3.13.

When $f \leq f_e$:

$$R_{\text{circle},1} = 10 \cdot \log_{10} \left(\frac{q_0^{2.5} \cdot f \cdot \left(1 + \frac{P}{2} + \frac{(f_e - f)^P}{f_e}\right) \cdot \pi}{P \cdot L^{1.3} \cdot c_0^{0.8} \cdot S} \right). \tag{3.8}$$

where S is the cross-section area of the ventilation duct and q_0 is the mass per unit area of the duct.

When $f_e < f \leq f_1$:

$$R_{\text{circle},2} = 10 \cdot \log_{10} \left(\frac{f^{(1.3 + 2 \cdot S)} \cdot \pi \cdot q_0^2}{P^3 \cdot L \cdot c_0^{0.88}} \right). \tag{3.9}$$

When $f_1 < f \leq f_R$:

$$R_{\text{circle},3} = 10 \cdot \log_{10} \left(\frac{P \cdot \pi^{2.55} \cdot q_0^2 \cdot f_1}{L^{\left(\frac{3+L}{L}\right)} \cdot c_0^{0.8} \cdot S^{0.6}} \right). \tag{3.10}$$

When $f \approx f_R$ (rounded down) $-$ one third octave band:

$$\text{Subtract } R_{\text{circle},3} \text{ with } 1 \cdot P. \tag{3.11}$$

When $f \approx f_R$ (rounded down):

$$\text{Subtract } R_{\text{circle},3} \text{ with } 3 \cdot P. \tag{3.12}$$

When $f > f_R$:

$$R_{\text{circle},4} = \text{ the largest of } \begin{cases} R_{\text{circle},3} \\ 40 \cdot \log_{10} \left(q_0^{1.27} \cdot L^{-0.5} \cdot \left(\frac{f}{f_R}\right)^2 \right). \end{cases} \tag{3.13}$$

76

The newly developed theory matches measurement data for all six configurations when only a sealant is applied with minor deviations. For the weighted sound reduction index, the error between measured data and theory is 0–1 dB. Results are displayed in Section 5.3.

3.5.2 Sound Reduction for Rectangular Ducts, Updates of Existing Theory According to Measurement Result

For the sound reduction of the rectangular duct, the theory is originally calculated with the Imperial system in Ref. [35]. This article aims to describe calculations using the SI-system, factors have therefore been listed in Table 3.1, which enables both systems to be used. Physical quantities and units are displayed in Table B1. It is strongly recommended to use the SI-system when using the following equations. The equations describing the new adapted theory follow where a and b describe the longest and smallest dimensions of the rectangular duct cross section. Then, the surface area A_0 and the cross-area A_i are calculated as Equations 3.14 and 3.15:

$$A_0 = 12 \cdot L \cdot (a+b) \cdot F1, \tag{3.14}$$

$$A_i = a \cdot b \cdot F2. \tag{3.15}$$

Table 3.1: Factors that should be used depending on whether the Imperial or the SI system is used.

Variable	Imperial units	SI-units	Equation Number
F1	1	129	3.14
F2	1	1550	3.15
F3	24134	613	3.17
F4	1	0.093	3.18
F5	1	0.00107	3.19
F6	1	0.205	3.20
F7	1	0.083	3.21

Before calculating the sound reduction for rectangular ducts, the cut-off frequency [13] and the cross-over frequency [33] need to be determined according to Equations 3.16 and 3.17. Plane mode transmission is dominant below f_L and above f_L, multi-mode transmission is dominant [33]:

$$f_1 = \frac{0.5 \cdot c_0}{a},$$ (3.16)

$$f_L = \frac{F3}{\sqrt{a \cdot b}}.$$ (3.17)

It is important that a and c_0 in Equation 3.16 uses the same length-unit (m and m/s or inch and inch/s). The sound reduction index is described in Equation 3.18:

$$R_{\text{rectangular}} = TL_{\text{out}} + TL_{\text{in}} - 10 \cdot \log_{10} \left(\left(\frac{Q}{4\pi r L} + \frac{4}{A_R} \right) \cdot F4 \right) - 10 \cdot \log_{10} \left(\frac{A_0^2}{A_i} \right)$$
$$+ 7 - 2C - 10 \cdot \log_{10} \left(\frac{A}{M_{\text{duct}}} \right).$$ (3.18)

The transmission loss when sound breaks out, TL_{out}, can be described as Equations 3.19 to 3.21 depending on if the frequency is below or above the cross-over frequency, f_L.

When $f \le f_L$:

$$TL_{\text{out}} = 10 \cdot \log_{10} \left(\frac{f \cdot q_0^2 \cdot F5}{a + b} \right) + 17,$$ (3.19)

and when $f > f_L$:

$$TL_{\text{out}} = 20 \cdot \log_{10} \left(f \cdot q_0 \cdot F6 \right) - 31,$$ (3.20)

with a rule that:

$$
TL_{\text{out}} = \begin{cases} \geq 10 \cdot \log_{10}\left(24 \cdot L \cdot \left(\frac{1}{a} + \frac{1}{b}\right) \cdot F7\right) \\ \\ \leq 41 \end{cases} \quad . \tag{3.21}
$$

The transmission loss when sound breaks in, TL_{in}, can be described as Equations 3.22 and 3.23 depending on if the frequency is below or above f_1.

When $f \leq f_1$:

$$
TL_{\text{in}} = \text{ the largest of} \begin{cases} TL_{\text{out}} + 4 - 10 \cdot \log_{10}\left(\frac{a}{b}\right) + 20 \cdot \log_{10}\left(\frac{f}{f_1}\right) \\ \\ 10 \cdot \log_{10}\left(\frac{P \cdot L}{2 \cdot S}\right). \end{cases} \tag{3.22}
$$

When $f > f_1$:

$$
TL_{\text{in}} = TL_{\text{out}} - 3. \tag{3.23}
$$

The internal loss factor, C, is calculated according to Equation 3.24 followed by Equations 3.25 and 3.26 and can be neglected if the length of the ventilation duct is small and specifically if the duct is unlined [13]:

$$
C = 10 \cdot \log_{10}\left(\frac{1 - e^{-(\tau + \beta) \cdot L}}{(\tau + \beta) \cdot L}\right), \tag{3.24}
$$

$$
\beta = \frac{\Delta L_1}{4.34}, \tag{3.25}
$$

$$
\tau = \frac{P}{S} \cdot 10^{-TL_{\text{out}}/10}. \tag{3.26}
$$

Finally, the sound attenuation per unit length in the duct, ΔL_1, needs to be determined. The variable is dependent on the shape and size of the ventilation duct according to Ref. [138] in Figure 3.8 with the sound attenuation in dB per meter.
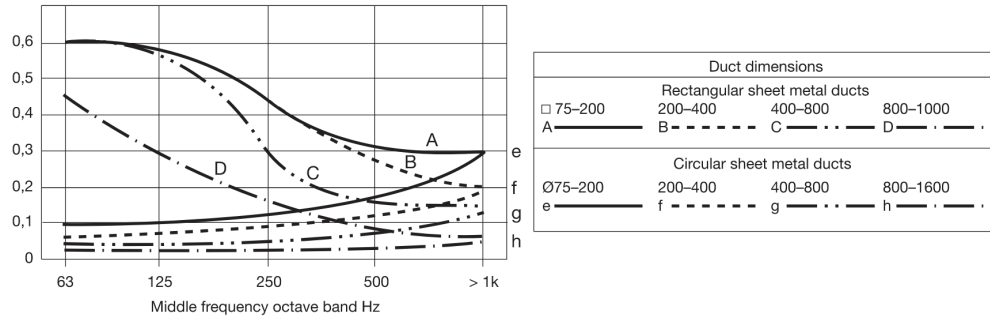
Figure 3.8: Sound attenuation in straight sheet metal ventilation ducts per meter from Lindab with 1 mm thickness for different shapes and dimensions [138].

3.5.3 Measurement Result Compared to Developed and Adapted Theories according to Nilsson

The sound reduction for the three different ducts can be calculated according to equations in Section 3.5.1 and Section 3.5.2, which can be combined with the sound reduction of the measured reference wall with Equation 3.4. The proposed and adapted theories are compared with measurements when the duct goes through wall C when only a sealant is applied according to Figure 3.9. The same precision is seen for the two other tested walls, A and B, which are displayed in Figure B7 and Figure B8.
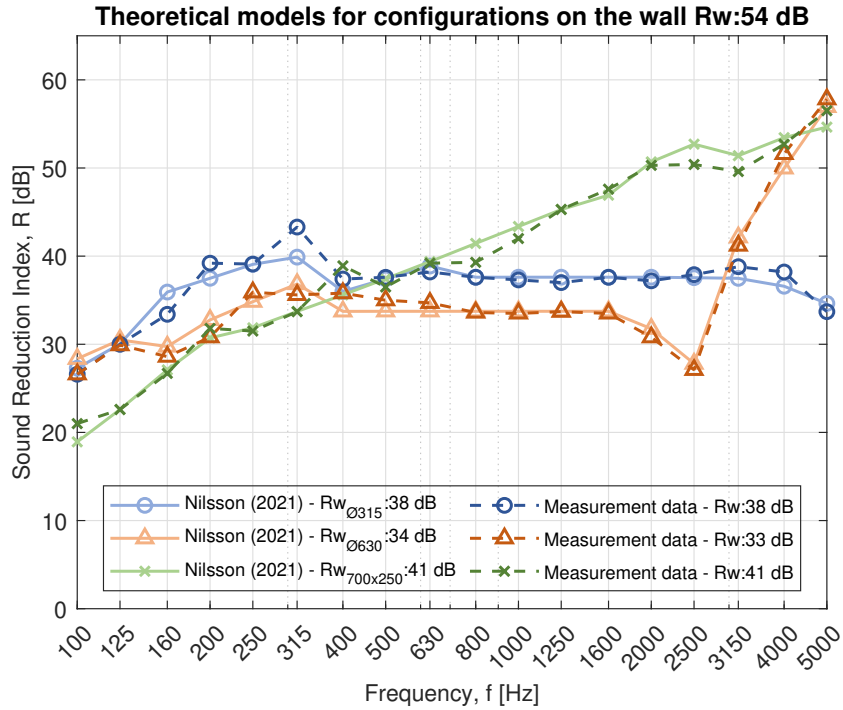
Figure 3.9: Theoretical analysis with the proposed theory, Nilsson (2021). Configurations for ducts of dimensions Ø315, Ø630 and 700x250 mm through wall C (sound reduction index R_w 54 dB).

3.6 Discussion

The new proposed theory for circular ducts is based on a few factors that have not been changed in the laboratory such as the length and the mass per unit area. Since the existing combined theory named Ver (1983) + Reynolds (1990) matches measurement data to some extent (Figure 3.5 and Figure 3.6), it can be used to validate the newly proposed theory which makes it more secure to apply to actual buildings. By iteration, the proposed theory was compared with existing theories so that changes in length and mass per unit area have the same impact. The proposed theory for circular ducts does not consider the sound attenuation, C, inside the duct because it is considerably small for circular ducts, especially with the length that was tested in the lab. The factor could be added to the presented equations if wanted. The measurements indicate that the main factor parameter affecting the sound reduction is the

length closest to the wall. This can be observed when treatment close to the wall is applied for wall A (with the lowest sound reduction index) as described in Ref. [35]. It is therefore unlikely that a 20-m-long ventilation duct will have a larger impact than a ventilation duct with a length of 15 m since the sound will attenuate in the duct and breakout from the duct (mainly close to the wall). The length is considered in the equations to calculate the sound reduction of both the ventilation duct and the wall combined with the ventilation duct. That length parameter might need to be changed in the theory to a standard maximum length, which has to be determined and verified in the lab or in the field for various configurations.

The weighted sound reduction index does not increase significantly when changing the wall from a sound reduction index of 46 dB to 54 dB (namely wall B to C), see measurement data in Figure B8 and Figure 3.9. However, it changes between walls A and B as depicted in Figure B7 and Figure B8. This happens because the radiated sound from the ventilation duct is dominant compared to the wall. The ventilation duct thereby dictates the value for the sound reduction index for the walls with a higher sound reduction index. With this observation, it is concluded that calculations for walls B and C with a sound reduction index of 46 and 54 dB, respectively, are more valid than wall A with 35 dB. However, this could also mean that the proposed model is less accurate at predicting sound reduction when the difference in sound insulation between the ventilation duct and the separating wall is small.

When analyzing measurement data, differences between lab and field values should be considered. In the field, more variables affect the sound reduction than only the ventilation duct, which is why the lab and field values in the product datasheet differ. On the other hand, treatments that have been applied in the lab are optimized for a higher sound reduction than expected in the field for the same type of configuration. Therefore, the same treatments might not be needed on the ventilation ducts in the field to fulfill the sound reduction index that is required for the separated wall construction. This can be concluded from Equation 3.4 that describes the combined sound reduction for the wall and the ventilation duct. Another factor to be considered is the flow inside the ventilation duct. The lab measurements were made with

a closed ventilation duct unlike the setup in the field where there is a flow of air inside the duct. This can have an impact on the sound reduction of the combined system, although Craik [150] highlighted that the airflow does not have a practical impact on the system for airflow velocity up to 30 m/s.

When applying different treatments to the configurations in the field, the length of the ventilation duct needs to be considered. A direct application is assessed to work for the treatments where only part of the ventilation ducts are covered, 600–1200 mm on both sides of the wall. For more demanding treatments, the dimensions of the rooms must be considered, as well as the sound reduction of the wall. In a large room, parts of the sound power will successively attenuate and breakout with the length of the duct. However, if the sound reduction of the wall is high, the whole ventilation duct still might need to be covered with heavy stone wool regardless of the dimensions of the rooms and the length of the ventilation duct. The different treatments are demonstrated in Ref. [35] for the nine configurations. Other treatments than wrapping the ventilation duct with stone wool may be more efficient for some configurations.

Several interesting aspects can be discovered when analyzing variations between rectangular and circular ducts. For wall A, 35 dB, applying a sealant is sufficient for the rectangular duct. For the circular ducts, stone wool was necessary to cover the surface area at a length of 600–1200 mm. The sound reduction curve for the rectangular duct increases relatively linearly with frequency, unlike the circular ducts. For the circular ducts, the sound reduction is constant with the frequency between f_1 and f_R, which is also described in Ref. [35]. The reason why a few simple treatments are needed for combination 35/700x250 is that the sound reduction curve for the wall is similar in shape and value to the sound reduction curve of the ventilation duct. If only the surface area of the duct is considered as a factor, then the same treatments (only applying sealant) should be enough for the larger circular duct (630 mm) and the rectangular duct since they almost have the same surface area/circumference (P_{630}: 1.98 m^2, $P_{700x250}$: 1.90 m^2). This is not the case because the shape and setup are different. For the

rectangular duct, more connections are required as they do not come in large sections, usually between 1–2 m. Circular ducts usually come in sections of 3 m. Therefore, the rectangular ducts have more coupling connectors in their system than the circular ducts, which gives more sound attenuation via the material of the ventilation ducts. This could be a reason for the different needs of treatments between the different ventilation ducts through wall A. On the other hand, when increasing the sound reduction index of the wall to 46 and 54 dB (wall B and C), the same treatments are required. Further investigation of the measurement data leads to the following aspects:

- The first interesting difference is the deviation of the sound reduction for the circular duct at the ring frequency. However, this factor has no meaning when the whole ventilation duct is covered with heavy stone wool.

- The rectangular duct has a high sound reduction in the higher frequencies, one reason could be the higher damping in the system with more connectors, but for the middle frequencies, 160–1200 Hz, it is not as sufficient as the wall's sound insulation.

- For the circular ducts, the sound reduction curve is flat above the cut-off frequency. When the circular ventilation ducts are wrapped with stone wool, the sound reduction is successively increasing. However, the flat trend of the curve only shifts when the whole ventilation duct is covered with stone wool.

- For lower sound reduction indices of the test walls, the rectangular duct needs fewer treatments than the circular 630 mm duct. When the sound reduction index of the wall increases, both the rectangular and circular ventilation duct needs to be covered completely since they are not sufficient in the middle frequencies and because of the ring frequency for the circular duct.

Instead of developing a new theory for circular ducts, the prediction scheme according to Heckl and Müller [128] could be used or described with equations and thereby be adjusted as

the rectangular duct theory. However, the prediction scheme seems hard to use since a graph needs to be shifted with outputs from equations. Therefore, another approach was taken in this study with iterations to match the measurement result for these ducts. A similar model for rectangular ducts cannot be developed with enough accuracy since measurements were only made with one sample size of the rectangular duct.

The frequency span for the measurements is 50–5000 Hz but the analysis and theories start from 100 Hz. Frequencies below 100 Hz were not considered since the frequency span of the standard regulation for offices and schools starts from 100 Hz in, for example, Sweden [155]. Contrary to that, sound reduction for frequencies below 100 Hz is considered in Swedish dwellings [156]. However, the diameter of the ventilation ducts in dwellings is often below 315 mm unlike offices, schools and hospitals where larger dimensions are common. Since ventilation ducts in dwellings have smaller diameters, they have less impact on the sound insulation. Therefore, the analysis starts from 100 Hz instead of 50 Hz.

3.7   Conclusions

The aim of the study was to model the sound reduction of a combined system with a separating wall and a ventilation duct through it.

A new theory is proposed for circular ducts, and it matches measurement data for a combined system with few deviations according to the proposed model. The same agreement between measurements and existing theory for rectangular ducts is yielded with some modifications, mainly for lower frequencies, together with the proposed model.

From measurement data, it is concluded that the part of the ventilation duct closest to the wall is the main factor affecting the sound reduction. For some configurations, it is enough to only apply stone wool around the surface area of the duct closest to the wall on each side but the reduction of sound insulation at the ring frequency only disappears when the whole ventilation duct is covered. The same treatments presented here and in Ref. [35] may be

dissimilar in the field since they are optimized for lab values. Wrapping ventilation ducts with stone wool yields effective results but other treatments can be more efficient for some configurations.

For lower sound reduction indices of the test walls, the shape of the ventilation ducts and the number of coupling connectors in the system are dependent and determine the type of treatments needed. For higher sound reduction indices of the wall, the surface area is the factor that controls which treatments are required.

3.8   Additional work

The theories from Vér [13], Reynolds [33], and Long [34] are sensitive to changes in the units (FT and SI). This is visible in Figures 3.5 and 3.6, where minor modifications in factors from the theory by Vér [13] result in a more accurate estimation compared to measurements (see the curve "Ver (1983) + Reynolds (1990)"). Based on the shape of the transmission loss model curve for breakout and breakin, Vér [13] yields a satisfactory result compared to measurements for circular ducts compared to the other theories. For rectangular ventilation ducts, the theories perform similarly, but the theory from Vér [13] is slightly more accurate. Examples with modified factors for each theory and ventilation duct are presented in Figure 3.10, Figure 3.11, and Figure 3.12. The curves in Figures 3.10 to 3.12, are calculated following Equation 3.27:

$$R_{\text{combined}} = 10 \cdot \log_{10} \left(\frac{S_{\text{wall}} + M_{\text{duct}}}{S_{\text{wall}} \cdot 10^{-R_{\text{wall}}/10} + M_{\text{duct}} \cdot 10^{-R_{\text{duct}} \cdot Z/10}} \right), \tag{3.27}$$

where Z is the factor shown in Figures 3.10-3.12. Equation 3.27 is based on Equation 3.4 with the added factor, Z. An interesting observation is that the theory according to Vér [13] performs best with the same factor, $Z = 0.75$, for all three ducts, unlike the other theories.
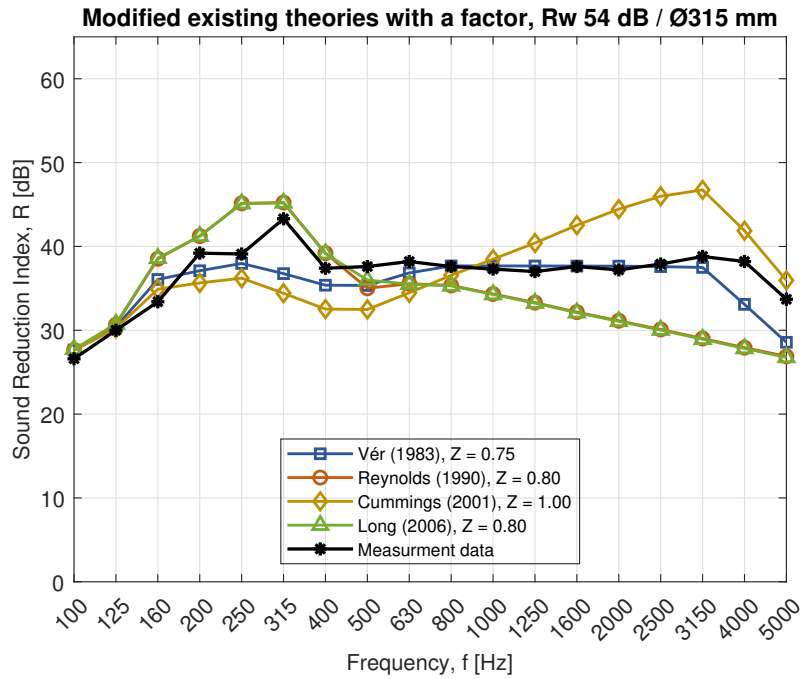
Figure 3.10: Existing theories that are multiplied with a factor to fit more accurately compared to measurement data. Setup with a circular ventilation duct, diameter 315 mm, through wall C, with a measured weighted sound reduction index of R_w 54 dB.
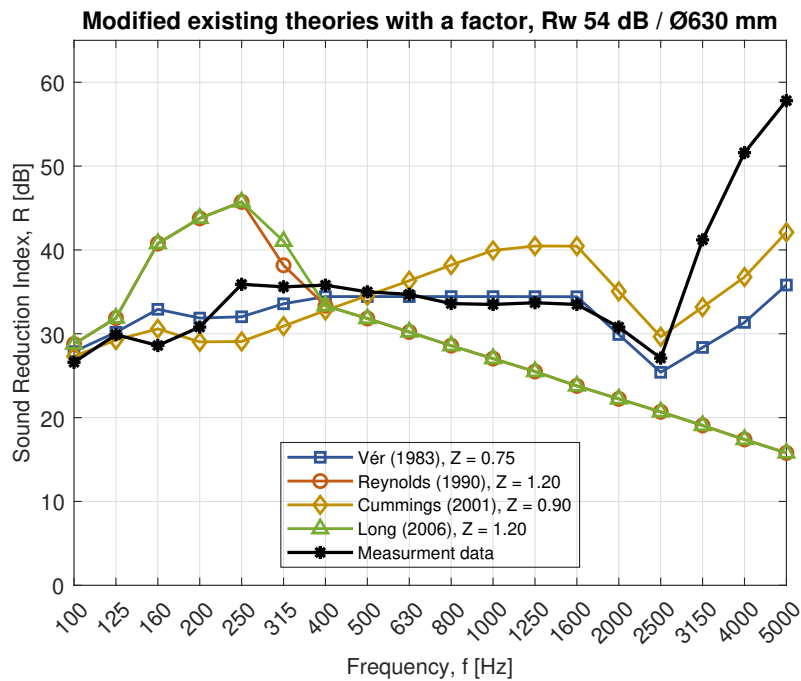
Figure 3.11: Existing theories that are multiplied with a factor to fit more accurately compared to measurement data. Setup with a circular ventilation duct, diameter 315 mm, through wall C, with a measured weighted sound reduction index of R_w 54 dB.
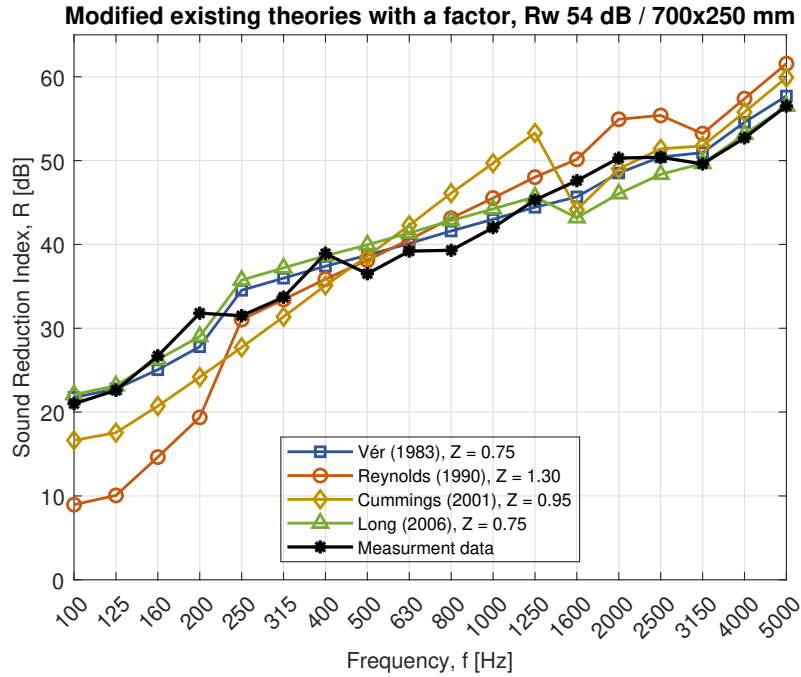
Figure 3.12: Existing theories that are multiplied with a factor to fit more accurately compared to measurement data. Setup with a circular ventilation duct, 700×250 mm, through wall C, with a measured weighted sound reduction index of R_w 54 dB.

In conclusion, the presented transmission model in Ref. [126] performs well with either the developed theories in the paper or with the theory from Vér [13] (see Section 2.5.2), with some larger deviations above f_R for circular ducts. With the theory from Vér [13], Equation 2.31 should be replaced with Equation 3.27 where $Z = 0.75$.

Observe that the formulated theories in this chapter are based on the transmission model in Figure 3.1 with a few assumptions. Therefore, if the results from the different theories do not align with the measurements, it does not indicate that the theories themselves are wrong but rather that they do not fit the presented model.

CHAPTER 4

ACOUSTICAL TREATMENTS ON VENTILATION DUCTS THROUGH WALLS: EXPERIMENTAL RESULTS AND NOVEL MODELS

Résumé

La réduction du bruit est complexe à estimer pour les traitements acoustiques des conduits de ventilation à travers les murs. Différents traitements acoustiques sont disponibles pour les conduits de ventilation, comme notamment le revêtement intérieur (absorption le long du périmètre intérieur), le calorifugeage extérieur (isolation acoustique extérieure), les silencieux et les plafonds suspendus. Des études antérieures ont examiné comment les silencieux et le revêtement intérieur affectent la transmission du son dans les conduits de ventilation. Cependant, il existe peu de théories permettant de prédire l'effet du calorifugeage extérieur en combinaison avec les gaines de ventilation et la manière dont la réduction totale du bruit est affectée. Cet article vise à étudier différents traitements acoustiques et à développer des modèles théoriques lorsque le calorifugeage externe avec de la laine de roche est utilisé pour réduire la transmission indirecte du bruit aérien via la surface des conduits de ventilation. Des modèles théoriques sont développés pour le calorifugeage externe et comparés aux données de mesure. Les mesures et la théorie sont généralement en bon accord sur la bande de tiers d'octave comprise entre 100 et 5000 Hz. Les modèles développés précisent que la distance la plus proche du mur a le principal impact sur la réduction du bruit pour un système combiné

d'un mur avec un conduit de ventilation. Les plafonds suspendus et les silencieux s'avèrent suffisants en tant que traitements acoustiques pour certaines combinaisons de conduits de ventilation et de murs. Toutefois, le calorifugeage extérieur semble être la seule solution efficace dans les bureaux et les écoles lorsqu'une grande gaine de ventilation traverse un mur à forte réduction acoustique.

Abstract

Sound reduction is complex to estimate for acoustical treatments on ventilation ducts through walls. Various acoustical treatments are available for ventilation ducts, including internal lining (absorption along the inner perimeter), external lagging (external sound insulation), silencer, and suspended ceilings. Previous studies have examined how silencers and the internal lining affect the sound transmission of ventilation ducts. However, there are few theories to predict the effect of external lagging in combination with ventilation ducts and how the total sound reduction is affected. This article aims to investigate different acoustical treatments and develop theoretical models when external lagging with stone wool is used to reduce flanking sound transmission via the surface area of ventilation ducts. Theoretical models are developed for external lagging and compared with measurement data. Measurements and theory are generally in good agreement over the third-octave band range of 100–5000 Hz. The developed models clarify that the distance closest to the wall has the main impact on sound reduction for a combined system with a wall and a ventilation duct. Suspended ceilings and silencers are found to be enough as acoustical treatments for certain combinations of ventilation ducts and walls. However, external lagging seems to be the only effective solution in offices and schools when a large ventilation duct passes through a wall with high sound reduction.

Keywords: ventilation duct, external lagging, flanking sound transmission, breakout, breakin, sound reduction

4.1 Introduction

This chapter is a copy of a journal article published in MDPI Acoustics in 2022 [127].

Ventilation ducts usually have a significant impact on a wall's sound reduction and treatments are often required to fulfill different acoustic regulations. In a previous study [126], the authors provide updated models for calculating the sound reduction index of circular and rectangular ventilation ducts through walls with different sound reduction indices, without treatment. The theory in [126] is based on laboratory measurements from a previous work by the first author [35] and the models show good agreement with measurements. The amount of acoustical treatment increases with the dimension of the ventilation ducts and with the sound reduction index of the wall. There are various treatments that a designer can choose to reduce the flanking path that arises when a ventilation duct is mounted through a wall. The treatments should be adapted to the problem that needs to be solved.

When sound travels via the ventilation duct, it can travel via both the material and the air inside the duct. In this article, sound attenuation is defined as the damping of sound by the air and by the material on the inside of the duct, and sound transmission is defined as the transfer of sound between different rooms; thus, sound attenuation is a part of the sound transmission. The sound can also travel between rooms via the slit between the ventilation duct and the wall.

The first important treatment is to minimize the leakage in the connection between the ventilation duct and the wall with a sealant. Otherwise, if a slit-shaped aperture is left untreated, the sound reduction will decrease significantly. Westerberg [157] performed measurements on how the sound reduction of a wall with no leakage is reduced when a pipe is mounted through a wall with a wooden cylinder. The wooden cylinder, mounted in the middle of the pipe, had a smaller diameter than the pipe itself, thus creating a slit-shaped circular aperture between the cylinder and the pipe. The article shows reduced sound insulation at higher frequencies with leakage. C Yang et al. [158] analyzed the sound transmission of an opening with and without an acoustic sealant. They concluded that an acoustic sealant increases the sound reduction at

the off-resonance frequencies of the system. Several studies have also investigated circular and slit-shaped apertures [159–162].

Sound attenuation can increase by installing an internal lining (absorption) along the inner perimeter of the ventilation duct. The inner lining acts as an absorber, which thereby decreases the sound transmission between rooms if they share the same ventilation duct. The acoustic performance of duct lining depends on several factors, including the geometry of the duct, the placement of the lining, and the acoustic properties of the lining material [137]. Generally, there are two types of lining materials: locally reacting and bulk-reacting linings. The difference between them is the number of directions that the liners permit propagation; locally reacting linings permit propagation only in the direction normal to the duct and bulk-reacting linings permit propagation in more than one direction [137]. The sound attenuation in ducts with linings is investigated in several studies [134–136, 163–165]. Bibby and Hodgson [133] concluded that the lining thickness does not affect high-frequency performance. The thickness mainly affects the low-frequency area, and a 25 mm thick liner is not effective enough [133]. Bibby and Hodgson [133] also concluded that a 100 mm thick liner might be excessive. The use of internal lining as a treatment is appropriate in many scenarios since it affects both the sound attenuation and the sound transmission.

Another method to increase the sound attenuation is with silencers. The use of silencers is also an effective way to reduce the transmission of sound between rooms because they act both as an absorbing material for air circulating inside and reduce the sound traveling through the material. Three different types of HVAC duct silencers are used according to ASHRAE [139] and they are named dissipative, reactive, and active. Dissipative silencers typically use perforated metal to cover an acoustic grade fiberglass. Reactive silencers use tuned perforated metal to cover tuned chamber voids with fibrous material. Lastly, active duct silencers produce inverse sound waves to cancel the unwanted noise, typically for low frequencies [139]. Several articles describe the methods to calculate the transmission or insertion loss in silencers [140–145], although ASHRAE [139] states that data should be

obtained from measurements according to ASTM E477 [146] for dissipative and reactive silencers when used in calculations.

With a suspended ceiling, sound transmission through ventilation ducts is reduced since they are usually placed above the ceiling. The sound transmission of suspended ceilings is dependent on the thickness, the density, and the porosity of the ceiling material. Laboratory measurements can determine how much the sound transmission decreases between two rooms with a common plenum (volume above the suspended ceiling) depending on the used suspended ceiling. ISO 10848-2 [166] describes this with a weighted normalized sound level difference for suspended ceilings named $D_{n,c,w}$. ASTM E1414 [167] instead describes the plenum sound path transmission loss with a ceiling attenuation class named *CAC* The transmission path, measured according to these standards, is dependent on the transmission loss of the suspended ceiling, but also the sound absorption and propagation in the plenum [168]. Refs. [169–172] conducted several measurements on different ceilings together with the sound absorption. Measurements based on $D_{n,c,w}$ and *CAC* describe the transmission loss when the plenum is shared between two rooms and the standards require that plenum walls are lined with some type of absorption. If the walls of a room go all the way up to the ceiling, less plenum absorption occurs, which is often the case with high sound reduction requirements between rooms. Values presented with $D_{n,c,w}$ and *CAC* should therefore be used with special consideration.

Lastly, the ventilation duct can be covered with external lagging (external sound insulation). One common application with this acoustical treatment is to solve an already existing breakout noise problem [1, 14], but it can also be a part of an early design. External lagging on ventilation ducts includes both covering with gypsum boards to form an enclosure or by wrapping the duct with a fibrous material, such as glass fiber or stone wool [1, 14]. The latter increases the surface mass and therefore decreases the sound transmission. Cummings [36] presents a method to model external lagging on rectangular ducts based on an electrical analogous circuit model. The theory is compared to measurements with a fairly good agreement, according to

Cummings [14]. Another prediction model by Venkatesham, Munjal, and Tiwari [37] is based on the four-pole parameters with some comparison against measurement data. The authors conclude that their model is appropriate for predicting insertion loss at lower frequencies, from 500 Hz and below [37]. The theoretical models above are not investigated further in this article since they primarily focus on rectangular ducts and when a ventilation duct is completely wrapped.

The purpose of this article is to investigate different acoustical treatments and develop theoretical models when external lagging with stone wool is used to reduce the flanking sound transmission via the surface area of ventilation ducts. Furthermore, the use of different acoustical treatments is discussed for various scenarios.

4.2   Theory

A previous article from the authors [126] investigates how the surface area of a ventilation duct affects sound reduction and presents theoretical models to calculate the combined sound reduction index of a duct wall. The initial model was based on Figure 4.1, which presents how the sound travels from the sending room to the receiving room if only the surface area affects the sound transmission. Elements 1 and 7 in Figure 4.1 describe the sound power in the different rooms and Elements 3 and 5 describe the sound power inside the ventilation duct. Elements 2 and 6 indicate the sound transmission loss of breakin and breakout between the sending and receiving room along the surface area of the ventilation duct, marked with different patterns. Lastly, Element 4 is the sound attenuation inside the ventilation duct and the damping of sound increases with the length of the ventilation duct. The model in Figure 4.1 could occur in the field when a ventilation duct passes by a room without any air diffuser.

Scenarios that include air diffusers can be illustrated according to Figure 4.2 where air diffusers can be on one or two sides of the wall. The model in Figure 4.2 has two more paths included, which are denoted as Elements 2a and 6a. They describe the sound transmission

loss of break-in and breakout via the air diffusers. The path from Element 2a to 6a can be described by the term crosstalk.

The use of internal lining affects path number 4 and therefore improves the scenarios described in Figure 4.1 and Figure 4.2. The use of external lagging only affects break-in and breakout through the surface area described as Elements 2 and 6 in Figure 4.2.
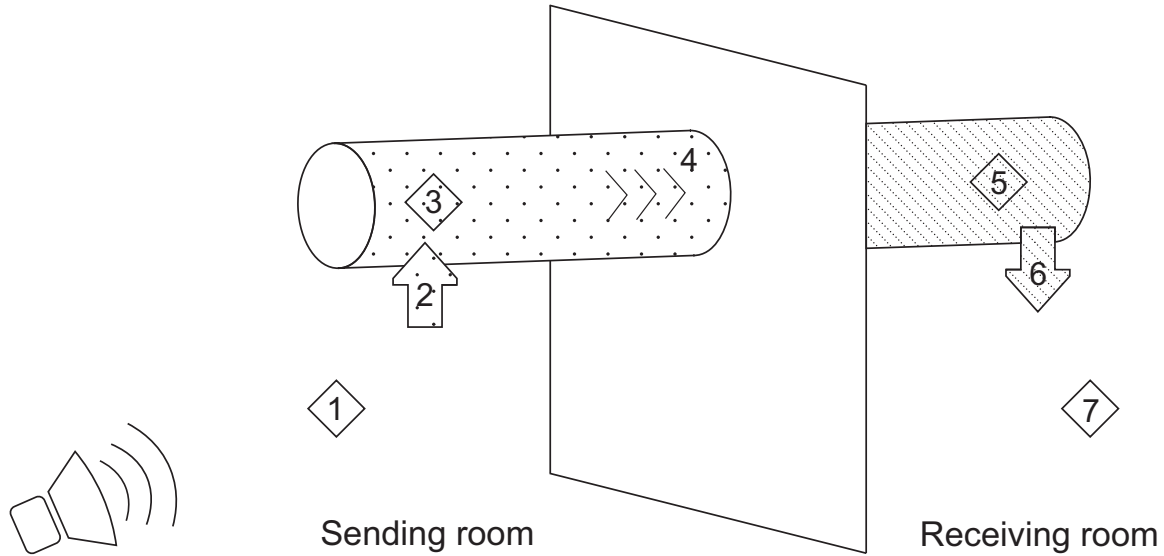
Figure 4.1: Illustration model of how sound travels from the sending room to the receiving room if only the surface area affects the sound transmission.
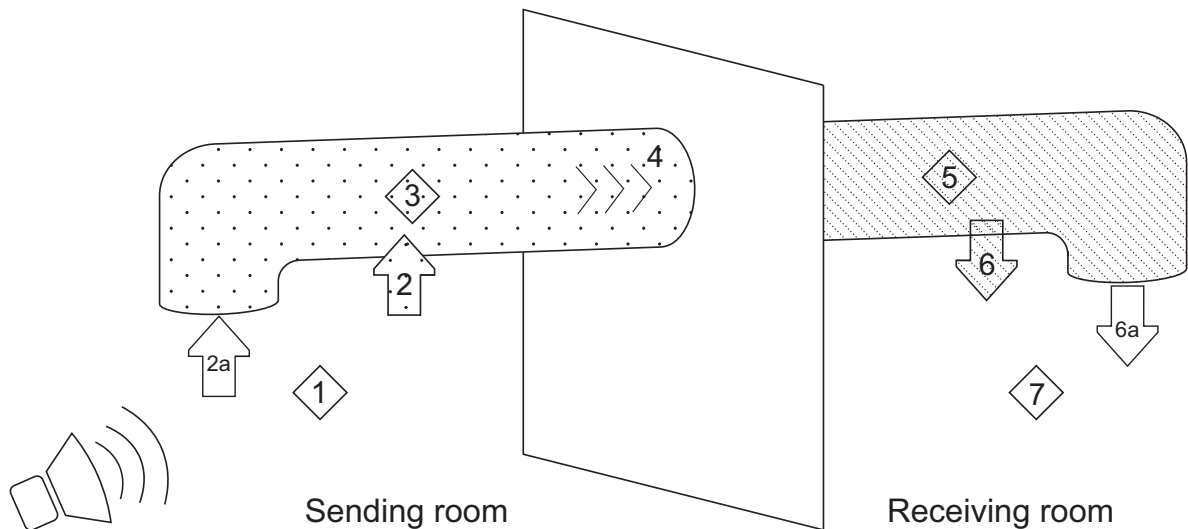
Figure 4.2: Illustration model of how sound travels from the sending room to the receiving room if the surface area and air diffusers affects the sound transmission.

The use of a silencer affects different paths depending on the placement, which is illustrated in Figure 4.3. If the silencer is placed in position a marked as blue, it primarily affects Element 2a. Sound is still able to break-in at the remaining path between the silencer and the wall. However, if the silencer is placed in position b marked as green, Elements 2, 2a and 4 are affected. Therefore, the placement of a silencer can be critical depending on the problem that needs to be solved. A ceiling between the sending room and the ventilation duct primarily affects Element 2 since the air diffusers (placed at Elements 2a and 6a) usually goes through the ceiling.

The placement of silencers, related to Figure 4.3, can be adapted to external lagging using similar principles. If external lagging is placed on a limited surface of the ventilation duct in position b, sound will break into the ventilation duct longer away from the wall, which is more advantageous compared to position a.
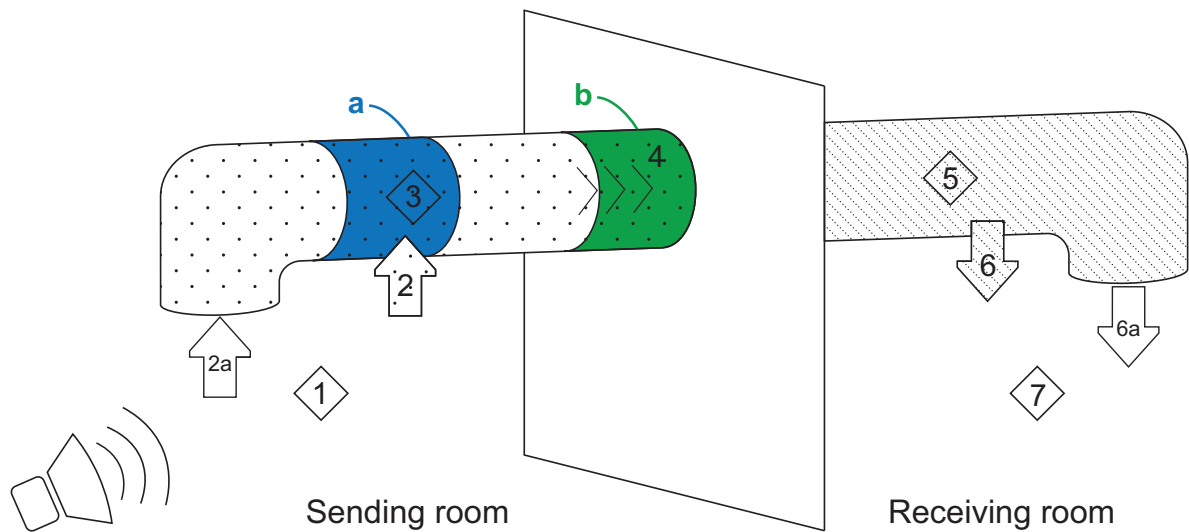
Figure 4.3: Illustration model of how sound travels from the sending room to the receiving room if the surface area and air diffusers affects the sound transmission. Two areas on the ventilation duct in the sending room are marked with blue and green colors together with the letters a and b that describe different areas for acoustical treatments.

Ventilation ducts have a few acoustical properties that theoretical models in general should consider. Both rectangular and circular ventilation ducts have different acoustic cross modes, and the cut-off frequency is the lowest of these modes [33], described in Equations 4.1 and

4.2 [139]. Sound transmission loss of break-in and breakout for circular ventilation ducts is also dependent on the ring frequency presented in Equation 4.3 [13, 29]. The ring frequency can be described as the frequency where an equivalent circular ring exhibits axisymmetric free vibrations [173]. The sound transmission loss for rectangular ducts is divided into other areas with a different frequency, called the longitudinal or cross-over frequency presented in [22, 33], and seen in Equation 4.4. Plane mode transmission dominates below the cross-over frequency and multi-mode transmission dominates above [33]. The calculated values are presented in Table C2.

$$f_{1,\text{circular}} = \frac{0.586 \cdot c_0}{d}. \tag{4.1}$$

$$f_{1,\text{rectangular}} = \frac{0.5 \cdot c_0}{a}. \tag{4.2}$$

$$f_R = \frac{c_L}{P}. \tag{4.3}$$

$$f_L = \frac{613}{\sqrt{a \cdot b}}. \tag{4.4}$$

The cut-off frequency in Equations 4.1 and 4.2 is dependent on the speed of sound in air, c_0, and the diameter of the circular duct, d, or the longest dimension of the rectangular duct, a. The ring frequency in Equation 4.3 is determined by the speed of sound of the ventilation duct material, c_L, and the perimeter of the circular duct, P. The longitudinal or cross-over frequency in Equation 4.4 is dependent on the longest and shortest dimension of the rectangular duct, a and b.

A system with a wall, a ventilation duct and external lagging with different lengths can be described with a combined sound reduction according to Equation 4.5:

$$R_{\text{combined}} =$$

$$= 10 \cdot \log_{10} \left(\frac{S_{\text{wall}} + M_{\text{duct}} + M_{\text{wrap}}}{S_{\text{wall}} \cdot 10^{-\frac{R_{\text{wall}}}{10}} + M_{\text{duct}} \cdot 10^{-\frac{R_{\text{duct}}}{10}} + M_{\text{wrap}} \cdot 10^{-\frac{(R_{\text{duct}} + R_{\text{wrap}})}{10}}} \right). \quad (4.5)$$

4.3 Method

The experimental part was performed according to [35] and took place in the sound transmission laboratory at Lund University, LTH, Faculty of Engineering, Division of Acoustics. The laboratory consists of two horizontal rooms, separated by a heavy wall with an opening where a 10 m^2 mock-up wall can be constructed (Figure 4.4a). The experimental part in Ref. [35] tested three different types of walls. Lab measurements yielded R_{w} of 35, 46, and 54 dB according to ISO 717-1:2013 [174] and *STC* of 35, 46, and 53 dB according to ASTM E413-16 [175]. The edges, between the mock-up wall and the heavy wall, were covered with sealant on all sides.

Two circular and one rectangular ventilation ducts were used together with the three different walls in Ref. [35]. The dimensions of the ventilation ducts were Ø315 and Ø630 mm for the circular duct and 700 × 250 mm for the rectangular duct. Both ends of the ventilation duct were plugged with a metal plate, with two gypsum boards and sealant on the inside of the plates (see Figure 4.4c and Figure 4.4d), since the main objective was to measure how the surface area affects the sound transmission. The connection was made airtight between the metal plate and the ducts with a rubber or foam lining (Figure 4.4b) on the metal plates.

(a)

(b)

(c)

(d)

Figure 4.4: Pictures from the measurements in Ref. [35]: (a) The finished mounted wall; (b) Foam lining for rectangular duct; (c) Cover cap for the circular duct: rubber lining, gypsum boards and sealant around the border; (d) Cover cap for the rectangular duct: foam lining and gypsum boards.

The impact of the ventilation ducts on the test walls was quantified by measuring the walls without any holes, as shown in Figure 4.4a. The measurements with no holes represent reference values, R_{wall}, that are used in Equation 4.5. Different treatments were applied on the duct and the main treatments are presented below. Treatments are only applied if the measured combined sound reduction index with duct and wall is below the reference wall. A sealant was applied between the ventilation duct and the wall for all cases below. More information about the measurements can be obtained in Ref. [35, 126].

1. External lagging with 50 mm stone wool, density of 100 kg/m^3, closest to the wall with a length of 600 mm.

2. External lagging with 50 mm stone wool, density of 100 kg/m^3, closest to the wall with a length of 1200 mm.

3. External lagging with 50 mm stone wool, density of 100 kg/m^3, closest to the wall with a length of 1800 mm.

4. External lagging with 50 mm stone wool, density of 100 kg/m^3, along the whole duct.

5. External lagging with 100 mm stone wool, density of 100 kg/m^3, closest to the wall with a length of 1800 mm. The rest of the duct is covered with 50 mm stone wool, density of 100 kg/m^3.

The different walls are further on described as the following types, measured in the laboratory according to Ref. [35].

- Wall A. Sound reduction index: $R_\text{w} = 35$ dB or sound transmission class: $STC = 35$ dB

- Wall B. Sound reduction index: $R_\text{w} = 46$ dB or sound transmission class: $STC = 46$ dB

- Wall C. Sound reduction index: $R_\text{w} = 54$ dB or sound transmission class: $STC = 53$ dB

Pictures from the measurements in [35] are displayed in Figure 4.5; different treatments with external lagging (external sound insulation) are applied on different ventilation ducts according to cases 1–5 above.

Figure 4.5: Pictures from the measurements in Ref. [35] in one of the rooms: (a) Circular 630 mm duct, treatment according to case 3; (b) Circular 630 mm duct, treatment according to case 5; (c) Circular 315 mm duct, treatment according to case 4; (d) Rectangular duct, 700 × 250 mm, treatment according to case 4.

4.4   Theoretical Models with External Lagging

The improvement of external lagging with stone wool according to different cases presented under Section 4.3 can be expressed with developed theoretical models. The models are based on measurements from [35] and previous theoretical models from [126], which describes the sound reduction of the ventilation duct. The models are developed with an analytical approach. For circular ducts, the equations are divided into different frequency areas depending on the cut-off frequency, f_1, and the ring-frequency, f_R. For rectangular ducts, the equations are instead divided into frequency areas depending on the cut-off frequency, f_1, and the

longitudinal (or cross-over) frequency, f_L. Units for different variables are presented in Table C1. Calculated values for frequencies presented in Equations 4.1–4.4 are displayed in Table C2.

4.4.1 Theoretical Models with External Lagging for Circular Ducts

In the development of theoretical models for circular ducts, the wrapping length closest to the wall proved to be the most important parameter when the ventilation duct was partially covered with external lagging. Equation 4.5 was therefore modified to consider this in Equation 4.6 below. It is important to note that R_{wrap} only describes the addition of sound reduction caused by the external lagging and that R_{duct} needs to be included to the total sound reduction described in Equation 4.6:

$$
R_{\text{circular,combined,wrap}} =
$$

$$
10 \cdot \log_{10} \left(\frac{S_{\text{wall}} + M_{\text{duct}} + M_{\text{wrap}}}{S_{\text{wall}} \cdot 10^{\frac{-R_{\text{wall}}}{10}} + M_{\text{wrap}} \cdot 10^{\frac{-(R_{\text{wrap}}+R_{\text{duct}})}{10}} + \left(\frac{L-L_{\text{wrap}}}{L} \right)^4 M_{\text{duct}} \cdot 10^{\frac{-R_{\text{duct}}}{10}}} \right). \tag{4.6}
$$

When the ventilation duct is completely covered with external lagging, $L_{\text{wrap}} = L$, one term disappears automatically from the equation above. R_{wrap} can be calculated with the equations below, R_{duct} can be calculated using Ref. [126] and R_{wall} can be obtained from the manufacturers (laboratory measurements), by calculations with a building acoustic software, or by calculations with equations from the literature.

Ref. [126] introduces a new equation that specifies another frequency area that is dependent on the cut-off frequency for circular ducts, presented in Equation 4.7. The calculated values are presented in Table C2.

$$
f_e = \frac{f_{1,\text{circular}}}{1.9}. \tag{4.7}
$$

4.4.1.1 Theoretical Models When Circular Ventilation Ducts Are Partly Wrapped

A theoretical model is developed when a circular ventilation duct is partly covered with external lagging and the sound reduction, depending on frequency, is divided into four main zones according to Equations 4.8–4.13, which together describe R_{wrap}.

When $f \leq f_e$:

$$R_{\text{circular,partly,1}} = 10 \cdot \log_{10} \left(\frac{q_{\text{wrap}}^{0.7}}{2 \cdot S \cdot \pi \cdot \left(S + 1.9 \cdot \frac{\max(f_e - f,\, 100)^{0.8/\sqrt{d}}}{f_{1,\text{circular}}} \right)} \right), \quad (4.8)$$

where S is the cross-section area of the ventilation duct and q_{wrap} is the mass per unit area of the external lagging.

When $f_e < f \leq f_{1,\text{circular}}$:

$$R_{\text{circular,partly,2}} = 10 \cdot \log_{10} \left(\frac{q_{\text{wrap}} \cdot f}{S \cdot c_0 \cdot \pi^2} \right). \quad (4.9)$$

When $f_{1,\text{circular}} < f \leq f_R$:

$$R_{\text{circular,partly,3}} = 10 \cdot \log_{10} \left(\frac{\sqrt{\max\left(f - f_{1,\text{circular}},\, 100\right)} \cdot q_{\text{wrap}}^3 \cdot 2.2 \cdot \left(\frac{L - L_{\text{wrap}}}{L} \right)}{P^2 \cdot \pi^2 \cdot f_{1,\text{circular}}^{0.3}} \right), \quad (4.10)$$

where L is the total length of the ventilation duct and L_{wrap} is the length of the external lagging. The ring frequency does not only cause a drop in sound reduction at the nearest one third octave band, denoted as $f_{R,\text{rounded}}$, but also at the one third octave band below that, denoted as $f_{R,\text{rounded}-1/3}$.

When $f \approx f_R$ (rounded down) $-$ one third octave band:

$$\text{Subtract } R_{\text{circular,partly,3}} \text{ with } P \cdot \left(L - L_{\text{wrap}} \right). \quad (4.11)$$

When $f \approx f_R$ (rounded down):

$$\text{Subtract } R_{\text{circular,partly,3}} \text{ with } 2P \cdot \left(L - L_{\text{wrap}}\right). \tag{4.12}$$

When $f > f_R$:

$$R_{\text{circular,partly,4}} = 10 \cdot \log_{10} \left(f^{0.1} \cdot q_{\text{wrap}}\right). \tag{4.13}$$

4.4.1.2 Theoretical Models When Circular Ventilation Ducts Are Completely Wrapped

The sound reduction index increases significantly when the whole circular ventilation duct is covered with external lagging according to Equations 4.14–4.17, which together describe R_{wrap}. Ref. [35] presents the basic equations to estimate the sound reduction, which are further developed in this article.

When $f \leq f_e$:

$$R_{\text{circular,full,1}} = 10 \cdot \log_{10} \left(\frac{q_{\text{wrap}}^2}{2 \cdot S \cdot \pi \cdot \left(S + 1.9 \cdot \frac{\max(f_e - f, \, 100)^{0.8/\sqrt{d}}}{f_{1,\text{circular}}}\right)} \right). \tag{4.14}$$

When $f_e < f \leq f_{1,\text{circular}}$:

$$R_{\text{circular,full,2}} = 10 \cdot \log_{10} \left(\frac{q_{\text{wrap}}^{2.7} \cdot f}{S \cdot c_0^{1.4} \cdot \pi^2 \cdot \frac{P}{2}} \right). \tag{4.15}$$

When $f_{1,\text{circular}} < f \leq f_R$:

$$R_{\text{circular,full,3}} = 10 \cdot \log_{10} \left(\frac{\max\left(f - f_{1,\text{circular}}, \frac{40 \cdot q_{\text{wrap}}}{P^2}\right)^2 \cdot q_{\text{wrap}}^2}{P^2 \cdot \pi^2 \cdot f_{1,\text{circular}}} \right). \tag{4.16}$$

When $f > f_R$:

$$R_{\text{circular,full,4}} = 10 \cdot \log_{10} \left(f \cdot q_{\text{wrap}}\right). \tag{4.17}$$

4.4.2 Theoretical Models with External Lagging for Rectangular Ducts

Similar to circular ducts, in the development of theoretical models for rectangular ducts, the wrapping length closest to the wall proved to be the most important parameter when the ventilation duct was partially covered with external lagging. Equation 4.5 was therefore adjusted to form Equation 4.18 with the same principles made for Equation 4.6. The combined sound reduction index of the wall, the rectangular ventilation duct, and external lagging as acoustical treatment can be described according to Equation 4.18. As mentioned before, note that R_{wrap} only describes the addition of the sound reduction caused by the external lagging and that R_{duct} needs to be included to the total sound reduction caused by that path described in Equation 4.18:

$$R_{\text{rectangular,combined,wrap}} =$$

$$10 \cdot \log_{10} \left(\frac{S_{\text{wall}} + M_{\text{duct}} + M_{\text{wrap}}}{S_{\text{wall}} \cdot 10^{\frac{-R_{\text{wall}}}{10}} + M_{\text{wrap}} \cdot 10^{\frac{-(R_{\text{wrap}} + R_{\text{duct}})}{10}} + \left(\frac{L - L_{\text{wrap}}}{L} \right)^2 M_{\text{duct}} \cdot 10^{\frac{-R_{\text{duct}}}{10}}} \right) . \quad (4.18)$$

R_{wrap} can be calculated with equations below, R_{duct} can be calculated using Ref. [126] and R_{wall} can be obtained from the manufacturers (laboratory measurements), by calculations with a building acoustic software, or by calculations with equations from the literature.

4.4.2.1 Theoretical Models When Rectangular Ventilation Ducts Are Partly Wrapped

A theoretical model is developed when a rectangular ventilation duct is partly covered with external lagging (wrapped) and the sound reduction depending on frequency is divided into three main zones according to Equations 4.19–4.21, which together describe R_{wrap}.

When $f \leq f_{1,\text{rectangular}}$:

$$R_{\text{rectangular,partly,1}} = 10 \cdot \log_{10} \left(\frac{q_{\text{wrap}}^{1.5} \cdot \left(0.5 + \frac{L_{\text{wrap}}}{L} \right)^{1.2} \cdot f_{1,\text{rectangular}}^{0.7}}{f \cdot S \cdot \pi^2} \right). \qquad (4.19)$$

When $f_{1,\text{rectangular}} < f \leq f_L$:

$$R_{\text{rectangular,partly,2}} = 10 \cdot \log_{10} \left(\frac{\max \left(f - f_{1,\text{rectangular}}, \frac{10 \cdot L_{\text{wrap}}}{L} \right)^{0.2} \cdot q_{\text{wrap}}^3}{P \cdot \pi^2 \cdot f_{1,\text{rectangular}}^{0.2}} \right). \qquad (4.20)$$

When $f > f_L$:

$$R_{\text{rectangular,partly,3}} = 10 \cdot \log_{10} \left(\sqrt{f \cdot q_{\text{wrap}}} \right). \qquad (4.21)$$

4.4.2.2 Theoretical Models When Rectangular Ventilation Ducts Are Completely Wrapped

Similar to circular ducts, the sound reduction increases significantly when the whole rectangular ventilation duct is covered with external lagging (wrapped) according to Equations 4.22–4.24, which together describe R_{wrap}. Ref. [35] presents the basic equations to estimate the sound reduction, which are further developed in this article.

When $f \leq f_{1,\text{rectangular}}$:

$$R_{\text{rectangular,full,1}} = 10 \cdot \log_{10} \left(\frac{q_{\text{wrap}}^{2.1}}{10 \cdot S \cdot \pi} \right). \qquad (4.22)$$

When $f_{1,\text{rectangular}} < f \leq f_L$:

$$R_{\text{rectangular,full,2}} = 10 \cdot \log_{10} \left(\frac{\max \left(f - f_{1,\text{rectangular}}, 50 \right)^{1.8} \cdot q_{\text{wrap}}^3}{P \cdot \pi^2 \cdot f_{1,\text{rectangular}}^{1.4}} \right). \qquad (4.23)$$

When $f > f_L$:

$$R_{\text{rectangular,full,3}} = 10 \cdot \log_{10} \left(f \cdot q_{\text{wrap}} \right). \tag{4.24}$$

4.5   Results

4.5.1   Measurement Results Compared to the Developed Theoretical Models

The sound reduction for the three different ventilation ducts with different lengths of external lagging combined with the sound reduction of the walls can be calculated according to equations in Section 4.4.1 and Section 4.4.2. The developed models are based on an analytical approach.

Measurement results compared to the developed theories are presented in Figure 4.6, Figure 4.7 and Figure 4.8 for Wall C with the highest sound reduction index of $R_w = 54$ dB and sound transmission class of $STC = 53$ dB. The calculations, compared to measurements for Walls A and B with lower sound reduction indices and sound transmission classes, are displayed in Figure C1, Figure C2, Figure C3, Figure C4 and Figure C5 described under Section 4.3.
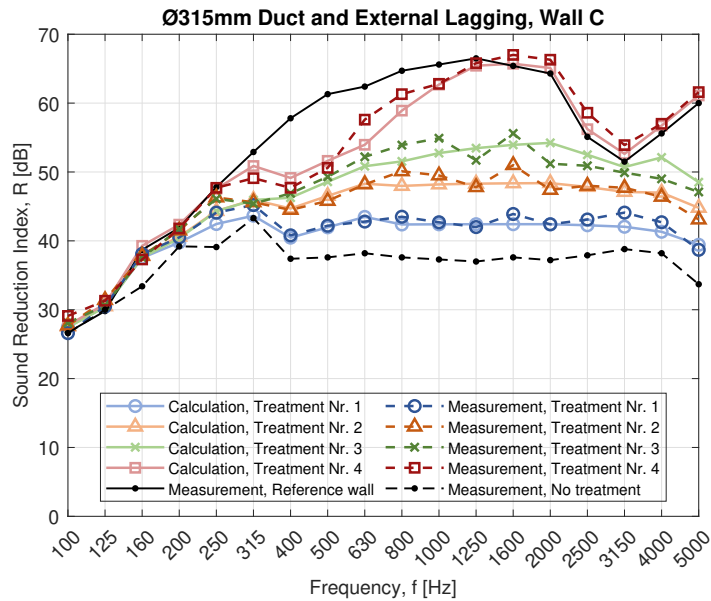
Figure 4.6: Theoretical models compared to measurements with external lagging as acoustic treatment. Ventilation duct with Ø315 mm through wall C with a sound reduction index of R_w = 54 dB. External lagging is mounted at partial lengths of 0.6–1.8 m (Treatment 1–3) and full length (Treatment 4) with 50 mm stone wool, density of 100 kg/m^3, closest to the wall.
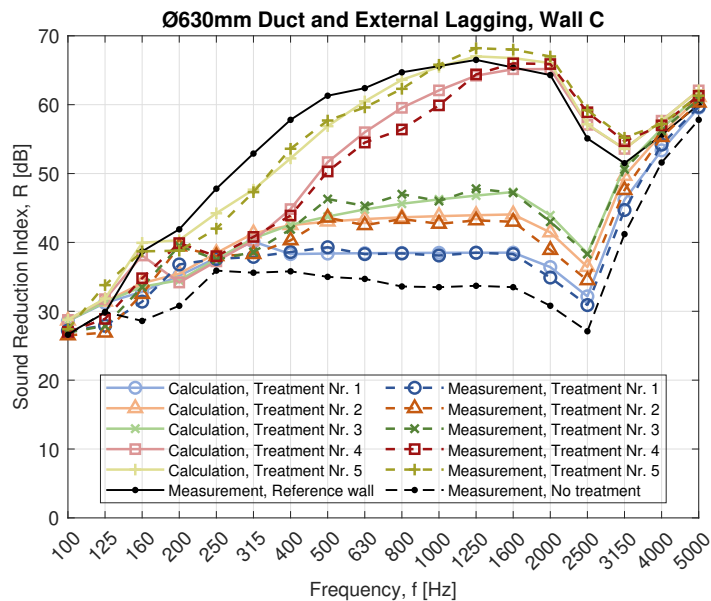
Figure 4.7: Theoretical models compared to measurements with external lagging as acoustic treatment. Ventilation duct with Ø630 mm through wall C with a sound reduction index of R_w = 54 dB. External lagging is mounted at partial lengths of 0.6–1.8 m (Treatment 1–3) and full length (Treatment 4 and 5) with 50 mm and 100 mm stone wool, density of 100 kg/m^3, closest to the wall.
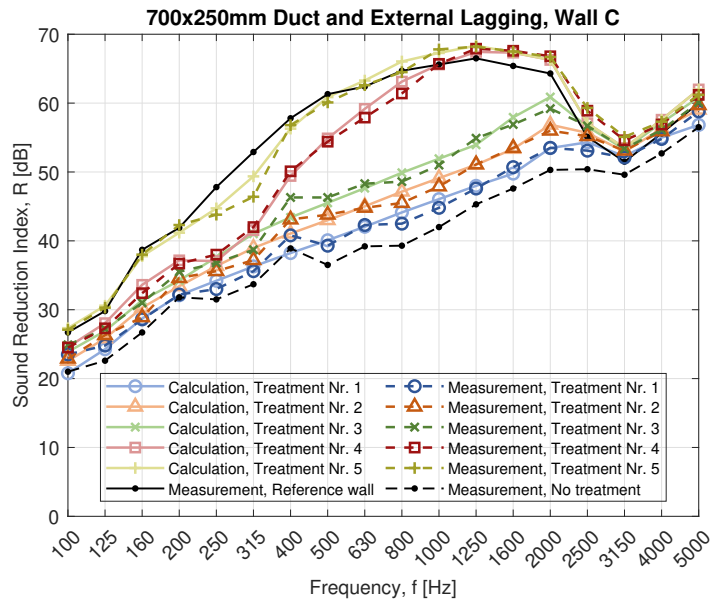
Figure 4.8: Theoretical models compared to measurements with external lagging as acoustic treatment. Ventilation duct with dimension: 700×250 mm through wall C with a sound reduction index of $R_w = 54$ dB. External lagging is mounted at partial lengths of 0.6–1.8 m (Treatment 1–3) and full length (Treatment 4 and 5) with 50 mm and 100 mm stone wool, density of 100 kg/m^3, closest to the wall.

4.5.2 Suspended Absorbent Ceilings: Estimated Calculations

Suspended ceilings have a positive effect on the sound reduction when a ventilation duct passes through a wall. The sound reduction for an absorbent ceiling can be estimated based on sound pressure insulation values, D_{pr}, from different products measured according to ISO 11546-1 [176]. The values measured according to Ref. [176] are expressed for one ceiling and the model in Figure 4.1 could include one suspended ceiling in each room. The total sound reduction addition can be estimated and added in Equation 4.5 instead of R_{wrap}.

Laboratory measurements with sound pressure insulation values, D_{pr}, have been obtained for two different types of ceilings. The first one, called Ceiling A, is built up with 40 mm absorbent tiles. The second, called Ceiling B, is built up with a gypsum board behind 40 mm absorbent tiles. Ceiling B will therefore have higher sound insulation compared to Ceiling A.

Estimated calculations are presented in Figure 4.9 and Figure 4.10 with Ceiling A and B

together with Wall C and the three different ventilation ducts investigated in this paper. The calculations assume that suspended absorbent ceilings are mounted in both rooms, with a model based on Figure 4.1, and that the total sound pressure insulation is almost twice the sound pressure insulation of one ceiling. The calculations could therefore be overestimating the sound reduction, meaning that the positive effect of suspended ceilings presented in Figure 4.9 and Figure 4.10 are lower than presented. Calculations for Wall B are presented in Figure C6 and Figure C7. Calculations for Wall A are not presented since the difference in sound reduction is minor between the reference wall and when an untreated ventilation duct passes through. Similar results and conclusions can be expected for Wall A as for Wall B.
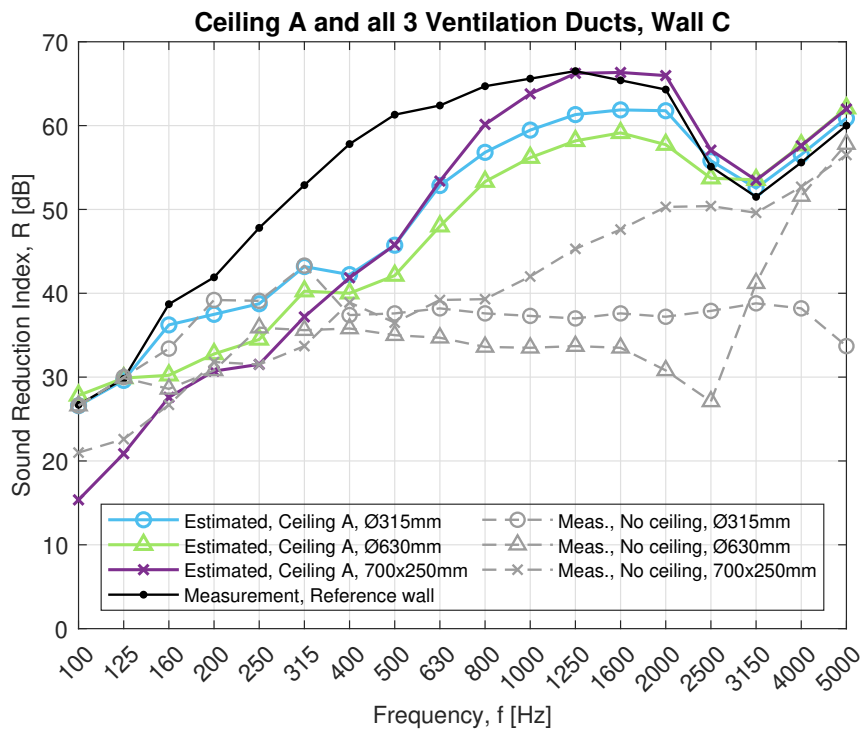
Figure 4.9: Estimated theory with a suspended absorbent ceiling, Ceiling A, as acoustical treatment. Ventilation duct with dimensions of Ø315, Ø630 and 700×250 mm through wall C with a sound reduction index of $R_w = 54$ dB.
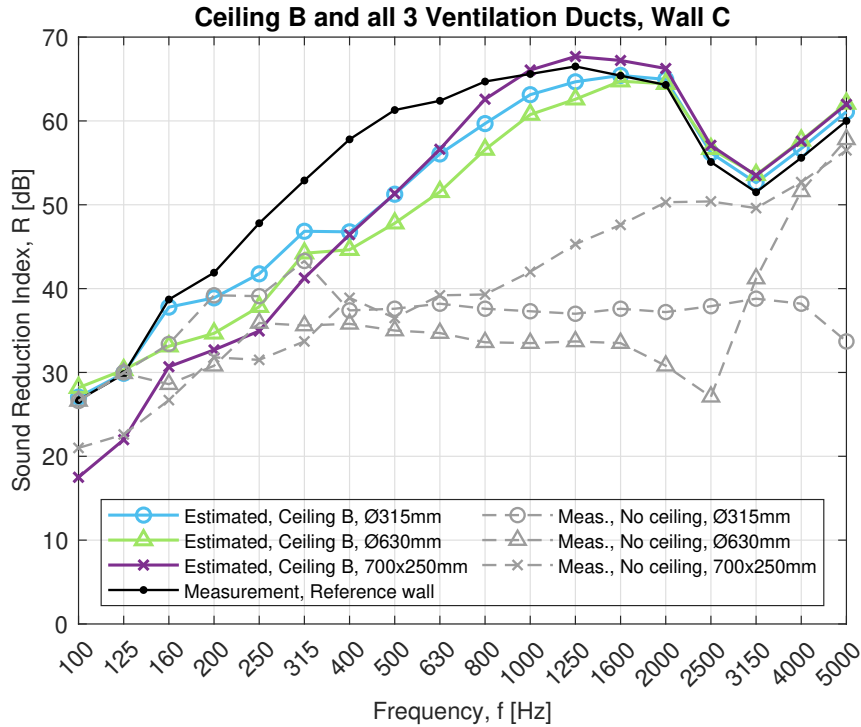
Figure 4.10: Estimated theory with a suspended absorbent ceiling, Ceiling B, as acoustical treatment. Ventilation duct with dimensions of Ø315, Ø630 and 700×250 mm through wall C with a sound reduction index of $R_w = 54$ dB.

4.6 Discussion

The agreement between measurements from [35] and new developed theoretical models in [126], combined with the models under Section 4.4.1 and Section 4.4.2, is sufficient with few minor deviations for certain frequency bands. However, some consideration needs to be taken around and below the frequency named f_e since the difference is very small between the reference wall and when a ventilation duct passes through the wall without treatments. Further studies are therefore required with a wall that has higher performance in a low frequency to model the combined sound reduction index around and below f_e. Nonetheless, the developed theory in this study models different wrapping lengths with high accuracy. The uncertainties of the models are the duct length since the length was constant, and the shape of rectangular ducts since only one rectangular duct was tested.

The frequency range between f_1 and f_R / f_L (circular or rectangular duct) is most affected when external lagging with stone wool is applied as an acoustical treatment on the ventilation ducts. The difference is very large if the ventilation duct is covered with external lagging along parts of its surface area or if the whole ventilation duct is covered. When the ventilation duct with a diameter of 630 mm is covered with 50 mm stone wool at a length of 1800 mm (Treatment 3), the sound reduction increases at the ring frequency $\left(f_{R,630} = 2554 \text{ Hz} \approx 2500 \text{ Hz}\right)$ with 11 dB compared to no treatments (see Figure 4.7). However, when the rest of the duct is covered (length of 1200 mm), the increase is in total 32 dB, meaning that the extra 1200 mm yields an improvement of 21 dB. The improvement is clearest for the larger circular ventilation duct, but similar improvements are visible for the smaller circular duct in Figure 4.6. Furthermore, for the rectangular ventilation duct and treatment 3, the sound reduction increases around the cross-over frequency $(f_{L,700} = 1465 \text{ Hz} \approx 1600 \text{ Hz})$ with 9 dB compared to no treatments (see Figure 4.8). Moreover, when the rest of the rectangular ventilation duct is covered (length of 1200 mm), the increase is in total 20 dB, meaning that the extra 1200 mm yields an improvement of 11 dB.

Measurements and the developed models consider the fact that the area of the ventilation duct closest to the wall has the greatest positive effect on the combined sound reduction index. Similar principles can be adapted to the placement of silencers, meaning that a silencer has the best effect on the sound transmission and attenuation if it is placed directly against the wall.

Measurements indicate that external lagging with stone wool can be used as an effective acoustical treatment for both small and large ventilation ducts combined with walls of both low and high sound reduction indices. However, other treatments may be more effective to use in some scenarios. Moreover, suspended ceilings are often used in buildings, which will improve the sound insulation to some extent. Depending on the choice of suspended ceiling, fewer treatments may be required if a ventilation duct passes through a wall above the suspended ceiling. Estimated calculations of suspended ceilings with absorbent tiles show that they can work as a main acoustical treatment for large ventilation ducts through walls

with a sound reduction up to $R_\mathrm{w} = 46$ dB, see Figure C6 and Figure C7. However, they are not sufficient for walls with $R_\mathrm{w} = 54$ dB even if the suspended ceiling is built up with a 40 mm absorber and a gypsum board (see Figure 4.9 and Figure 4.10). More treatments are thereby required in addition to a suspended ceiling for walls with higher sound reduction indices. The calculations presented in Figure 4.9, Figure 4.10, Figure C6 and Figure C7 could be overestimated, meaning that the sound reduction might be lower. Therefore, consideration needs to be taken when analyzing these results, specifically when a large ventilation duct passes through walls with a sound reduction of around $R_\mathrm{w} = 46$ dB.

It should be noted that a ceiling with gypsum boards will acquire a high sound insulation and in some cases be enough as an acoustic treatment for the model presented in Figure 4.1. However, the problems with larger ventilation ducts often occur in schools, offices, and hospitals and the room acoustic requirements need to be considered. Therefore, it might not be possible to have a ceiling with gypsum boards because the sound absorption will not be sufficient. In addition to a suspended ceiling with absorption, other treatments may be necessary to fulfill the requirements.

One effective solution, in addition to suspended ceilings, is to connect a silencer to the ventilation duct system. However, the sound attenuation of a silencer decreases with the diameter of the ventilation duct based on various technical data sheets from suppliers. Some suppliers offer silencers with a divider in the center, called a baffle, which helps to improve the surface damping area of the silencer, but it might not be enough for larger ventilation ducts.

Crosstalk in ventilation duct systems describes when the sound travels via air diffusers between rooms, displayed by Elements 2a and 6a in Figure 4.2. External lagging is, for this scenario, not helpful as an acoustic treatment because it only affects break-in and breakout of the ventilation duct, described as Element 2 and 6 in Figure 4.2. When both the sound reduction due to flanking and crosstalk needs to be solved, a silencer might be the optimal solution since silencers are an effective way of solving both the sound attenuation and the sound transmission between two rooms connected with a ventilation duct.

It is important for designers to consider the scenarios displayed in Figure 4.1 and Figure 4.2 to find an optimal solution when choosing acoustical treatments and further studies are required when different acoustical treatments are combined to produce a design scheme.

4.7 Conclusions

The purpose of this article was to investigate different acoustical treatments and develop theoretical models when external lagging is used on parts or on the whole ventilation duct to reduce flanking sound transmission.

The number of acoustical treatments required depends on several factors, including the dimensions and shape of the ventilation duct, the sound reduction of the wall and the connection between the duct and the wall. Moreover, the number of treatments will also depend on whether there are air diffusers connected to the ventilation ducts to supply the different rooms with air.

Theoretical models are developed for external lagging (wrapping with stone wool) on ventilation ducts as an acoustic treatment through walls. The models take the wrapping length into consideration and measurement data agrees with the developed theory with few deviations for certain frequency bands. The models clarify that the distance closest to the wall has the main impact on the sound reduction for the combined system.

Suspended ceilings with a 40 mm absorber could be enough as an acoustical treatment to prevent the sound from propagating via the surface area of the ventilation duct when it passes through walls of lower sound reduction indices of around $R_\mathrm{w} = 35$ dB or sound transmission classes around $STC = 35$ dB. Furthermore, suspended ceilings with a 40 mm absorber and a gypsum board behind could be enough for walls with R_w and STC up to 46 dB.

The whole system, including wall, ventilation duct, air diffusers, and suspended ceiling, must be investigated when acoustical treatments are proposed. This article mainly investigated how the surface area of ventilation ducts and suspended ceilings affect the sound transmission. Sometimes, other treatments instead of external lagging may be more effective, such as the

use of silencers, and in some cases, the suspended ceiling could be enough. However, external lagging seems to be the only effective solution in offices and schools when a large ventilation duct passes through a wall with high sound reduction.

4.8   Additional work

Weighted sound reduction index values are presented in Table 4.1 for the configurations in Figures 4.6-4.8 and in Figures C1-C5.

Table 4.1: Weighted sound reduction indices for different treatment configurations.

Configuration	Measurement, R_w [dB]	Estimation, R_w [dB]
Wall A, Vent $\varnothing$315, Treatment 1	36	36
Wall A, Vent $\varnothing$630, Treatment 1	33	35
Wall A, Vent $\varnothing$630, Treatment 2	36	36
Wall B, Vent $\varnothing$315, Treatment 1	42	42
Wall B, Vent $\varnothing$315, Treatment 2	45	45
Wall B, Vent $\varnothing$630, Treatment 1	37	38
Wall B, Vent $\varnothing$630, Treatment 2	41	42
Wall B, Vent $\varnothing$630, Treatment 3	43	43
Wall B, Vent $\varnothing$630, Treatment 4	47	46
Wall B, Vent 700x250, Treatment 1	42	42
Wall B, Vent 700x250, Treatment 2	44	44
Wall B, Vent 700x250, Treatment 3	45	45
Wall C, Vent $\varnothing$315, Treatment 1	43	42
Wall C, Vent $\varnothing$315, Treatment 2	48	47
Wall C, Vent $\varnothing$315, Treatment 3	51	51
Wall C, Vent $\varnothing$315, Treatment 4	53	53
Wall C, Vent $\varnothing$630, Treatment 1	38	38
Wall C, Vent $\varnothing$630, Treatment 2	42	43
Wall C, Vent $\varnothing$630, Treatment 3	45	45
Wall C, Vent $\varnothing$630, Treatment 4	50	50
Wall C, Vent $\varnothing$630, Treatment 5	54	54
Wall C, Vent 700x250, Treatment 1	43	43
Wall C, Vent 700x250, Treatment 2	46	46
Wall C, Vent 700x250, Treatment 3	48	48
Wall C, Vent 700x250, Treatment 4	50	50
Wall C, Vent 700x250, Treatment 5	54	54

CHAPTER 5

EFFECTS OF BUILDING HEIGHT ON THE SOUND TRANSMISSION IN CROSS-LAMINATED TIMBER BUILDINGS – AIRBORNE SOUND INSULATION

Résumé

Les bâtiments construits en bois lamellé-croisé (CLT) suscitent un intérêt croissant dans de très nombreux pays. Le CLT étant un produit durable, il peut aider l'industrie du bâtiment à réduire les émissions de gaz à effet de serre. En outre, les bâtiments construits en CLT sont de plus en plus hauts, ce qui augmente la charge sur les jonctions et les éléments de construction localisés aux étages inférieurs du bâtiment. Plusieurs études ont examiné l'impact de la charge sur la transmission du son entre les appartements. La majorité d'entre elles ont constaté qu'une augmentation de la charge pouvait avoir un effet négatif sur l'isolation acoustique verticale. Cependant, les résultats sont limités à quelques mesures ou éléments de construction, et ne portent que sur les jonctions avec des couches intermédiaires résilientes. Cet article a pour but d'étudier si la hauteur du bâtiment, et donc la charge, affecte l'isolation verticale contre les bruits aériens entre des appartements situés à différents étages dans différents bâtiments en bois lamellé-croisé, avec ou sans la présence d'intercalaires viscoélastiques, et de quantifier l'effet. Quatre bâtiments en CLT avec différents systèmes de construction, différentes hauteurs et la présence d'intercalaires viscoélastiques dans les jonctions ont été mesurés. L'isolation des bruits aériens entre différentes pièces d'appartement a été mesurée verticalement pour

les étages inférieurs et supérieurs. La différence d'isolation aux bruits aériens a été calculée séparément pour chaque bâtiment, et les mesures indiquent que l'isolation verticale aux bruits aériens diminue à mesure que l'on descend dans les bâtiments. Par conséquent, les résultats montrent qu'une augmentation de la charge, causée par un nombre croissant d'étages, a un effet négatif sur l'isolation des bruits aériens verticaux.

Mots clés: bois lamellé-croisé (CLT), charge, hauteur du bâtiment, couche intermédiaire viscoélastique, acoustique du bâtiment, isolation contre les bruits aériens

Abstract

Buildings constructed with cross-laminated timber (CLT) are increasing in interest in several countries. Since CLT is a sustainable product, it can help the building industry to reduce greenhouse gas emissions. Furthermore, buildings constructed with CLT are increasing in building height, thereby increasing the load on the junctions and structural building elements further down in the building. Several studies have investigated how the load impacts the sound transmission between apartments. The majority found that an increasing load could have a negative effect on the vertical sound insulation. However, the findings are limited to a few measurements or building elements, and the studies only investigate junctions with resilient interlayers. This article aims to investigate if the building height, and thereby the load, affect the vertical airborne sound insulation between apartments on different stories in different cross-laminated timber buildings, with or without the presence of viscoelastic interlayers, and to quantify the effect. Four CLT buildings with different building systems, building heights, and the presence of viscoelastic interlayers in the junctions were measured. The airborne sound insulation between different apartment rooms was measured vertically for stories on the lower and higher levels. The difference in airborne sound insulation was calculated separately for each building, and the measurements indicate that the vertical airborne sound insulation reduces further down in the buildings. Therefore, results show that increasing load, by an increasing number of stories, has a negative effect on the vertical airborne sound insulation.

Keywords: cross-laminated timber (CLT), load, building height, viscoelastic interlayer, building acoustic, airborne sound insulation

5.1 Introduction

This chapter, except Section 5.5, is a copy of a journal article published in Building and Environment in 2023 [177].

Wooden buildings, in general, and cross-laminated timber (CLT) buildings, in particular, are increasing in interest in many countries [9]. There are few materials that can match wood in terms of environmental benefits [92]. Thus, wood plays an important role in future buildings to reduce global energy-related CO_2 emissions from the building industry by replacing steel and concrete [3–6, 8, 178]. Cross-laminated timber is a sustainable product made with several layers of lumber boards stacked in alternating directions, most often with an odd number of layers and usually between three to seven layers [9, 179]. Moreover, CLT has been a game-changer for tall buildings in wood, and it is reported possible to build up to around 40 stories with CLT as of this moment [180–182]. The tallest wooden building as of this year is the Ascent tower in Wisconsin, according to CTBUH [183], with a height of around 87 m in 25 floors, constructed with both CLT and glued-laminated timber (glulam). With the possibility of constructing tall buildings in CLT, the increasing building height directly leads to increasing loads lower down in the building. Furthermore, the increasing loads could have an impact on the elasticity of junctions, as suggested by Ref. [16] and thus affecting the sound transmission between apartments on different stories [16].

In order to fulfill different acoustical requirements in wooden buildings, viscoelastic interlayers are often used, and they can be placed between load-bearing walls and floors to reduce the flanking sound transmission in junctions [11]. Several laboratory measurements have presented a higher vibration reduction index with resilient interlayers compared to without for CLT-elements [18, 110–113]. Bolmsvik Bolmsvik and Brandt [114] concluded that elastomers, which are a type of viscoelastic interlayers, have a positive effect on the sound reduction for frequencies above 70 Hz for the measured laboratory mockup configuration used. Other literatures have also confirmed the potential benefits of resilient interlayers [40, 106, 115,

184]. However, elastic interlayers change the distribution of sound energy in the structure, and they can be implemented to minimize flanking transmission in a specific direction only [115]. The elastic interlayer does not change the total energy in the system. Instead, it changes the distribution of energy between different elements [106], which is observed in measurements by Ref. [113], where the vibration reduction index of the floor-to-floor path overall decreases when resilient layers are added for an X-junction with a continuous floor slab.

Previous studies have measured how the number of stories, or the load, impacts the airborne or flanking sound transmission. Ref. [108] investigated how the number of stories impacts the airborne sound transmission between apartments for a lightweight wooden frame building with elastic strips in the junctions between volume elements. Measurements show that there is a difference over the different stories and that the sound insulation increases higher up in the building. Stiffer elastic strips were used above the first and second floors, and a softer elastic strip was used above the third, and final, floor. However, authors in Ref. [108] suggest that the result is caused by a mismatch in the relation between the load and the stiffness of the elastic strip and therefore, not by the load itself.

Timpte [18] collected laboratory measurement data from several institutes and compared an L-junction of CLT consisting of a floor and a wall with and without resilient layers and with and without external load. The comparison between no load and load with a resilient layer shows that the vibration reduction index increases when a load is applied for frequencies between 125 and 1000 Hz. Similar results are presented without a resilient layer in Ref. [18] with some exceptions on certain frequencies. Hörnmark [19] measured the vibration reduction index in a real CLT building on a junction between different stories, namely between stories 4 to 5 and 5 to 6. The result indicates that the vibration reduction index reduces with increased load for the path wall to wall, opposite to what was found in Ref. [18]. However, only a one-story difference was measured in one building. Moreover, measurements were performed with the transient method, but measurements of the receiving and sending levels were not simultaneously measured, which could have an effect on the result. According to ISO 10848-1

[88], both elements' velocity levels should be measured simultaneously when using transient structure-borne excitation.

Bard, Davidsson, and Wernberg [16] have investigated vibrations induced by a tapping machine in a multi-family wooden frame building. The top of the floor structure is constructed with a mix of CLT and glued laminated T beams that together form a stiff I-beam. The ceiling, on the bottom of the floor structure, is built up with wooden beams and battens together with gypsum boards. Viscoelastic interlayers with different stiffnesses depending on floor level are also placed in the junction. The authors in Ref. [16] concluded that junctions attenuate vibrations better higher up in the building for most of the measured frequencies, which is in agreement with findings in Ref. [19] and opposite what was presented in Ref. [18]. Furthermore, the authors in Ref. [16] suggest that the result could be explained by the difference in load between the junctions.

Authors in Ref. [185] have investigated how the load affects a junction with a flexible interlayer, and natural rubber with high resilience was used together with two reinforced concrete slabs. Three different loads were applied, and the result showed that an increase in load yielded a lower vibration reduction index for frequencies between 200 and 5000 Hz, with some discrepancies around 1250 Hz. The authors in Ref. [185] further explain that an increasing load increases the dynamic stiffness of the joint.

Previous studies [16, 18, 19, 108, 185] mentioned above have investigated how the number of stories, or the load, affects the sound insulation or the vibration reduction index between apartments or different building elements. However, the findings are for specific junctions or between specific rooms in a building in each paper and the findings are therefore limited. Furthermore, only junctions with the presence of resilient interlayers were studied in actual buildings. Moreover, the results are, in some cases contradictory to each other, but overall, most of them conclude that increasing load could have a negative effect on the acoustic performance of junctions. The actual difference in airborne sound insulation with increasing load is not thoroughly investigated in previous research. There are no detailed field estimations

of the effect of the building height for various building solutions in CLT, and specifically no estimations without viscoelastic interlayers.

The purpose of this paper is to investigate if the building height, and thereby the load, has an effect on the vertical airborne sound insulation between apartments on different stories in different cross-laminated timber buildings. Furthermore, if the load has an effect on the result, the aim is thereafter also to quantify or estimate the difference in vertical airborne sound insulation.

5.2   Materials and Method

5.2.1   Cross-laminated timber (CLT)

Cross-laminated timber is a sustainable product made with several layers of lumber boards stacked in alternating directions and most often with an odd number of layers, usually between three to seven layers [9, 179]. CLT is a lightweight solid engineering wood panel with good seismic and thermal performance [91]. In terms of acoustic, heavy mass or low bending stiffness usually result in good acoustic performance, and the sound insulation generally decreases around the critical frequency [93]. Treatments with viscoelastic interlayers in the junctions are sometimes required to increase the acoustic performance because CLT is lightweight, illustrated in Figure 5.1. Treatments are chosen depending on how different flanking paths are suppressed.

CLT elements usually have a critical frequency between 100 and 500 Hz, according to Refs. [93, 95]. Furthermore, Ref. [186] found that for 3-ply CLT assemblies, the critical frequency is around 500 Hz. Moreover, CLT has lumber boards stacked in alternating directions and, thereby, different modulus of elasticity in the major and minor directions. Therefore, it is suggested that the difference in modulus of elasticity between a CLT panel's major and minor axis yields different critical frequencies, resulting in not just one dip in a specific third-octave band but instead a range of third-octave bands where the sound insulation is decreased for a

CLT element [94].

The frequency area of interest for CLT elements is, therefore, not only in the low-frequency region, which is often highlighted as an important factor for lightweight buildings [20, 96, 97] but also in the mid-frequency area around 500 Hz.

Figure 5.1: Junction with cross-laminated timber and elastomers as viscoelastic interlayers.

5.2.2 Elastomers

Elastomers used to reduce flanking sound transmission in CLT junctions can be made of polyurethane which is a type of polymer [103]. Elastomers can exhibit properties between an elastic solid and a viscous liquid, thus behaving like a viscoelastic material [99–101] and the behavior is frequency dependent [102]. Viscoelastic damping is displayed in many polymeric and elastomeric materials, and after deformation, molecular chains relax and recover, resulting in damping [101]. An elastomer can be modeled as a spring with a specific stiffness, and they are selected based on the calculated load [101, 103–105]. Figure 5.2 displays several different viscoelastic materials from different manufacturers, and the different colors represent different stiffnesses.
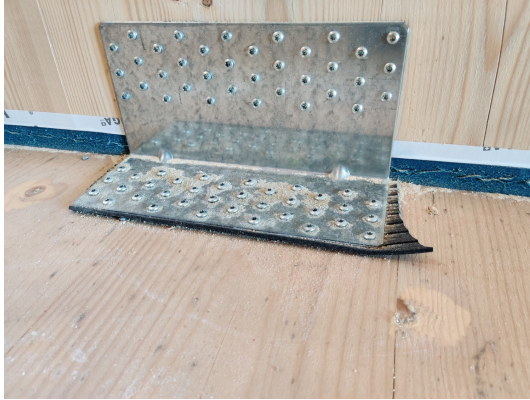
Figure 5.2: Viscoelastic interlayers from different manufacturers in a building (left) and as samples (right).

Ref. [106] show that the transmission loss for a junction is frequency dependent with an elastic interlayer, compared to a rigid junction without an elastic interlayer which is nearly independent of frequency. Measurements by Ref. [107] of resilient materials used in floating floor systems show that the dynamic stiffness decreases when the thickness of the resilient material increases. Moreover, elastomers not utilized or selected for the correct load could have lower vibration-damping properties, as suggested by Ref. [108]. However, measurements show that stiff interlayers that are not utilized still have a contribution to floor vibration [109].

The vibration reduction index of a junction depends on several factors, including the presence of viscoelastic interlayers, mentioned in Section 1, but also the type of connectors and screws, which was tested with many variations in laboratory measurements by several studies [18, 116, 117].

5.2.3 Project description

Airborne sound insulation measurements were conducted in three different projects situated in different locations in Sweden before people had moved in. The projects are in this article described as projects A, B, and C. In each project, the same floor plan is used for several stories. Measurements between different stories were conducted and compared between the same type of rooms to minimize the number of affecting parameters. To summarize, the

volume, surface dividing area, and principal construction were the same. Moreover, the rooms had no furniture in them. The thickness of the CLT slab and walls differ in project A between the stories, described further down. However, the thickness of the CLT walls and floors is always increasing, or the same, further down in the building. Otherwise, the main parameter that differs in the measurements between different stories is the load on the junctions and the stiffness of the viscoelastic interlayers dependent on the load.

Project A was measured in two separate buildings, building 1 with twelve stories, and building 2 with ten stories. The system, in both buildings in project A, is built up with CLT, a suspended gypsum ceiling, and concrete above an impact sound insulation board. Furthermore, 6 mm viscoelastic interlayers are placed under the CLT walls in building 2 with different stiffnesses depending on the load. Moreover, there are no viscoelastic interlayers in building 1. Figure 5.3 illustrates a junction between two stories in project A with an overview of the construction, different layers, and viscoelastic interlayers. The junctions are connected with brackets and nails/screws. The thickness of the CLT walls and floors decreases higher up in the building. Walls and ceilings are covered with gypsum boards. In project A, building 1, measurements were conducted between stories 3–4 and mainly 9–10, with few exceptions in one apartment where measurements were conducted between stories 8–9. In project A, building 2, measurements were conducted between stories 3–4 and 8–9.
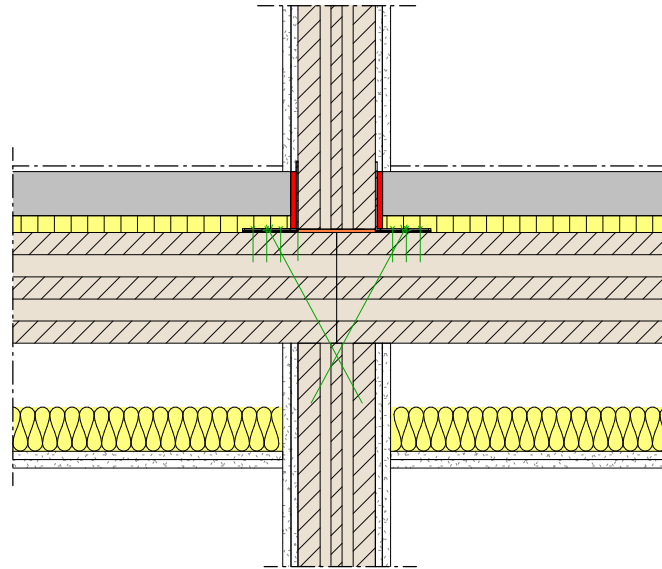
Figure 5.3: Overview of the construction, different layers, and viscoelastic interlayers used in project A – building 2. For project A – building 1, viscoelastic interlayers under the CLT walls are removed. Yellow color is chosen for insulation, red and orange colors are selected for the viscoelastic interlayers.

Project B has three connected buildings. Measurements in project B were conducted in the building with the most stories, 6 in total, between stories 2–3 and 4–5. The system in project B is built up with CLT, a suspended gypsum ceiling, and a raised resilient floor. Furthermore, 25 mm viscoelastic interlayers are placed under the CLT walls with different stiffnesses depending on the load. Figure 5.4 illustrates a junction between two stories in project B with an overview of the construction, different layers, and the viscoelastic interlayer. The junctions are connected with brackets and screws. The thickness of the CLT walls and floors is the same on each story. One wall in some rooms has a visible CLT surface, but most walls and all ceilings are covered with gypsum boards.

Project C is constructed as one building with eight stories. Measurements in project C were conducted between stories 3–4 and 7–8. The system in project C is built up with volume modules of CLT, with a raised resilient floor. Viscoelastic interlayers are placed between the volume modules. Figure 5.5 illustrates a junction between two stories in project C with an overview of the construction, different layers, and the viscoelastic interlayers. The thickness

of the CLT walls and floors is the same on each story. Furthermore, both walls and ceilings have visible CLT surfaces.
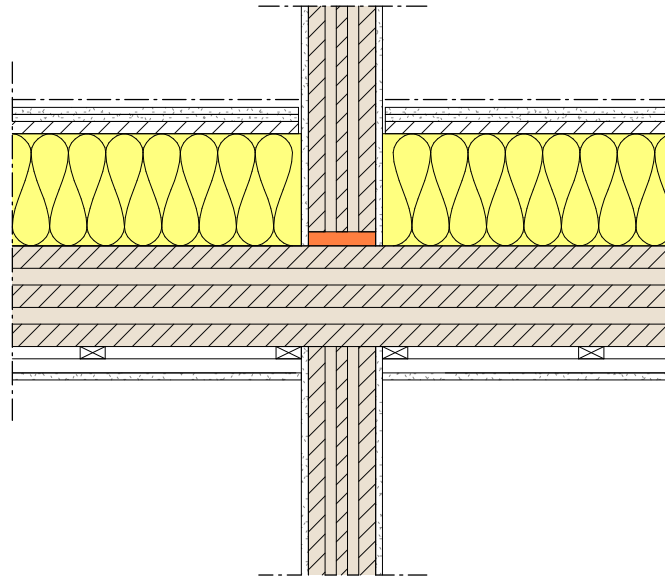
Figure 5.4: Overview of the construction, different layers, and the viscoelastic interlayer used in project B. Yellow color is chosen for insulation, and orange color is selected for the viscoelastic interlayer.
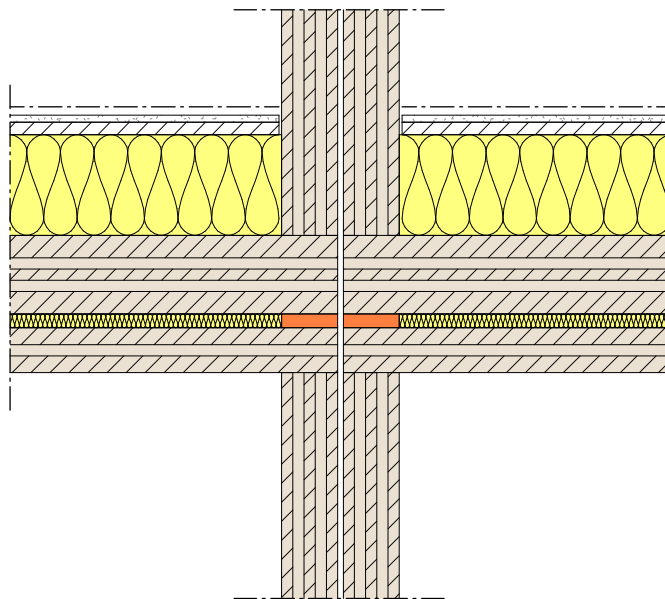
Figure 5.5: Overview of the construction, different layers, and the viscoelastic interlayer used in project C. Yellow color is chosen for insulation, and orange color is selected for the viscoelastic interlayer.

An illustration of where the different measurements took place, depending on the story, project, and building, is displayed in Figure 5.6. Measurements are evaluated for each building separately by subtracting the differences in vertical airborne sound insulation between low and high stories accordingly: $D_{\mathrm{n}T,\mathrm{high}} - D_{\mathrm{n}T,\mathrm{low}}$. The floor plans are the same where the sound insulation is evaluated. Therefore, the only main difference is the load on the junction. Moreover, for Project A – Building 2, Project B and Project C, the stiffness of the viscoelastic interlayers is different depending on the load on the junctions.
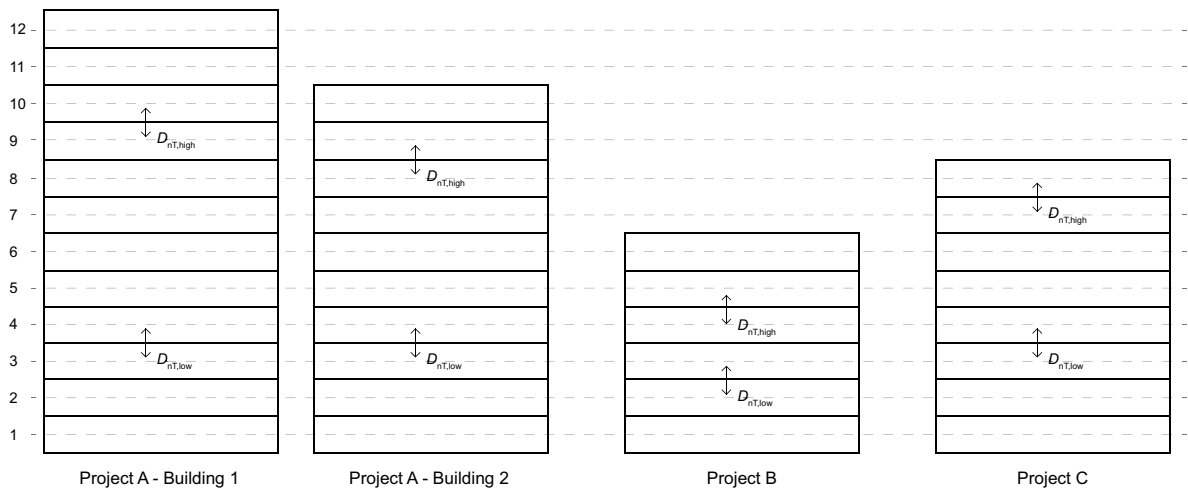
Figure 5.6: Illustration where measurements took place on different stories for each project and building.

5.2.4 Measurement method

The airborne sound insulation mainly depends on the difference in sound pressure level between the sending room, L_{p1}, and the receiving room, L_{p2}. This level difference, described as D in ISO 16283-1 is frequency dependent and presented in Equation 5.1 [83]:

$$D = L_{p1} - L_{p2}. \tag{5.1}$$

Corrections can be applied depending on the physical quantity requested. In a laboratory, corrections typically include the equivalent sound absorption area in the receiving room and the separating area of the test element [86, 87]. In the field in many European countries,

corrections typically include a ratio between the measured reverberation time, T, and a standard reverberation time, T_0. The physical quantity, described as D_{nT} in ISO 16283-1 [83] or *NNR* in ASTM E336 [84], is presented in Equation 5.2:

$$D_{nT} = L_{p1} - L_{p2} + 10 \cdot \log_{10}\left(\frac{T}{T_0}\right). \tag{5.2}$$

The airborne sound insulation in the described projects was measured in the field according to ISO 16283-1 [83] and evaluated according to Equation 5.2 and ISO 717-1 [174] with the standardized level difference. An omnidirectional loudspeaker was placed on a tripod in two different positions in the sending room, one corner position and one other position. The sound pressure level was thereafter measured in the sending and receiving room with sweeping patterns, mainly a cylindrical type, according to ISO 16283-1 [83]. The sound pressure level was measured in two different positions in each room for every loudspeaker position, each with a duration of 15 s. The reverberation time in the receiving room was measured using the interrupted noise method, with one loudspeaker position and three fixed microphone positions with two measurements in each position according to the engineering method in ISO 3382-2 [153].

5.2.5 Flanking sound transmission

The sound insulation between two rooms in a finished building includes all different flanking paths that affect the result together with the direct path. The direct path, together with six first-order flanking paths, is illustrated in Figure 5.7. For rectangular rooms directly above each other, 12 first-order flanking paths are usually defined [71]. First-order flanking paths are in this article described as the paths that include one junction, one source surface, and one receiving surface. Measurements in a laboratory, on the other hand, are designed to suppress the different flanking paths [85, 87].
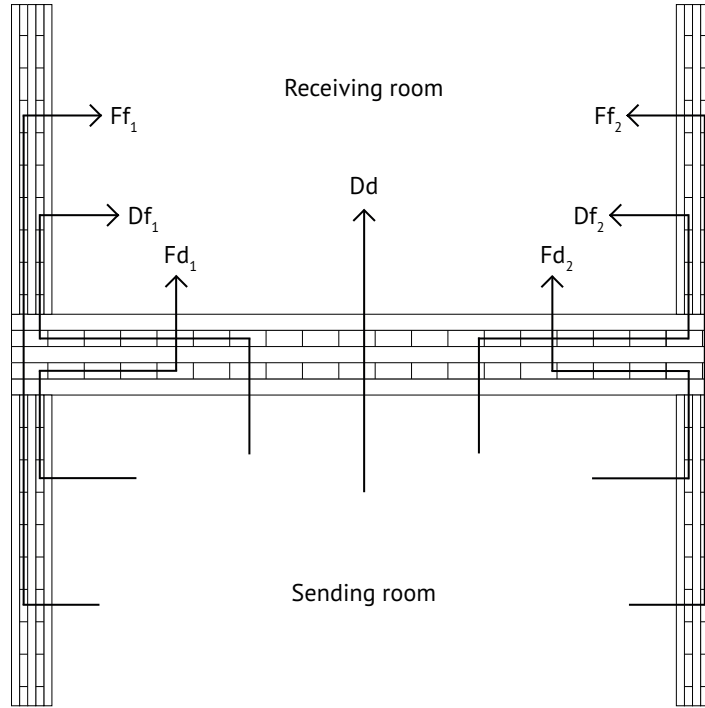
Figure 5.7: Illustration of different sound transmission paths including both the direct sound transmission path and 6 first-order flanking sound transmission paths.

The flanking airborne sound transmission paths are defined in ISO 12354-1 [39]. The sound reduction, including direct airborne sound transmission, R_d, and flanking airborne sound transmission, R_f, is described in Equation 5.3. The equation could be used both during a design phase to predict the sound insulation in the field, and afterward to verify the building's performance. The standard, Ref. [39], also mentions two other paths, defined as R_e and R_s. The first one is the sound transmission from components mounted in the separating element, and the second one is the indirect flanking airborne sound transmission. These paths are not included in Equation 5.3 in this article. The parameter, n, in Equation 5.3 is defined as the number of flanking elements accordingly:

$$R' = R_d + \sum_{f=1}^{n} R_f, \qquad (5.3)$$

The flanking airborne sound transmission is for each path described according to Equation 5.4, based on the simplified model in Ref. [39]. The indexes i and j are described as the source

and receiving surfaces of the structure defined for each flanking path. The sound reduction index for each element, included in the defined flanking path, is described with R_i and R_j in Equation 5.4:

$$R_f = \frac{R_i + R_j}{2} + \Delta R_{ij} + K_{ij} + 10 \cdot \log_{10}\left(\frac{S_s}{l_0 \cdot l_{ij}}\right), \tag{5.4}$$

where S_s is the area of the separating element, l_0 is a reference coupling length and l_{ij} is the coupling length of the junction between the separating and the flanking element. ΔR_{ij} is defined as the sound reduction improvement by additional lining on the source and/or receiving side of the flanking element [39]. Each flanking sound transmission path is described with the vibration reduction index, K_{ij}, presented in Equation 5.4 and described in Equation 5.5 [88]:

$$K_{ij} = \frac{D_{v,ij} + D_{v,ji}}{2} + 10 \cdot \log_{10}\left(\frac{l_{ij}}{\sqrt{a_i \cdot a_j}}\right), \tag{5.5}$$

where $D_{v,ij}$ and $D_{v,ji}$ in Equation 5.5 are describing the direction-averaged velocity level differences between the sending and receiving elements. Furthermore, a_i and a_j are the equivalent absorption lengths of fictional totally-absorbing junctions of each element, i and j, when the critical frequency is assumed to be 1000 Hz. The equivalent absorption lengths are dependent on several factors, including the structural reverberation time of each element [88].

5.2.6 Measurement uncertainty

Measurements of the sound transmission in the field between apartments could vary depending on several factors: including room volume, dividing surface, junctions but also the measurement procedure and the workmanship [187]. Craik and Steel [187] measured the airborne sound transmission of, more or less, identical situations of concrete floors in a building to determine the variation due to the workmanship. They used ten test floors, with one being a control floor that was measured in between every test and the measured rooms had some minor variations of the room dimensions. After a deduction of the variation due to the measurement

procedure, measurements resulted in a variation of 1.5–2 dB per third-octave band for the workmanship. Trevathan and Pearse [188] used a similar approach as Ref. [187] to separate the variation due to the measurement procedure from the variation due to the workmanship. However, walls in 12 pairs of nominally identical dwellings were measured instead of floors with the same room volume and surface area in Ref. [188]. The study resulted in an average third-octave band standard deviation of 1.1 dB due to the workmanship. Ref. [108] measured the airborne sound transmission between lightweight timber floors with nominally identical construction, and measurements resulted in a standard deviation of 0.8 dB due to the workmanship. Simmons [189] found that the weighted sound reduction index variation was 1.0 dB in a round-robin test with eight participating laboratories and seven different floors.

Variations in the airborne sound transmission between apartments in a wood-based system were found to be largest between 50 and 100 Hz in Ref. [17]. Moreover, the variations above 2000 Hz were concluded to be related to the background noise because of excellent performance in high-frequency sound insulation for wooden constructions. Furthermore, variations between floor numbers of 2–3 dB in Ref. [17] are suggested to be attributed to the increasing stiffness of the elastic interlayers on the lower floors, with higher load, between 125 and 630 Hz. In addition, elastomers are found to be primarily effective at high frequencies [17].

Variation due to the method was investigated in Ref. [190] for a lightweight wooden construction with fixed microphone positions and for impact sound levels. The standard deviations due to the method were found to be 0.4 dB from 100 Hz to 0.8 dB from 50 Hz. This study focuses on the airborne sound insulation. However, variations in the method are, to some extent, still applicable from studies on impact sound insulation. Ref. [190] also studied the variation due to the method for manual sweeps where similar results in standard deviation were found as for fixed positions. However, the relative difference in sound level varies to a higher degree between fixed and manually swept microphones in low frequencies.

Measurements in this study in the three different projects were performed by the same

operator (the first author). The same measurement procedure, including loudspeaker and measurement positions, was applied in the same room pairs over the different stories to minimize the variation of the results. Furthermore, Ref. [191] measured the sound insulation in a CLT building and found that the variations due to the measurement procedure were minor compared to the total variations in the building.

5.3   Measurement results and discussion

5.3.1   Results for each project and initial discussion

In total, 58 vertical airborne sound insulation measurements were conducted over the three projects in four different buildings. Furthermore, each project has varying junctions, different dividing elements, different floor plans, and a varying total number of stories.

Project A was measured in two buildings, one with and one without viscoelastic interlayers between the load-bearing CLT walls and the floors. Measurements in project A - building 1 varies with 5–6 stories and this building has no viscoelastic interlayers in the junctions. The difference in vertical airborne sound insulation between high and low stories is displayed in Figure 5.8. Measurements show that there is an overall positive difference in airborne sound insulation between high and low stories, indicating that the airborne sound insulation increases higher up in the building with decreasing load on the junctions. The difference is highest between 500 and 3150 Hz, with minor negative deviations for certain measurements and frequencies below and above the interval. Mean values for small rooms (bedrooms) and larger rooms (living rooms) are displayed separately, and most values are positive, with a few values around 0 dB difference. The deviation between stories is highest for mean values in bedrooms between 500 and 3150 Hz.
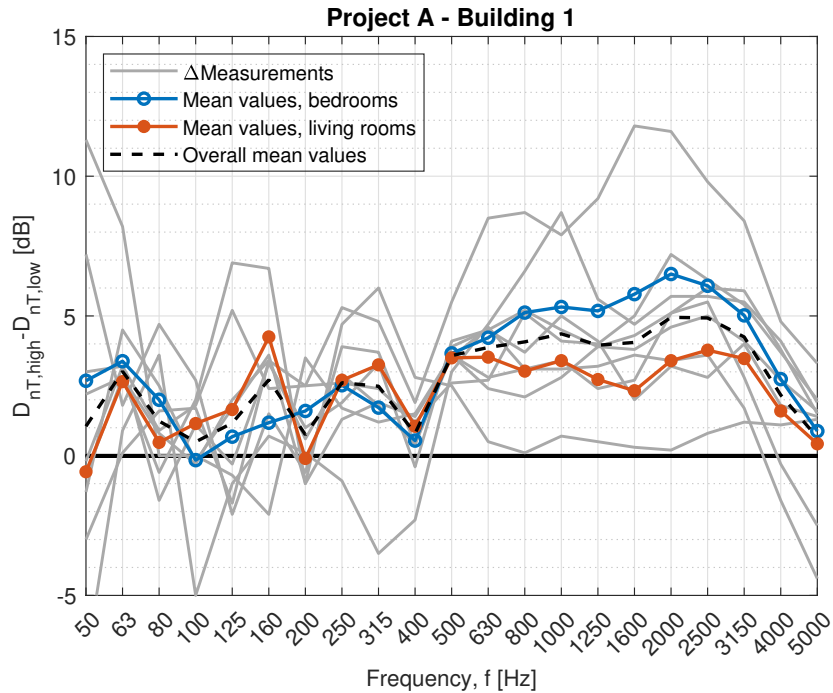
Figure 5.8: Difference in vertical airborne sound insulation between rooms situated in high and low stories for project A, building 1 without viscoelastic interlayers in the junctions.

Measurements in project A - building 2 varies with five stories and this building has viscoelastic interlayers in the junctions. The difference in vertical airborne sound insulation between high and low stories is displayed in Figure 5.9. Measurements also show that there is an overall positive difference in airborne sound insulation between high and low stories, indicating that the airborne sound insulation increases higher up in the building with decreasing load on the junctions. Mean values for small rooms (bedrooms) and larger rooms (living rooms) are displayed separately, and most values are positive, with a few values around 0. The difference in mean values is overall positive, with a difference of 2–5 dB, with some minor deviations between 80 and 200 Hz. In contrast to building 1, there are not the same differences in the sound insulation for small and larger rooms between high and low stories for building 2 in project A.
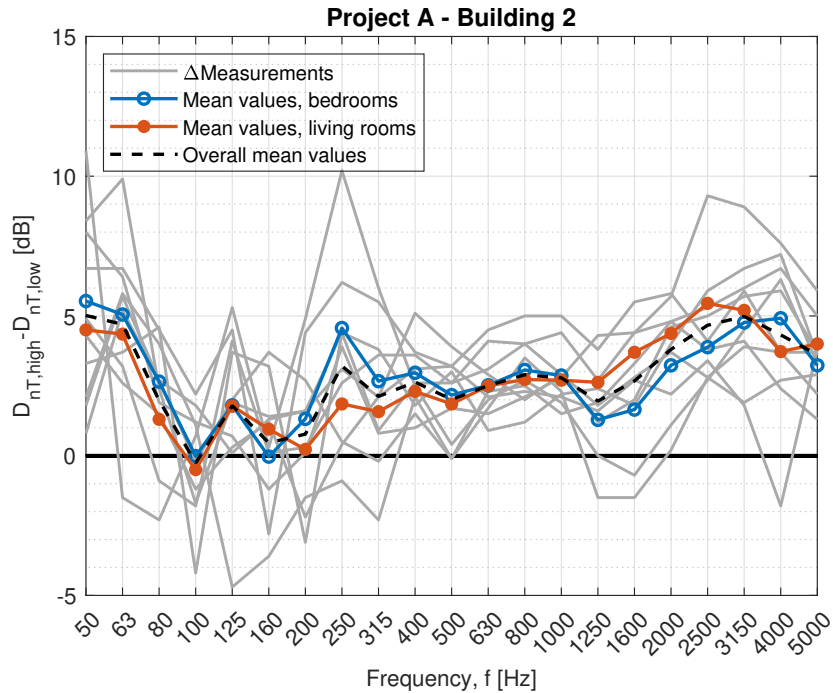
Figure 5.9: Difference in vertical airborne sound insulation between rooms situated in high and low stories for project A, building 2 with viscoelastic interlayers in the junctions.

Project B was measured in one building with viscoelastic interlayers between the load-bearing CLT walls and the floors. Measurements in project B vary with two stories, and the difference in vertical airborne sound insulation between high and low stories is displayed in Figure 5.10. Measurements show that there is an overall positive difference in airborne sound insulation between high and low stories, indicating that the airborne sound insulation increases higher up in the building with decreasing load on the junctions. The difference is highest around 160 Hz, with minor negative deviations between 50 and 100 Hz and overall positive values above 250 Hz. Mean values for small rooms (bedrooms) and larger rooms (living rooms) are displayed separately, and the difference between stories is highest for mean values in living rooms.
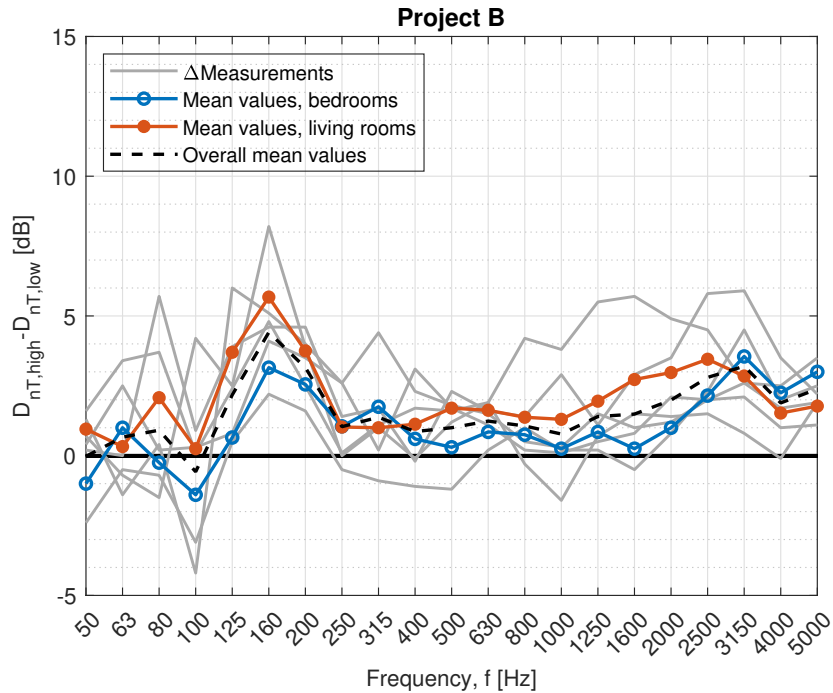
Figure 5.10: Difference in vertical airborne sound insulation between rooms situated in high and low stories for project B with viscoelastic interlayers in the junctions.

Project C was measured in one building with viscoelastic interlayers between the load-bearing CLT walls and the floors. Measurements in project C vary with four stories, and the difference in vertical airborne sound insulation between high and low stories is displayed in Figure 5.11. Measurements show that there is an overall positive difference in airborne sound insulation between high and low stories, indicating that the airborne sound insulation increases higher up in the building with decreasing load on the junctions. The difference is highest between 250 and 2000 Hz, with minor negative deviations for certain measurements below and above the interval. Mean values for small rooms (bedrooms) and larger rooms (living rooms) are displayed separately, and the difference between stories is highest for mean values in bedrooms.
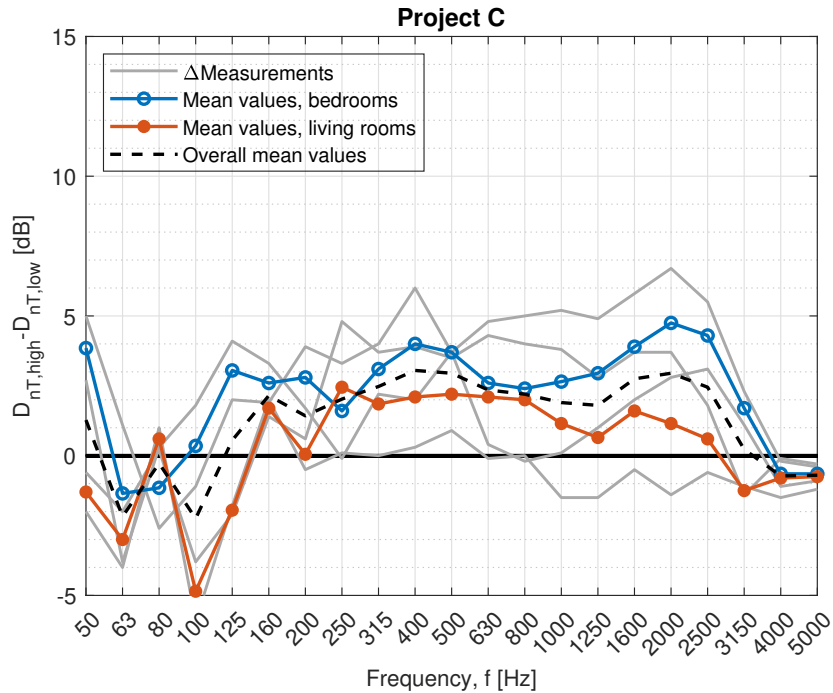
Figure 5.11: Difference in vertical airborne sound insulation between rooms situated in high and low stories for project C with viscoelastic interlayers in the junctions.

The measurements in each project indicate a difference in sound insulation between stories. The sound insulation between stories improves higher up in the building from around 200 Hz. The same type of difference in airborne sound insulation between stories is also observed in Ref. [108]. Moreover, similar principles are also observed for the vibration reduction index in Ref. [19]. Since the dividing floor structure is more or less the same over the different stories, it is not likely an explanation for the differences. Furthermore, in project A, thinner CLT walls and floors are used higher up in the building, which should acoustically perform worse and not better. Therefore, the difference in sound insulation between stories should be explained by the flanking paths, related to Equation 5.4, and thereby the load on the junctions rather than the direct path.

Previous studies with a related subject on lightweight timber buildings, mentioned above, shows that the airborne sound insulation or the vibration reduction index improves higher up in the building [19, 108]. Both buildings have viscoelastic interlayers in the junction to reduce the flanking sound transmission. One possible explanation is that a higher load, due to

more stories above the junctions, results in stiffer viscoelastic interlayers and, therefore, more sound transfers in the junctions. This explanation correlates well with the projects measured in this article that have viscoelastic interlayers in the junctions and measurements in previous studies [19, 108]. However, in project A, the airborne sound insulation was measured in two similar buildings with one significant difference. Building 2 has viscoelastic interlayers under the load bearing CLT walls and in building 1, the viscoelastic interlayers are removed. Furthermore, treatments on the walls and the floors are the same in both buildings with similar plan orientations. Therefore, the difference in stiffness of the viscoelastic interlayers, dependent on the load and, thereby, the number of stories, is not the whole explanation behind the difference in vertical airborne sound insulation between high and low stories measured in the presented CLT buildings. The main factor that changes in the measurements is the load on the junction, which could have the largest effect on the difference in sound insulation between stories, regardless of the presence of viscoelastic interlayers or not in the junction for CLT buildings. Similar results are observed in Refs. [16, 185]. Furthermore, Ref. [185] explains that the decrease of vibration reduction index in the junction due to increased load is because of the increased stiffness of the joint.

5.3.2   Measurement uncertainties and variations

Measurements in the different projects vary with several decibels depending on the apartment type and rooms. This variation is likely caused by the variations in flanking sound transmission paths by the building elements and the vibration reduction index over the same story.

There are some differences in the dimensions of the cross-laminated timber walls and floors depending on stories in project A, where the thickness is reduced higher up in the building. However, this should result in a lower standardized level difference on the higher stories compared to the lower ones and, therefore, negative values in the figures because thinner walls and floors usually perform acoustically worse. Instead, the opposite is observed for the majority of the measurements.

The same measurement procedure was applied in all projects for the room pairs, meaning that the same loudspeaker and measurement positions were used in the same type of rooms in both the lower and higher stories. Moreover, the same operator (the first author) performed all measurements presented in the article. The remaining variations are, therefore, likely due to the construction, load, and the workmanship. As stated in section 5.2.6, workmanship have a variation of between 0.8 and 2 dB per third octave band [108, 187, 188]. However, the value of the variation in the lower interval, around 1 dB, was concluded between apartments that were identical in room shape, which is consistent with the compared results in the measured projects. Consequently, the measurement variation due to workmanship for this study is estimated to be around 1 dB per third-octave band.

The variation due to the construction should be minimal in the calculated result because the same type of junctions and constructions are used in the compared rooms (higher and lower stories). Viscoelastic interlayers were also carefully selected in each project for different stories during the design phase to have a suitable stiffness for the load, unlike the project in Ref. [108]. Therefore, it is unlikely that the explanation for the variations in the measurements is due to a wrong selected stiffness of the viscoelastic interlayers for the load.

The reverberation time was only measured in 3 measurement positions with a total of 6 measurements together with one loudspeaker position. The reason was partly to save time on the measurement site but also because the geometry of the rooms is rectangular and, therefore, not an odd shape. However, the reverberation time should not affect the result because the same type of room pairs are measured and compared with each other. There are very small, if any, differences between the rooms on the different stories. Moreover, according to ISO 3382-2 [153], it is accepted to use three measurement positions with a total of 6 measurements together with one loudspeaker position when the result is used as a correction term to other engineering-level measurements.

It is reasonable to argue that the variation between floors is mainly due to the load on the junctions with three statements. First, the variation due to the measurement procedure

is found to be small in comparison with the total variations in buildings [191]. Second, the observed variation due to the workmanship is found to be around 1 dB for the airborne sound transmission when the rooms are similar [108, 188]. Third, if the variations were mainly due to the workmanship or the measurement procedure, a systematic difference would be observed with values spread more evenly around a 0 dB difference, which is not the case.

5.3.3 Extended discussion and analysis

5.3.3.1 Comparison of measurement mean values for each project and building

Figure 5.12 compares the mean values for each project and building to visualize the difference in airborne sound insulation between stories. Furthermore, the scale on the y-axis is shifted to visualize the difference between the different projects and buildings easier. The mean values indicate that there is a noticeable difference in vertical airborne sound insulation between stories, as confirmed earlier, and the mean values have a positive effect starting from around 125 Hz. However, the results have a spread of several decibels over the frequency range, and there is no clear correlation between the improvement and the different buildings.

The difference in the number of stories between high and low levels for the measurement results variates between two to six stories depending on the project and the building. By dividing the result in Figure 5.12 with the difference in the number of stories for each measurement in each project and building, a linear correlation between the number of stories and airborne sound insulation improvement is observed, see Figure 5.13. A linear correlation is however an assumption. If measurements were carried out on each story, a more precise estimation would be achieved. However, there was not enough time on the building site to test all rooms over the different stories due to a tight time schedule of the building contractors. Overall, there is a good agreement between the difference in vertical airborne sound insulation per story for each project for frequencies between 250 and 2000 Hz with a linear correlation. The improvement in sound insulation further up in the building is vaguely apparent in low frequencies. However, the improvement is clearly apparent in mid-frequencies, around the

suggested region for the critical frequencies of CLT panels, and also in higher frequencies. Above 2000 Hz, the mean values are spread and reduced, which is likely due to the background noise. Both the direct and the flanking sound transmission usually have a lower influence in high frequencies, meaning that the receiving values measured in the different rooms are affected, to a higher degree, by the background noise because there is a limit in sound power from the sound source. Therefore, the difference in high frequencies is expected to be higher than the ones presented in the table in Figure 5.13 when used in predictions. Furthermore, the difference in low frequencies for measurements could be caused by the direct sound transmission because of the different floor structures in the projects and the variation in measurement procedure which increases for low frequencies [17, 187]. However, one peak stands out compared to the other projects in the measurements for project B around 160 Hz in Figure 5.13, which is discussed further in Section 5.3.3.2.
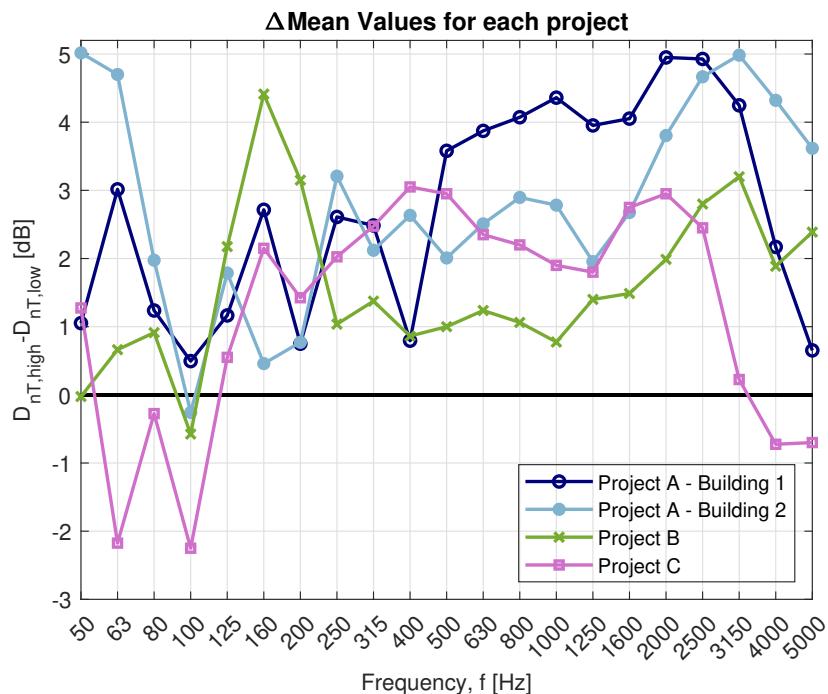
Figure 5.12: Mean values of the difference in vertical airborne sound insulation between high and low stories for each building and project.
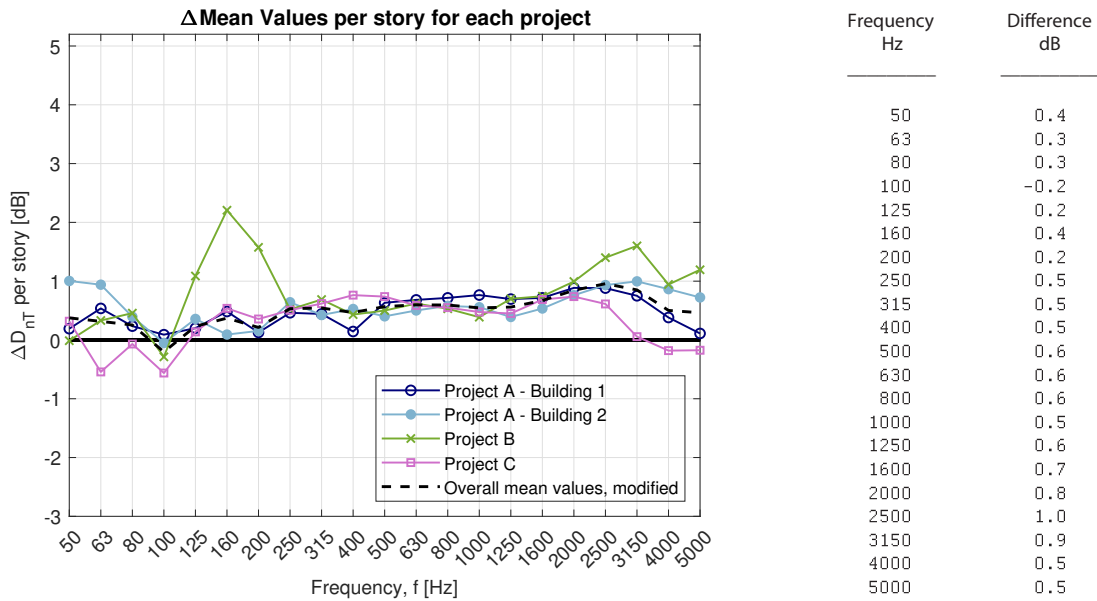
Figure 5.13: Mean values of the difference in vertical airborne sound insulation between high and low stories, per story, for each building and project. Moreover, the overall mean value curve is shown with modifications between 125 and 200 Hz. Alongside the diagram is a table with rounded values for the modified mean value curve with the difference between high and low stories, per story.

5.3.3.2 Deviation in mean values for project B around 160 Hz

Project B uses a thick viscoelastic interlayer, and it is the thickest viscoelastic interlayer used in the different projects measured. Measurements collected by Timpte [18] display that there is a local drop in the vibration reduction index for resilient interlayers with and without load around 250 Hz and that the load changes the vibration reduction index the most around that peak. However, the result contradicts what was observed in measurements in this article and other studies [16, 19, 108, 185]. Crispin et al. [185] show that the vibration reduction index with the minor load increases by over 5 dB around 315 Hz for an elastic interlayer of natural rubber compared to measurements with high load, and more peaks occur around 630 Hz. They observe that the peaks shift to higher frequencies when the load increases. In addition, they present a possible explanation that "these maxima occur in the frequency range where the magnitude of the shear impedance of the interlayer matches the magnitudes of the point impedance on the plate edge" [185]. The peak around 160 Hz observed in project

B in Figure 5.13 could be caused by the combination between stiffness and thickness of the viscoelastic interlayer and the load combined with some visible CLT walls because the combination between load and stiffness varies over stories. Another explanation could be related to the mounting procedure of CLT elements. Viscoelastic interlayers are designed to be compressed when loaded to an optimal state and further down in the building; they are designed for a load when the whole building is finished and when people have moved in. For project B, brackets were mounted on each story, holding the walls in place. The load will likely be divided partly on the viscoelastic interlayers and partly via the brackets when more and more stories are mounted if the brackets are not dismounted and mounted again when the whole building is finished. Therefore, the viscoelastic interlayers on the lower stories may not be in their optimal state, which could have a more significant effect on thicker viscoelastic interlayers at certain frequencies. In combination with the system of the building, this could be another explanation for the peak around 160 Hz. The peak is indicated in all measurements for project B, which indicates that it is correlated with the design system, see Figure 5.10.

Because of the peak around 160 Hz in Figure 5.13 for project B, the overall mean value curve is modified to not include values between 125 and 200 Hz from project B since it is suggested before that it is related to the specific design system of the project.

5.3.3.3   Comparison in mean values with and without elastomer in the junctions

In Figure 5.14, measurements from project A were measured with a difference between five and six stories. To evaluate the difference between the buildings with and without elastomers for the effect of load on the junction, measurements are adapted to a difference of five stories.

In Figure 5.14, the difference in sound insulation between stories is the largest without an elastomer for the interval between 500 and 2000 Hz and similar for the other frequencies. This result indicates that the stiffness of the elastomer has less effect on the difference in vertical airborne sound transmission between stories at high and low levels in the building. The result also show that the actual load is the primary dependent factor for the difference,

with or without an elastomer, in cross-laminated timber buildings.
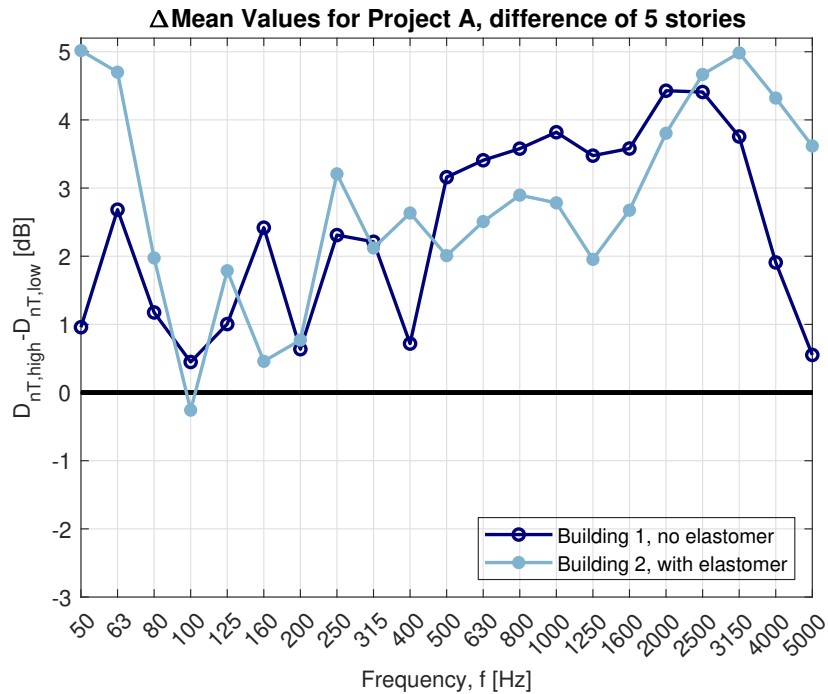
Figure 5.14: Mean values of the difference in airborne sound insulation between high and low stories, with a difference of 5 stories, for building 1 and 2 in project A.

5.3.3.4 Difference in room volumes and room modes

Measurements in the different projects have various room volumes, and for some rooms, the floor area is smaller than 10 m^2. The small floor area makes it difficult to follow the requirements in ISO and ASTM regarding minimum distances between room boundaries, loudspeaker, and microphone position. However, measurements in this article focus on the difference in sound insulation between high and low stories. Therefore, the effect of smaller rooms has less significance because the same measurement method is applied in the same room configurations.

Measurement data in Figures 5.8 to 5.11 show differences in sound insulation depending on if the room volume is large or small, but the result variates, and no clear conclusion can be made from the result. In project A, building 1, differences are more or less the same except for mid to high frequencies, where bedrooms show bigger differences in sound insulation

between high and low stories. In project A, building 2, rooms with larger and smaller volumes show similar differences between high and low stories. For project B, rooms with larger volumes have a bigger difference between high and low stories compared to rooms with smaller volumes. On the contrary, in project C, the opposite is indicated: rooms with smaller volumes have a bigger difference between high and low stories compared to rooms with larger volumes. Measurements in project B and C are not of the same numbers compared to project A, which could be one of the reasons why the effect of room volume changes between projects. Nevertheless, the result is still clear that the load affects the sound insulation.

Larger rooms have a more diffuse sound field than small rooms [191], indicating that results in larger rooms are more accurate. However, smaller rooms have bigger flanking surface areas in relation to the surface area of the dividing element, compared to a large room, which implies higher flanking sound transmission. Therefore, a bigger difference should be visible for small rooms compared to large rooms. Anyhow, measurements show minor differences in mean values for large and small rooms when the difference in airborne sound insulation is compared between high and low stories.

Rooms with identical dimensions, and thereby same volumes, have the same eigenfrequencies, which, according to Ref. [192] in Ref. [191], leads to a strong acoustic coupling. Furthermore, Ref. [193] highlights that this acoustic coupling generates large variations in sound level difference between normal room modes that are perpendicular to the dividing element, and particularly when the room dimensions are the same. Measurements in this study were made vertically with the same floor plan per project and building, and each measurement had the same volume for sending and receiving room. However, the room modes should not have a significant difference on the result since the difference in vertical airborne sound insulation between high and low stories is evaluated and not the actual values between apartments.

5.3.3.5 Application of the result to other projects and buildings

Measurements in this article have focused on buildings constructed with CLT elements. Airborne and impact sound insulation measurements in concrete houses showed no specific difference in weighted indices depending on the number of stories [194]. However, concrete houses may have a lower effect on the flanking sound transmission compared to wooden buildings, and specifically buildings with CLT elements that have a large radiating surface area. Furthermore, if flanking paths are more suppressed, the difference in sound insulation between stories is likely less relevant. In addition, junctions in concrete buildings can be considered stiffer than junctions with CLT elements. Therefore, the increase in load might have a lower effect on the stiffness of the junction in concrete buildings compared to CLT buildings. Consequently, the same result in this article cannot be expected in a concrete building, and specifically in a building with low-flanking sound transmission.

Since the measured airborne sound insulation is a combination of different transmission paths, including the direct transmission path and flanking transmission paths, the effect of the load on the junction is likely different depending on the project and the acoustical treatments. The values presented in Figure 5.13 are mean values for all measurements. Therefore, they should be used as an overall estimation for a project when the flanking transmission paths have an influence on the sound insulation. For a more precise model, the flanking sound transmission paths, and specifically the vibration reduction index, must be investigated further with the same principles as this article.

5.3.3.6 Weaknesses and justifications of the presented result

Figure 5.13 show how the airborne sound insulation improves per story. Another alternative would be to correlate the airborne sound insulation improvement with the load. However, the load on each junction could vary over the whole wall, and it could also differ depending on the load-bearing walls. Moreover, since the vertical airborne sound insulation between apartments is a combination of at least 13 different sound transmission paths for a rectangular

room with four walls, different elements, and potentially also different vibration reduction indices of junctions make it complicated to quantify how much the load affects the result. There could be a few flanking paths that more or less determines the airborne sound insulation between different rooms. Each flanking path could be estimated by Equation 5.4, but the equation consists of many unknown factors, such as the vibration reduction index. If the load on the junctions were compared with the airborne sound insulation, all paths with different load combinations would be considered, which could have a negative impact on the accuracy of the result. Therefore, it is more reliable to instead use the number of stories as a factor and not the actual load.

This article has investigated vertical airborne sound insulation, which is a result of both the direct path and all the flanking paths, presented in Equation 5.3, and also other paths described further in ISO 12354-1 [39]. Measurements show that the increase in the number of stories, or the increase in load, has a negative effect on the vertical airborne sound insulation between stories. This effect is likely caused by the flanking sound transmission because the main factor that changes between measurements is the number of stories where the measurements took place. To evaluate this further, vibration reduction index measurements of the junction are required where the difference in velocity levels over the junction is measured and calculated as described in Equation 5.5.

5.4   Conclusions

The purpose was to investigate if the building height, and thereby the load, has an effect on the vertical airborne sound insulation between apartments on different stories in different cross-laminated timber buildings.

Measurement data on several projects and buildings with a different number of stories and various building systems show that the load has a negative effect on the vertical airborne sound insulation between dwellings. Measurements also indicate that the load has a similar

effect regardless of the presence of elastomers. With or without elastomers, increasing load yields a higher sound transmission between apartments and, therefore, lower sound insulation.

Measurements were tested between two and six-story differences for buildings with a total of six to twelve stories. The result shows that the vertical airborne sound insulation can differ up to 5 dB in third-octave bands between single measurements, caused by the difference in the number of stories, with reduced sound insulation further down in the building. In addition, the mean difference per story over the measured frequency range is calculated to 0.5 dB. Although 0.5 dB is a low number, a difference of 6 levels in a CLT building is expected to have a mean difference of 3 dB, which starts to have a more significant effect. Furthermore, if the mean value difference is applicable to higher buildings with more levels than investigated in this study, a 10-story difference or more could yield a mean difference in vertical airborne sound insulation of a minimum of 5 dB, which has a significant effect. Therefore, with increasing building height in high-rise CLT buildings, the load on the junction should be considered to choose the right treatments and to ensure good sound insulation performance, specifically at the lower levels. Moreover, if the load is not considered, measurement results could vary significantly between stories, which could have a significant effect on the final evaluation of the project. Thus, negatively affect the well-being of future occupants, specifically for CLT buildings.

Measurement result also highlights the importance of measuring the sound insulation on different levels in buildings made with CLT and not only focusing the measurements on a specific level in the building. By measuring on different levels, a more suitable average of the acoustical performance of the project is achieved since the load is concluded to have an effect on the airborne sound insulation between apartments.

For further investigation, measurements are needed in more wooden lightweight high-rise buildings below and above ten stories, with various building systems, to verify similarities with the result in this study and to determine the effect for higher buildings.

5.5 Additional work

After publication of the article [177], more work was made both to understand the measurement uncertainties and to precise the estimations per story.

5.5.1 Measurement method uncertainty

When measurements in general, but specifically in the field, are used in estimations, it is necessary to evaluate the uncertainties. In Section 5.3.2, measurement uncertainties due to several factors were described. With this in mind, the uncertainties due to the measurement method were evaluated in a new CLT building. This new CLT building was not part of the previous evaluations in this chapter, and vertical airborne measurements were made between living rooms in two apartments vertically adjacent to each other. The measurements followed the procedure in Section 5.2.4. A total of 10 measurement series were performed to evaluate the uncertainties caused by the measurement method correctly, and the result is presented in Figure 5.15, where all ten measurements are displayed. The level difference is presented without considering the reverberation time since the same time was used within each measurement pair, as discussed in Section 5.2.4.

The spread between individual measurements is not visible in Figure 5.15. To closer evaluate the uncertainties, relative differences are calculated and presented in Figure 5.16. The lowest standard deviation of the relative differences was calculated for each measurement, and measurement 4 yielded the lowest standard deviation. Thus, measurement 4 is used as a reference value to present the relative differences by taking Meas.4-Meas.X where X is an integer between 1-10. The spread is overall higher at lower frequencies, which is common and found in previous literature [17]. The spread is also increasing at higher frequencies above 2500 Hz, likely due to the background noise found in Ref. [17]. In general, the spread is acceptable, with slight deviations in mid-frequencies.
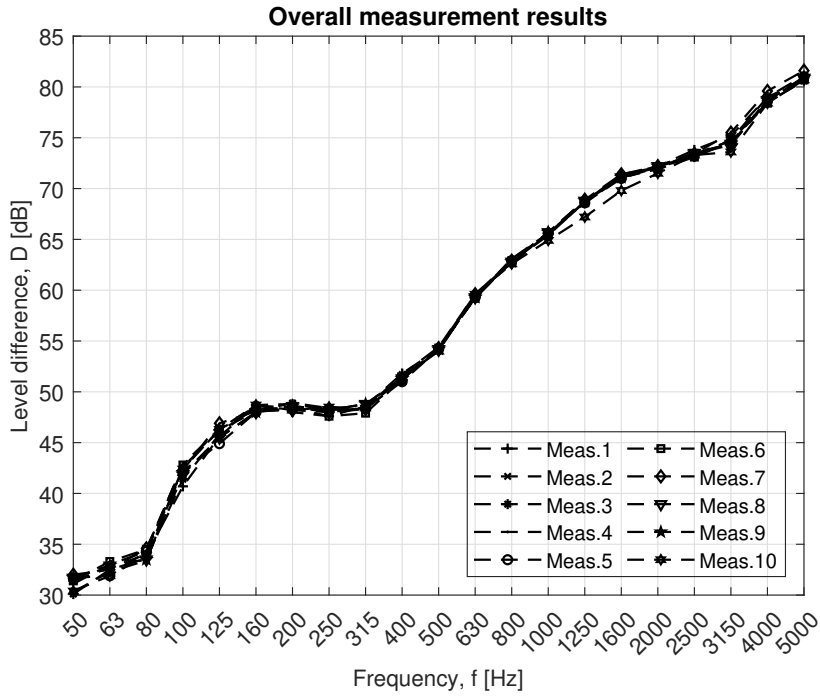
Figure 5.15: Vertical airborne sound insulation measurements, measured a total of 10 times between the same apartments.
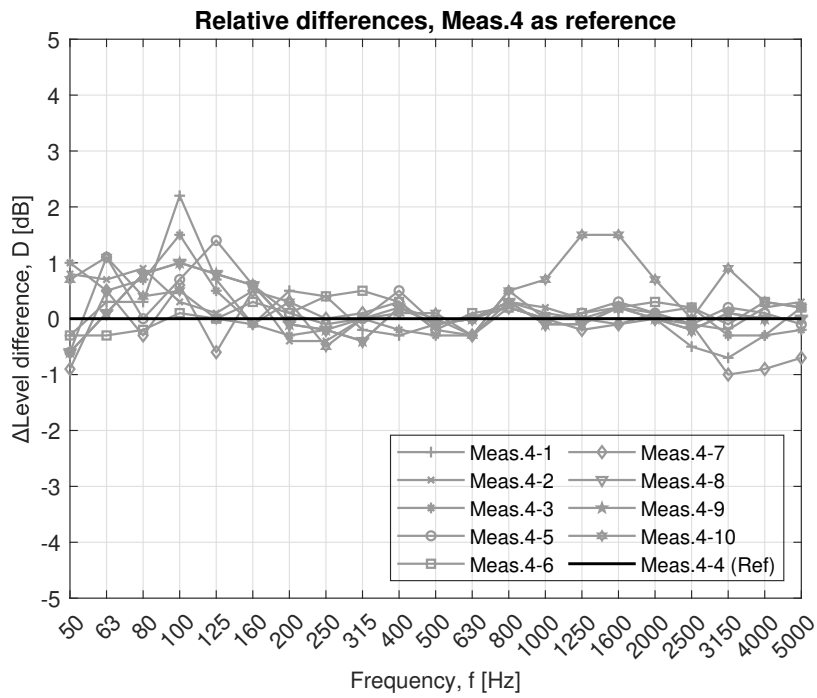
Figure 5.16: Relative differences for measurements between the same rooms. Meas.4 is used as a reference.

Additionally, the standard deviation per third-octave frequency band is calculated separately in Figure 5.17. It is evident in Figure 5.17 that higher deviations occurred for lower and higher frequencies in the measurements.
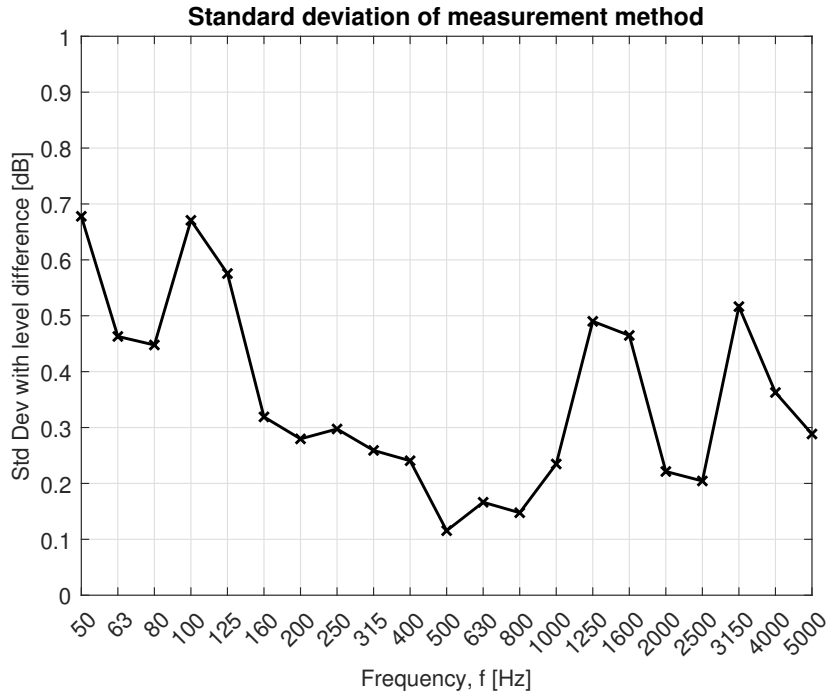
Figure 5.17: Standard deviation of the measurement method, vertical airborne sound insulation.

With the evaluated uncertainties in the measurement method, previous estimations should be displayed with the standard deviation due to the measurement method. Prior to that, some adjustments are required. The standard deviation curve in Figure 5.17 is for one measurement of the sound insulation, and it applies to measurements at the higher and the lower stories. Consequently, the difference in sound insulation between two measurements across various stories is influenced by two standard deviations. The standard deviation for the difference between two measurements, σ_{diff}, is calculated using Equation 5.6:

$$\sigma_{\text{diff}}(f) = \sqrt{\sum_{n=1}^{i} \sigma_n(f)^2},\tag{5.6}$$

where σ_n is the standard deviation of the measurement method and i is the number of standard

deviations (two in this case). By modifying the result in Figure 5.17 with Equation 5.6, the result in Figure 5.18 is formed. The standard deviation presented in Figure 5.18 can be used along with the presented data in Figures 5.8 to 5.12.
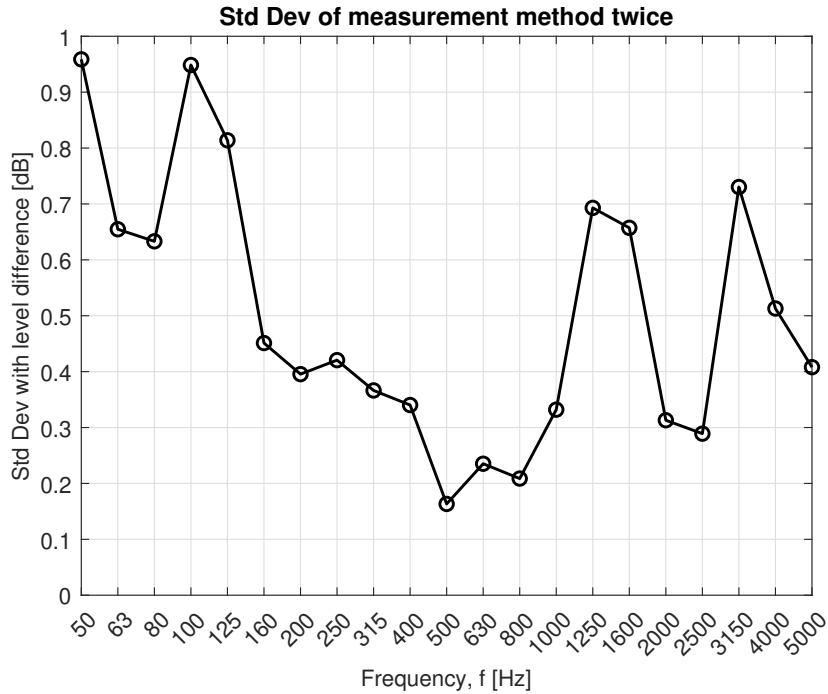
Figure 5.18: Standard deviation of the measurement method, difference in vertical airborne sound insulation.

The standard deviation curve presented in Figure 5.18 does not accurately reflect the estimations per story in Figure 5.13 without additional modifications. The values in Figure 5.13 are calculated from Figure 5.12, where the curves are divided with the difference in the number of stories for each measurement pair. Thus, the same approach should be used to calculate the standard deviation in Figure 5.18 per story for each measurement pair, $\sigma_{\text{n, diff per story}}$, following Equation 5.7, where the differences are assumed to be identically distributed across the number of stories:

$$\sigma_{\text{n, diff per story}}(f) = \frac{\sigma_{\text{diff}}(f)}{\Delta \text{Number of stories}}. \tag{5.7}$$

The standard deviation per story for each measurement pair, $\sigma_{\text{n, diff per story}}(f)$, is combined to

one average standard deviation per story using the root mean square (RMS) method according to Equation 5.8:

$$\sigma_{\text{per story}}(f) = \sqrt{\frac{\sum_{n=1}^{i} \sigma_{n,\text{diff per story}}(f)^2}{k}}, \qquad (5.8)$$

where k is the number of measurement pairs. Lastly, the overall standard deviation of the measurement method per story from the measurements in the article [177] is achieved and presented in Figure 5.19.
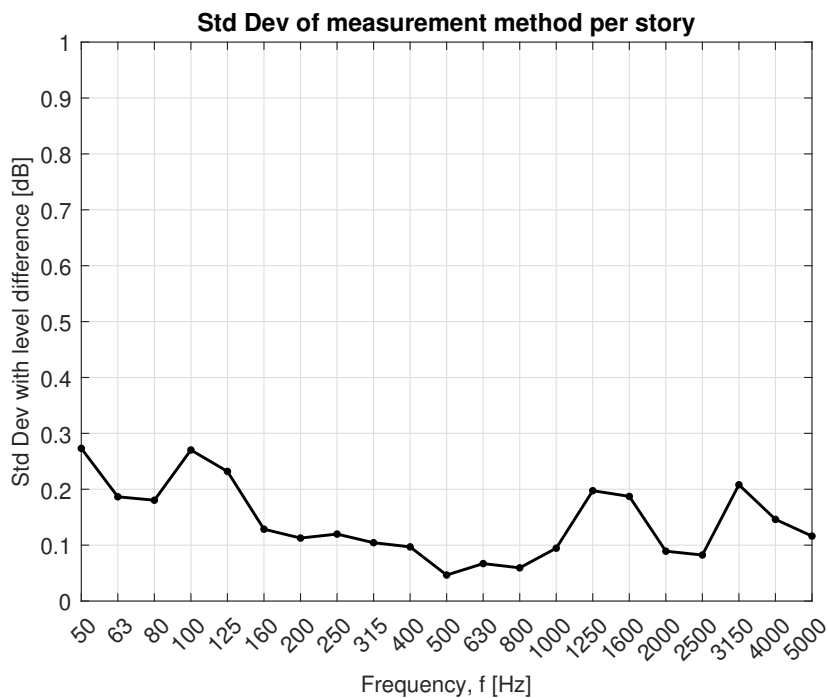
Figure 5.19: Standard deviation of the measurement method, difference in vertical airborne sound insulation per story.

5.5.2 Measurements on each story

Schoenwald et al. [117] highlighted in a paper that the vibration reduction index only decreased with an increased load of a simulated first story in a laboratory and that the vibration reduction index remained, more or less, unchanged with more load. The vibration reduction index affects the flanking sound transmission, and a lower vibration reduction index leads to higher

flanking sound transmission and worse sound insulation if the flanking transmission paths affect the total sound insulation.

Measurements named "high" in this chapter and in the article [177] primarily focused on the upper stories before people had moved in. Thus, the findings in this chapter could, to some extent, result from the difference in the initial load of the first story following the result found in Ref. [117]. To properly investigate this, measurements were conducted in a building with the same construction system as Project A between several apartments on top of each other in two different types of rooms. Measurements were performed following the procedures in Section 5.2.4 in a bedroom and a living room between stories, illustrated in Figure 5.20.

Buiing simlar to Project A
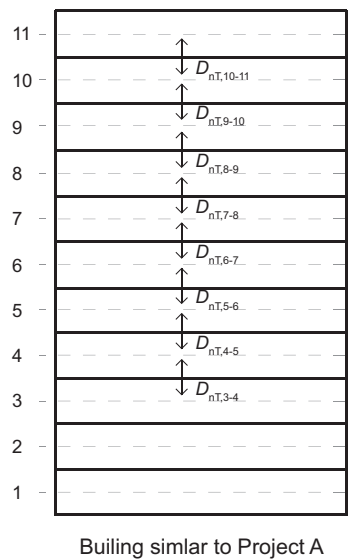
Figure 5.20: An illustration where measurement occurred in the project similar to building A where the vertical airborne sound insulation was measured on each story with CLT.

Initial evaluation of the weighted standardized level difference reveals interesting findings. In Tables 5.1 and 5.2, differences are observed in the weighted standardized level difference for the living rooms and the bedrooms. The highest vertical measurement in the building (between stories 10-11) is used as a reference value, and vertical airborne sound insulation values across different stories are subtracted from the reference value. A positive value signifies a decreased sound insulation with increased load on the junctions lower down the building.

The differences between stories are higher in the living room than in the bedroom, likely

due to the flanking sound transmission. The living room is built up with four load-bearing CLT walls, while the bedroom only contains two load-bearing CLT walls. Therefore, larger differences are anticipated in the living room, Table 5.1, compared to the bedroom, Table 5.2.

It is essential to highlight that with few flanking surfaces, the building height effect is expected to have a minor impact on the sound insulation. The differences are overall decreasing with the number of stories, and it is more apparent in the living room (see Table 5.1). Furthermore, the difference in sound insulation is most significant on the higher floors, and the effect diminishes slightly lower down the building.

Table 5.1: Weighted airborne sound insulation differences [dB] per story in the living room. Reference values are used on stories 10-11 and positive values represent a decrease in sound insulation lower down the building.

Stories	3-4	4-5	5-6	6-7	7-8	8-9	9-10	10-11
$\Delta D_{\mathbf{n}T,w}$	5	4	3	3	2	3	1	0
$\Delta D_{\mathbf{n}T,w,50}$	4	3	3	3	2	2	2	0

Table 5.2: Weighted airborne sound insulation differences [dB] per story in the bedroom. Reference values are used on stories 10-11 and positive values represent a decrease in sound insulation lower down the building.

Stories	3-4	4-5	5-6	6-7	7-8	8-9	9-10	10-11
$\Delta D_{\mathbf{n}T,w}$	3	3	3	3	3	2	1	0
$\Delta D_{\mathbf{n}T,w,50}$	4	4	3	3	3	3	2	0

Tables 5.1 and 5.2 present the differences in weighted values, and variations across third-octave frequency bands could provide valuable insights. The differences between measurements at various stories in the building are displayed in Figures 5.21 and 5.22. The data is calculated by subtracting the measurements on different stories ($D_{\mathrm{n}T,10-11}$, $D_{\mathrm{n}T,9-10}$, $D_{\mathrm{n}T,8-9}$, $D_{\mathrm{n}T,7-8}$, $D_{\mathrm{n}T,6-7}$, $D_{\mathrm{n}T,5-6}$, $D_{\mathrm{n}T,4-5}$, $D_{\mathrm{n}T,3-4}$) from the measurements at the highest story ($D_{\mathrm{n}T,10-11}$), see Figure 5.20 for clarification.
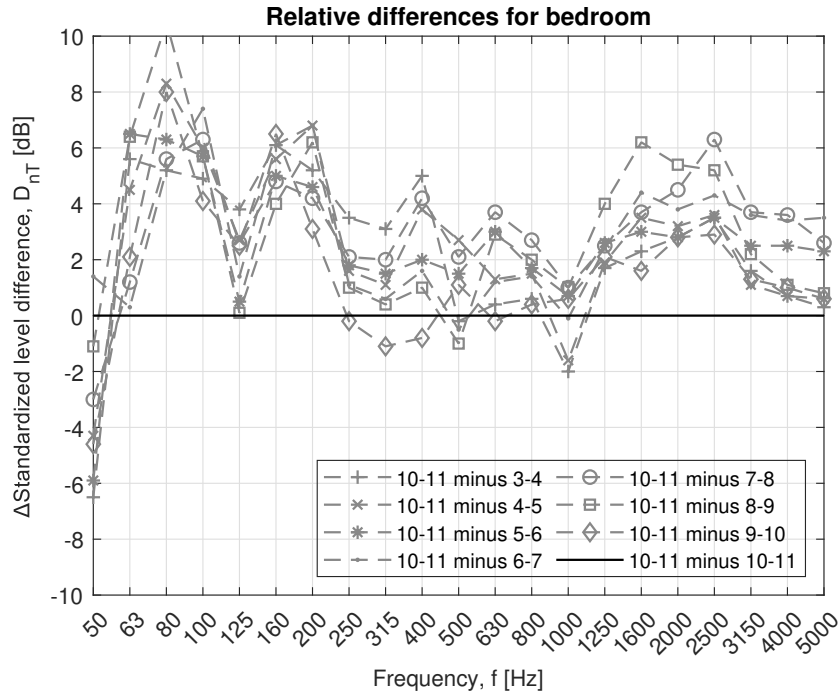
Figure 5.21: Relative vertical airborne sound insulation differences between measurements in the bedrooms at the highest story compared to the other stories.
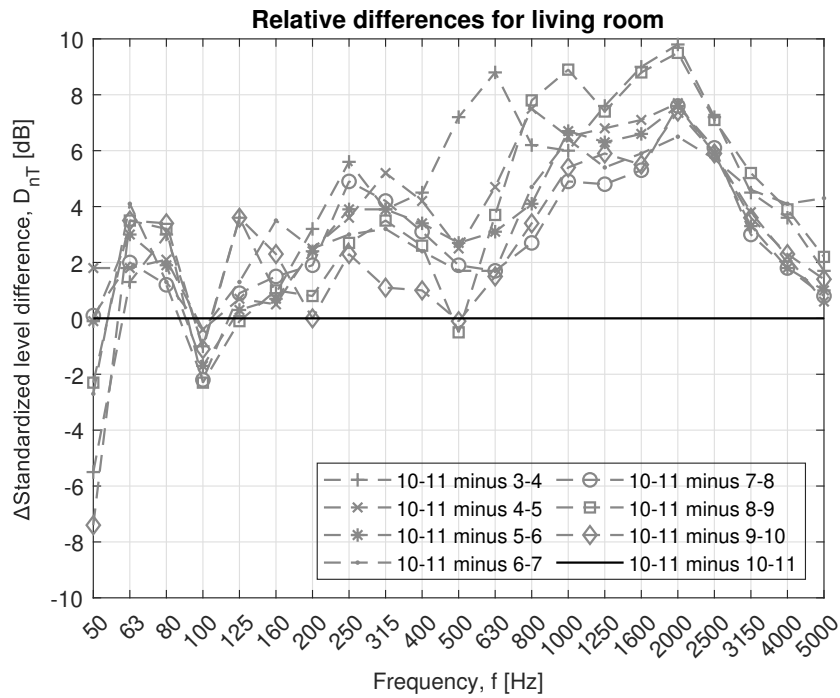
Figure 5.22: Relative vertical airborne sound insulation differences between measurements in the living rooms at the highest story compared to the other stories.

The curves in Figures 5.21 and 5.22 are mainly positive, with minor deviations at specific frequency bands for certain measurements. Positive values indicate a worse sound insulation lower down the building, and the result agrees with previous findings.

However, as highlighted in a paper by Schoenwald et al. [117], initial loading after the first story should not yield a notable difference. Thus, measurements from the lowest story should instead be subtracted from the measurements on the different stories. In Figure 5.23, relative differences between measurements at different stories are illustrated separately. Measurements between stories 3-4 are subtracted from measurements at the various stories.

Overall, measurements in Figure 5.23 show that the airborne sound insulation is decreasing over the number of stories (lower down the building), even after a few stories down. This decrease is represented by positive values in Figure 5.23. The effect is somewhat smaller lower down the building compared to higher floors. Altogether, the building height effect has the most significant impact on the vertical airborne sound insulation highest up in the building, and the differences stabilize lower down the building.

The uncertainties caused by the measurement method have a larger effect when the vertical airborne sound insulation is measured and evaluated on each story, compared to if the sound insulation is measured with a few stories difference and divided with the difference in number of stories. Thus, evaluations should be based on measurements with a few story differences, as presented in Ref. [177].

This chapter demonstrates that an increasing building height results in worse sound insulation lower down the building, likely due to higher loads on the junctions. According to Crispin et al. [185], these higher loads on junctions increase the dynamic stiffness of the joint, leading to a more significant transfer of sound energy over the junction. Furthermore, the increased loads can result in a larger contact area in the junction between the CLT elements, thereby resulting in more flanking sound transmission.
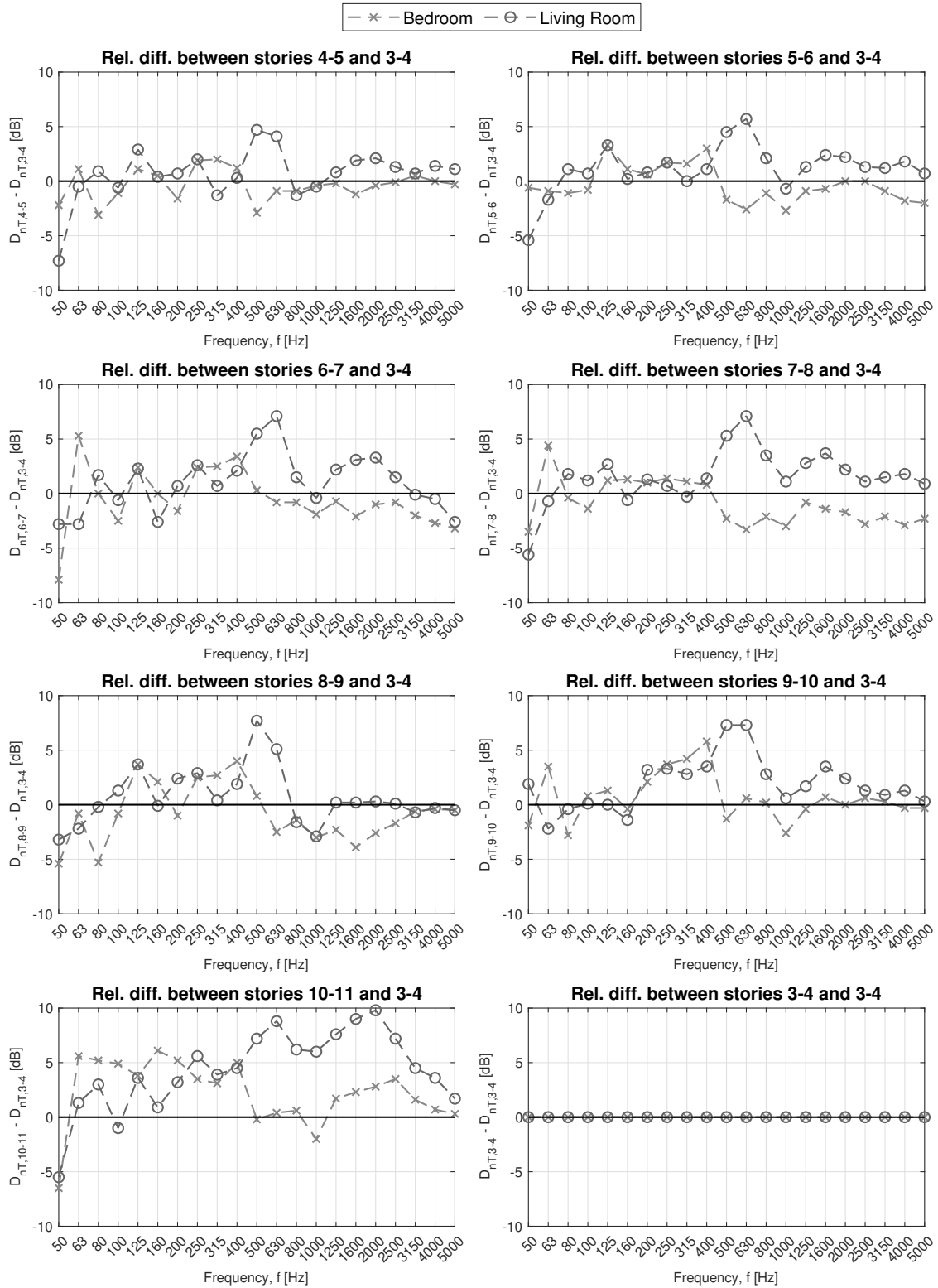
Figure 5.23: Relative vertical airborne sound insulation differences between measurements at the lowest story compared to the other stories.

The mean value difference per story is evaluated for all measurements, and the result is presented in Figures 5.24 and 5.25 where a one-story difference is used. The differences per story are not always positive in the graphs, indicating that the sound insulation at certain frequency bands is not decreasing lower down the building. However, the measurements are, to a higher degree, more affected by uncertainties in the measurement method. Moreover, the curves' overall mean value differences are calculated to 0.3 dB for the bedroom and 0.5 dB for the living room. The overall mean value differences align well with the findings presented earlier in this chapter and the article [177] for the three projects. The result suggests that the vertical airborne sound insulation tends to decrease lower down the building, but randomly selected vertical measurements with a one-story difference may not show substantial differences.
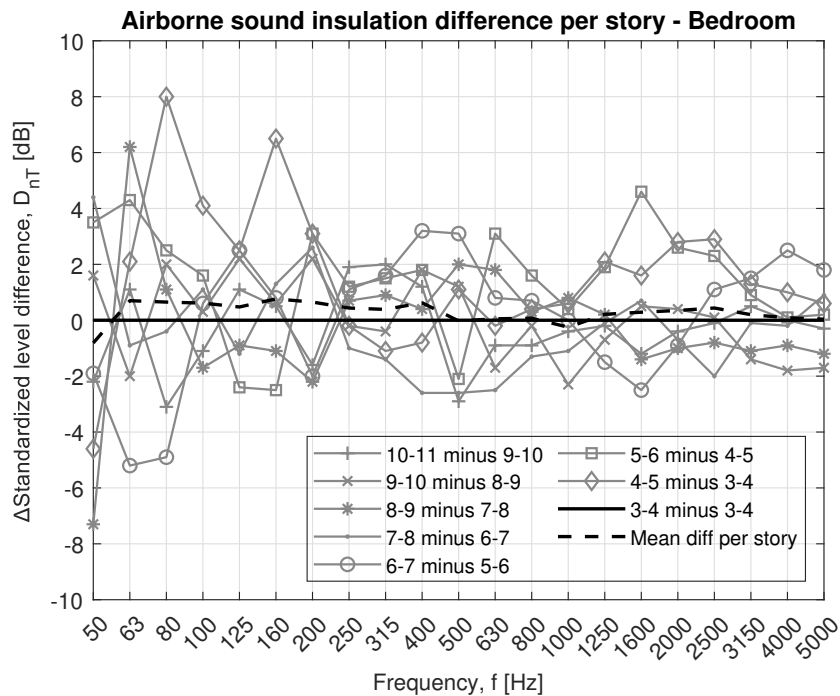
Figure 5.24: Vertical airborne sound insulation differences per story in the bedroom.
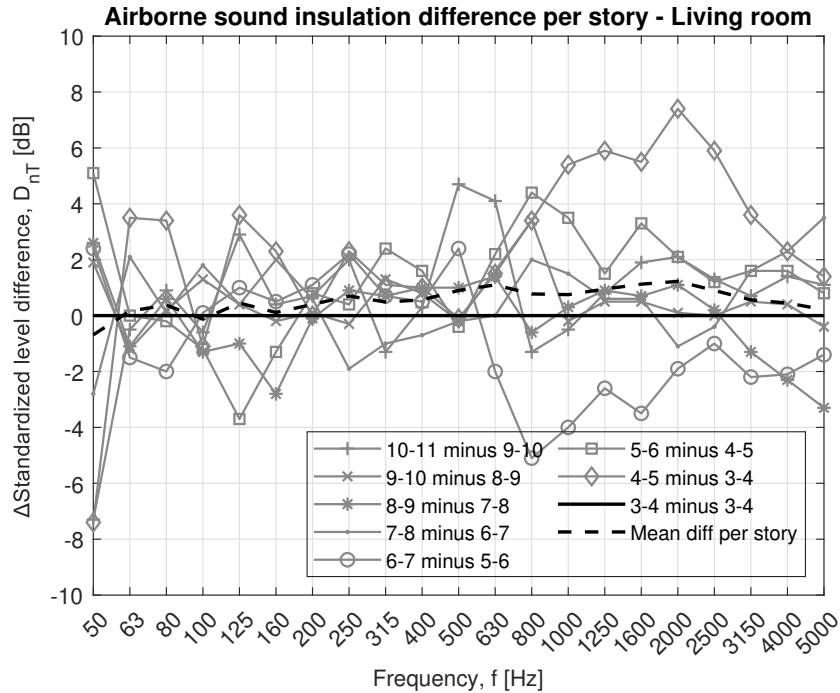
Figure 5.25: Vertical airborne sound insulation differences per story in the living room.

5.5.3 Improved estimation of the building height effect

Two additional differences in vertical airborne sound insulation between stories 3-4 and 8-9 are incorporated into the existing set of measurements outlined in this chapter and the article [177]. Consequently, Figure 5.26 expresses a more precise estimation curve, illustrating all differences alongside the overall mean prediction curve.

The standard deviation (SD) of all measurement differences from Figure 5.26 are presented with the mean estimation curve in Figure 5.27, alongside the standard deviation of the measurement method per story from Figure 5.19. These two standard deviations are combined using Equation 5.6 to also show the total standard deviation of the mean estimation curve for the difference in sound insulation per story.

The values from Figure 5.27 are presented in Table D1, rounded to one decimal.
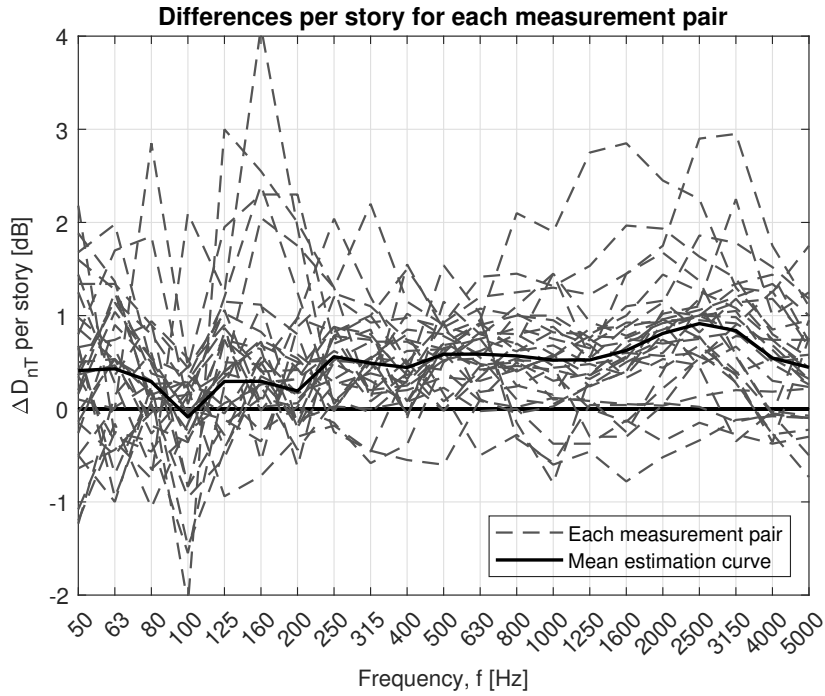
Figure 5.26: Differences in vertical airborne sound insulation per story for each measurement pair.
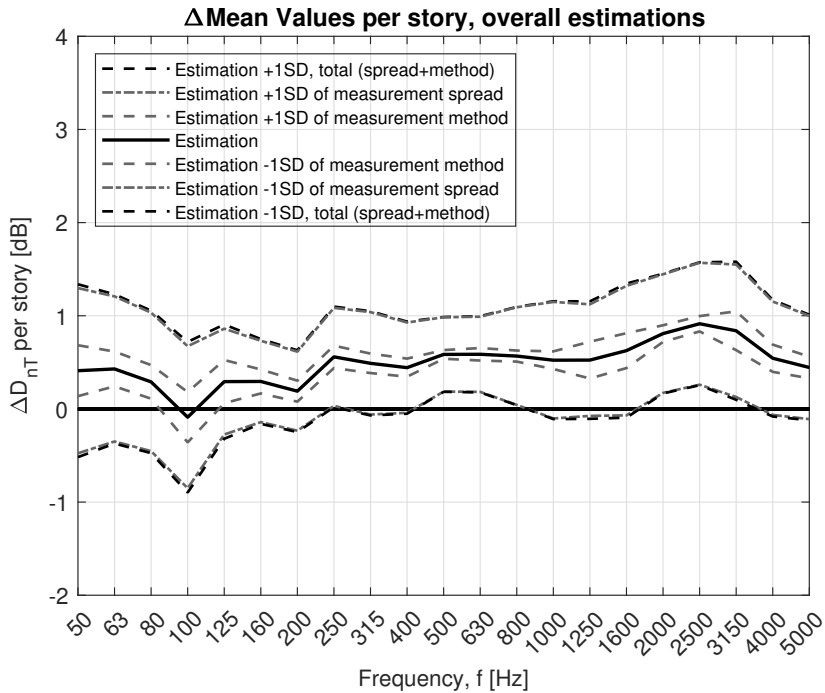
Figure 5.27: Mean values per story for both the estimation curve along with several standard deviations (SD) regarding the measurement spread of the measurement pair, the measurement method, and both of them combined.

Lastly, estimations of the decrease in sound insulation per story are presented in Figure 5.28. Actual values are presented in Table D2. The curves in Figure 5.28 are based on Figure 5.27 and Table D1, where negative values are ignored and set to 0 since an improvement lower down the building is not expected. Positive values in Figure 5.28 indicate a decrease in airborne sound insulation lower down the building. The effect of flanking means that the flanking transmission via the CLT elements is expected to be low/normal/high compared to other transmission paths and background noises. More specifically, low effect means that flanking is limited and has a minimal effect on the sound insulation. High effect of flanking means that the flanking paths determine the sound insulation and that many flanking paths or large surface areas contribute to lower sound insulation. Normal effect is between low and high effect and can be considered the general case for most rooms. Values are presented in Table D2.
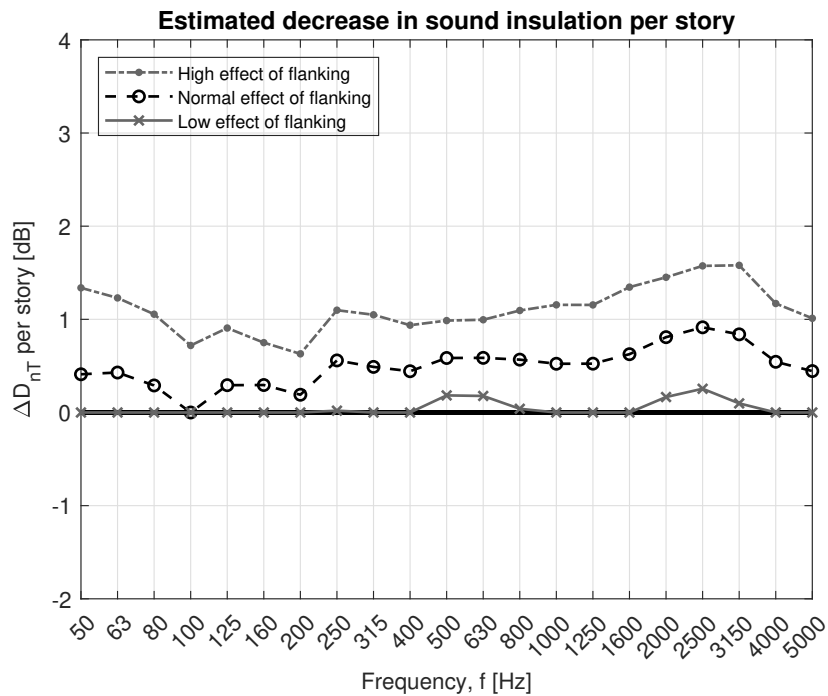
Figure 5.28: Estimations of the decrease in sound insulation per story lower down the building with various effects of flanking. Values are presented in Table D2.

CHAPTER 6

MOUNTING TECHNIQUE OF ACCELEROMETERS AND EFFECT OF BEARING DIRECTION OF CLT ELEMENTS

Résumé

Les mesures de l'indice de réduction des vibrations $\left(K_{ij}\right)$ sur le terrain présentent certaines difficultés comparativement aux mesures en laboratoire. Tout d'abord, la mesure nécessite l'accès à un chantier de construction pendant le court laps de temps où les éléments en bois lamellé-croisé (CLT) sont apparents. Deuxièmement, les entrepreneurs en bâtiment sont souvent soumis à un calendrier serré. Il est donc important de trouver une solution qui minimise le temps de mesure sur le chantier. De plus, les mesures du facteur K_{ij} sur le terrain incluent plusieurs types de jonctions avec différentes directions d'appui qui peuvent être importantes. Cet article vise à évaluer deux techniques différentes de montage d'accéléromètres sur des éléments CLT et à discuter de l'influence de la direction des roulements sur la différence de niveau de vibration des jonctions. Les données de mesure indiquent qu'il y a peu de différences entre les techniques de montage avec de la cire d'abeille ou du ruban adhésif double face lorsque les accéléromètres sont fixés sur des éléments en CLT. De plus, les mesures sur le terrain indiquent que le niveau de vibration diminue avec l'augmentation des lamelles sur le même élément CLT. Le ruban adhésif double face est un substitut adéquat à la cire d'abeille sur le terrain pour le montage d'accéléromètres sur des éléments CLT, avec quelques limitations aux hautes fréquences. Les données de mesure concluent que le sens d'appui des éléments

CLT peut influencer l'indice de réduction des vibrations d'une jonction.

Abstract

Vibration reduction index (K_{ij}) measurements in the field have some challenges compared to laboratory measurements. Firstly, the measurement requires access to a construction site during the short time span when the cross-laminated timber (CLT) elements are apparent. Secondly, building contractors are often on a tight time schedule. Therefore, it is important to find a solution that minimizes the measurement time on site. Moreover, K_{ij} measurements in the field include several types of junctions with different bearing directions which may be of importance. This paper aims to evaluate two different mounting techniques with accelerometers on CLT elements and to discuss how the bearing direction could affect the vibration level difference of junctions. Measurement data indicate few deviations between mounting techniques with beeswax or double-sided adhesive tape when accelerometers are attached to CLT elements. Furthermore, field measurements indicate that the vibration level will decrease with increased lamellas over the same CLT element. Double-sided adhesive tape is an adequate substitute for beeswax in the field for mounting accelerometers on CLT elements, with some limitations at high frequencies. Measurement data concludes that the bearing direction of CLT elements can influence the vibration reduction index of a junction.

Keywords: bearing direction, cross-laminated timber, mounting technique, vibration reduction index

6.1 Introduction

This chapter is a copy of a conference paper presented at Internoise 2022 in Glasgow, Scotland [98].

Flanking sound transmission paths play an important role when the airborne sound reduction is measured in the field since these values will be lower than those obtained in the laboratory. The flanking paths can be measured with the vibration reduction index K_{ij}. However, K_{ij} measurements on cross-laminated timber (CLT) in the field have some complications since they require access to a construction site during the short time span when the cross-laminated timber elements are apparent. Therefore, it is important to find a solution that minimizes the measurement time on site.

Several studies have investigated the impact of flanking transmission paths for concrete and masonry structures [195–199]. The standard ISO 12354-1 specifies calculation models for direct and indirect flanking transmission paths to estimate the airborne sound insulation between adjacent rooms [39]. The indirect paths are mainly described with empirical formulas, based on the mass difference of connected elements, characterized by the vibration reduction index, K_{ij} [39]. Many empirical formulas in ISO 12354-1 describe heavy structures such as concrete and masonry. The standard also provides empirical formulas of junctions with framed lightweight constructions and CLT elements [39].

CLT is increasing in popularity in several countries as a building element [89]. The product has a good environmental profile and can compete with other traditional structure materials since it has excellent strength and stiffness properties [90]. Several studies have measured the vibration reduction index of CLT elements and mainly in the laboratory (mock-ups), but more data is needed [116, 117, 121, 200, 201]. Ref. [200] have compared measurements of K_{ij} against the empirical values in ISO 12354-1 [39] and results show that measured values in the laboratory deviate from the values in the standard. ISO 12354-1 should be used with special consideration when estimating the impact of different flanking sound transmission

paths for CLT elements. More measurements and studies are required for different junction types to achieve high precision calculations. The vibration reduction index for CLT elements is typically measured in the laboratory, which may not reflect the field results. To decide whether there is a difference, vibration reduction index measurements on CLT elements in the field are needed.

Vibration measurements on an element shall be performed with accelerometers that are mounted directly on the surface according to ISO 10848-1 [88]. The accelerometers must have sufficient efficiency and low noise to obtain an adequate signal-to-noise ratio. Furthermore, the mass of the accelerometers should be small enough to minimize the effect of mass loading [88]. ISO 10848-1 mentions that the fixing of accelerometers should be stiff in the normal direction of the surface and the standard suggests the use of beeswax or petroleum wax, with some caution regarding weak fixing which could cause measurement errors at high frequencies [88].

Beeswax as a mounting technique implies some difficulties in the field when measuring the vibration reduction index on CLT elements. Since beeswax does not adhere well to the surface without a little preparation, mounting each accelerometer requires some time, and the beeswax will not stick if the accelerometer is moved. Additionally, beeswax requires a certain temperature to function properly based on measurements conducted both during winter and summer on CLT elements in the field. The temperature is usually very low inside the buildings when measurements take place during the winter period. The primary reason is that the climate shell is often built simultaneously with indoor construction and vibration measurements cannot usually take place after the work has started indoors. A laboratory or mock-up is not affected by this problem because the climate is controlled, unlike a field situation. Due to its ability to work with temperature changes, double-sided tape proves to be a suitable option. Moreover, mounting time decreases since the tape can be left on the CLT elements without losing its effectiveness during the measurement period. However, double-sided tape is not mentioned in the ISO 10848-1 [88], and therefore, the mounting technique requires evaluation before it is

used in practice.

CLT elements in the field typically vary significantly more compared to the ones tested in the laboratory in size, various openings, and bearing directions. A corner room in an apartment with four CLT walls will have two façades and two internal walls with multiple floor elements connected. The bearing direction of the floor in one room is usually oriented the same way and if the bearing direction has an impact on the vibration reduction index, then the room will have a minimum of four different junction types. The junctions in that room will consist of two T-junctions (façade) with the bearing direction of the floor parallel and perpendicular to the junction, and two X-junctions (internal walls), also with different bearing directions in relation to the junctions. If the bearing direction has an impact on the sound reduction index, and if it is not considered during calculation, then the measurements will not match the calculations to a certain degree.

The purpose of this paper is to evaluate two different mounting techniques with accelerometers on CLT elements (beeswax and double-sided tape) and to discuss how the bearing direction could affect the vibration level difference of junctions.

6.2   Cross-Laminated Timber

Cross-laminated timber (CLT) is an engineered wood product made of different layers of kiln-dried dimension lumber boards stacked in alternating directions (crosswise 90°) and glued into place. CLT elements always consist of an odd number of layers, usually between three to seven, and the orientation of lamellas provides improved dimensional stability [89]. The panels are prefabricated, and they can be cut with high precision with CNC (Computer Numerical Controlled) routers. The finished product is stiff, strong, and stable which makes it suitable for several applications including floors, walls, and roofs [90]. Wood has three principal axes with respect to grain direction and growth rings. Lumber boards, therefore, have three different moduli of elasticity depending on the axis (longitudinal, radial, and tangential)

[92]. CLT panels will, therefore, also have different moduli of elasticity depending on the global axes. Moreover, due to alternative direction of the lumber boards, CLT elements will have different moduli of elasticity depending on the bearing direction [90]. A T-junction with CLT walls and a CLT floor is illustrated in Figure 6.1 with different bearing directions in relation to the walls (perpendicular and parallel to the junction). Most often, the strongest load-bearing direction is parallel to the boards on the outer layer [90] which is illustrated in Figure 6.1.
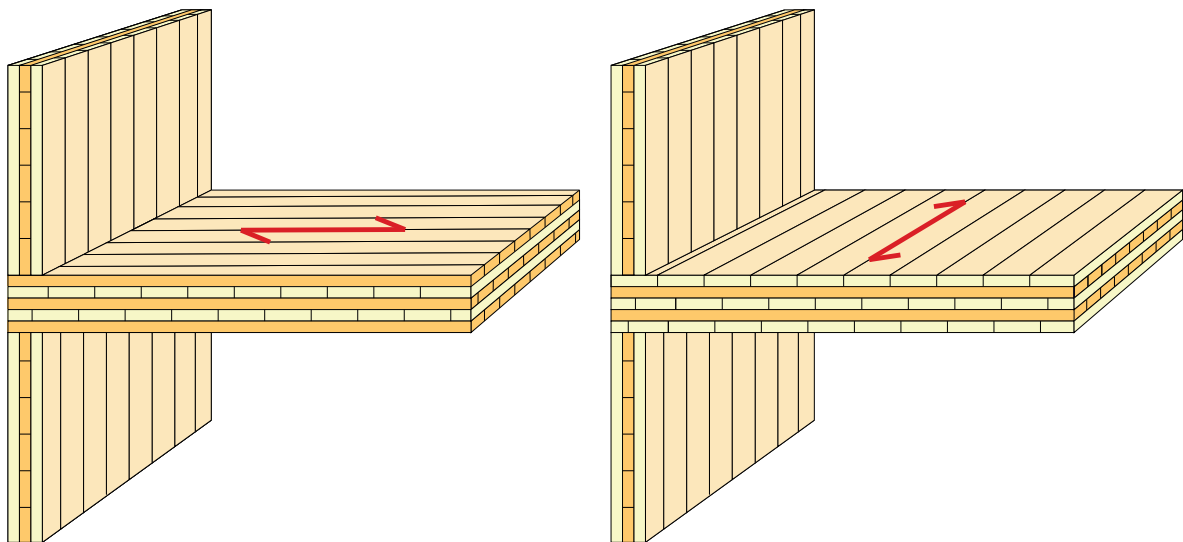
Figure 6.1: T-junctions of CLT elements with two different bearing directions. To the left: Bearing direction perpendicular to the junction. To the right: Bearing direction parallel to the junction.

6.3   Vibration Reduction Index

Vibration measurements should be executed according to ISO 10848-1 [88] to calculate the vibration reduction index. Vibrations can be measured both with acceleration and velocity. However, acceleration is preferred prior to velocity when measuring the structural reverberation time to avoid signal processing affecting the decay curve. The averaged velocity level can be calculated according to Equation 6.1:

$$L_v = 10 \log_{10} \left(\frac{\frac{1}{T_\mathrm{m}} \cdot \int_0^{T_\mathrm{m}} v^2(t)\, dt}{v_0^2} \right), \tag{6.1}$$

where v is the velocity over time and v_0 is the reference velocity level [88].

Flanking transmission paths between two elements, i and j, can be quantified with the vibration reduction index in Equation 6.2 known as K_ij [88] which is expressed in decibels:

$$K_\mathrm{ij} = \overline{D_\mathrm{v,ij}} + 10 \cdot \log_{10} \left(\frac{l_\mathrm{ij}}{\sqrt{a_\mathrm{i} \cdot a_\mathrm{j}}} \right). \tag{6.2}$$

$\overline{D_\mathrm{v,ij}}$ in Equation 6.2 is described as the direction-averaged velocity level difference, which is calculated as the mean value between the velocity level difference $D_\mathrm{v,ij}$ (when element i is excited) and $D_\mathrm{v,ji}$ (when element j is excited) [88] according to Equation 6.3:

$$\overline{D_\mathrm{v,ij}} = \frac{1}{2} \cdot \left(D_\mathrm{v,ij} + D_\mathrm{v,ji} \right). \tag{6.3}$$

The vibration reduction index in Equation 6.2 is also dependent on the common junction length, l_ij, and the equivalent sound absorption length for each element, a_i and a_j according to Equation 6.4:

$$a_\mathrm{j} = \frac{2.2 \cdot \pi^2 \cdot S_j}{T_\mathrm{s,j} \cdot c_0 \cdot \sqrt{\frac{f}{f_\mathrm{ref}}}}. \tag{6.4}$$

S_j is the surface area of the element, $T_\mathrm{s,j}$ is the structural reverberation time of the element (dependent on frequency), c_0 is the speed of sound in air, f is the frequency and f_ref is the reference frequency, $f_\mathrm{ref} = 1000$ Hz [88].

6.4 Measurement Setup

6.4.1 Mounting technique

The impact of different mounting techniques (beeswax and double-sided tape) was measured on a CLT wall with several configurations. The test configuration mainly consisted of four accelerometers and a transient excitation source with multiple impacts of a hammer. Accelerometers were mounted at different positions on a CLT wall according to Figure 6.2.
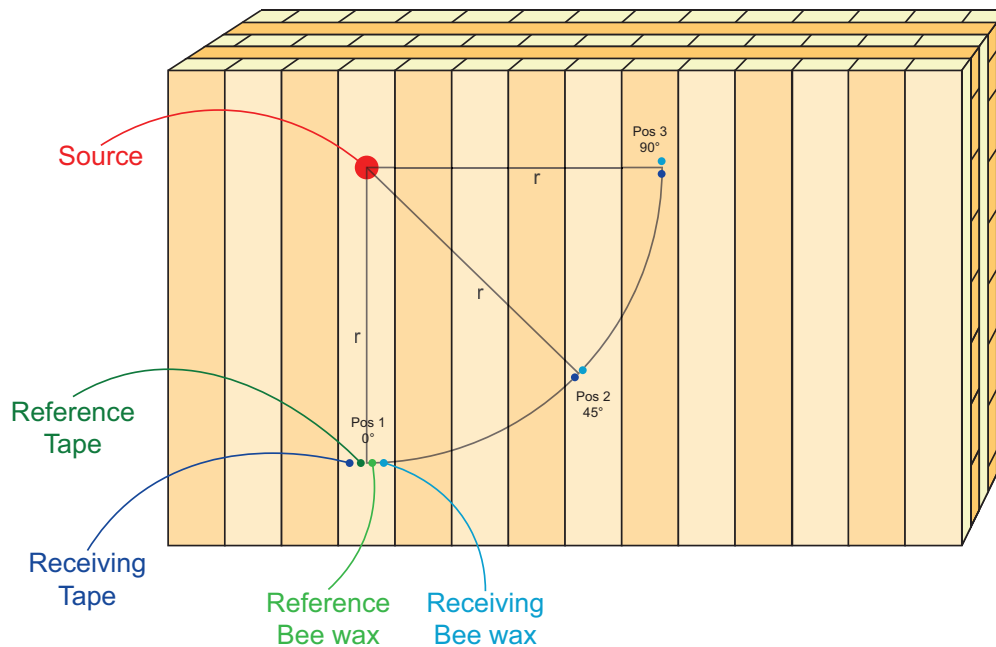
Figure 6.2: Measurement setup on the CLT wall.

In the first position, four accelerometers were placed on the same board and at the same distance from the excitation source (see also Figure 6.3a from the field measurement). Two accelerometers were attached with beeswax and the remaining two were attached with double-sided tape. One accelerometer was also placed close to the source to measure the power input (not illustrated in Figure 6.2). One accelerometer of each mounting technique was moved from position 1 to positions 2 and 3 (see Figure 6.2), oriented 45 and 90 degrees from the reference position. In Figure 6.3b, receiving accelerometers are placed in position 3. Six

excitations with the impact hammer were conducted on the CLT wall over a period of 30 seconds and the measured vibration was linearly averaged. The test was repeated so that two measurements were conducted for each position. The difference in velocity level of different mounting techniques was calculated as $L_{v,\text{bee wax}} - L_{v,\text{tape}}$ for each position and measurement. The two measurements for each position were then linearly averaged and compared with each other.

(a)   (b)
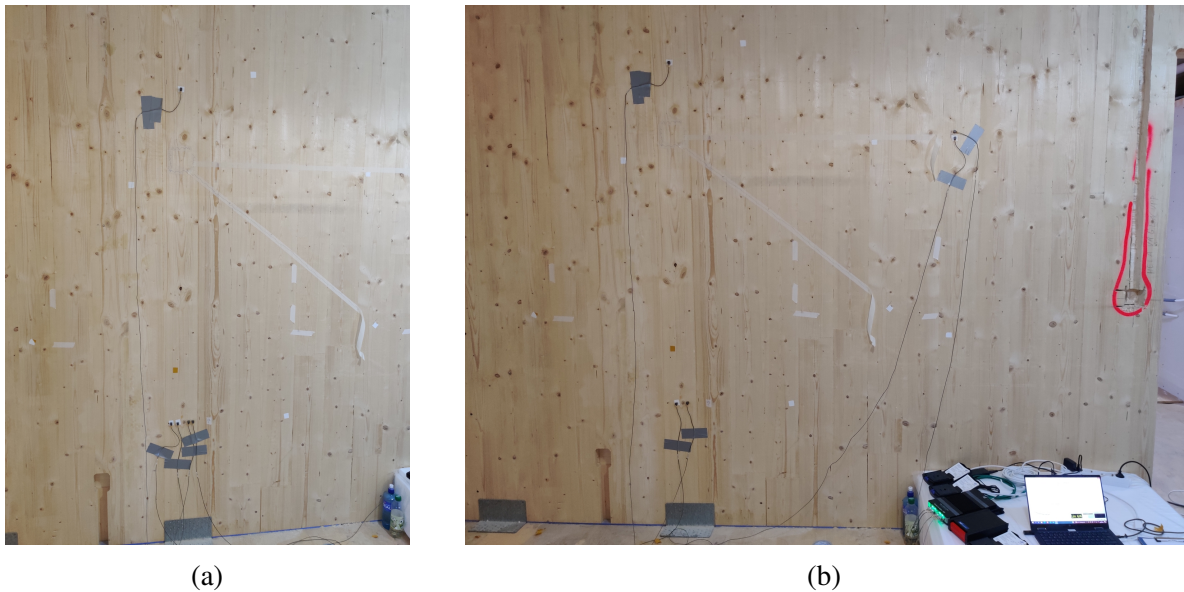
Figure 6.3: Pictures on the CLT wall in the field: (a) Receiving accelerometers at position 1; (b) Receiving accelerometers at position 3.

6.4.2   Bearing Direction

Two different test methods were conducted to investigate how the vibration level differs when the bearing direction was oriented perpendicular to the junction compared to parallel to the junction. The first simplified test method was based on the setup in Figure 6.2, measurement pictures are presented in Figure 6.3. Two accelerometers were used as reference values at position 1 where one was fixed with beeswax and the other with tape. Two accelerometers were used to measure receiving values at positions 1-3 with different mounting techniques as described before. The idea of the test was to understand how the velocity level changes over the CLT element if the accelerometers are placed on the same outer lumber board (of the

CLT wall's five layers) as the one getting excited, or if they are moved around with the same distance from the source. In theory, the vibrations need to travel through more lumber boards to directly excite the board closest to the accelerometer. The measured receiving values at positions 1-3 were subtracted from the reference values at position 1 for each position and each mounting technique.

The second test method was performed in accordance with ISO 10848-1 [88] where the vibration reduction index of a junction was determined. The measurements consisted of seven accelerometers, four on the source element and three on the receiving element, and an impact hammer. Several measurements were conducted for each flanking path of the junction with different positions of accelerometers and impact hammer. Two different junctions were tested in the same apartment with similar attributes, except that the bearing direction differed. The room, in which the measurements were conducted, is displayed in Figure 6.4 with markings on how the bearing direction was oriented. Measurement pictures are presented in Figure 6.5 for both junctions. The floor in Figure 6.4 is oriented parallel in relation to junction 1 and perpendicular in relation to junction 2. The vibration reduction index of both junctions was measured in two identical apartments and the difference of each junction was calculated for each flanking path according to ISO 10848-1 [88].
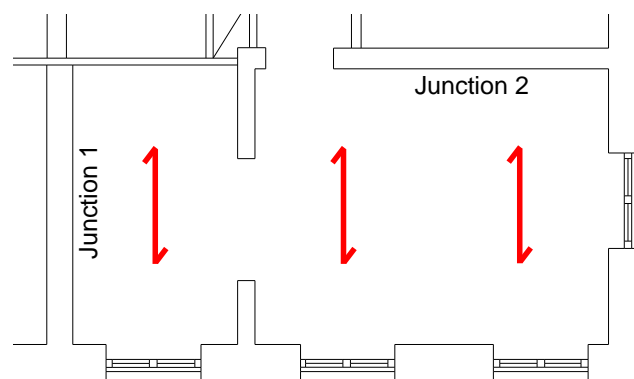
Figure 6.4: Plan drawing of two measured junctions in one apartment with different bearing directions. The bearing direction of the floor is parallel in relation to junction 1 and perpendicular in relation to junction 2.
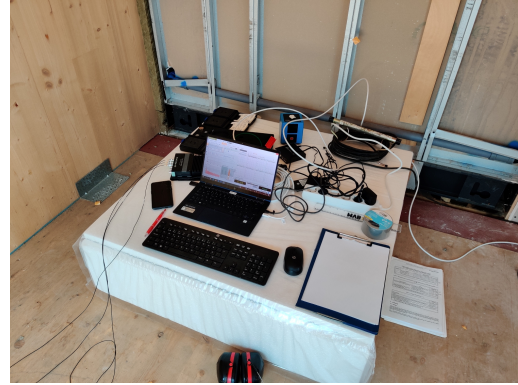
Figure 6.5: Pictures on the two measured junction types in the field: (a) Accelerometers placed on the receiving element for junction type 1; (b) Measurement setup; (c) Accelerometers placed on the source element for junction type 2; (d) Close-up on the used impact hammer.

6.5 Measurement Results

Velocity level measurement results on the same CLT wall with tape and beeswax are presented in Figure 6.6 for different positions according to Figure 6.2. The result is calculated by subtracting the receiving velocity levels for each position and mounting technique from the reference velocity levels at position 1 for each mounting technique. The impact of both the bearing direction and mounting technique can be observed in Figure 6.6.
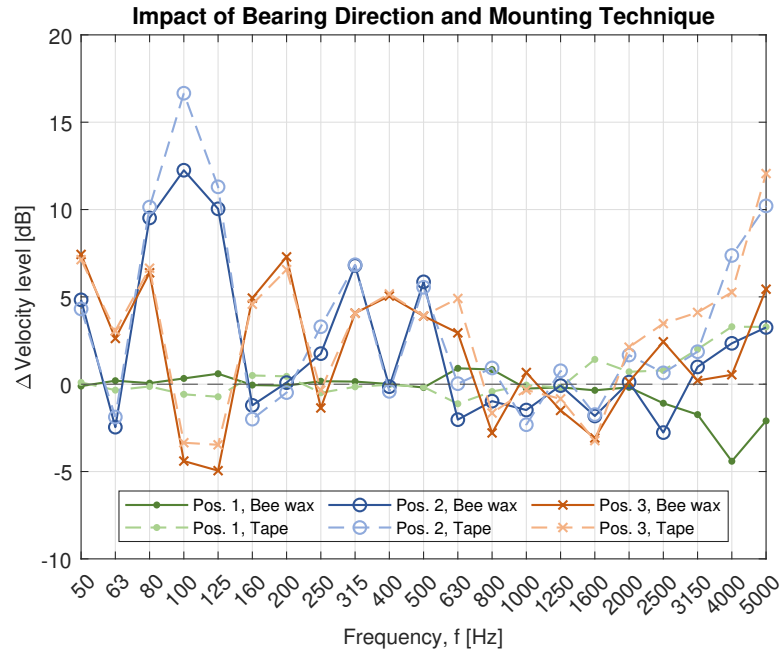
Figure 6.6: The impact of bearing direction and mounting technique for positions 1-3 on the CLT wall (see Figure 6.2).

The green line, Pos 1: 0°, have both the reference and receiving accelerometers on the same outer lumber board, positioned close to each other, and the velocity level difference is therefore expected to be around zero. The result indicates that the velocity levels are reduced over the CLT wall when the accelerometers are placed on lumber boards that are not directly excited, with a few exceptions for certain frequency bands. Furthermore, Figure 6.6 also indicates that the difference is small between the two mounting techniques for frequencies below 2.5 kHz, again with some exceptions for certain frequency bands.

6.5.1 Mounting Technique

The impact of different mounting techniques with beeswax and tape, with measurement setup according to Figure 6.2, can be calculated as the difference in measured velocity levels at each position. The receiving velocity levels for each position with tape are subtracted from the velocity level with beeswax and presented in Figure 6.7. The measurement result indicates that the mounting technique with beeswax has higher sensitivity than tape at high frequencies,

meaning that weak fixing is more likely to occur for tape at higher frequencies.
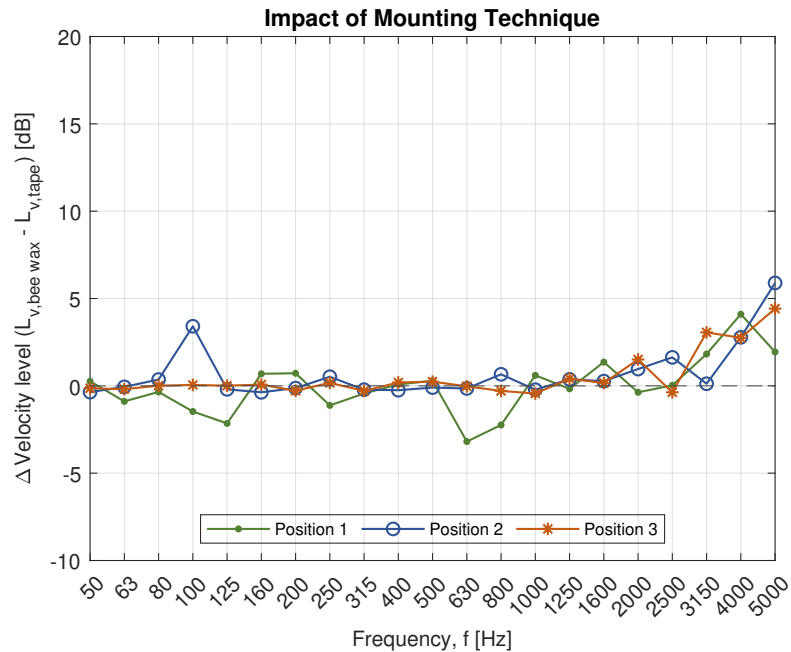
Figure 6.7: The difference in mounting techniques with beeswax and double-sided tape for positions 1-3 on the CLT wall, according to Figure 6.2.

6.5.2 Bearing Direction

The impact of bearing directions is displayed with several measurements and with two different test methods in Figure 6.8. Two curves, with yellow and red colors, illustrate test method 1. The measurements for method 1 are evaluated by subtracting the receiving velocity levels at positions 2 and 3 respectively from the reference velocity level at position 1 for each mounting technique. The mean value is thereafter calculated for the different mounting techniques and presented in Figure 6.8 (beeswax with yellow and double-sided tape with red). Values above zero indicate that the velocity level is higher when the bearing direction of the floor is oriented perpendicular in relation to the junction, compared to a parallel bearing direction in relation to the junction.

Furthermore, two grey curves are presented in Figure 6.8 which illustrates test method 2. The grey curves describe the difference in vibration reduction index between the two junctions

for each apartment. The difference is calculated by subtracting the vibration reduction index of junction 2 (bearing direction perpendicular to the junction) from the vibration reduction index of junction 1 (bearing direction parallel to the junction), $K_{ij,junction1} - K_{ij,junction2}$, for the flanking transmission paths that include the floor. The mean value of the different paths for each apartment is displayed with the grey curves in Figure 6.8. Once again, values above zero indicate that the vibration reduction index is higher when the bearing direction is oriented parallel to the junction, meaning that the measured receiving velocity levels are higher when the bearing direction is oriented perpendicular in relation to the junction. Finally, the mean value of test method 2 is illustrated with a black curve.
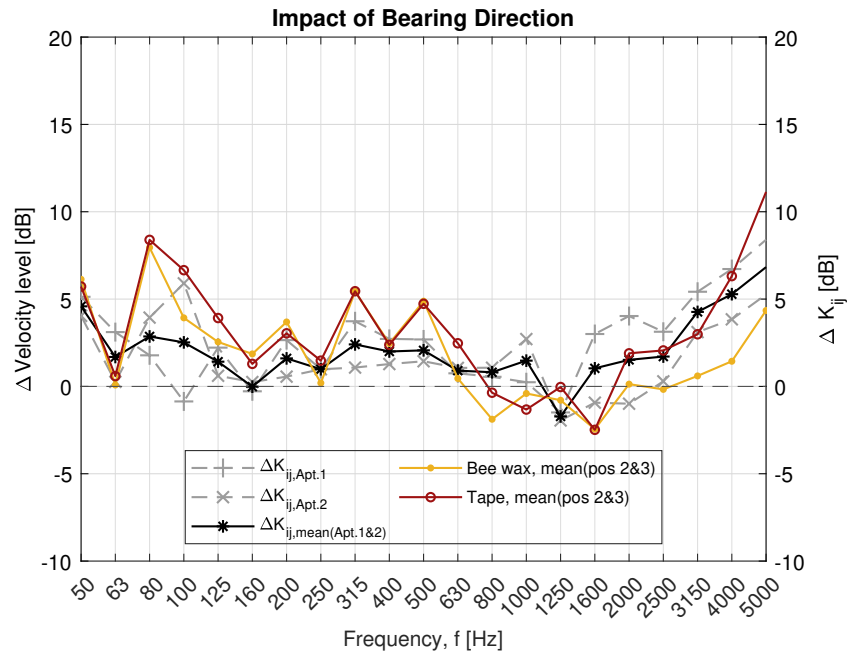
Figure 6.8: Difference of bearing directions in relation to junctions. The left y-axis describes the velocity level difference with the two tested mounting techniques (yellow and red lines). The right y-axis describes the vibration reduction index difference between two junctions (grey and black curves) with different bearing directions in relation to the junction (perpendicular and parallel).

The measurement result of both test methods has the same trend, and the values correspond with each other to a certain degree. Measurements from both test methods indicate that there is a difference between different bearing directions. Overall, the values presented in Figure 6.8

178

are positive, indicating that the favorable placement of a floor is when the bearing direction is parallel in relation to the junction.

6.6 Discussion

Field measurements on CLT elements imply several difficulties, including limited measurement time on the site since the contractors are often on a tight time schedule. It is therefore important to find optimal solutions that minimize the time spent on the site, while still making sure to record accurate results. ISO 10848-1 suggests the use of beeswax or petroleum wax as a mounting technique to fix the accelerometers on the elements. However, wax is mainly functional around room temperature and not during cold weather conditions, and the mounting time increases since wax requires some preparation before usage compared to double-sided tape. Measurements were therefore performed on a CLT wall with two different mounting techniques, with beeswax and double-sided tape according to Figure 6.2. Results indicate small differences in receiving velocity levels at different positions on the CLT element with double-sided tape compared to beeswax for most frequency bands, see Figures 6.6-6.7, and the result is similar for all positions, with some exceptions at certain frequency bands. However, double-sided tape performs differently than beeswax at higher frequencies, above 2.5 kHz (Figure 6.7), with a difference of around 5 dB. ISO 10848-1 mentions that weak fixing could occur with beeswax which could cause measurement errors at high frequencies, and measurements show that this could also be the case with double-sided tape. Moreover, it seems to be more likely that double-sided tape ends up in measurement errors due to the weak fixing of the accelerometers, compared to beeswax, at higher frequencies since beeswax records higher receiving velocity levels.

Although double-sided tape induces more issues at high frequencies compared to beeswax, it is still a suitable option for field measurements. The frequency area that is of most interest for CLT constructions is from 50 Hz up to around 1 kHz, since that frequency range most

often determines the sound reduction index of the constructions, concluded from several measurements on CLT buildings and elements by the authors and by Ref. [202–204]. Therefore, measurement uncertainties at high frequencies are less relevant compared to the time saved when measuring the vibration reduction index in the field. Double-sided tape is therefore an adequate substitute for beeswax in the field since the difference in velocity level is small between the two tested mounting techniques for frequencies below 2.5 kHz, for the frequency area of most importance. Moreover, vibration reduction index measurements are determined by the difference in velocity levels and not the actual velocity levels for each accelerometer position, suggesting that the uncertainties might even out the result. However, double-sided tape should be used with caution and the results and conclusions are mainly valid for CLT constructions. The same conclusion might not be valid for velocity level measurements on light-frame constructions.

Another interesting observation from the measurements is the difference in velocity levels for each mounting technique on the same lumber board at Pos 1: 0°. The velocity levels measured simultaneously by the accelerometer on the same lumber board, at the same distance from the source, varies between 0-1 dB between 10 Hz to 2.5 kHz, and above 2.5 kHz, the difference is around 3-5 dB (see Figure 6.8). The difference in high frequencies could, once again, depend on weak fixing but it could also depend on where the accelerometers are placed on the outer lumber board since CLT and wood itself is not a homogenous construction and material [92].

The bearing direction of CLT floors typically varies depending on the layouts of different rooms in relation to the bearing CLT walls. A corner room with four CLT walls can have a minimum of four different junction types which could affect the sound reduction index between dwellings. Field measurements of the vibration reduction index were performed in a multi-family building with several stories and with different bearing directions in relation to the junction (perpendicular and parallel), described as test method 2. The result indicates that there is a difference in vibration reduction index depending on the orientation of the

bearing direction. Vibration levels tend to be higher on the receiving element when the bearing direction is perpendicular to the junction, meaning that the vibration reduction index of a junction is higher when the bearing direction is parallel to the junction. The difference in vibration reduction index varies, on average, between 0 to 5 dB depending on the frequency with a mean value of 2.1 dB over the whole frequency range, 50 Hz to 5 kHz. Orientation of the bearing direction could therefore have an impact of several dB on the weighted sound reduction index between two apartments. These results are concluded in two apartments for different flanking transmission paths. In addition, measurements were performed on the wall where mounting techniques were evaluated, described as test method 1. This test method indicates similar results as test method 2, meaning that the receiving vibration levels are higher when the boards are oriented perpendicular compared to parallel, in relation to the junctions.

The result from both test methods thereby explains, to a certain degree, why some rooms with similar geometry and structural build-up of walls and floor could have different sound insulation properties between apartments. However, the explanation is far more complex than just the bearing direction which probably represents a small contribution to the difference of the total sound insulation between apartments.

6.7 Conclusions

The purpose of the paper was to evaluate two different mounting techniques with accelerometers on CLT elements (beeswax and double-sided tape) and to discuss how the bearing direction could affect the vibration level difference of junctions.

Double-sided adhesive tape is an adequate substitute for beeswax in the field for mounting accelerometers on CLT elements, with some limitations at high frequencies where it is more likely that weak fixing will occur.

Measurement data with two different test methods concludes that the bearing direction of CLT elements, in relation to junctions, can influence the vibration reduction index of different

flanking transmission paths. The favorable placement of a floor is when the bearing direction is parallel in relation to the junction. Therefore, the orientation of the bearing direction, in relation to junctions, could affect the total measured sound insulation between apartments.

CHAPTER 7

EFFECTS OF BUILDING HEIGHT ON THE SOUND TRANSMISSION IN CROSS-LAMINATED TIMBER BUILDINGS – VIBRATION REDUCTION INDEX

Résumé

Les bâtiments en bois de grande hauteur sont de plus en plus populaires et leur structure comprend généralement du bois lamellé-croisé. Les bâtiments plus hauts entraînent des charges plus élevées sur les jonctions situées plus bas dans le bâtiment, ce qui, d'après la littérature, a un effet négatif sur l'isolation acoustique. Cette étude a consisté à mesurer l'indice de réduction des vibrations dans quatre bâtiments en bois lamellé-croisé différents, dont la hauteur et les détails de jonction varient. Au total, 12 jonctions ont été mesurées à la fois à des niveaux élevés et bas dans les bâtiments. Parmi celles-ci, 10 jonctions avaient des intercalaires résilients avec différentes rigidités dépendant de la charge quasi-permanente conçue, tandis que 2 jonctions n'avaient pas d'intercalaires résilients. Les résultats indiquent que l'indice de réduction des vibrations diminue plus bas dans le bâtiment, principalement pour la trajectoire mur-mur. Les résultats sont cohérents pour toutes les jonctions mesurées au-dessus de 400 Hz pour la trajectoire mur-mur et pour la majorité des mesures de la gamme de fréquences restante, 400 Hz et en dessous. La différence observée dans l'indice de réduction des vibrations pourrait avoir un impact significatif sur le résultat final si un immeuble de grande hauteur comporte plusieurs voies latérales qui affectent l'isolation acoustique entre

deux appartements, ce qui doit être pris en compte lors de la phase de conception. Des effets similaires ont été observés pour les bâtiments avec et sans couches intermédiaires résilientes dans les jonctions.

Mots clés: indice de réduction des vibrations, hauteur des bâtiments, bois lamellé-croisé, acoustique des bâtiments, isolation acoustique

Abstract

High-rise wooden buildings are increasing in popularity, and they typically include cross-laminated timber in the structure. Taller buildings result in higher loads on the junctions lower down in the building, which are suggested in the literature to negatively affect the sound insulation. This study involved measurement of the vibration reduction index in four different CLT buildings, varying in height and junction details. A total of 12 junctions were measured at both high and low levels in the buildings. Among these, 10 junctions had resilient interlayers with different stiffnesses dependent on the designed quasi-permanent load, while 2 junctions lacked resilient interlayers. The results indicated that the vibration reduction index decreases lower down in the building mainly for the Wall–Wall path. The findings were consistent for all measured junctions above 400 Hz for the Wall–Wall path and for the majority of the measurements of the remaining frequency range, 400 Hz and below. The observed difference in the vibration reduction index could significantly impact the final result if a high-rise building has several flanking paths that affect the sound insulation between two apartments, and this needs to be considered during the design phase. Similar effects were shown for buildings both with and without resilient interlayers in the junctions.

Keywords: vibration reduction index, building height, cross-laminated timber, building acoustics, sound insulation

7.1 Introduction

This chapter, except Section 7.6, is a copy of a journal article published in MDPI Buildings in 2023 [205].

Wooden buildings are increasing in popularity and usage for various constructions, including multi-family houses, schools, and offices. Moreover, the maximum building height is gradually growing with more stories, which increases the load lower down in the building. Cross-laminated timber (CLT) is typically used in some parts of the construction of high-rise wooden buildings. CLT is built up from several layers of stacked lumber boards that are glued together in a crosswise pattern. Generally, the crosswise pattern is 90 degrees, a minimum of three glued layers are used, and the CLT elements consist of an odd number of layers. Due to the crosswise pattern and laminating process, improved dimensional stability is provided for the elements, and CLT has high strength and stiffness properties [9]. While various papers on wind, fire, and seismic performance exist for high-rise wood buildings [206–221], few investigate the acoustic factors. Previous research on acoustics in wood has mainly focused on sound transmission through single elements in a laboratory and the sound transmission in finished smaller buildings or mockups.

Several laboratories measured the performance of CLT elements with and without additional layers, including Refs. [186, 222–228]. Vardaxis, DB Hagberg, and Dahlström [229] measured various configurations of CLT slabs, focusing on layers of wet and dry solutions above the CLT. Sabourin [230] measured the sound insulation properties of CLT elements for floors and walls with different thicknesses and additional linings. Loriggiola et al. [122] measured several configurations of CLT walls with frames and panels. Hongisto et al. [231] measured many wooden and concrete constructions, including CLT floors with additional layers. Moreover, some articles, including Refs. [93, 94, 232–236], focused on theoretical estimations and evaluations based on measurements to predict the sound insulation properties of CLT elements. Lin, CT Yang, and Tsay [237] compared several calculation methods with

the measurement results of CLT walls combined with frames and panels. Bader Eddin et al. [50] used an artificial neural network approach to predict the sound insulation properties of different lightweight floors based on 252 standardized laboratory measurements with good accuracy. Furthermore, sound radiation models and finite element methods were developed in a few papers [46, 204, 238–240] for CLT plates, which are used to predict sound insulation.

In the literature, several authors collected and measured the vibration reduction index of CLT elements, including Refs. [110, 113, 118, 121, 241, 242]. Schoenwald et al. [117] presented vibration reduction index measurements of CLT elements via different connection methods that are used to predict the flanking sound transmission. Pérez and Fuente [123] measured the velocity level difference in a CLT mock-up building where, amongst other combinations, different resilient materials were used. Additionally, a more extensive mock-up test of several sound parameters, including the vibration reduction index, was conducted in the ADIVBois Acoustic Mockup [243].

A large set of measurements have been collected by various authors in the literature described above. Moreover, some researchers have observed whether the load on junctions affects the sound transmission. Ref. [117] found that the load on a junction affected the flanking sound transmission in a laboratory, but only on the initial loading of the first simulated story; further loading after that had no effect. Morandi et al. [116] expected to see a difference when adding a load on a CLT slab during measurements of the vibration reduction index in a laboratory. Conversely, they found no significant difference when a load was added, which they argue could have been caused by the construction process. Mecking, Kruse, and Schanda [112] found that an extra load marginally lowered the vibration reduction index of an L-junction. Crispin et al. [185] showed that an increasing load results in a higher dynamic stiffness of the joint and a lower global vibration reduction index for two concrete elements connected with a flexible interlayer of natural rubber. The measurements from Refs. [112, 116, 117] were on CLT elements from laboratories, where a field situation could be simulated. In other papers, field measurements in finished buildings were evaluated, and it was suggested

that the load affects the sound transmission between apartments. Ref. [108] found that the load could have a negative effect on the flanking sound transmission in a lightweight timber construction. However, the authors suggested that this is caused by a mismatch between the load and stiffness of the resilient interlayers. Ref. [16] found that the impact sound insulation was worse lower down in the building, which they argue is due to less elasticity in the lower junctions because of the higher constraints being applied. Hörnmark [19] measured the vibration reduction index in a finished building and found that increasing the load negatively affects the vibration reduction index. However, measurements were performed with a transient method, and the vibration levels were not simultaneously recorded, which contradicts the recommendations in ISO 10848-1 [88].

Some of the previously mentioned studies [16, 19, 108, 112, 116, 117, 185] either measured the vibration reduction index in a laboratory or in the field, and few junctions and combinations were investigated in each paper. Moreover, only a few papers described in numbers or curves how significant the influence of the building height is, while others mainly commented on whether it has an effect. There is a need to thoroughly investigate whether the difference in building height affects the sound transmission between stories in the field and how significant the effect is. In a recent study by E Nilsson et al. [177], the authors performed 58 airborne sound insulation measurements over several stories in four buildings with different building systems and junction details. The results showed that the airborne sound insulation decreases lower down in the buildings. Moreover, Ref. [177] found that the airborne sound insulation decreases at a mean value of 0.5 dB per story over the frequency range. For a six-story difference, a 3 dB decrease in airborne sound insulation is, therefore, expected. The findings in Ref. [177] can be used for an overall estimation but strongly depend on the presence of the flanking sound transmission. Additionally, the study did not describe how the impact sound insulation is affected. For more precise estimations, measurements of the K_{ij} in several buildings are needed to determine the effect of the flanking sound transmission.

In an attempt to further investigate how the load might affect the sound insulation in

finished buildings, vibration reduction index measurements in real buildings are required, as also highlighted in Ref. [177]. The purpose of this paper is to present findings from measurements and evaluations of the vibration reduction index of several CLT buildings with different junction details at different stories. The goal is to find correlations between the difference in K_{ij} and the load or the number of stories that can be used in predictions.

7.2 Vibration Reduction Index and Measurement Method

The vibration reduction index, K_{ij}, was measured on 12 junctions in four different building projects made with cross-laminated timber. The junctions were categorized in pairs (six pairs in total), where one junction pair was measured at a low level and a high level in a building (see Figure 7.1). The junctions within each junction pair are at the same location in a plane view with the same boundary conditions. Thus, the only main difference within the same junction pair is the load on the junction, with a few exceptions described further down for each building project.
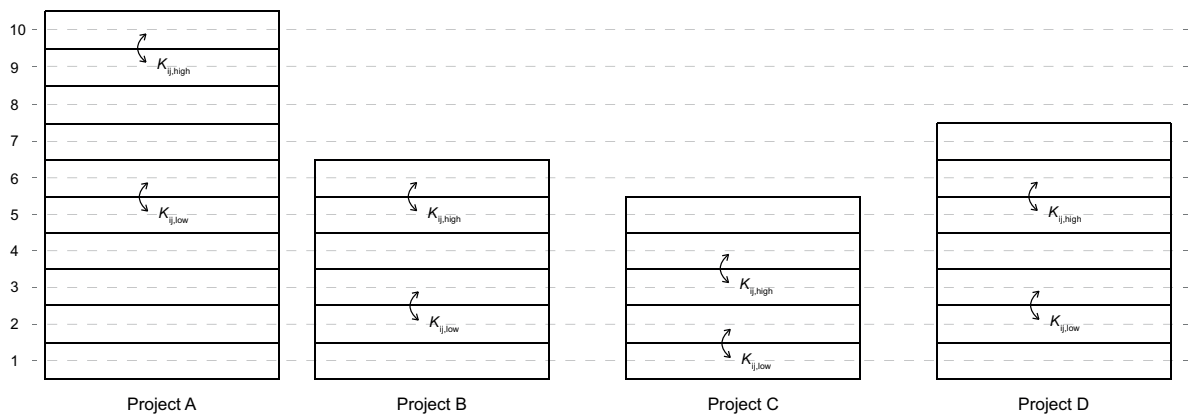
Figure 7.1: Overview of the number of stories for each project and where measurements took place at high and low stories.

The vibration reduction index, K_{ij}, was measured based on the standard ISO 10848-1 [88] and was calculated according to Equation 7.1:

$$K_{ij} = \overline{D_{v,ij}} + 10 \cdot \log_{10}\left(\frac{l_{ij}}{\sqrt{a_i \cdot a_j}}\right), \qquad (7.1)$$

where $\overline{D_{v,ij}}$ is the direction-averaged velocity level difference, l_{ij} is the junction length, and a_i and a_j are the equivalent junction lengths of the elements. The standard [88] was developed for laboratory measurements, and no measurement standard exists for the field. However, similar principles can be applied to field situations with some caution. For example, in a field situation, the operator should take note of potential flanking paths that are not first-order flanking paths. Here, first-order flanking paths are defined as paths including one junction, one source surface, and one receiving surface. ISO 10848-1 [88] describes two different measurement methods, either a transient or a steady-state method. Indeed, excitation with a steady-state method (like a shaker) is more reliable than a transient method (like a hammer), as shown in the literature [244, 245]. Moreover, measurement with a shaker is the preferred method, but an impact hammer can be used as long as simultaneous measurements on the sending and receiving elements are performed according to the standard [88]. However, it is not reasonable to bring a shaker to field measurements due to the weight of the device, handling it on-site without access to elevators, and the limited time available because of ongoing building work. Furthermore, Ref. [121] found no significant difference between measurement methods with a hammer or a shaker for CLT elements. To measure the direction-averaged velocity level difference, the velocity level difference between elements i and j ($D_{v,ij}$) and between elements j and i ($D_{v,ji}$) is measured. Then, $\overline{D_{v,ij}}$ is calculated according to Equation 7.2:

$$\overline{D_{v,ij}} = \frac{D_{v,ij} + D_{v,ji}}{2}, \qquad (7.2)$$

The velocity level difference was measured with accelerometers attached to the surface, and seven to nine accelerometers were used in total, depending on the size of the CLT plates. The measurement equipment consisted of accelerometers of type 4507 B 004 from Brüel & Kjær (Virum, Denmark), two LAN-XI of type 3050-A-060 from Brüel & Kjær, and an impact

hammer of type 8210 also from Brüel & Kjær. The accelerometers were calibrated with a vibration calibrator of type VC20 from Metra (MMF) (Radebeul, Germany), and the software BK Connect (mainly version 26.0.0.241) from Brüel & Kjær was used to record, process, and analyze the data. The impact hammer is a part of the transient method, and it is shown in Figure 7.2a. Different hardnesses (soft, medium, tough, and hard) can be used at the tip of the hammer. On-site tests showed that there is a small difference in the result among the different tips for CLT elements. This was also found in Ref. [121] but with different tips. However, it was more challenging to excite the structure with the softest tip, and the accelerometers detected some airborne sound produced by the hardest tip. Moreover, the difference in the reverberation time of a test element was negligible between the medium tip and the tough tip when struck with different strengths, as suggested in Ref. [88], to test the measurement method. Thus, either the tough or the medium tip was used in the measurements depending on the situation at the site. The same tip was always used within the same junction pair. Furthermore, since it was the difference in the vibration reduction index between stories that is of interest, and since the junction details and measurement method were the same in each junction pair, the measurement procedure was expected to have a minor impact on the test result accuracy.

(a)   (b)
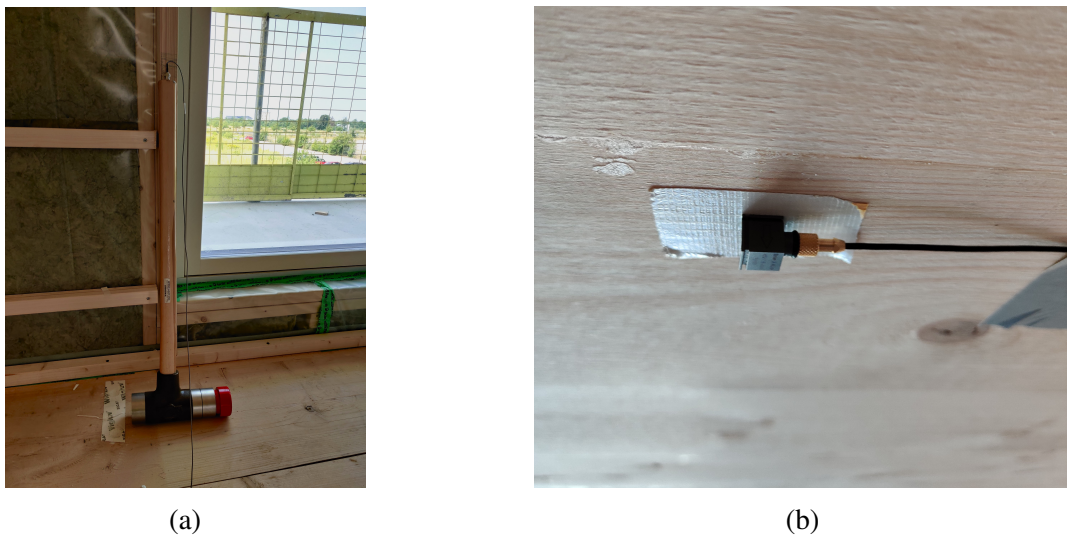
Figure 7.2: Measurement pictures of the equipment: (a) impact hammer with tough tip; (b) accelerometer mounted with double-sided tape.

For each junction, two to three excitation positions were used when measuring the difference in the average velocity level between the measured elements ($D_{v,ij}$ and $D_{v,ji}$). The standard [88] specifies a minimum of four excitation positions for Type A elements (for example, CLT). However, this is not always suitable for field measurements because of the size of the elements and openings, even if the minimum distances are vaguely considered. In general, three excitation positions were used in the projects. However, two junctions in project A could only fit two positions, which was considered adequate, since the difference in the vibration reduction index was of interest, and since the same measurement method was applied for each junction pair. Along the two to three excitation positions, a minimum of three accelerometers were used at each element for each excitation position according to the procedure in Ref. [88]. The accelerometers were also moved around at different positions on the element, and the measurement procedure concerning minimum distances was followed based on Ref. [88]. The excitation and measurement positions were always on the same side as the flanking paths. For example, when measuring the Ceiling–Wall flanking path, the excitation positions and measurement positions of the ceiling/floor were performed on the ceiling instead of the floor. Furthermore, simultaneous measurements of sending and receiving elements were performed, which is strongly recommended by the standard when using the transient method. Measurement positions were recorded with accelerometers attached to the surface with double-sided tape (see Figure 7.2b). The standard [88] specifies that the fixing of accelerometers should be stiff in the direction normal to the surface of the elements, which is not always suitable for measurements on site, as highlighted in Ref. [98]. Thus, double-sided tape is used, and this works similarly to beeswax for frequencies up to 3150 Hz. For 3150 Hz and above, a weak fixing of the accelerometers could occur and cause errors that need to be considered [98]. Indeed, it is preferred to mount the accelerometers with screws and magnets to the CLT, instead of using beeswax or double-sided tape, to avoid weak fixing. However, this was only possible in some projects.

The structural reverberation time was measured using the same principles and procedure

for the difference in average velocity levels between elements. Here, the standard specifies a minimum of three excitation positions, which is more in line with the procedure followed in the different projects. The structural reverberation times, $T_{s,j}$ and $T_{s,i}$, were used to calculate the equivalent absorption lengths, a_j and a_i, according to Equation 7.3:

$$a_j = \frac{2.2 \cdot \pi^2 \cdot S_j}{T_{s,j} \cdot c_0 \cdot \sqrt{\frac{f}{f_{\text{ref}}}}}, \tag{7.3}$$

where S_j is the surface area of the element measured, c_0 is the speed of sound in air, f is the frequency, and f_{ref} is the reference frequency (equal to 1000 Hz [88]). The evaluation of the decay curves to determine the structural reverberation time followed the procedure in Refs. [88, 153]. The evaluation range should be between 5–15 dB, according to Ref. [88]. However, shorter evaluation ranges are preferred in Ref. [246], as also highlighted in Ref. [88]. An evaluation range of 10 dB was, therefore, used, as recommended in Ref. [88].

The airborne sound produced due to impacts of the hammer was recorded by disconnecting the accelerometers from the sending and receiving elements, letting them hang in the air while the cables were attached to the elements with duct tape. The measurements in question were used to evaluate whether the airborne sound produced by the hammer, with different tips, influenced the result, while measuring the vibration reduction index.

The four building projects measured in this paper have CLT as the bearing structure for interior walls and floors. Some projects also had CLT in the facades. In this paper, the junction types (X and T) consisted of two walls and a floor. For the X-junctions, the floor was on both sides of the walls, either continuous or divided. For the T-junctions, the floor stopped in line with the two walls, with no other connections afterward.

Project A was a 10-story building with a 6 mm viscoelastic interlayer between the floor and the walls above it. The CLT elements were connected with brackets that are mounted directly onto the CLT without resilient interlayers (see Figure 7.3a). The measurements for project A were performed on six junctions, yielding three junction pairs: two interior X-junction pairs and one facade T-junction pair. The difference in the number of stories between the

measurements for project A was four stories for all three junction pairs. All the junctions in project A consisted of 180 mm thick CLT floor elements. All three junctions measured lower down in the building consisted of 160 mm thick CLT wall elements. For the junctions higher up in the building in project A, all three consisted of 120–140 mm thick CLT wall elements (120 mm for the upper wall elements at all three junctions, and 140 mm for the lower wall elements at all three junctions). The junctions called Int.Wall 2 had continuous floors, while the junctions called Int.Wall 1 had no continuous floors.

The measurements for project B took place in a six-story building with a 25 mm viscoelastic interlayer between the floor and the walls above it. The CLT elements were connected with brackets and screws, and a thin resilient interlayer was located on the lower part of the brackets against the floor (see Figure 7.3b). Two X-junctions with continuous floors (one junction pair) were measured with a three-story difference. Both junctions consisted of 180 mm thick CLT floor elements and 120 mm thick CLT wall elements.

Project C was a five-story building (including the attic) with a 12 mm viscoelastic interlayer between the floor and the walls above it. The CLT elements were connected with brackets that are mounted directly onto the CLT–wall, with a 6 mm resilient interlayer between the bracket and the CLT floor (see Figure 7.3c). Measurements were performed on two T-junctions, yielding one junction pair over a two-story difference. Both junctions consisted of 240 mm thick CLT floor elements and 120 mm thick CLT wall elements.

Measurements for project D took place in a seven-story building without a resilient interlayer in the vertical junctions (between floors and walls). The CLT floors and walls were connected with brackets and screws, also without a resilient interlayer (see Figure 7.3d). One junction pair, consisting of two interior X-junctions with a three-story difference, was measured, and the floors were not continuous for the junctions. Both junctions consisted of 250 mm thick CLT floor elements and 130 mm thick CLT wall elements.

A description of the thicknesses and the static E-modulus for the resilient interlayers that were used in the measured vertical CLT junctions is presented in Table E1.

(a)

(b)

(c)
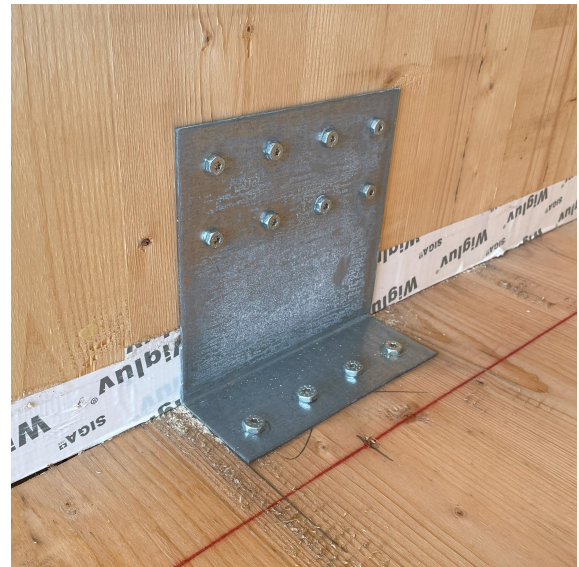
(d)

Figure 7.3: Measurement pictures of the different junction details. (a) Junction detail for project A with a 6 mm viscoelastic interlayer between CLT wall and floor and no interlayers between bracket and CLT elements. (b) Junction detail for project B with a 25 mm viscoelastic interlayer between CLT wall and floor and a thin resilient interlayer between bracket and CLT elements. (c) Junction detail for project C with a 12 mm viscoelastic interlayer between CLT wall and floor and a 6 mm resilient interlayer between bracket and CLT-elements. (d) Junction detail for project A with no interlayers in the vertical junctions.

7.3 Results

7.3.1 Evaluation of Structural Reverberation Time

ISO 10848-1 [88] suggests that measurements with an impact hammer should be evaluated with different strengths of the hammer blow, combined with different materials on the tip. Different materials are discussed in Section 7.2. To evaluate the strength of the hammer blow, measurements of the reverberation time for two floors in project C are compared and displayed in Figure 7.4. The hammer was struck from both the ceiling and the floor. The impacts on the ceiling were lower in strength than on the floor.
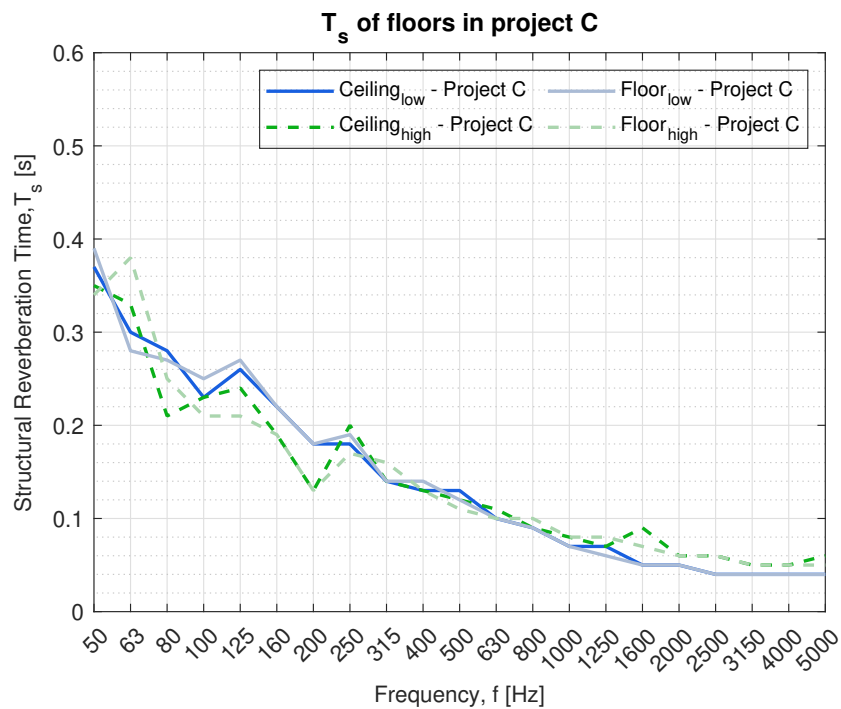
Figure 7.4: Difference in structural reverberation time of floors in project C when an impact hammer was struck from under (ceiling) and above (floor). Dashed curves represent the floor at the higher story, and solid lines represent the floor at the lower story.

The result in Figure 7.4 indicates that there was a small difference in reverberation time between the measurements overall. A comparison was made between lines of the same type, for example, solid dark blue compared to solid light blue. Furthermore, the measurements of

different floors in project C showed a small variation in reverberation time in comparison to each other.

7.3.2   Vibration Reduction Index Measurements

Based on vibration reduction index measurements from four CLT projects with a total of 12 junctions consisting of 36 flanking paths, the results indicated that there is a difference in the vibration reduction index between apartments located on high stories compared to those located on low stories. In Figure 7.5, the difference in the vibration reduction index for the Wall–Wall path is displayed for all projects. The T-junctions (facades) are shown with dashed lines, and the X-junctions (interior walls) are displayed with solid lines. A positive difference in Figure 7.5 indicates that the vibration reduction index is decreasing lower down in the building. Overall, there was a positive difference for all curves above 400 Hz. Furthermore, below 400 Hz, the curves in Figure 7.5 vary around 0 dB, with most of the curves also being positive. Initially, the curves have no good correlation, and one of the dashed curves is much higher than the rest. The results above 3150 Hz had a higher uncertainty due to the accelerometer mounting technique.

The difference in the vibration reduction index for the Wall–Ceiling path is displayed for all projects in Figure 7.6. Similar to the result in Figure 7.5, the curves were mainly positive with some variations around 0 dB, indicating that the vibration reduction index was decreasing lower down in the building where the load on the junctions was higher. However, the curves were more consistent with each other, and a more apparent correlation was seen without adjustments. The results above 3150 Hz had a higher uncertainty due to the accelerometer mounting technique.
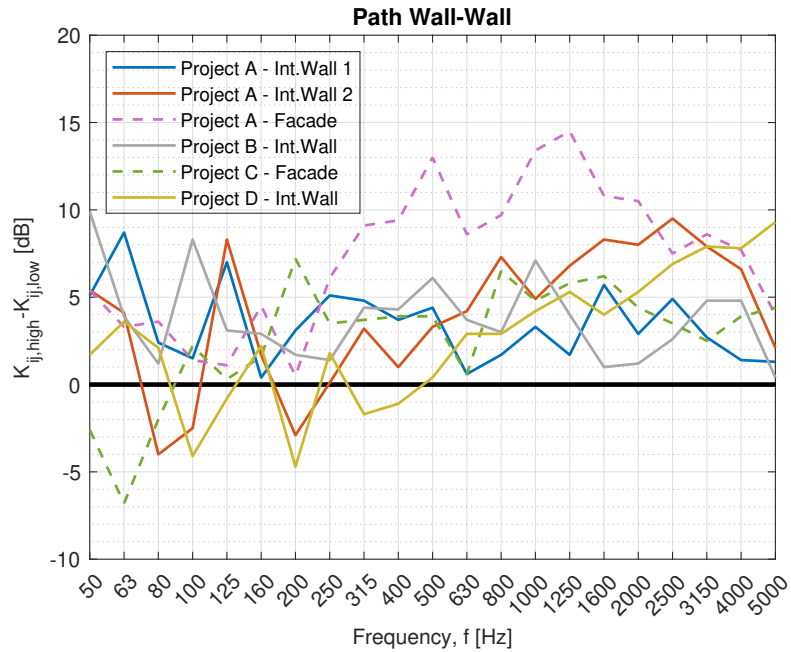
Figure 7.5: Difference in vibration reduction index for the Wall–Wall path between apartments situated at high and low stories for four different projects. Dashed curves represent T-junctions (facades), and solid lines represent X-junctions (interior walls).

Figure 7.6: Difference in vibration reduction index for the Wall–Ceiling path between apartments situated at high and low stories for four different projects. Dashed curves represent T-junctions (facades), and solid lines represent X-junctions (interior walls).

Lastly, the difference in vibration reduction index for the Wall–Floor path is displayed for all projects in Figure 7.7. The same result was not found here compared to the curves shown in Figure 7.5 and Figure 7.6. A few curves in Figure 7.7 vary more around 0 dB. Overall, the mean value was still positive (indicating that the vibration reduction index was decreasing lower down in the building) but not as apparent. Moreover, the curves were not consistent with each other, and no correlation was found without adjustments. Again, results above 3150 Hz had a higher uncertainty due to the accelerometer mounting technique.
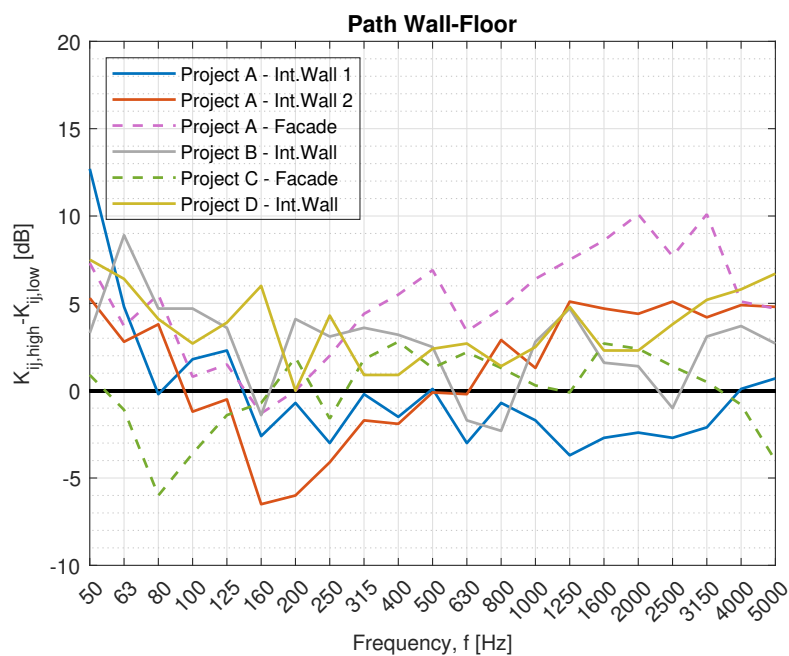
Figure 7.7: Difference in vibration reduction index for the Wall–Floor path between apartments situated at high and low stories for four different projects. Dashed curves represent T-junctions (facades), and solid lines represent X-junctions (interior walls).

7.4   Discussion

The junction pairs measured for the four projects have a different number of stories between them and different loads that affect the junctions. Thus, correlations with these factors are interesting to analyze in further detail.

7.4.1 Measurements Correlated with the Load

First, a correlation factor including the load was used to compare the results. Different load combinations could be used to find a suitable correlation factor, including combinations of the actual load when measurements took place and the quasi-permanent load combination that was used to choose the resilient interlayers in the finished buildings. However, it was only possible to obtain the load combinations for finished buildings. For these load combinations, the quasi-permanent load was relevant to use since it directly affected the choice of stiffness of the resilient interlayers in the junctions on the different stories for three of the four projects (one project had no resilient interlayers in the junctions). The load correlation factor according to Equation 7.4 is used:

$$\frac{\Delta K_{ij}}{0.08 \cdot \log_{10}\left((1.2\pi)^{(\Delta \text{Load}+14)}\right)}, \tag{7.4}$$

where ΔLoad is the quasi-permanent load in kN/m, and the result is displayed in Figure 7.8, Figure 7.9 and Figure 7.10 for the various paths. The y-axes in Figure 7.8, Figure 7.9 and Figure 7.10 are based on a reference number divided by the denominator in Equation 7.4, called the mean load correlation factor. This factor used the mean value of the ΔLoad from all the measurements in this article. The correlation factor in Equation 7.4 was first developed based on an iterative process. Later, it was adjusted so that the y-axis for both correlation methods matched (correlation with the number of stories and correlation with the load).

For the Wall–Wall path, mean value curves are displayed for X-junctions and T-junctions, since a correlation is found between the junction pairs and the difference between the X-junctions and T-junctions. The correlation is accurate for the T-junctions above 200 Hz, where the curves follow each other. However, for 200 Hz and below, the curves do not correlate with the load factor proposed in Equation 7.4. For the X-junctions, a good correlation is found for frequencies above 500 Hz. The correlation is also quite good for frequencies 500 Hz and below, but with slightly higher deviations. Overall, the correlation factor in Equation

7.4 results in a better correlation between the curves in Figure 7.8 compared to the results in Figure 7.5.

Figure 7.8: Difference in vibration reduction index for the Wall–Wall path, correlated with the load according to Equation 7.4, between apartments situated at high and low stories for four different projects. Dashed curves represent T-junctions (facades), and solid lines represent X-junctions (interior walls). Black curves represent mean value prediction curves.

For the Wall–Ceiling transmission path, the correlation factor according to Equation 7.4 does not show a good correlation between the curves in Figure 7.9. Thus, the black mean value curves are not displayed in Figure 7.9.

For the Wall–Floor transmission path, the correlation factor according to Equation 7.4 again does not show a good correlation between the curves in Figure 7.10. As a result, the black mean value curves are not displayed in Figure 7.10 either.
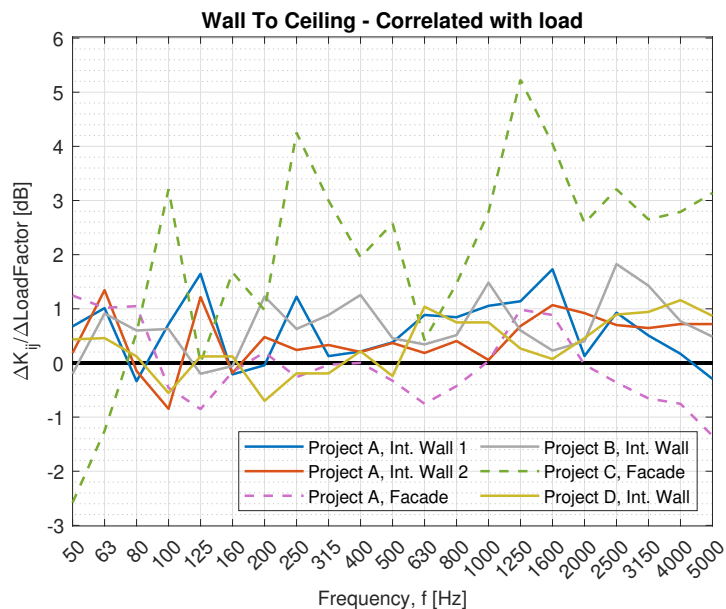
Figure 7.9: Difference in vibration reduction index for the Wall–Ceiling path, correlated with the load according to Equation 7.4, between apartments situated at high and low stories for four different projects. Dashed curves represent T-junctions (facades), and solid lines represent X-junctions (interior walls).
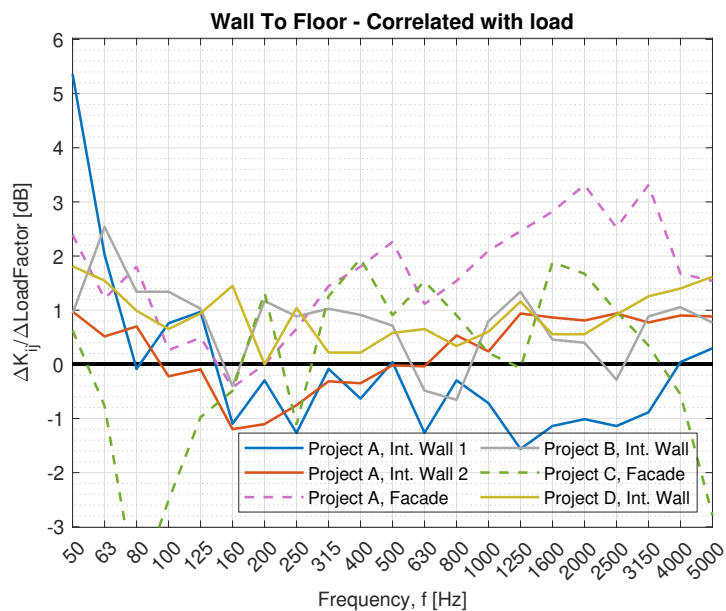
Figure 7.10: Difference in vibration reduction index for the Wall–Floor path, correlated with the load according to Equation 7.4, between apartments situated at high and low stories for four different projects. Dashed curves represent T-junctions (facades), and solid lines represent X-junctions (interior walls).

The common denominator between the Wall–Floor and Wall–Ceiling paths is the floor itself, and the floor is not a vertical element in contrast to the walls. Hence, this factor could be attributed to the lack of promising results in correlation with the load for the vibration reduction index paths that include the floor. It could also explain why the correlation performs well when only vertical elements, such as walls, are considered.

It would be interesting to correlate the result with a load combination when the measurements occurred. However, the same principal loads per story are more or less affecting the junctions when the measurements take place among the different projects, since measurements are made just after the CLT elements are mounted for each project. Thus, a correlation factor with the number of stories could show similar results, if we assume a linear correlation between the stories.

7.4.2 Measurements Correlated with the Number of Stories

As an alternative to correlating the result with the load, the difference in the number of stories within each junction pair is used according to the story correlation factor in Equation 7.5:

$$\frac{\Delta K_{ij}}{\Delta \text{Number of stories}}, \tag{7.5}$$

and the results are displayed in Figure 7.11, Figure 7.12 and Figure 7.13. The y-axes in Figure 7.11, Figure 7.12 and Figure 7.13 are based on a reference number that is divided by the denominator in Equation 7.5, called the mean story correlation factor. This factor uses the mean value of the ΔNumber of stories from all the measurements in this article. The same reference number is used for correlations with the load and the number of stories. A somewhat better correlation is seen with the number of stories in Figure 7.11 compared to the load in Figure 7.8 for the Wall–Wall path for both the T-junctions and X-junctions. This is statistically evaluated for the whole frequency range up to 3150 Hz, with both the root-mean-square error (RMSE) and the mean absolute error (MAE). Both are assessed, since the RMSE is more sensitive than the MAE to outliers [247]. However, varying results are obtained by evaluating

the RMSE and the MAE for different frequency regions (low (50–200 Hz), mid (250–1000 Hz), and high (1250–5000 Hz)) according to Hopkins [38]. The high-frequency region in this article was chosen as 1250–3150 Hz instead of 1250–5000 Hz because of a higher uncertainty in the measurement method for frequencies above 3150 Hz. The correlation with the load was found to be the best for the X-junctions at higher frequencies, while the correlation with the number of stories was found to be the best at lower frequencies for both the X- and T-junctions. The correlation with the load at higher frequencies was found to perform similarly as the correlation with the number of stories for the T-junctions. Both correlation methods performed similarly for the mid-frequency region, although the number of stories performed slightly better. The overall mean prediction values per story were calculated as 1.0 dB for the X-junctions and 1.6 dB for the T-junctions. The detailed prediction values are displayed in Figure E1, and the statistical results are shown in Figure E2.
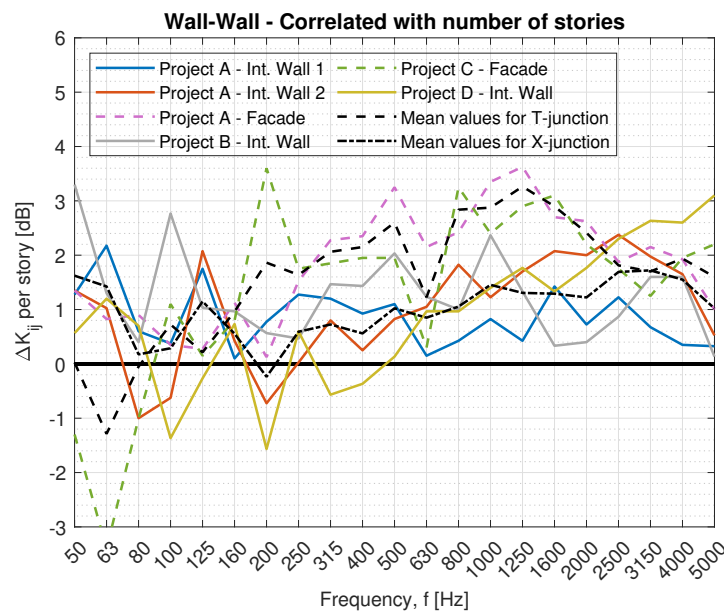
Figure 7.11: Difference in vibration reduction index for the Wall–Wall path, correlated with the number of stories according to Equation 7.5, between apartments situated at high and low stories for four different projects. Dashed curves represent T-junctions (facades), and solid lines represent X-junctions (interior walls). Black curves represent mean value prediction curves.
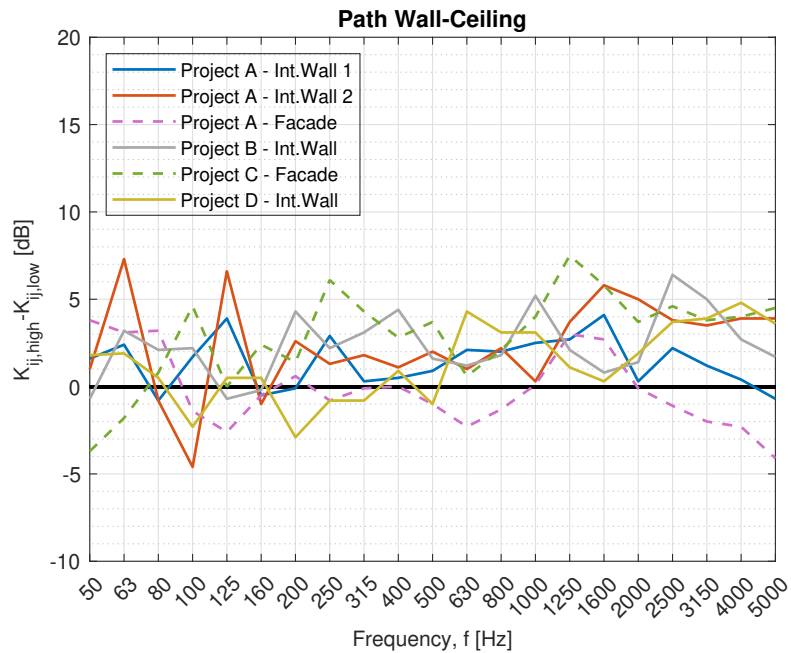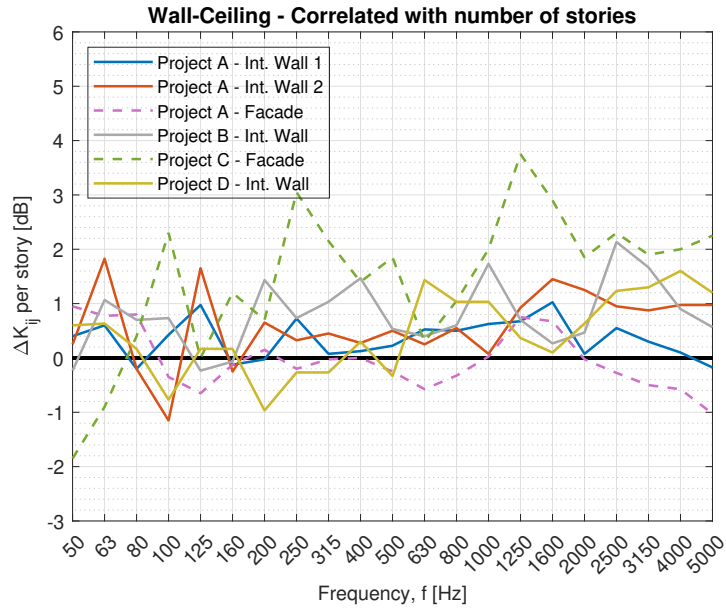
Figure 7.12: Difference in vibration reduction index for the Wall–Ceiling path, correlated with the number of stories according to Equation 7.5, between apartments situated at high and low stories for four different projects. Dashed curves represent T-junctions (facades), and solid lines represent X-junctions (interior walls).
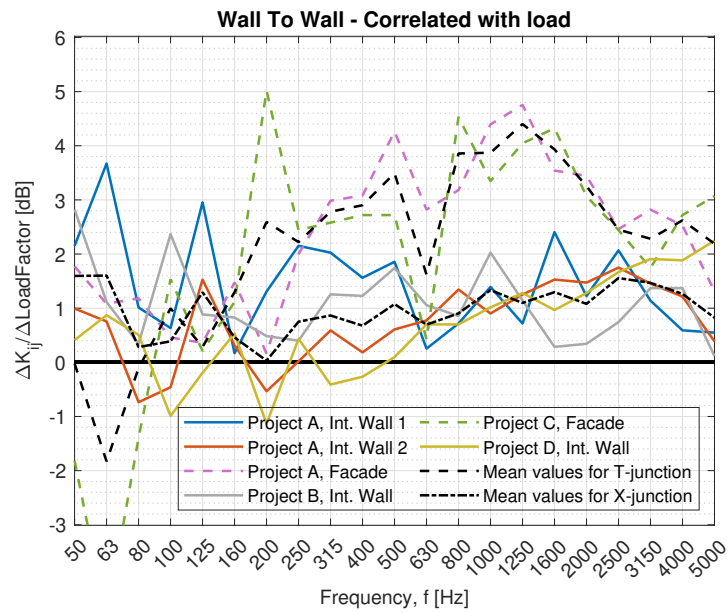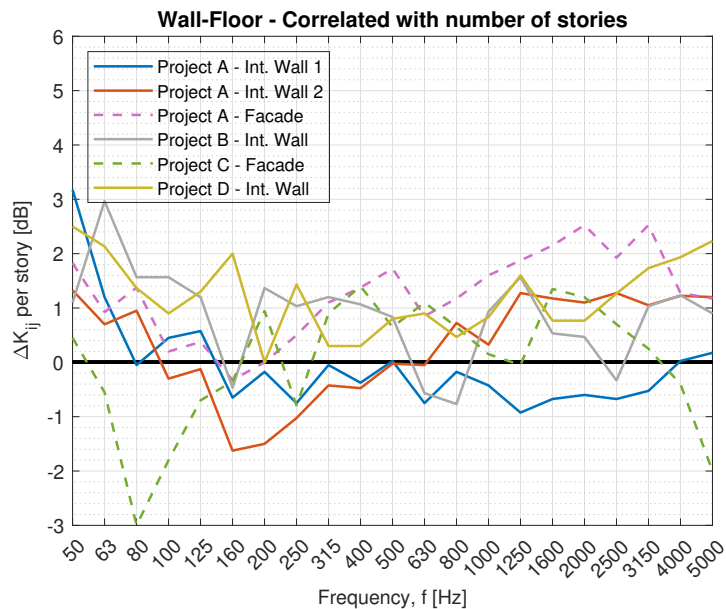

Figure 7.13: Difference in vibration reduction index for the Wall–Floor path, correlated with the number of stories according to Equation 7.5, between apartments situated at high and low stories for four different projects. Dashed curves represent T-junctions (facades), and solid lines represent X-junctions (interior walls).

For the Wall–Ceiling transmission path, the correlation factor according to Equation 7.5 does not show a good correlation among the curves in Figure 7.12. However, the correlation factor according to Equation 7.5 in Figure 7.12 performs better than the correlation factor according to Equation 7.4 in Figure 7.9.

For the Wall–Floor transmission path, the same result as the Wall–Ceiling path, as shown above, is found in Figure 7.13. The correlation factor according to Equation 7.5 performs better in Figure 7.13 than the correlation factor according to Equation 7.4 in Figure 7.10, and the correlation is not good between the curves in Figure 7.13.

The correlation factors in Equations 7.4 and 7.5 mainly depend on the difference in load or the number of stories. They could be improved by including frequency-dependent correlations, since there could be different behaviors around, for example, the various critical frequencies of the systems. By including other parameters in Equations 7.4 and 7.5, better correlations could be achieved, specifically in the mid- and lower-frequency regions below 400 Hz, where a lower correlation is seen compared to the higher frequencies above 400 Hz. However, more vibration reduction index measurements of various junction details in CLT are needed in the field to include more parameters in the correlations.

7.4.3 In-Depth Analysis

The quasi-permanent load combination is chosen as the input for the load correlation factor (Equation 7.4), since that load combination is used when the resilient interlayers are dimensioned. A slightly worse correlation is observed with the load compared to the number of stories for frequencies in the mid and low regions. One possible explanation for this outcome may be the choice of resilient interlayers compared to the actual load. Even if the resilient interlayers are designed for the right load, they are chosen based on a load interval that could cover a broad load range from some manufacturers. Furthermore, K_{ij} is measured on the CLT elements while they are visible, long before the building is completed. The load is, therefore, different when measurements occur compared to the designed load values in the

finished building, including larger dead loads and live loads. With this argument, the load when measurements occur should be used instead of the designed load in a finished building. However, the load when measurements take place is not representative for the chosen stiffness of the resilient interlayers in the finished building. The relation between the load and stiffness is expected to be more relevant, since the resilient interlayers' stiffness could directly affect the vibration reduction index, as shown for some materials in Refs. [116, 242]. Moreover, load combinations of just the bare CLT are only possible to be retrieved for some projects. Also, as argued at the end of Section 7.4.1, load combinations with only the bare CLT could have roughly the same correlation as the number of stories, if a linear correlation is assumed between the different stories.

The different stiffnesses of the resilient interlayers are chosen based on the quasi-permanent load, as previously described. Thus, stiffer resilient interlayers are chosen lower down in the building compared to the upper levels. As the literature [116, 242] shows, stiffer resilient interlayers contribute to a higher vibration transmission over a junction. Therefore, it could be argued that the result obtained in this study is related to the difference in stiffness of the resilient interlayers over the number of stories. However, as shown in project D, junctions without resilient interlayers show similar results as junctions with resilient interlayers. Furthermore, a previous paper [177] that measured the airborne sound transmission in similar buildings found the same similarity as shown in this paper. While the difference in stiffness of the resilient interlayers over the number of stories might have an effect, this does not solely explain the result found in this study. Therefore, an increasing load is found to negatively affect the vibration reduction index with or without resilient interlayers in the junctions, and a higher flanking sound transmission is expected at lower levels in the buildings. The explanation, as the previous literature suggested [185], is that an increasing load yields stiffer junctions that result in a lower vibration reduction index. Hence, the load on the junctions needs to be considered with increasing stories in high-rise buildings.

The measurement results for the paths including the floor/ceiling show a slightly positive

difference overall between K_{ij} at high and low stories, with a smaller K_{ij} lower down in the building. Moreover, analysis indicates that the Wall–Wall path yields a better result with the correlation factors than paths including the floor, compared to with no correlations. The difference in correlation performance could be caused by the fact that a floor is not affected to the same degree by the load as a vertical element, like a wall. However, the junction itself should be affected and have a result on the vibration reduction index. Furthermore, measurements of the directional average velocity level difference show that the velocity level difference varies more depending on the direction when the floor/ceiling is included, compared to the Wall–Wall path. For the Wall–Wall path, the velocity level difference is almost identical in either direction. Whether this is due to the measurement procedure or other physical parameters is uncertain at the moment and requires further investigation.

The measurements in Ref. [117] showed that the load primarily affects the vibration reduction index up to an initial load of the first story and that an additional increased load does not change the acoustical propagation properties. The measurements of the junctions in this paper described as high are junctions that are situated on the upper stories. Measurements also take place when the CLT elements are visible. The load is, therefore, smaller when measurements occur compared to a finished building. Thus, the result shown in this paper could be related to the same findings seen in Ref. [117]. However, the measurements in Ref. [177] were not at the highest stories, and the airborne sound insulation was measured in the finished buildings with the right load where a difference per story was found. Furthermore, a correlation between the number of stories and the load yields a good result in this paper over the frequency span for the Wall–Wall path and specifically for the T-junctions above 200 Hz. In contrast, the same correlation accuracy is not found for the two other paths, which could be more related to the findings in Ref. [117]. Consequently, the mean value curves, presented in Figure E1, can be used when estimating the decrease in sound insulation and the need for additional treatments lower down in the building. However, they should be used with some caution, since they are field measurements and were only verified by one operator in four

buildings. Additional measurements of the junctions in finished buildings, for each story, are needed to find more accurate estimations. This includes measurements where the difference in the number of stories is higher than four, to see if the effect is similar for even taller high-rise buildings than the ones measured in this paper.

7.5   Conclusions

The purpose of this study was to evaluate the vibration reduction index of several CLT buildings with different junction details at different stories, based on in situ measurements.

The measurements in this study indicate that the number of stories, or the load, has a negative effect on the vibration reduction index of the junctions in CLT buildings. A higher flanking sound transmission and a decrease in sound insulation are expected lower down in the building. The statement is supported by measurements from several buildings with various junction types, as shown in Figure 7.3. Also, the same tendency is seen for junctions without resilient interlayers. Therefore, the number of stories, or the load, is the primary factor for the building height effect, rather than the difference in the stiffness of the resilient interlayers.

The measurements were evaluated between two- and four-story differences, where individual junction pairs for the Wall–Wall path can differ by more than 10 dB in the vibration reduction index for specific third-octave band frequencies. In addition, the mean difference per story for the Wall–Wall path was calculated as 1.0 dB for the X-junctions and 1.6 dB for the T-junctions, with a decreasing vibration reduction index lower down in the building. If several flanking paths affect the sound insulation, and if the building has several stories, these factors can significantly affect the final result. Consequently, the number of stories, or the load, needs to be considered during the design phase for acoustical treatments.

7.6 Additional work

After publication of the article [205], more work was made to understand the measurement uncertainties.

7.6.1 Measurement method uncertainty

Measurements in the field have uncertainties caused by the measurement method, and it is important to quantify when they are used in estimations. Measurement uncertainties due to several factors were described in Section 5.3.2. With this in mind, the uncertainties due to the measurement method for the velocity level difference were evaluated in a CLT building. Velocity level differences of a junction between a floor and a wall without a resilient interlayer between the CLT elements were measured. The measurement procedure followed the procedure in Section 7.2, but only one direction was evaluated, and only the velocity level difference. A total of 6 measurement series were performed to evaluate the uncertainties caused by the measurement method properly, and the result is presented in Figure 7.14, where all six measurements are displayed.

The spread between individual measurements is not clearly visible in Figure 7.14, and relative differences are calculated and presented in Figure 7.15 to evaluate the spread closer. Here, the lowest standard deviation of the relative differences was calculated for each measurement, and measurement 5 yielded the lowest standard deviation. Thus, it is used as a reference value to present the relative differences by taking Meas.5-Meas.X where X is an integer between 1-6. The spread is overall higher at frequencies from 2000 Hz and above, likely due to the mounting conditions of the accelerometers (weak fixing) as discussed in Section 6.4.1. The spread is generally acceptable, with minor deviations in low and mid-frequencies. Additionally, the standard deviation per third-octave frequency band is calculated separately in Figure 7.16. It is here clear that the higher frequencies have higher deviations.
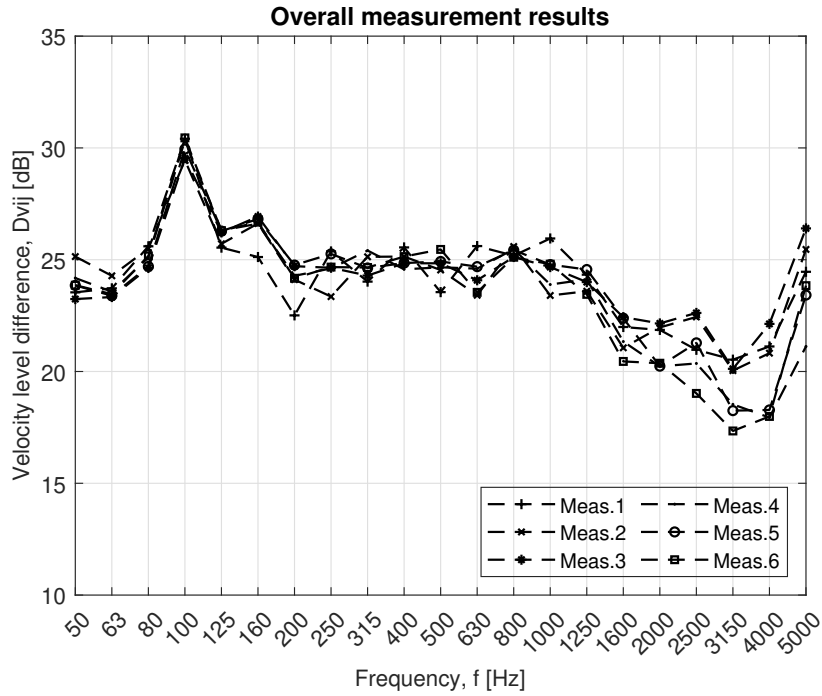
Figure 7.14: Velocity level difference measurements, measured a total of 6 times in a junction.
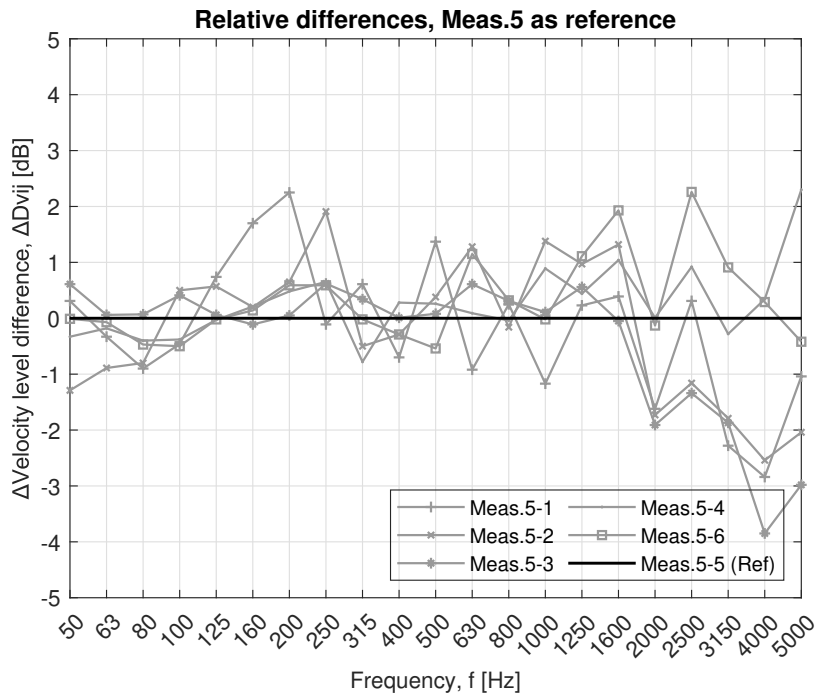
Figure 7.15: Relative differences for measurements between the same junction transmission path. Meas.5 is used as a reference.
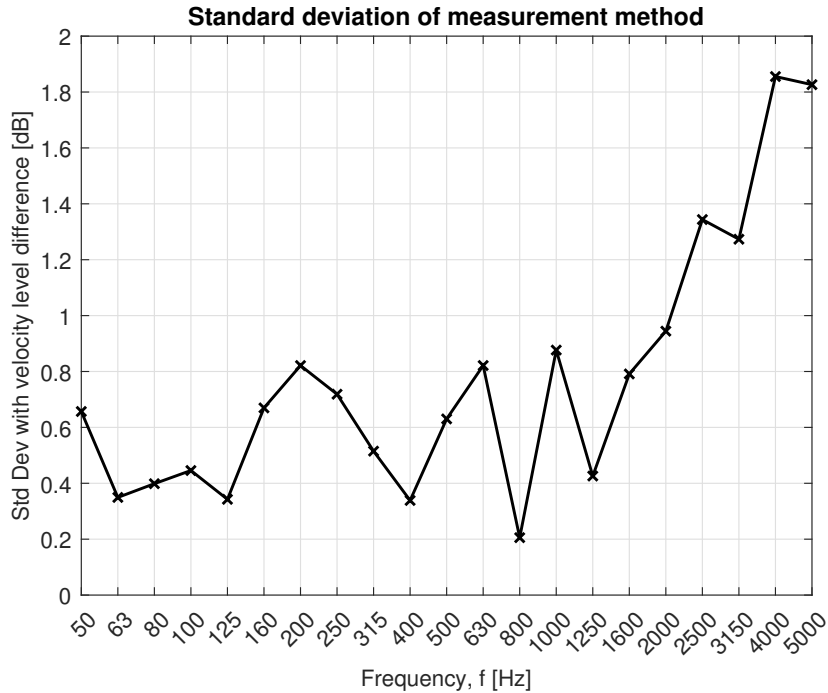
Figure 7.16: Standard deviation of the measurement method with the velocity level difference.

Considering the measurement uncertainties, previous estimations should be displayed with the standard deviation due to the measurement method. Prior to that, some adjustments are required. The measurement uncertainty applies to both the measurements at the higher and lower stories. Consequently, the difference in sound insulation across various stories is influenced by two standard deviations. The standard deviation for the difference between measurements, σ_{diff}, is calculated using Equation 5.6.

By modifying the result in Figure 7.16 with Equation 5.6, the result in Figure 7.17 is formed. The standard deviation presented in Figure 7.17 can be used along with the presented data in Figures 7.5 to 7.7.
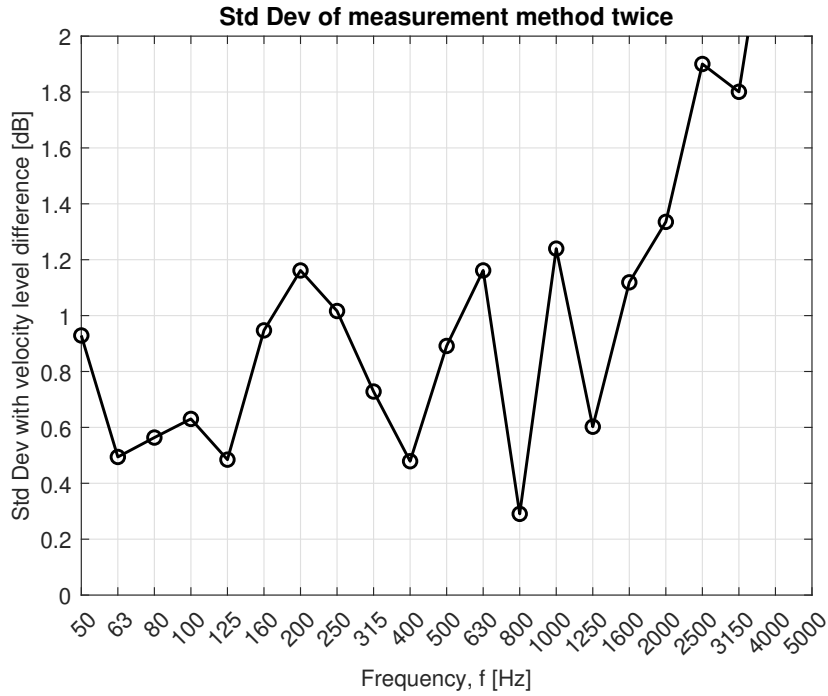
Figure 7.17: Standard deviation of the measurement method with the velocity level difference twice.

However, the standard deviation presented in Figure 7.17 does not accurately reflect the estimations per story in Figure 7.11 without additional modifications. The values in Figure 7.11 are calculated from Figure 7.5 where the curves are divided with the difference in the number of stories for each measurement pair. Thus, the same approach should be used to calculate the standard deviation in Figure 7.17 per story for each measurement pair, $\sigma_{n,\text{diff per story}}$, following Equation 5.7, where the differences are assumed to be identically distributed across the number of stories.

The standard deviation per story for each measurement pair, $\sigma_{n,\text{diff per story}}(f)$, is combined to one average standard deviation per story, and the root mean square (RMS) method can be used following Equation 5.8. Lastly, the overall standard deviation from the measurement method per story is achieved and presented in Figure 7.18. The uncertainties for the case with load are not evaluated since the result with the number of stories is overall more accurate.
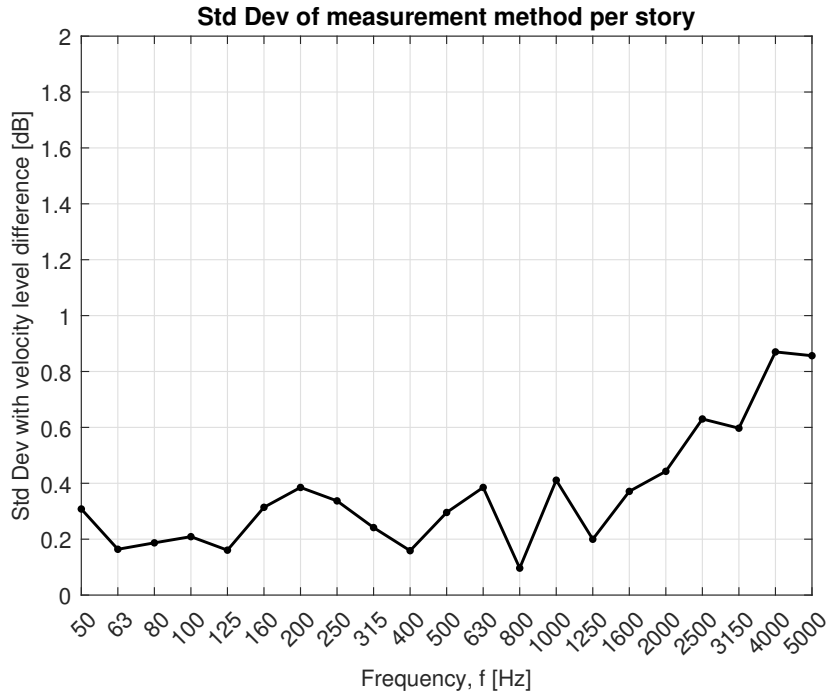
Figure 7.18: Standard deviation of the measurement method with the velocity level difference per story.

7.6.2 General comments

In this chapter, the results presented, along with those in Ref. [205], may be influenced to a higher degree by the fact that the initial load affects the difference most. In Ref. [205], measurements were made on the higher stories in the buildings with visible CLT elements. As a result, the load on the junctions is far from the designed load when the buildings are finished. Consequently, the outcomes reported in this chapter and Ref. [205] may not necessarily be related just to the overall difference lower down the building but more related to the initial load decrease. This assertion aligns well with the conclusions drawn in Ref. [177], where the differences between stories were observed to be smaller than those reported in Ref. [205].

Nevertheless, the findings in Ref. [205] offer intriguing insights. Firstly, the building height effect significantly impacts the vibration reduction index, with a worse performance in sound insulation lower down the building. Secondly, vibration reduction index measurements on CLT junctions conducted in a laboratory environment without additional loads on the

junctions are anticipated to yield more favorable results than those achievable in the field. A load corresponding to the first story should be applied following Ref. [117] and what was found in Section 5.5.2. Therefore, K_{ij} values of vertical junctions from a laboratory setting without additional loads on the junctions should be used cautiously for predictive or estimative purposes. However, existing K_{ij} values of vertical junctions from laboratory measurements without an applied load can be used with less caution if corrections from Ref. [205] and this chapter are used. Average correction values for different transmission paths of vertical junctions are illustrated in Figures 7.19, 7.20, and 7.21 along with the standard deviation from 7.18, where negative values are ignored and set to 0 since an improvement lower down the building is not expected. Positive values in Figures 7.19, 7.20, and 7.21 indicate a decrease in vibration reduction index. Values are presented in Tables E2, E3, and E4.
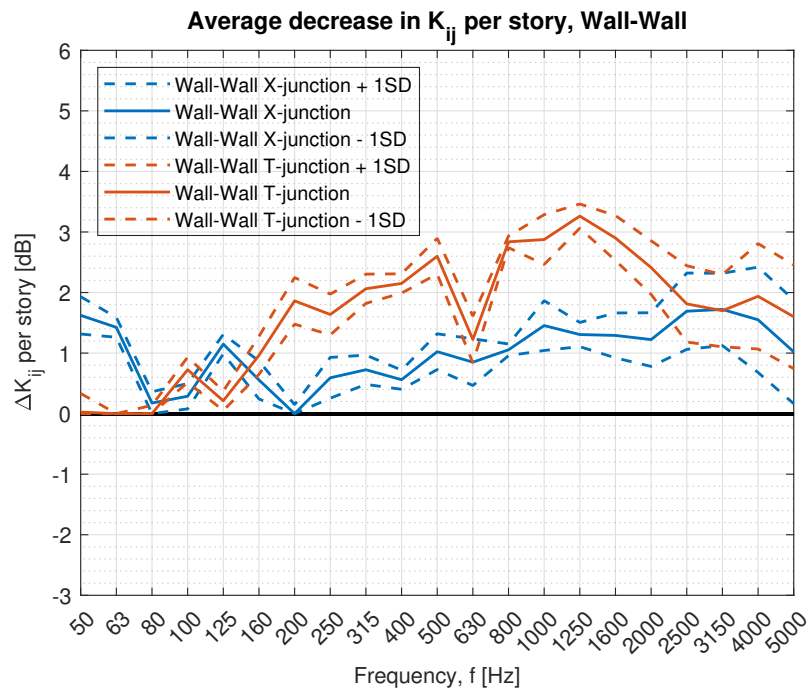
Figure 7.19: Estimations of the decrease in vibration reduction index per story lower down the building for the wall-wall path, plus and minus one standard deviation of the measurement method. Values are presented in Table E2.
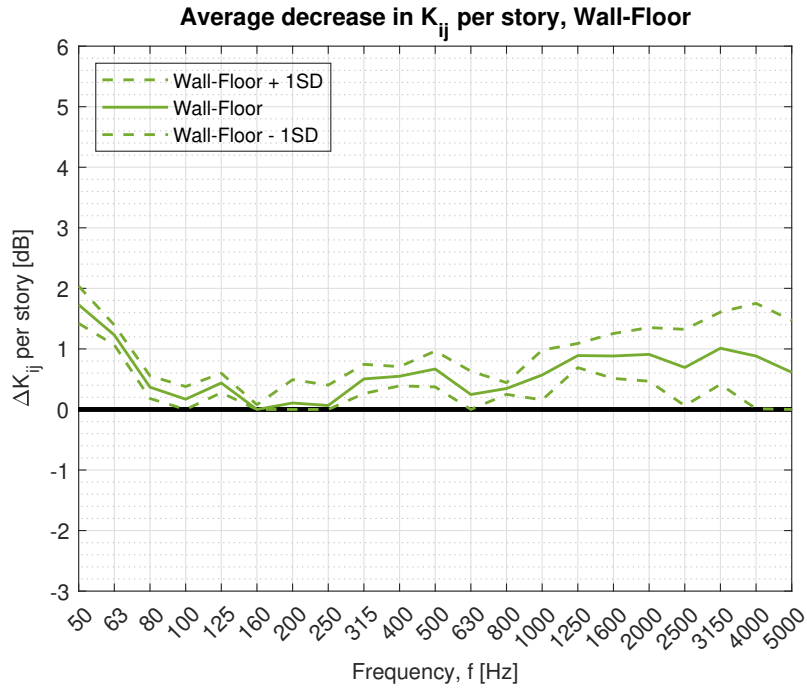
Figure 7.20: Estimations of the decrease in vibration reduction index per story lower down the building for the wall-floor path, plus and minus one standard deviation of the measurement method. Values are presented in Table E3.
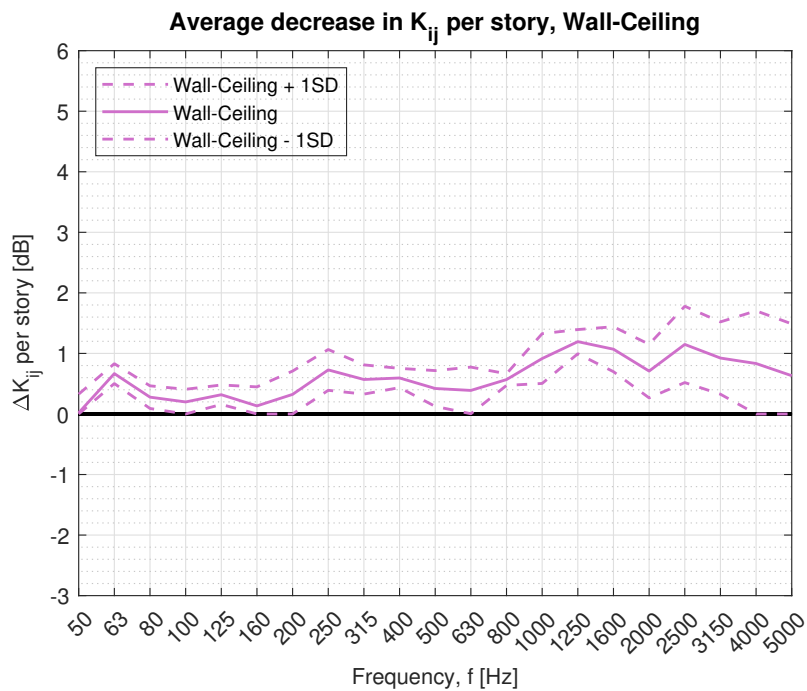
Figure 7.21: Estimations of the decrease in vibration reduction index per story lower down the building for the wall-ceiling path, plus and minus one standard deviation of the measurement method. Values are presented in Table E4.

CHAPTER 8

CONCLUSIONS AND FUTURE PROSPECTS

8.1   Conclusions

The presented thesis demonstrates several estimations for parameters affecting lightweight buildings' flanking airborne sound insulation. A sound transmission path model for a wall with a continuous ventilation duct through it can estimate the sound reduction of three types of ventilation ducts (Chapter 3). Depending on the separating construction, the necessary treatments with external lagging and the combination with a suspended ceiling can be estimated based on a partial or completely wrapped duct (Chapter 4). A comprehensive understanding of the building height effect in cross-laminated timber buildings is shown, and a decrease in sound insulation of more than 0.5 dB per story lower down the building is found (Chapters 5 and 7).

The first study (Chapter 3) focused on estimating the sound reduction of a combined system with a separating wall and a ventilation duct. The proposed estimation for circular ducts and modifications of the existing theory for rectangular ducts demonstrated good agreement with measurement data with the proposed transmission path model. The study emphasized that the part of the ventilation duct nearest to the wall affects the improvement in sound reduction most with external lagging of stone wool. Moreover, wrapping with stone wool proves effective, but treatment choice depends on several factors, such as the sound reduction of the direct path and the duct configuration.

The second study (Chapter 4) focuses on acoustical treatments, mainly external lagging on

ventilation ducts, to limit the flanking sound transmission via the ventilation duct. Estimations that consider the duct's shape and whether it is partly or completely wrapped with stone wool are developed. The part of the duct closest to the wall is identified as a primary factor to improve the sound reduction. However, for high sound reduction requirements, it is not enough to only partly cover the ventilation duct with external lagging of stone wool. Suspended absorbing ceilings are shown to be effective for lower sound reduction requirements without additional treatments on the ducts, but external lagging becomes essential with high sound reduction requirements.

The third study (Chapter 5) investigated the effect of the building height on the vertical airborne sound insulation in four cross-laminated timber buildings. Based on measurements performed in buildings with varying numbers of floors and different construction systems, it was observed that the load affects the vertical airborne sound insulation negatively, regardless of the presence of resilient interlayers between load-bearing CLT elements. In conclusion, a decrease in sound insulation of 0.5 dB per story is expected lower down the building. However, it depends on how much the flanking sound transmission affects the sound insulation in relation to other transmission paths. The study emphasizes the need to consider the number of stories during the design phase for acoustical treatments.

The fourth study (Chapter 6) evaluated mounting techniques for accelerometers on CLT elements and discussed how the bearing direction could affect the vibration reduction index. It concluded that double-sided adhesive tape is a suitable substitute for beeswax, with exceptions at higher frequencies where a greater risk of weak fixing exists. Moreover, two different test methods conclude with measurements that the bearing direction of the floor influences the vibration reduction index of a junction with CLT elements. Measurements show that a floor should be oriented with a parallel bearing direction in relation to the junction for the junction that is most critical in the room.

The fifth study (Chapter 7) investigated the effect of the building height on the vibration reduction index of four CLT buildings with different junction details at various stories. Similar

to airborne sound insulation measurements, a worse sound insulation was found lower down the buildings. A reduction of more than 1.0 dB was found when measuring the vibration reduction index. Moreover, it is found that the building height effect is more significant in T-junctions (facade) compared to X-junctions (interior wall). However, estimations of the building height effect with the vibration reduction should be used more cautiously since they are based on less data than the airborne measurements.

8.2   Future Work

The estimations presented in this thesis provide valuable insights into optimizing the acoustic performance of buildings by reducing the variability in sound insulation values typically observed in lightweight buildings. While several parameters have been considered, further research is imperative to refine the proposed estimations and to explore estimations for additional parameters influencing flanking sound insulation in lightweight buildings.

In our analysis of various ventilation duct types, a constant length was maintained, potentially limiting our understanding of the duct's surface area and the effect of a line source. For instance, a line source assumption is questionable for lengths of less than one meter, warranting further investigation. Additionally, it would be worthwhile to compare estimations across other sizes of ventilation ducts, particularly rectangular ones, as only one was included in the measurement series.

Considering acoustical treatments on ventilation ducts, varying thicknesses and densities of external lagging with stone wool presents an intriguing avenue for further inquiry. Our analysis was based on measurements involving one density but with two thicknesses. Testing and comparison against the developed estimations with more thicknesses and densities would likely increase the accuracy of the estimations since the surface density of the applied external lagging is a part of the estimations. Moreover, assessing the effect of external lagging with stone wool in combination with suspended ceilings would be valuable to ensure that the effect

in the estimations is appropriate, or to determine if adjustments are required.

Regarding the bearing direction effect of Cross-Laminated Timber (CLT) elements, our study observed an effect in a limited set of measurements using two different methods. Moving forward, additional measurements with varying junction types and CLT element thicknesses are needed. Furthermore, floors constructed with Laminated Veneer Lumber (LVL) are also interesting to examine, given the consistent orientation of laminae in the building material.

The building height effect was confirmed in this thesis with airborne sound insulation measurements and vibration reduction index measurements. While the decrease in sound insulation is most visible on higher levels, the decrease is still visible and present further down the buildings with CLT as bearing elements. Moving forward, additional measurements with different building systems, including wooden frame houses, LVL, and concrete buildings are needed. With a minor effect of flanking, the number of stories between measurements at higher and lower stories must be increased for the observed difference to be larger than the uncertainties caused by the measurement method and the workmanship. Lastly, the estimations in this study are limited to a ten-story building, and measurements in buildings with more stories are therefore of interest.

REFERENCE LIST

1. Hassan OAB. Building Acoustics and Vibration: Theory and Practise. Building Acoustics and Vibration. Singapore: World Scientific Publishing Company, 2009. DOI: 10.1142/7165

2. United Nations Environment Programme. Global Status Report for Buildings and Construction: Towards a Zero-emission, Efficient and Resilient Buildings and Construction Sector. Report. Nairobi, Kenya, 2020

3. Robertson AB, Lam FCF, and Cole RJ. A Comparative Cradle-to-Gate Life Cycle Assessment of Mid-Rise Office Building Construction Alternatives: Laminated Timber or Reinforced Concrete. Buildings 2012; 2:245–70. DOI: 10.3390/buildings2030245

4. Gustavsson L, Pingoud K, and Sathre R. Carbon Dioxide Balance of Wood Substitution: Comparing Concrete- and Wood-Framed Buildings. Mitig Adapt Strat Glob Change 11 2006; 11:667–91. DOI: 10.1007/s11027-006-7207-1

5. Gerilla GP, Teknomo K, and Hokao K. An environmental assessment of wood and steel reinforced concrete housing construction. Building and Environment 2007; 42:2778–84. DOI: 10.1016/j.buildenv.2006.07.021

6. Padilla-Rivera A, Amor B, and Blanchet P. Evaluating the Link between Low Carbon Reductions Strategies and Its Performance in the Context of Climate Change: A Carbon Footprint of a Wood-Frame Residential Building in Quebec, Canada. MDPI AG 2018; 10. DOI: 10.3390/su10082715

7. Buchanan AH and Honey BG. Energy and carbon dioxide implications of building construction. Energy and Buildings 1994; 20:205–17. DOI: 10.1016/0378-7788(94)90024-8

8. Nässén J, Hedenus F, Karlsson S, and Holmberg J. Concrete vs. wood in buildings – An energy system approach. Building and Environment 2012; 51:361–9. DOI: 10.1016/j.buildenv.2011.11.011

9. Karacabeyli E and Gagnon S. Canadian CLT Handbook. Vol. 1. Point-Claire, QC, Canada: FPInnovations, 2019

10. Rindel JH. Sound Insulation in Buildings. Boca Raton: CRC Press, Taylor & Francis Group, 2018

11. Forssén J, Kropp W, Brunskog J, Ljunggren S, Bard D, Sandberg G, Ljunggren F, Ågren A, Hallström O, Dybro H, Larsson K, Tillberg K, Jarnerö K, Sjökvist LG, Östman B, Hagberg K, Bolmsvik Å, Olsson A, Ekstrand CG, and Johansson M. Acoustics in wooden buildings, State of the art 2008, Vinnova project 2007-01653. Report. Stockholm, Sweden: SP Trätek (Technical Research Institute of Sweden), 2008

12. Hagberg K. Dimensionering av flerbostadshus med trästomme – en balansgång. Bygg & teknik 3/22 2022. Accessed 2024-02-09. Available from: `https://byggteknikforlaget.se/dimensionering-av-flerbostadshus-med-trastomme-en-balansgang/`

13. Vér IL. Prediction of Sound Transmission through Duct Walls; Breakout and Pickup. Report. American Society of Heating, Refrigerating and Air-Conditioning Engineers Research Project, 1983

14. Cummings A. Sound transmission through duct walls. Journal of Sound and Vibration 2001; 239:731–65. DOI: `10.1006/jsvi.2000.3226`

15. Bader Eddin M, Ménard S, Bard Hagberg D, and Kouyoumji JL. Modeling field measurements of sound insulation performance for multi-layered CLT-based floor systems: A means of prediction model using artificial neural networks. Building and Environment 2023. DOI: `10.1016/j.buildenv.2023.110561`

16. Bard D, Davidsson P, and Wernberg PA. Sound and Vibrations investigations in a multi-family wooden frame building. *In proceedings of the 20th International Congress on Acoustics (ICA)*. Sydney, Australia, 23–27 August. 2010

17. Öqvist R and Ljunggren F. Variations in sound insulation from 20 Hz in lightweight dwellings. Noise Control Engineering Journal 2018; 66:56–65. DOI: `10.3397/1/37666`

18. Timpte A. Vibration Reduction Indices of Cross Laminated Timber Structures. Dataset. Accessed 2024-02-09. 2017. Available from: `https://www.th-rosenheim.de/fileadmin/fakultaeten/ang/Labore_ANG/Labor_fuer_Schallmesstechnik/Download/2017-03-23_Documentation_Kij.pdf`

19. Hörnmark J. Acoustic performance of junctions in cross laminated timber constructions. Master's thesis. Chalmers University of Technology, Göteborg, Sweden, 2019

20. Caniato M, Bettarello F, Ferluga A, Marsich L, Schmid C, and Fausti P. Acoustic of lightweight timber buildings: A review. Renewable and Sustainable Energy Reviews 2017; 80:585–96. DOI: `10.1016/j.rser.2017.05.110`

21. Cummings A. Low frequency acoustic transmission through the walls of rectangular ducts. Journal of Sound and Vibration 1978; 61:327–45. DOI: `10.1016/0022-460x(78)90384-x`

22. Cummings A. Approximate Asymptotic Solutions for Acoustic Transmission through the Walls of Rectangular Ducts. Journal of Sound and Vibration 1983; 90:211–27. DOI: `10.1016/0022-460x(83)90529-1`

23. Cummings A. Higher order mode acoustic transmission through the walls of rectangular ducts. Journal of Sound and Vibration 1983; 90:193–209. DOI: 10.1016/0022-460x(83)90528-x

24. Astley RJ and Cummings A. A finite element scheme for acoustic transmission through the walls of rectangular ducts: Comparison with experiment. Journal of Sound and Vibration 1984; 92:387–409. DOI: 10.1016/0022-460x(84)90387-0

25. Cummings A. Low frequency sound transmision through the walls of rectangular ducts: Further comments. Journal of Sound and Vibration 1979; 63:463–5. DOI: 10.1016/0022-460x(79)90692-8

26. Cummings A. Design charts for low frequency acoustic transmission through the walls of rectangular ducts. Journal of Sound and Vibration 1981; 78:269–89. DOI: 10.1016/s0022-460x(81)80038-7

27. Cummings A. Stiffness control of low frequency acoustic transmission through the walls of rectangular ducts. Journal of Sound and Vibration 1981; 74:351–80. DOI: 10.1016/0022-460x(81)90304-7

28. Cummings A. Low frequency acoustic radiation from duct walls. Journal of Sound and Vibration 1980; 71:201–26. DOI: 10.1016/0022-460x(80)90347-8

29. Cummings A and Chang IJ. A finite difference scheme for acoustic transmission through the walls of distorted circular ducts and comparison with experiment. Journal of Sound and Vibration 1986; 104:377–93. DOI: 10.1016/0022-460x(86)90296-8

30. Cummings A, Chang IJ, and Astley RJ. Sound transmission at low frequencies through the walls of distorted circular ducts. Journal of Sound and Vibration 1984; 97:261–86. DOI: 10.1016/0022-460x(84)90322-5

31. Cummings A and Chang IJ. Noise breakout from flat-oval ducts. Journal of Sound and Vibration 1986; 106:17–33. DOI: 10.1016/s0022-460x(86)80171-7

32. Chang IJ and Cummings A. Higher order mode and multimode acoustic transmission through the walls of flat-oval ducts. Journal of Sound and Vibration 1986; 108:157–64. DOI: 10.1016/s0022-460x(86)80319-4

33. Reynolds DD. Hvac Systems Duct Design. Third Ed. Chapter 11 - Noise control. Chantilly, VA, USA: Sheet Metal and Air Conditioning Contractors' National Association, 1990

34. Long M. Architectural Acoustics. Chapter 14. Boston, MA, USA; Oxford, UK: Academic Press, 2006 :872

35. Nilsson E. Hur genomföring av ventilationskanaler påverkar lättregelväggars ljudisolering. Accessed 2024-02-09. Master Thesis. Lund University, 2020. Available from: http://lup.lub.lu.se/student-papers/record/9010166

36. Cummings A. The effects of external lagging on low frequency sound transmission through the walls of rectangular ducts. Journal of Sound and Vibration 1979; 67:187–201. DOI: `10.1016/0022-460x(79)90483-8`

37. Venkatesham B, Munjal ML, and Tiwari M. Prediction of Breakout Noise from Acoustically Lagged Rectangular HVAC Ducts. Building Acoustics 2009; 16:313–28. DOI: `10.1260/135101009790291246`

38. Hopkins C. Sound Insulation. 1st Edition. London: Routledge, 2007 :648. DOI: `10.1201/9781003070788`

39. International Organization for Standardization. Building acoustics — Estimation of acoustic performance of buildings from the performance of elements — Part 1: Airborne sound insulation between rooms. (ISO 12354-1:2017). Geneva, Switzerland, 2017

40. Cremer L, Heckl M, and Petersson BAT. Structure-Borne Sound. third ed. Springer Berlin, Heidelberg, Germany, 2005

41. Craik RJM and Smith RS. Sound transmission through lightweight parallel plates. Part II: structure-borne sound. Applied Acoustics 2000; 61:247–69. DOI: `10.1016/S0003-682X(99)00071-7`

42. Craik RJM and Smith RS. Sound transmission through double leaf lightweight partitions - part I: airborne sound. Applied Acoustics 2000; 61:223–45. DOI: `10.1016/S0003-682X(99)00070-5`

43. Craik RJM. Non-resonant sound transmission through double walls using statistical energy analysis. Applied Acoustics 2003; 64:325–41. DOI: `10.1016/S0003-682X(02)00051-8`

44. Shen C, Xin FX, and Lu TJ. Theoretical model for sound transmission through finite sandwich structures with corrugated core. International Journal of Non-Linear Mechanics 2011; 47:1066–72. DOI: `10.1016/j.ijnonlinmec.2011.09.014`

45. Shen C, Xin FX, and Lu TJ. Sound transmission through lightweight double-leaf partitions: theoretical modelling Author links open overlay panel. Journal of Sound and Vibration 2005; 286:817–47. DOI: `10.1016/j.jsv.2004.10.020`

46. Yang Y, Fenemore C, Kingan MJ, and Mace BR. Analysis of the vibroacoustic characteristics of cross laminated timber panels using a wave and finite element method. Journal of Sound and Vibration 2021; 494. DOI: `10.1016/j.jsv.2020.115842`

47. Qian C, Ménard S, Bard D, and Negreira J. Development of a Vibroacoustic Stochastic Finite Element Prediction Tool for a CLT Floor. MDPI Applied Science 2019; 9. DOI: `10.3390/app9061106`

48. Guigou-Carter C and Villot M. Modelling of Sound Transmission through Light-weight Elements with Stiffeners. Building Acoustics 2003; 10:193–209. DOI: `10.1260/135101003322662005`

49. Zimmermann A. Acoustical Performance of Wooden Lightweight Industrialized Buildings. University of Quebec at Chicoutimi. Master Thesis. 2021

50. Bader Eddin M, Ménard S, Bard Hagberg D, Kouyoumji JL, and Vardaxis NG. Prediction of Sound Insulation Using Artificial Neural Networks—Part I: Lightweight Wooden Floor Structures. MDPI Acoustics 2022; 4:203–26. DOI: `10.3390/acoustics4010013`

51. Bader Eddin M, Vardaxis NG, Ménard S, Bard Hagberg D, and Kouyoumji JL. Prediction of Sound Insulation Using Artificial Neural Networks—Part II: Lightweight Wooden Façade Structures. MDPI Applied Sciences 2022; 12:69–83. DOI: `10.3390/app12146983`

52. Sharp BH. A Study of Techniques to Increase the Sound Insulation of building elements. WR 73-5. 1973

53. Legault J and Atalla N. Numerical and experimental investigation of the effect of structural links on the sound transmission of a lightweight double panel structure. Journal of Sound and Vibration 2009; 324:712–32. DOI: `10.1016/j.jsv.2009.02.019`

54. Legault J and Atalla N. Sound transmission through a double panel structure periodically coupled with vibration insulators. Journal of Sound and Vibration 2010; 329:3082–100. DOI: `10.1016/j.jsv.2010.02.013`

55. Sas P, Bao C, Augusztinovicz F, and Desmet W. Active control of sound transmission through a double panel partition. Journal of Sound and Vibration 1995; 180:609–25. DOI: `10.1006/jsvi.1995.0102`

56. Oliazadeh P, Farshidianfar A, and Crocker MJ. Study of sound transmission through single- and double-walled plates with absorbing material: Experimental and analytical investigation. Applied Acoustics 2019; 145:7–24. DOI: `10.1016/j.apacoust.2018.09.014`

57. Díaz-Cereceda C, Poblet-Puig J, and Rodríguez-Ferran A. The finite layer method for modelling the sound transmission through double walls. Journal of Sound and Vibration 2012; 331:4884–900. DOI: `10.1016/j.jsv.2012.06.001`

58. Galbrun L. Vibration transmission through plate/beam structures typical of lightweight buildings: Applicability and limitations of fundamental theories. Applied Acoustics 2010; 71:587–96. DOI: `10.1016/j.apacoust.2010.01.009`

59. Oliazadeh P, Farshidianfar A, and Crocker MJ. Experimental study and analytical modeling of sound transmission through honeycomb sandwich panels using SEA method. Composite Structures 2022; 280. DOI: `10.1016/j.compstruct.2021.114927`

60. Poblet-Puig J, Vilaseca R, and Rodríguez-Ferran A. Numerical Modelling of Sound Transmission in Double Walls. *In proceedings of Euronoise*. Tampere, Finland. 2006

61. Churchill C and Hopkins C. Prediction of airborne sound transmission across a timber–concrete composite floor using Statistical Energy Analysis. Applied Acoustics 2016; 110. DOI: 10.1016/j.apacoust.2016.03.031

62. Nilsson AC. Wave propagation in and sound transmission through sandwich plates. Journal of Sound and Vibration 1990; 138:73–94. DOI: 10.1016/0022-460X(90) 90705-5

63. Wang DW, Ma L, and Wen ZH. Sound transmission through a sandwich structure with two-layered pyramidal core and cavity absorption. Journal of Sound and Vibration 2019; 459. DOI: 10.1016/j.jsv.2019.114853

64. Arjunan A, Wang CJ, Yahiaoui K, Mynors DJ, Morgan T, Nguyen VB, and English M. Development of a 3D finite element acoustic model to predict the sound reduction index of stud based double-leaf walls. Journal of Sound and Vibration 2014; 33:6140–55. DOI: 10.1016/j.jsv.2014.06.032

65. Smith RS. Sound Transmission Through Lightweight Parallel Plates. Doctoral Thesis. Heriot-Watt University, Department of Building Engineering and Surveying, 1997

66. Prasetiyo I. Investigation of sound transmission in lightweight structures using a waveguide finite element/boundary element approach. Doctoral Thesis. University of Southampton, Faculty of Engineering, the Environment Institute of Sound, and Vibration Research, 2012

67. Mosharrof MS. Sound Transmission Loss Through a Lightweight Double-Leaf Panel. Doctoral Thesis. Auckland University of Technology, School of Engineering, Computer and Mathematical Sciences, 2018

68. Wareing RR. Investigation and Prediction of the Sound Transmission Loss of Plywood Constructions. Doctoral Thesis. University of Canterbury, Mechanical Engineering, 2014

69. Davy JL, Fard M, Dong W, and Loverde J. Empirical corrections for predicting the sound insulation of double leaf cavity stud building elements with stiffer studs. Acoustical Society of America 2019; 145:703–13. DOI: 10.1121/1.5089222

70. Wallin HP, Bodén H, Carlsson U, Åbom M, and Glav R. Ljud och Vibrationer. KTH: Norstedts Tryckeri AB, 1999

71. Schoenwald S. Flanking sound transmission through lightweight framed double leaf walls - Prediction using statistical energy analysis. Doctoral Thesis. Technische Universiteit Eindhoven, 2008

72. Galbrun L. The prediction of airborne sound transmission between two rooms using first-order flanking paths. Applied Acoustics 2007; 69:1332–42. DOI: 10.1016/j. apacoust.2007.08.010

73. Poblet-Puig J. Numerical modelling of sound transmission in lightweight structures. Doctoral Thesis. Universitat Politecnica de Catalunya, 2008

74. Santos P, Mateus D, and Tadeu A. Predicting flanking sound transmission between two contiguous rooms. *In proceedings of ICSV12*. Lisbon, Portugal, 11-14 July. 2005

75. Bard D, Sonnerup J, and Sandberg G. Prediction model of the flanking transmission through a light-weight building construction utilizing fluid-structure interaction procedures. 2008. Lund University, Division of Enginnering Acoustics

76. Mahn J. Prediction of Flanking Noise Transmission in Lightweight Building Constructions: A Theoretical and Experimental Evaluation of the Application of EN12354-1. Doctoral Thesis. University of Canterbury. Department of Mechanical Engineering, 2009

77. Craik RJM. The contribution of long flanking paths to sound transmission in buildings. Applied Acoustics 2001; 62:29–46. DOI: 10.1016/S0003-682X(00)00020-7

78. Bolmsvik Å, Linderholt A, and Jarnerö K. FE modeling of a lightweight structure with different junctions. *In proceedings of Euronoise*. Prague, 10-13 June. 2012

79. Andersen LV, Kirkegaard PH, Dickow KA, Kiel N, and Persson K. Influence of wall surface and air modelling in finite-element analysis of sound transmission between rooms in lightweight buildings. *In proceedings of the 41st International Congress and Exposition on Noise Control Engineering (Inter-Noise)*. New York City, USA, August 19-22. 2012

80. Chin CS and Ji X. Analytical modelling of structure-borne sound transmission through I-junction using Chebyshev-Ritz method on cascaded rectangular plate–cavity system. Applied Acoustics 2019; 143:171–82. DOI: 10.1016/j.apacoust.2018.09.001

81. Paolini A, Kollmannsberger S, Winter C, Buchschmid M, Müller G, Rabold A, Mecking S, Schanda U, and Rank E. A high-order finite element model for vibration analysis of cross-laminated timber assemblies. Building Acoustics 2017; 24:135–58. DOI: 10.1177/1351010X17727126

82. Davy J, Mahn J, Guigou-Carter C, and Villot M. The prediction of flanking sound transmission below the critical frequency. The Journal of the Acoustical Society of America 2012; 132:2359–70. DOI: 10.1121/1.4746945

83. International Organization for Standardization. Acoustics — Field measurement of sound insulation in buildings and of building elements — Part 1: Airborne sound insulation. (ISO 16283-1:2014). Geneva, Switzerland, 2014

84. ASTM International. ASTM E336-20, Standard Test Method for Measurement of Airborne Sound Attenuation between Rooms in Buildings. Standard. West Conshohocken, PA, USA, 2020

85. International Organization for Standardization. Acoustics — Laboratory measurement of sound insulation of building elements — Part 5: Requirements for test facilities and equipment. (ISO 10140-5:2021). Geneva, Switzerland, 2021

86. International Organization for Standardization. Byggakustik – Mätning av ljudisolering hos byggnadselement i laboratorium – Del 2: Mätning av luftljudsisolering. (ISO 10140-2:2021). Geneva, Switzerland, 2021

87. ASTM International. ASTM E90-09, Standard Test Method for Laboratory Measurement of Airborne Sound Transmission Loss of Building Partitions and Elements. Standard. West Conshohocken, PA, USA, 2016

88. International Organization for Standardization. Acoustics — Laboratory and field measurement of flanking transmission for airborne, impact and building service equipment sound between adjoining rooms — Part 1: Frame document. (ISO 10848-1:2017). Geneva, Switzerland, 2017

89. Gagnon S, Bilek EM, Podesto L, and Crespell P. CLT Handbook - Cross-Laminated Timber. U.S. U.S. Department of Agriculture, Forest Service, Forest Products Laboratory, Binational Softwood Lumber Council (BSLC), 2013

90. Borgström E and Fröbel J. The CLT Handbook, CLT structures – facts and planning. Sundbyberg, Sweden: Swedish Wood, 2019

91. APA. Cross-Laminated Timber (CLT). Accessed 28 December 2023. 2023. Available from: `https://www.apawood.org/cross-laminated-timber`

92. Forest Products Laboratory. Wood handbook - Wood as an engineering material. Centennial. Madison, WI: U.S.: Department of Agriculture, Forest Service, Forest Products Laboratory, 2010

93. Dolezal F and Kumer N. Simplified model for sound insulation of cross laminated timber walls with external thermal insulation composite systems. *In proceedings of the 48th International Congress and Exposition on Noise Control Engineering (Inter-Noise).* Madrid, Spain, 16–19 June. 2019

94. Hagberg K, Thorsson P, Golger A, and Bard D. SEAP—Acoustic design tool for Stora Enso Building Solutions. *In proceedings of the 22nd International Congress on Acoustics (ICA).* Buenos Aires, Argentina, 5–9 September. 2016

95. Dolezal F, Teibinger M, and Bednar T. Flanking Transmission of Impact Noise at Solid Wood Structures. *In proceedings of the World conference on timber engineering WCTE.* Trentino, Italy, 20-24 June. 2010

96. Hagberg K and Bard D. Low Frequency Sound Transmission in Multifamily Wooden Houses. *In proceedings of the 43rd International Congress and Exposition on Noise Control Engineering (Inter-Noise).* Melbourne, Australia, November 16-19. 2014

97. Ljunggren F and Ågren A. Elastic Layers to Reduce Sound Transmission in Lightweight Buildings. Building Acoustics 2013; 20:25–42. DOI: `10.1260/1351-010X.20.1.25`

98. Nilsson E, Ménard S, Bard Hagberg D, and Hagberg K. Effect of Bearing Direction and Mounting Techniques on Cross-Laminated Timber Elements in the Field. *In proceedings of the 51st International Congress and Exposition on Noise Control Engineering (Inter-*

Noise). Glasgow, Scotland, 21-24 August. 2022 :1936–46. DOI: 10.3397/IN_2022_0274

99. Ward IM and Sweeney J. Mechanical Properties of Solid Polymers. third ed. John,Wiley & Sons, Ltd, United Kingdom, 2013

100. Capps RN. Elastomeric Materials for Acoustical Applications. Naval Research Laboratory, 1989

101. Harris CM and Piersol AG. Harris' Shock and Vibration Handbook. fifth ed. McGraw-Hill, NY, USA, 2002

102. Bolmsvik Å. Structural-acoustic Vibrations in Wooden Assemblies : Experimental Modal Analysis and Finite Element Modelling. phd. Department of Building and Energy Technology, Linnaeus University, Växjö, Sweden, 2013

103. Bolmsvik Å and Linderholt A. Damping elastomers for wooden constructions – dynamic properties. Wood Material Science & Engineering 2015; 10:245–55. DOI: 10.1080/17480272.2015.1046920

104. Bolmsvik Å, Linderholt A, Brandt A, and Ekevid T. FE modelling of light weight wooden assemblies – parameter study and comparison between analyses and experiments. Engineering Structures 2014; 73:125–42. DOI: 10.1016/j.engstruct.2014.04.028

105. Bolmsvik Å, Linderholt A, and Jarnerö K. FE Modeling of a Lightweight Structure with Different Junctions. *In proceedings of Euronoise*. Prague, Czech Republic. 2012

106. Craik RJM and Osipov AG. Structural isolation of walls using elastic interlayers. Applied Acoustics 1995; 46:233–49. DOI: 10.1016/0003-682x(95)98774-d

107. Kim KW, Jeong GC, Yang KS, and Sohn Jy. Correlation between dynamic stiffness of resilient materials and heavyweight impact sound reduction level. Building and Environment 2009; 44:1589–600. DOI: 10.1016/j.buildenv.2008.10.005

108. Öqvist R, Ljunggren F, and Ågren A. Variations in Sound Insulation in Nominally Identical Prefabricated Lightweight Timber Constructions. Building Acoustics 2010; 17:91–103. DOI: 10.1260/1351-010X.17.2.91

109. Jarnerö K, Bolmsvik Å, Linderholt A, and Olsson A. Effect of Flexible Supports on Vibration Performance of Timber Floors. *In proceedings of Euronoise*. Prague, Czech Republic. 2012

110. Schoenwald S, Kumer N, Wiederin S, Bleicher N, and Furrer B. Application of elastic interlayers at junctions in massive timber buildings. *In proceedings of the 23rd International Congress on Acoustics (ICA)*. Aachen, Germay, 9–13 September. 2019. DOI: 10.18154/RWTH-CONV-239722

111. Barbaresi L, Morandi F, Garai M, and Speranza A. Experimental measurements of flanking transmission in CLT structures. *In proceedings of the 22nd International*

Congress on Acoustics (ICA). Buenos-Aires, Argentina, 5-9 September. 2016. DOI: `10.1121/2.0000433`

112. Mecking S, Kruse T, and Schanda U. Measurement and calculation of sound transmission across junctions of solid timber building elements. *In proceedings of the 10th European Congress and Exposition on Noise Control Engineering (EuroNoise)*. Maastricht, Netherlands, 31 May - 3 June. 2015

113. Di Bella A, Dall'Acqua d'Industria L, Valluzzi MR, Pengo A, Barbaresi L, Di Nocco F, and Morandi F. Flanking transmission in CLT buildings: comparison between vibration reduction index measurements for different mounting conditions. *In proceedings of the 48th International Congress and Exposition on Noise Control Engineering (Inter-Noise)*. Madrid, Spain, 16-19 June. 2019

114. Bolmsvik Å and Brandt A. Damping assessment of light wooden assembly with and without damping material. Engineering Structures 2013; 49:434–47. DOI: `10.1016/j.engstruct.2012.11.026`

115. Osipov A and Vermeir G. Sound transmission in buildings with elastic layers at joints. Applied Acoustics 1996; 49:141–62. DOI: `10.1016/0003-682x(96)00016-3`

116. Morandi F, De Cesaris S, Garai M, and Barbaresi L. Measurement of flanking transmission for the characterisation and classification of cross laminated timber junctions. Applied Acoustics 2018; 141:213–22. DOI: `10.1016/j.apacoust.2018.07.009`

117. Schoenwald S, Zeitler B, Sabourin I, and King F. Sound insulation performance of Cross Laminated Timber Building Systems. *In proceedings of the 42nd International Congress and Exposition on Noise Control Engineering (Inter-Noise)*. Innsbruk, Austria, 15-18 September. 2013

118. Schoenwald S, Zeitler B, and Sabourin I. Analysis on Structure-borne Sound Transmission at Junctions of Solid Wood Double Walls with Continuous Floors. *In proceedings of Forum Acusticum*. Kraków, Poland, 7–12 September. 2014

119. Jarnerö K, Brandt A, and Olsson A. In situ testing of timber floor vibration properties. *In proceedings of the World Conference on Timber Engineering (WCTE)*. Trentino, Italy, 20-24 June. 2010

120. Jarnerö K, Brandt A, and Olsson A. Vibration properties of a timber floor assessed in laboratory and during construction. Engineering Structures 2015; 82:44–54. DOI: `10.1016/j.engstruct.2014.10.019`

121. Speranza A, Barbaresi L, and Morandi F. Experimental analysis of flanking transmission of different connection systems for clt panels. *In proceedings of the World Conference on Timber Engineering (WCTE)*. Vienna, Austria, 22-25 August. 2016

122. Loriggiola F, Dall'Acqua d'Industria L, Granzotto N, and Di Bella A. Acoustics behaviour of CLT structure: transmission loss, impact noise insulation and flanking transmission evaluations. *In proceedings of Acoustics*. Victoria, Australia, 10-13 November. 2019

123. Pérez M and Fuente M. Acoustic design through predictive methods in Cross Laminated Timber (CLT) panel structures for buildings. *In proceedings of the 42nd International Congress and Exposition on Noise Control Engineering (Inter-Noise)*. Innsbruk, Austria, 15-18 September. 2013

124. Mak CM and Wang Z. Recent advances in building acoustics: An overview of prediction methods and their applications. Building and Environment 2015; 91:118–26. DOI: 10.1016/j.buildenv.2015.03.017

125. Craik RJM and Mackenzie RK. The Transmission of Sound by Ventilation Ducts - a Design Guide. Applied Acoustics 1981; 14:1–5. DOI: 10.1016/0003-682x(81)90038-4

126. Nilsson E, Vardaxis NG, Ménard S, and Bard Hagberg D. Sound Reduction of Ventilation Ducts through Walls: Experimental Results and Updated Models. Acoustics 2021; 3:695–716. DOI: 10.3390/acoustics3040044

127. Nilsson E, Ménard S, Bard Hagberg D, and Vardaxis NG. Acoustical Treatments on Ventilation Ducts through Walls: Experimental Results and Novel Models. Acoustics 2022; 4:276–96. DOI: 10.3390/acoustics4010017

128. Heckl M and Müller HA. Pocketbook of Technical Acoustics. Springer, Berlin / Heidelberg, Germany, 1975

129. ASHRAE. Handbook — HVAC Applications. Atlanta, GA, USA: American society of Heating, Refrigerating, and Air conditioning Engineers, Inc, 2023. Chap. 49:49.1–49.58

130. Vigran TE. Building Acoustics. Boca Raton, FL, USA: CRC Press, 2008

131. Cummings A. The Attenuation of Sound in Unlined Ducts with Flexible Walls. Journal of Sound and Vibration 1994; 174:433–50. DOI: 10.1006/jsvi.1994.1286

132. Cummings A and Astley RJ. The Effects of Flanking Transmission on Sound-Attenuation in Lined Ducts. Journal of Sound and Vibration 1995; 179:617–46. DOI: 10.1006/jsvi.1995.0041

133. Bibby C and Hodgson M. Theoretical Analysis of lined-Duct sound attenuation. Canadian Acoustics 2013; 41. Accessed 2024-02-09:15–22. Available from: https://jcaa.caa-aca.ca/index.php/jcaa/article/view/2625

134. Astley RJ and Cummings A. A finite element scheme for attenuation in ducts lined with porous material: Comparison with experiment. Journal of Sound and Vibration 1987; 116:239–63. DOI: 10.1016/s0022-460x(87)81302-0

135. Cummings A. Sound attenuation in ducts lined on two opposite walls with porous material, with some applications to splitters. Journal of Sound and Vibration 1976; 49:9–35. DOI: 10.1016/0022-460x(76)90754-9

136. Astley RJ, Cummings A, and Sormaz N. A finite element scheme for acoustic propagation in flexible-walled ducts with bulk-reacting liners, and comparison with ex-

periment. Journal of Sound and Vibration 1991; 150:119–38. DOI: 10.1016/0022-460x(91)90406-a

137.   Ramli NB. Analytical modelling of sound transmission in a lined duct. Accessed 2024-02-09. Doctoral Thesis. University of Southampton, Engineering and the Environment, 2013. Available from: http://eprints.soton.ac.uk/id/eprint/361186

138.   Lindab. Lindab General Information and Theory. Accessed 2024-02-09. 2022. Available from: https://itsolution.lindab.com/LindabWebProductsDoc/PDF/Documentation/ADS/Lindab/Technical/GeneralInformationTheory-product-overview.pdf

139.   ASHRAE. Handbook- HVAC Applications. Atlanta, GA, USA: American society of Heating, Refrigerating, and Air conditioning Engineers, Inc, 1999

140.   Selamet A, Xu MB, Lee IJ, and Huff NT. Analytical approach for sound attenuation in perforated dissipative silencers. The Journal of the Acoustical Society of America 2004; 115:2091–9. DOI: 10.1121/1.1694994

141.   Bilawchuk S and Fyfe KR. Comparison and implementation of the various numerical methods used for calculating transmission loss in silencer systems. Applied Acoustics 2003; 64:903–16. DOI: 10.1016/s0003-682x(03)00046-x

142.   Cummings A. High Frequency Ray Acoustics Models for Duct Silencers. Journal of Sound and Vibration 1999; 221:681–708. DOI: 10.1006/jsvi.1999.2030

143.   Cummings A and Chang IJ. Sound attenuation of a finite length dissipative flow duct silencer with internal mean flow in the absorbent. Journal of Sound and Vibration 1988; 127:1–17. DOI: 10.1016/0022-460x(88)90347-1

144.   Kirby R. Simplified Techniques for Predicting the Transmission Loss of a Circular Dissipative Silencer. Journal of Sound and Vibration 2001; 243:403–26. DOI: 10.1006/jsvi.2000.3425

145.   Kirkby R and Mimani A. Attenuating sound in large ductwork using reactive and dissipative silencers. *In proceedings of the 6th conference on Noise and Vibration Emerging Methods (NOVEM)*. Ibiza, Spain, 7–9 May. 2018

146.   ASTM International. ASTM E477-13, Standard Test Method for Laboratory Measurements of Acoustical and Airflow Performance of Duct Liner Materials and Prefabricated Silencers. Standard. West Conshohocken, PA, USA, 2013

147.   Einarsson S and Svensson J. Ljudläckage vid Installationsgenomföringar. Statens Råd för Byggnadsforskning 1987. Stockholm, Sweden

148.   ASHRAE. Handbook — Fundamentals. Atlanta, GA, USA: American society of Heating, Refrigerating, and Air conditioning Engineers, Inc, 2019

149.   Jade N and Venkatesham B. Experimental study of breakout noise characteristics of flexible rectangular duct. Mechanical Systems and Signal Processing 2018; 108:156–72. DOI: 10.1016/j.ymssp.2018.02.015

150. Craik RJM. The noise reduction of the acoustic paths between two rooms interconnected by a ventilation duct. Applied Acoustics 1979; 12:161–79. DOI: 10.1016/0003-682X(79)90020-3

151. Lindab. NPU - Coupling. Accessed 2024-01-25. 2024. Available from: https://www.lindab.co.uk/Products/ventilation/spiral-ducting/safe-duct-fittings/couplings/npu/?sort=popularity&display=16&page=1

152. International Organization for Standardization. Acoustics — Laboratory measurement of sound insulation of building elements — Part 4: Measurement procedures and requirements. (ISO 10140-4:2021). Geneva, Switzerland, 2021

153. International Organization for Standardization. Acoustics — Measurement of room acoustic parameters — Part 2: Reverberation time in ordinary rooms. (ISO 3382-2:2008). Geneva, Switzerland, 2008

154. Arafa N, Tariq A, Mohany A, and Hassan M. Effect of Cylinder Location inside a Rectangular Duct on the Excitation Mechanism of Acoustic Resonance. Canadian Acoustics 2014; 42:33–40

155. Swedish Standards Institute. Acoustics – Sound classification of spaces in buildings – Institutional premises, rooms for education, preschools and leisure-time centres, rooms for office work and hotels. (SS 25268:2007+T1:2017). Stockholm, Sverige, 2018

156. Swedish Standards Institute. Acoustics – Sound classification of spaces in buildings – Dwellings. (SS 25267:2015). Stockholm, Sverige, 2015

157. Westerberg G. On the sealing of circular holes in a thick wall for the purpose of sound insulation. Applied Acoustics 1971; 4:115–29. DOI: 10.1016/0003-682X(71)90003-X

158. Yang C, Zhang X, Tao F, and Lam DC. A study of the sound transmission mechanisms of a finite thickness opening without or with an acoustic seal. Applied Acoustics 2017; 122:156–66. DOI: 10.1016/j.apacoust.2017.02.012

159. Kuo-Tsai C. Study of acoustic transmission through apertures in a wall. Applied Acoustics 1995; 46:131–51. DOI: 10.1016/0003-682X(95)00009-X

160. Poblet-Puig J and Rodríguez-Ferran A. Modal-based prediction of sound transmission through slits and openings between rooms. Journal of Sound and Vibration 2013; 332:1265–87. DOI: 10.1016/j.jsv.2012.09.044

161. Mechel FP. The acoustic sealing of holes and slits in walls. Journal of Sound and Vibration 1986; 111:297–336. DOI: 10.1016/S0022-460X(86)80163-8

162. Trompette N, Barbry JL, Sgard F, and Nelisse H. Sound transmission loss of rectangular and slit-shaped apertures: Experimental results and correlation with a modal model. Journal of the Acoustical Society of America 2009; 125:31–41. DOI: 10.1121/1.3003084

163. Tester BJ. The propagation and attenuation of sound in lined ducts containing uniform or "plug" flow. Journal of Sound and Vibration 1973; 28:151–203. DOI: 10.1016/S0022-460X(73)80102-6

164. Cummings A and Astley RJ. The effects of flanking transmission on sound attenuation in lined ducts. Journal of Sound and Vibration 1995; 179:617–46. DOI: 10.1006/jsvi.1995.0041

165. Howe MS. The attenuation of sound in a randomly lined duct. Journal of Sound and Vibration 1983; 87:83–103. DOI: 10.1016/0022-460X(83)90441-8

166. International Organization for Standardization. Acoustics—Laboratory and Field Measurement of Flanking Transmission for Airborne, Impact and Building Service Equipment Sound between Adjoining Rooms—Part 2: Application to Type B Elements When the Junction Has a Small Influence. (ISO 10848-2:2017). Geneva, Switzerland, 2017

167. ASTM International. ASTM E1414/E1414M-21a, Standard Test Method for Airborne Sound Attenuation between Rooms Sharing a Common Ceiling Plenum. Standard. West Conshohocken, PA, USA, 2021

168. Van Hout G. The Acoustic Performance of Suspended Ceiling Systems. 2016. Master's Thesis, University of Canterbury, Christchurch, New Zealand

169. Van Hout G and Reeve W. Effect of Plenum Absorption on Ceiling Attenuation. 2017. Accessed 2024-01-21. Available from: https://www.acoustics.org.nz/sites/www.acoustics.org.nz/files/journal/pdfs/Van%20Holt_G_NZA_2017.pdf

170. Halliwell RE and Quirt JD. Controlling interoffice sound transmission through a suspended ceiling. Journal of the Acoustical Society of America 1991; 90:1446–53. DOI: 10.1121/1.401937

171. Van Hout G, Pearse J, and Donohue B. Relationship between flanking noise through a common ceiling plenum and plenum absorption. *In proceedings of ACOUSTICS*. Brisbane, Australia, 9–11 November. 2016

172. Kruger K. The Effect of Various Parameters on the Sound Isolation between Offices with Suspended Ceilings. Canadian Acoustics 1988; 16

173. Cummings A. Acoustic Noise Transmission through Duct Walls. ASHRAE Trans. 1983; 91:48–61

174. International Organization for Standardization. Acoustics — Rating of sound insulation in buildings and of building elements — Part 1: Airborne sound insulation. (ISO 717-1:2020). Geneva, Switzerland, 2020

175. ASTM International. ASTM E413-16, Classification for Rating Sound Insulation. Standard. West Conshohocken, PA, USA, 2016

176. International Organization for Standardization. Acoustics—Determination of Sound Insulation Performances of Enclosures—Part 1: Measurements under Laboratory Conditions (for Declaration Purposes). (ISO 11546-1:1995). Geneva, Switzerland, 1995

177. Nilsson E, Ménard S, Bard D, and Hagberg K. Effects of building height on the sound transmission in cross-laminated timber buildings – Airborne sound insulation. Building and Environment 2023; 229. DOI: `10.1016/j.buildenv.2023.109985`

178. Buchanan AH and Honey BG. Honey, Energy and carbon dioxide implications of building construction. Energy and Buildings 1994; 20:205–17. DOI: `10.1016/0378-7788(94)90024-8`

179. Kurzinski S, Crovella P, and Kremer P. Overview of cross-laminated timber (CLT) and timber structure standards across the World. Mass Timber Construction Journal 2022; 5. DOI: `10.55191/MTCJ.2022.1`

180. Bowyer J, Bratkovich S, Howe J, Fernholz K, Frank M, Hanessian S, Groot H, and Pepke E. Modern Tall Wood Buildings: Opportunities for Innovation. Dovetail Partners, Inc., Minneapolis, USA 2016

181. Van De Kuilen JWG, Ceccotti A, Xia Z, Minjuan H, and Li S. Wood concrete skyscrapers. *In proceedings of the World conference on timber engineering WCTE*. Trentino, Italy, June 20-24. 2010

182. Van De Kuilen JWG, Ceccotti A, Xia Z, and He M. Very tall wooden buildings with cross laminated timber. Procedia Engineering 2011; 14:1621–8. DOI: `10.1016/j.proeng.2011.07.204`

183. CTBUH. CTBUH Certifies Ascent, Milwaukee, as the World's Tallest Mass Timber Hybrid Building. Accessed 28 December 2023. 2022. Available from: `https://www.ctbuh.org/ctbuh-news/ctbuh-certifies-ascent-worlds-tallest-timber`

184. Negreira J, Austrell PE, Flodén O, and Bard D. Characterisation of an elastomer for noise and vibration insulation in lightweight timber buildings. Building Acoustics 2014; 21:251–76. DOI: `10.1260/1351-010x.21.4.251`

185. Crispin C, Ingelaere B, Van Damme M, and Wuyts D. The Vibration Reduction Index Kij: Laboratory Measurements for Rigid Junctions and for Junctions with Flexible Interlayers. Building Acoustics 2006; 13:99–111. DOI: `10.1260/135101006777630427`

186. Hoeller C, Mahn J, Quirt D, Schoenwald S, and Zeitler B. RR-335 Apparent Sound Insulation in Cross-Laminated Timber Buildings. National Research Council Canada. Vancouver, BC, Canada, 2017

187. Craik RJM and Steel JA. The effect of workmanship on sound transmission through buildings: Part 1—Airborne sound. Applied Acoustics 1989; 27:57–63. DOI: `10.1016/0003-682X(89)90045-5`

188. Trevathan JW and Pearse JR. The effect of workmanship on the transmission of airborne sound through light framed walls. Applied Acoustics 2008; 69:127–31. DOI: `10.1016/j.apacoust.2006.09.001`

189. Simmons C. Uncertainty of measured and calculated sound insulation in buildings - results of a Round Robin Test. Noise Control Engineering Journal 2007; 55:67–75. DOI: 10.3397/1.2402312

190. Lofdahl M, Öqvist R, and Gruffman J. Variations in impact sound insulation from 20 Hz due to measurement uncertainty and workmanship. *In proceedings of the 46th International Congress and Exposition on Noise Control Engineering (Inter-Noise).* Hong Kong, August 27-30. 2017

191. Öqvist R, Ljunggren F, and Ågren A. On the uncertainty of building acoustic measurements – case study of a cross-laminated timber construction. Applied Acoustics 2012; 73:904–12. DOI: 10.1016/j.apacoust.2012.03.012

192. Kihlman T. Sound radiation into a rectangular room. Applications to airborne sound transmission in buildings. Acustica 1967; 18:11–20

193. Gibbs BM and Maluski S. Airborne sound level difference between dwellings at low frequencies. Building Acoustics 2004; 11:61–78. DOI: 10.1260/1351010041217202

194. Öqvist R and Johnsson R. Variationer i Ljudisolering i Platsbyggda Flerbostadshus i Betong. Bygg & teknik 2013 :21–4

195. Crispin C, Mertens C, Blasco M, Ingelaere B, Van Damme M, and Wuyts D. The vibration reduction index Kij: laboratory measurements versus predictions EN 12354-1 (2000). *In proceedings of the 33rd International Congress and Exposition on Noise Control Engineering (Inter-Noise).* Prague, Czech Republic, 22-25 August. 2004 :2071–7

196. Mahn J. Measurement of the vibration reduction index between concrete masonry walls and precast hollow core floors. National Research Council of Canada 2017. Construction: 2017/05/01

197. Hopkins C. Measurement of the Vibration Reduction Index, Kij on Free-Standing Masonry Wall Constructions. Building Acoustics 1999; 6:235–57. DOI: 10.1260/1351010991501437

198. Schiavi A and Astolfi A. The prediction of the vibration reduction index Kij for brick and concrete rigid junctions. Applied Acoustics 2010; 71:523–30. DOI: 10.1016/j.apacoust.2010.01.001

199. Esteban A, Cortés A, Villot M, and Martin C. Vibration Reduction Index Kij in Hollow Conctructions: Application of the European Standard EN12354 to the Spanish Constructions. *In proceedings of TechniAcustica.* Bilbao, Spain, 15-17 October. 2003

200. Dijckmans A, De Geetere L, and Ingelaere B. Laboratory measurements of the vibration reduction index Kij of Cross Laminated Timber (CLT) junctions. Belgian Building Research Institute 2018

201. Buchegger B. Flanking sound transmission in coupled panels of cross-laminated-timber. Doctoral thesis. PhD thesis. Technischen Universität Graz, 2019

202. Hagberg K and Bard D. Acoustic Requirements for a Sustainable Future. *In proceedings of CEES*. Coimbra, Portugal, 12-15 October. 2021

203. Hagberg K and Nilsson E. KL-trä - Optimering av Knutpuntker. Bygg & Teknik 2021; 4:21–3

204. Santoni A, Bonfiglio P, Fausti P, and Schoenwald S. Predicting sound radiation efficiency and sound transmission loss of orthotropic cross-laminated timber panels. *In proceedings of the 173rd Meeting of Acoustical Society of America and 8th Forum Acusticum*. Boston, MA, USA, 25–29 June. 2017. DOI: 10.1121/2.0000626

205. Nilsson E, Ménard S, Bard D, and Hagberg K. Effects of Building Height on the Sound Transmission in Cross-Laminated Timber Buildings—Vibration Reduction Index. Buildings 2023; 13. DOI: 10.3390/buildings13122943

206. Barber D. Fire Safety of Mass timber Buildings with CLT in USA. Wood and Fiber Science 2018; 50:83–95. DOI: 10.22382/wfs-2018-042

207. Barber D. Tall Timber Buildings: What's Next in Fire Safety? Fire Technology 2015; 51:1279–84. DOI: 10.1007/s10694-015-0497-7

208. Barber D, Rackauskaite E, Christensen E, and Schulz J. Exposed Mass Timber in High-Rise Structures: A Practical Discussion of a Complex Fire Problem. CTBUH Fire & Life Safety 2022; 1. Accessed 2024-02-09:32–9. Available from: https://global.ctbuh.org/resources/papers/download/4527-exposed-mass-timber-in-high-rise-structures-a-practical-discussion-of-a-complex-fire-problem.pdf

209. Gernay T and Ni S. Timber High Rise Buildings and Fire Safety. World Steel Association 2020. Accessed 2024-02-09. Available from: https://constructsteel.org/assets/uploads/2021/03/2020-WSA-Timber_Fire-final_report.pdf

210. Gorska C, Hidalgo JP, and Torero JL. Fire dynamics in mass timber compartments. Fire Safety Journal 2021; 120. DOI: 10.1016/j.firesaf.2020.103098

211. Hayajneh SM and Naser J. Fire Spread in Multi-Storey Timber Building, a CFD Study. Fluids 2023; 8. DOI: 10.3390/fluids8050140

212. Lazzarini E, Frison G, Trutalli D, Marchi L, and Scotta R. Comfort assessment of high-rise timber buildings exposed to wind-induced vibrations. The Structural Design of Tall and Special Buildings 2021; 30. DOI: 10.1002/tal.1882

213. Li Z and Tsavdaridis KD. Design for Seismic Resilient Cross Laminated Timber (CLT) Structures: A Review of Research, Novel Connections, Challenges and Opportunities. Buildings 2023; 13. DOI: 10.3390/buildings13020505

214. Xing Z, Wang Y, Zhang J, and Ma H. Comparative study on fire resistance and zero strength layer thickness of CLT floor under natural fire and standard fire. Construction and Building Materials 2021; 302. DOI: 10.1016/j.conbuildmat.2021.124368

215. Pan Y, Tannert T, Kaushik K, Xiong H, and Ventura CE. Seismic performance of a proposed wood-concrete hybrid system for high-rise buildings. Engineering Structures 2021; 238. DOI: 10.1016/j.engstruct.2021.112194

216. Loss C, Pacchioli S, Polastri A, Casagrande D, Pozza L, and Smith I. Numerical Study of Alternative Seismic-Resisting Systems for CLT Buildings. Buildings 2018; 9. DOI: 10.3390/buildings8110162

217. Sun X, Li Z, and He M. Seismic Reliability Assessment of Mid- and High-rise Post-tensioned CLT Shear Wall Structures. International Journal of High-Rise Buildings 2020; 9:175–85. DOI: 10.21022/IJHRB.2020.9.2.175

218. Teweldebrhan BT and Tesfamariam S. Seismic Design of CLT Shear-Wall and Glulam Moment-Resisting Frame Coupled Structure. Journal of Structural Engineering 2023; 149. DOI: 10.1061/JSENDH.STENG-12690

219. Hong HP and Yang SC. Reliability and fragility assessment of the mid- and high-rise wood buildings subjected to bidirectional seismic excitation. Engineering Structures 2019; 201. DOI: 10.1016/j.engstruct.2019.109734

220. Dernayka S, Ahmed D, Ajmal M, Asiz A, and Ayadat T. Comparison of Wind Induced Response of High-Rise Buildings with Reinforced Concrete and Cross Laminated Timber. *In proceedings of the International Structural Engineering and Construction.* Vol. 9. 2022. DOI: 10.14455/ISEC.2022.9(1).STR-21

221. Hajjaj R, Alhimeidi A, Sabbagh M, Alatallah A, Ahmed D, Asiz A, Ayadat T, Salman A, and Ouda OKM. Structural design and analysis of high-rise building using ultra-lightweight floor system. *In proceedings of the International Structural Engineering and Construction.* Valencia, Spain, 24–29 July. 2017. DOI: 10.14455/ISEC.res.2017.132

222. Byrick W. Laboratory data examining impact and airborne sound attenuation in cross-laminated timber panel construction. *In proceedings of the 44th International Congress and Exposition on Noise Control Engineering (Inter-Noise).* San Francisco, CA, USA, 9–12 August. 2015

223. Golden M and Byrick W. Laboratory Data Examining Impact and Airborne Sound Attenuation in Cross- Laminated Timber Panel Construction—Part 2. *In proceedings of the 45th International Congress and Exposition on Noise Control Engineering (Inter-Noise).* Hamburg, Germany, 21–24 August. 2016

224. Byrick W. Laboratory impact and airborne sound attenuation in cross-laminated timber construction using resiliently mounted ceilings and poured concrete toppings. *In proceedings of the Acoustics Week in Canada.* Vancouver, BC, Canada, 21–23 September. 2016

225. Ljunggren F. Innovative solutions to improved sound insulation of CLT floors. Developments in the Built Environment 2023; 13. DOI: 10.1016/j.dibe.2022.100117

226. Hindman DP and Golden MV. Acoustical Properties of Southern Pine Cross-Laminated Timber Panels. Journal of Architectural Engineering 2020; 26. DOI: 10.1061/(ASCE)AE.1943-5568.0000407

227. Ferk H, Leh C, Mosing M, Vavrik-Kirchsteiger S, and Nusser B. Sound. Wood. Austria — Selected measurement results of building components for multi-storey timber construction in Austria. *In proceedings of the 51st International Congress and Exposition on Noise Control Engineering (Inter-Noise)*. Glasgow, UK, 21–24 August. 2022

228. Beresford T and Chen J. Floor airborne and impact sound insulation performance of cross laminated timber vs. timber joist and concrete systems. *In proceedings of the HEAR TO LISTEN—Acoustics Adelaide*. Adelaide, Australia, 6–9 November. 2018

229. Vardaxis NG, Hagberg DB, and Dahlström J. Evaluating Laboratory Measurements for Sound Insulation of Cross-Laminated Timber (CLT) Floors: Configurations in Lightweight Buildings. Applied Sciences 2022; 12. DOI: 10.3390/app12157642

230. Sabourin I. Measurement of Airborne Sound Insulation of 8 Wall Assemblies; Measurement of Airborne and Impact Sound Insulation of 29 Floor Assemblies. National Research Council of Canada 2015. Report No. A1-006070.10, Ottawa, ON, Canada

231. Hongisto V, Alakoivu R, Virtanen J, Hakala J, Saarinen P, Laukka J, Linderholt A, Olsson J, Jarnerö K, and Keränen J. Sound insulation dataset of 30 wooden and 8 concrete floors tested in laboratory conditions. Data in Brief 2023; 49. DOI: 10.1016/j.dib.2023.109393

232. Ljunggren F. Sound insulation prediction of single and double CLT panels. *In proceedings of the 23rd International Congress on Acoustics (ICA)*. Aachen, Germany, 9–13 September. 2019

233. Krajči L, Hopkins C, Davy JL, and Tröbs HM. Airborne sound transmission of a cross-laminated timber plate with orthotropic stiffness. *In proceedings of Euronoise*. Prague, Czech Republic, 10–13 June. 2012

234. Fenemore C, Kingan MJ, and Mace BR. Application of the wave and finite element method to predict the acoustic performance of double-leaf cross-laminated timber panels. Building Acoustics 2023; 30. DOI: 10.1177/1351010X231162483

235. Simmons C. A systematic comparison between EN ISO 12354 calculations of CLT floors with a large set of laboratory and field measurements. *In proceedings of EuroNoise*. Madeira, Portugal, 25–27 October. 2021

236. Di Bella A, Granzotto N, Quartaruolo G, Speranza A, and Morandi F. Analysis of airborne sound reduction index of bare CLT walls. *In proceedings of the World Conference on Timber Engineering (WCTE)*. Seoul, Republic of Korea, 20–23 August. 2018

237. Lin JY, Yang CT, and Tsay YS. A Study on the Sound Insulation Performance of Cross-laminated Timber. Materials 2021; 14. DOI: 10.3390/ma14154144

238. Santoni A, Schoenwald S, Van Damme B, Tröbs HM, and Fausti P. Average Sound Radiation Model for Orthotropic Cross Laminated Timber Plates. *In proceedings of EuroRegio*. Porto, Portugal, 13–15 June. 2016

239. Santoni A, Schoenwald S, Fausti P, and Tröbs HM. Modelling the radiation efficiency of orthotropic cross-laminated timber plates with simply-supported boundaries. Applied Acoustics 2019; 143:112–24. DOI: 10.1016/j.apacoust.2018.08.022

240. Santoni A. Sound Radiation and Sound Transmission in Building Structures: Numerical Modelling and Experimental Validation. Ph.D. Thesis. University of Ferrara, Ferrara, Italy, 2016

241. Rabold A, Châteauvieux-Hellwig C, Mecking S, and Schramm M. Flanking transmission of solid wood elements in multi-storey timber buildings—input data and prediction models for airborne and impact sound excitation. *In proceedings of the 48th International Congress and Exposition on Noise Control Engineering (Inter-Noise)*. Madrid, Spain, 16–19 June. 2019

242. Neusser M and Bednar T. Construction details affecting flanking transmission in cross laminated timber structures for multi-story housing. *In proceedings of the 51st International Congress and Exposition on Noise Control Engineering (Inter-Noise)*. Glasgow, UK, 21–24 August. 2022. DOI: 10.3397/IN_2022_0159

243. Guigou Carter C, Balanant N, and Kouyoumji JL. Acoustic Performance Investigation of a CLT-Based Three-Floor Building. Buildings 2023; 13:213–22. DOI: 10.3390/buildings13081935

244. Murta BHP, Hoeller C, Sabourin I, and Zeitler B. Measurement of structural reverberation times for calculation of ASTC in upcoming NBCC. *In proceedings of the Acoustic Week in Canada*. Winnipeg, MB, Canada, 8–10 October. 2014. DOI: 10.13140/2.1.4760.5762

245. Bietz H and Wittstock V. Comparison of Different Methods for the Determination of Structure-Borne Noise Reverberation Time. *In proceedings of the CFA-DAGA'04*. Strasbourg, France, 22–25 March. 2004

246. Hopkins C and Robinson M. On the Evaluation of Decay Curves to Determine Structural Reverberation Times for Building Elements. Acta Acustica united with Acustica 2013; 99:226–44. DOI: 10.3813/AAA.918606

247. Pontius RG, Thontteh O, and Chen H. Components of information for multiple resolution comparison between maps that share a real variable. Environmental and Ecological Statistics 2007; 15:111–42. DOI: 10.1007/s10651-007-0043-y

APPENDICES

A   Appendix for Chapter 2

Table A1: Units for different variables used in the theory adapted from Vér [13].

Variable	Description	Unit
A	Total absorption area	ft^2
$A_{0,\text{ver}}$	Surface area factor of the duct	ft^2
a	Larger dimension of rectangular duct's cross section	in
a_{feet}	Larger dimension of rectangular duct's cross section	ft
b	Smaller dimension of rectangular duct's cross section	in
b_{feet}	Smaller dimension of rectangular duct's cross section	ft
d	Diameter of the circular duct	in
L	Length of the duct	ft
M_{duct}	Surface area of the duct	ft^2
P	Perimeter of the duct cross section	ft
r	Radial distance between the duct and observer location	ft
S	Area of the duct cross section	ft^2
S_{wall}	Area of the separating wall	ft^2
t	Thickness of the duct walls	in

Table A2: Units for different variables used in the theory adapted from Reynolds [33].

Variable	Description	Unit
A	Total absorption area	ft^2
$A_{0,rey}$	Surface area factor of the duct	ft*in
$A_{i,rey}$	Cross section factor of the duct	in^2
A_R	Room constant	ft^2
a	Larger dimension of rectangular duct's cross section	in
b	Smaller dimension of rectangular duct's cross section	in
d	Diameter of the circular duct	in
L	Length of the duct	ft
M_{duct}	Surface area of the duct	ft^2
q_0	Mass/unit area (surface density) of the duct	lb/ft^2
r	Radial distance between the duct and observer location	ft
S_{wall}	Area of the separating wall	ft^2

Table A3: Units for different variables used in the theory adapted from Long [34].

Variable	Description	Unit
A	Total absorption area	ft^2
$A_{0,long}$	Surface area factor of the duct	ft^2
$A_{i,long}$	Cross section factor of the duct	ft^2
A_R	Room constant	ft^2
a	Larger dimension of rectangular duct's cross section	ft
b	Smaller dimension of rectangular duct's cross section	ft
d	Diameter of the circular duct	ft
L	Length of the duct	ft
M_{duct}	Surface area of the duct	ft^2
P	Perimeter of the duct cross section	ft
q_0	Mass/unit area (surface density) of the duct	lb/ft^2
r	Radial distance between the duct and observer location	ft
S	Area of the duct cross section	ft^2
S_{wall}	Area of the separating wall	ft^2

B   Appendix for Chapter 3

Figure B1: Theoretical sound reduction index according to different theories compared to measurements for the configuration with a circular ventilation duct, diameter 315 mm, through wall A, with a measured weighted sound reduction index of R_w: 35 dB.

Figure B2: Theoretical sound reduction index according to different theories compared to measurements for the configuration with a circular ventilation duct, diameter 315 mm, through wall B, with a measured weighted sound reduction index of R_w: 46 dB.

Figure B3: Theoretical sound reduction index according to different theories compared to measurements for the configuration with a circular ventilation duct, diameter 630 mm, through wall A, with a measured weighted sound reduction index of R_w: 35 dB.
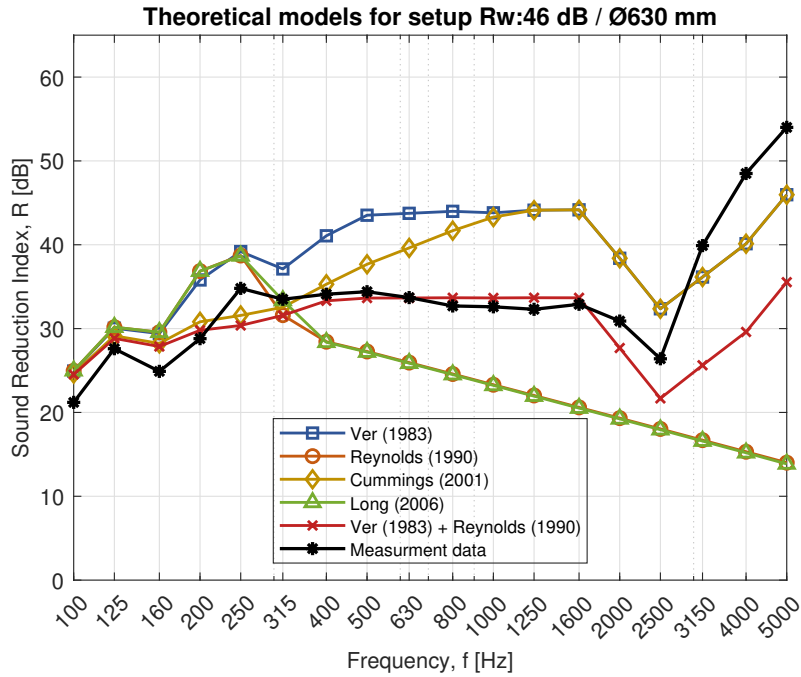
Figure B4: Theoretical sound reduction index according to different theories compared to measurements for the configuration with a circular ventilation duct, diameter 630 mm, through wall B, with a measured weighted sound reduction index of R_w: 46 dB.
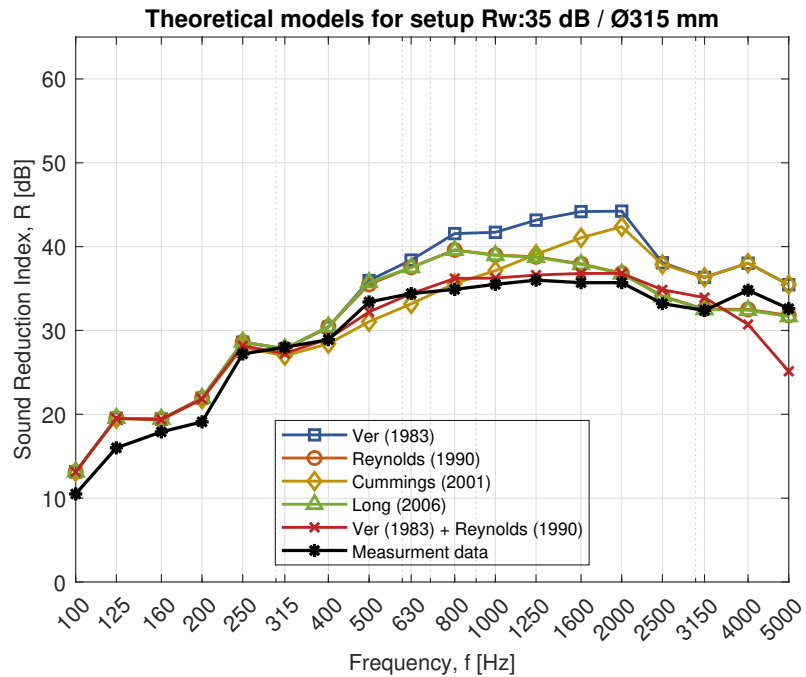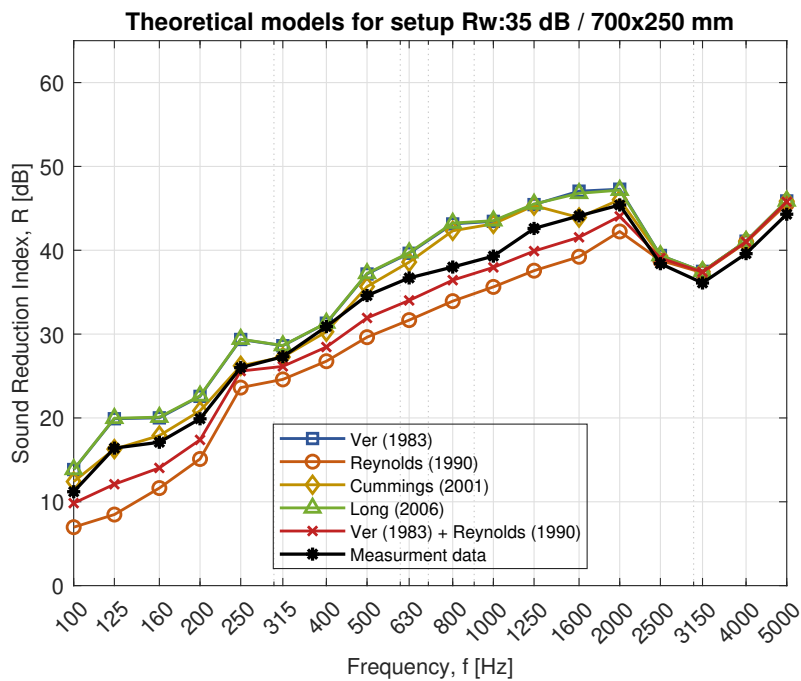

Figure B5: Theoretical sound reduction index according to different theories compared to measurements for the configuration with a rectangular ventilation duct, 700×250 mm, through wall A, with a measured weighted sound reduction index of R_w: 35 dB.
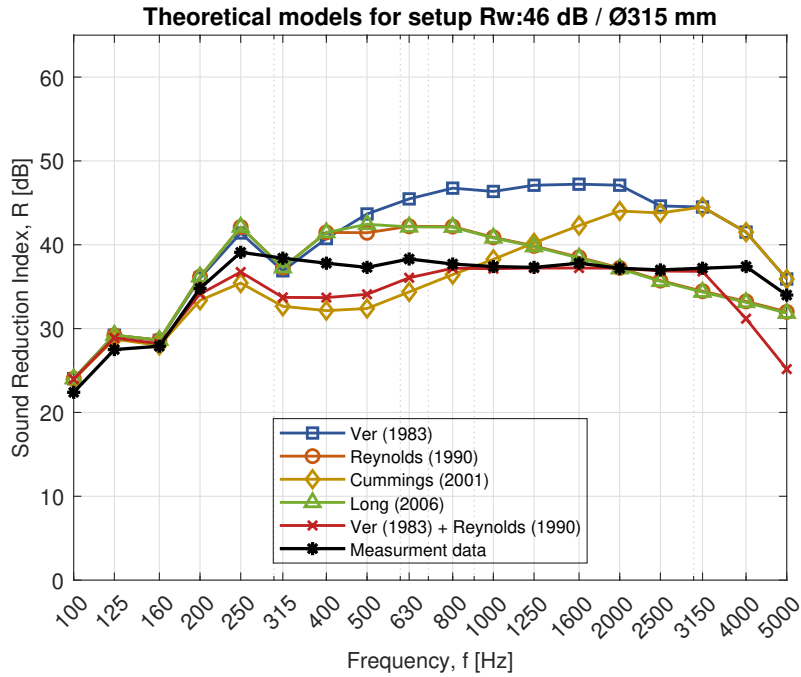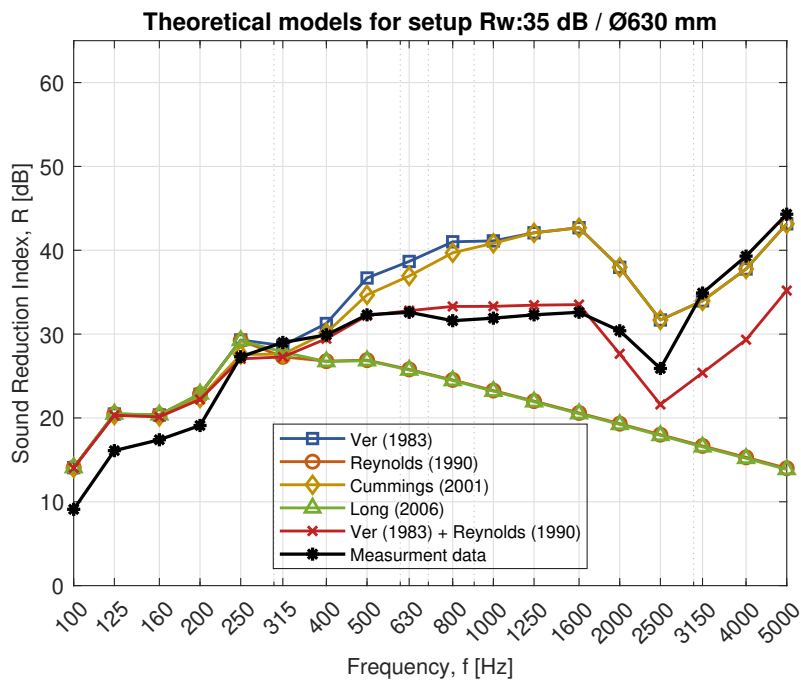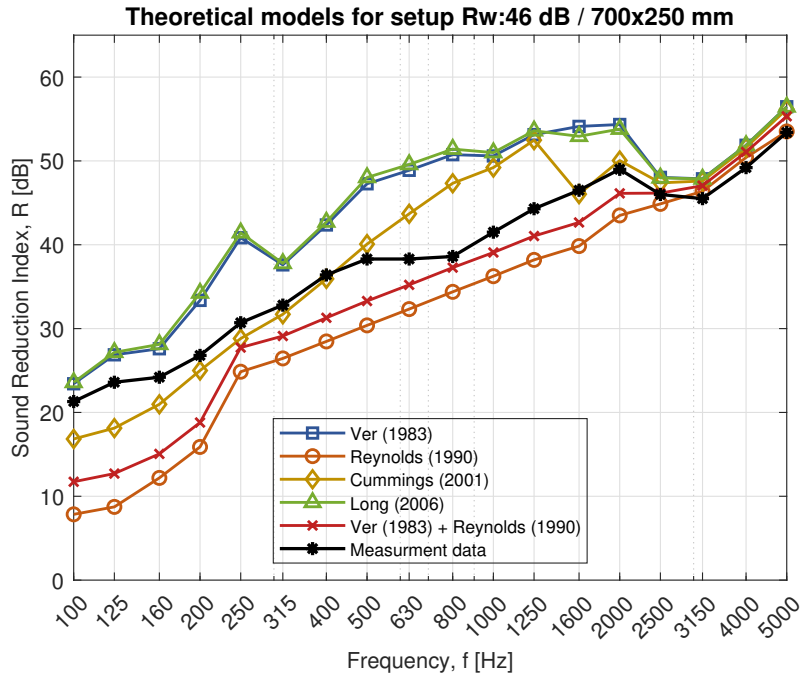
Figure B6: Theoretical sound reduction index according to different theories compared to measurements for the configuration with a rectangular ventilation duct, 700×250 mm, through wall B, with a measured weighted sound reduction index of R_w: 46 dB.
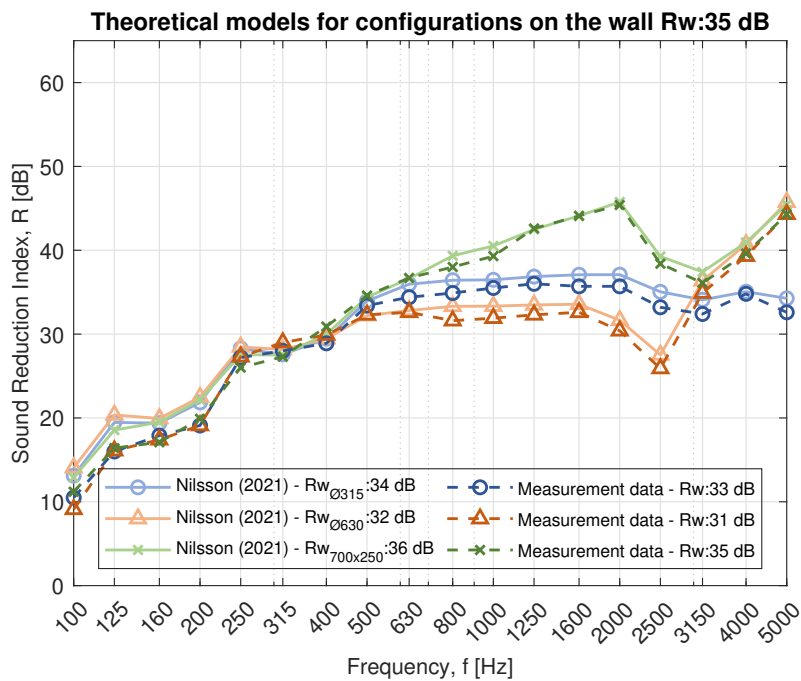

Figure B7: Theoretical analysis with the proposed theory, Nilsson (2021). Configurations for ducts of dimensions Ø315, Ø630 and 700x250 mm through wall A (sound reduction index R_w 35 dB).
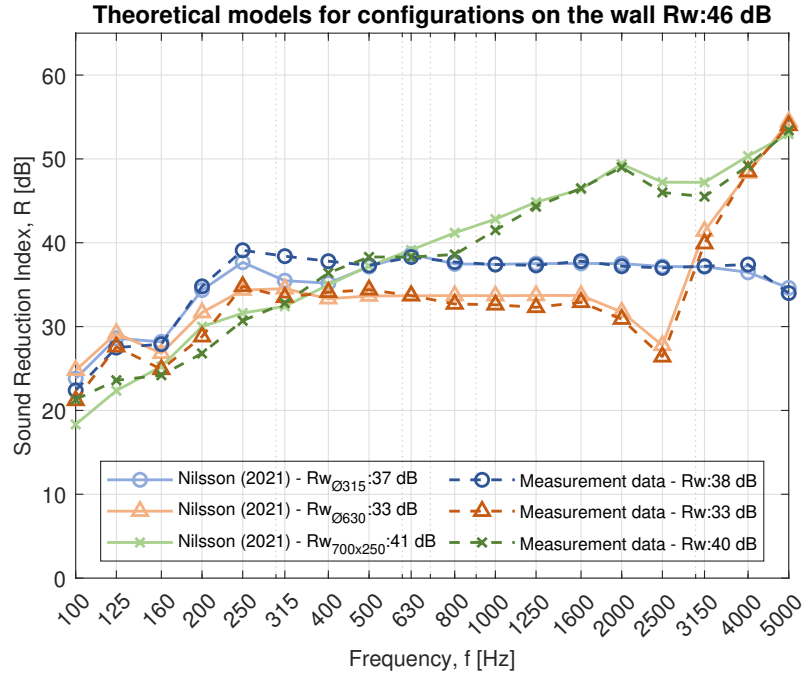
Figure B8: Theoretical analysis with the proposed theory, Nilsson (2021). Configurations for ducts of dimensions Ø315, Ø630 and 700x250 mm through wall B (sound reduction index R_w 46 dB).

Table B1: Units for different variables.

Variable	Unit Imperial/SI
A	Ft^2/m^2
A_R	Ft^2/m^2
M_{duct}	Ft^2/m^2
r	Ft/m
L	Ft/m
S_{wall}	Ft^2/m^2
c_0	Inch/s / m/s
d	Inch/m
c_L	Inch/s / m/s
P	Ft/m
S	Ft^2/m^2
q_0	Lb/ft^2/kg/m^2
a	Inch/m
b	Inch/m
A_0	Ft^2/m^2
A_i	Ft^2/m^2

C Appendix for Chapter 4

Ø315mm Duct and External Lagging, Wall A
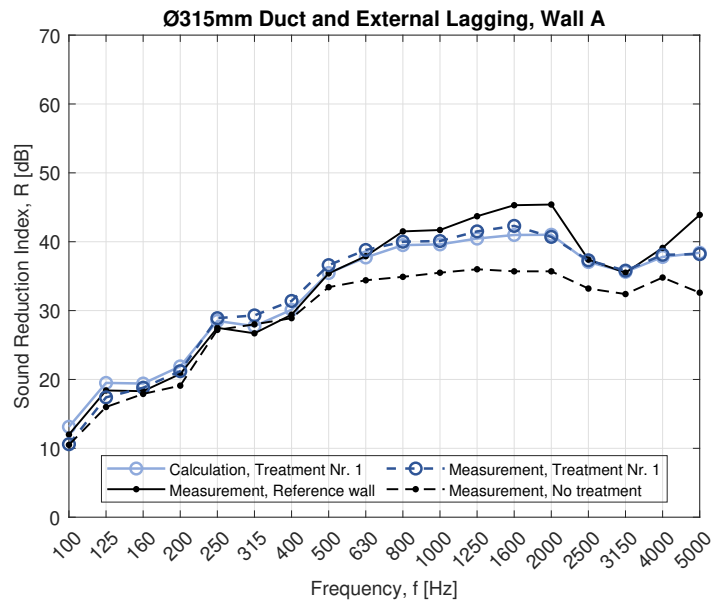
Figure C1: Theoretical models compared to measurements with external lagging as acoustic treatment. Ventilation duct with Ø315 mm through wall A with a sound reduction index of R_w = 35 dB. External lagging is mounted at a partial length of 0.6 m (Treatment 1) with 50 mm stone wool, density of 100 kg/m³, closest to the wall.
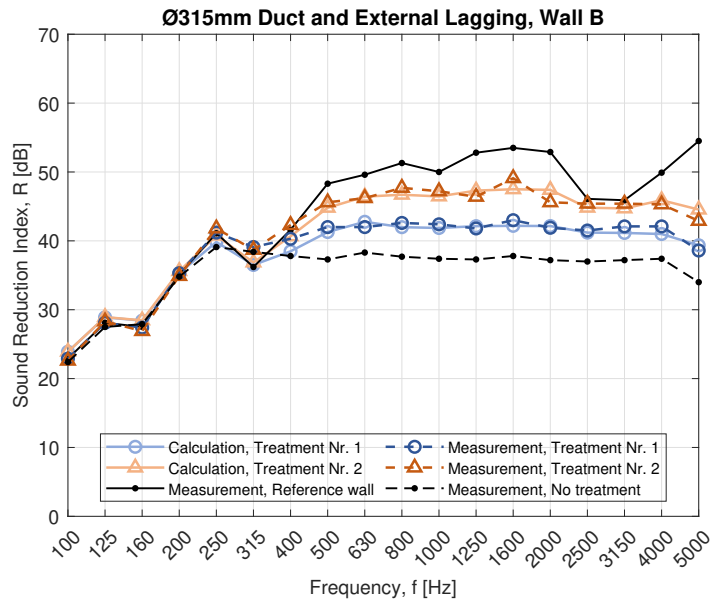
Figure C2: Theoretical models compared to measurements with external lagging as acoustic treatment. Ventilation duct with Ø315 mm through wall B with a sound reduction index of R_w = 46 dB. External lagging is mounted at partial lengths of 0.6–1.2 m (Treatment 1 and 2) with 50 mm stone wool, density of 100 kg/m³, closest to the wall.
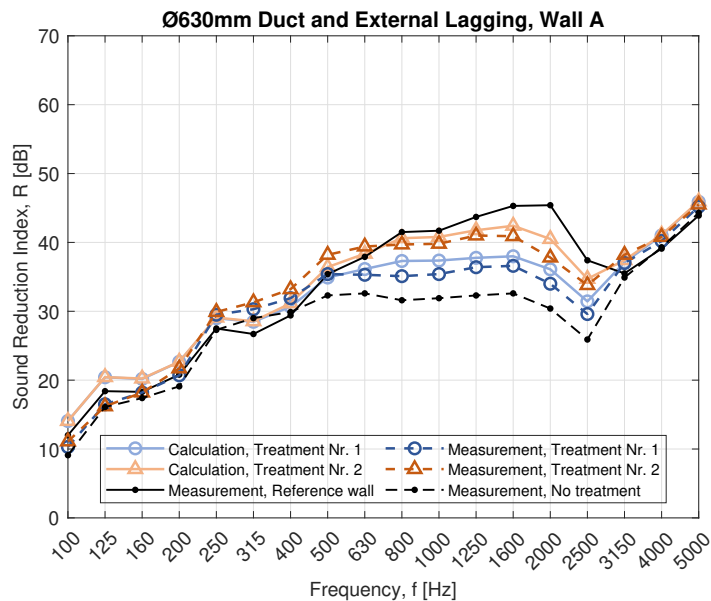
Figure C3: Theoretical models compared to measurements with external lagging as acoustic treatment. Ventilation duct with Ø315 mm through wall A with a sound reduction index of R_w = 35 dB. External lagging is mounted at partial lengths of 0.6–1.2 m (Treatment 1 and 2) with 50 mm stone wool, density of 100 kg/m³, closest to the wall.
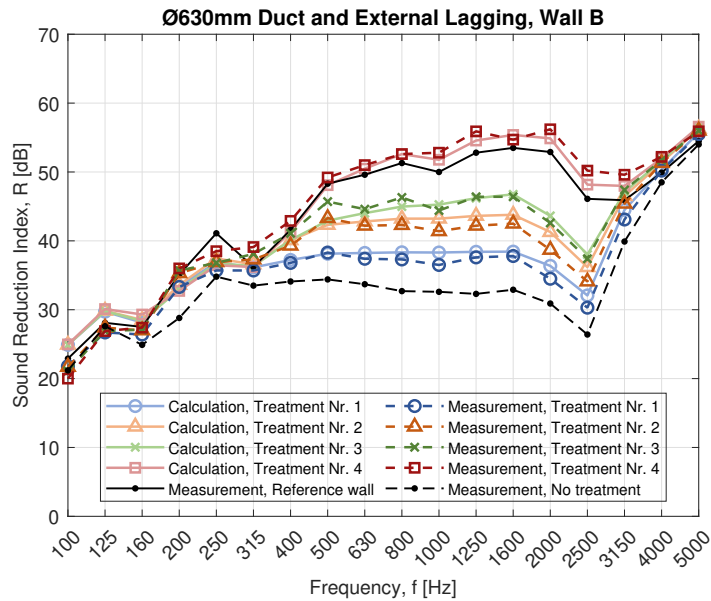
Figure C4: Theoretical models compared to measurements with external lagging as acoustic treatment. Ventilation duct with Ø315 mm through wall B with a sound reduction index of R_w = 46 dB. External lagging is mounted at partial lengths of 0.6–1.8 m (Treatment 1–3) and full length (Treatment 4) with 50 mm stone wool, density of 100 kg/m^3, closest to the wall.
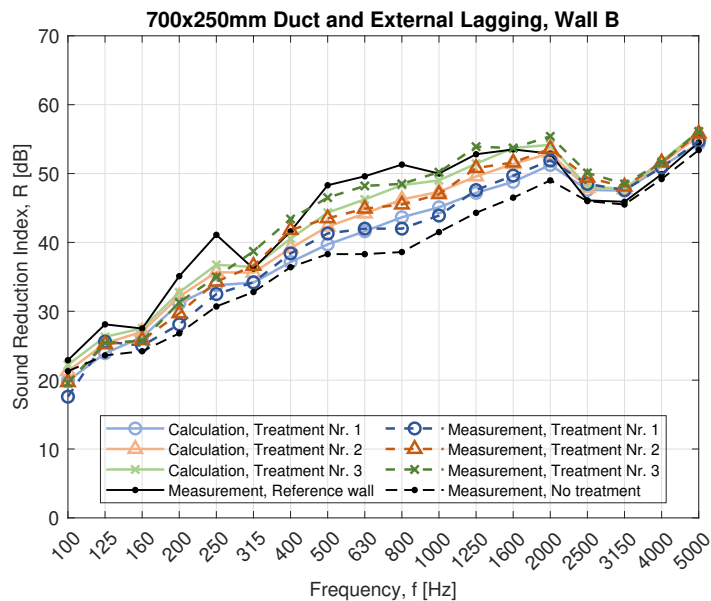
Figure C5: Theoretical models compared to measurements with external lagging as acoustic treatment. Ventilation duct with dimension: 700 × 250 mm through wall B with a sound reduction index of R_w = 46 dB. External lagging is mounted at partial lengths of 0.6–1.8 m (Treatment 1–3) with 50 mm stone wool, density of 100 kg/m^3, closest to the wall.
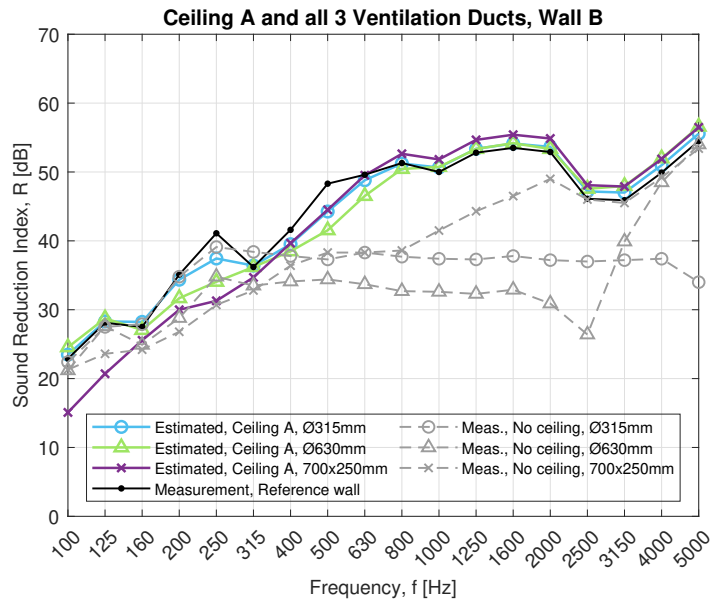
Figure C6: Estimated theory with a suspended absorbent ceiling, Ceiling A, as acoustical treatment. Ventilation duct with dimensions of Ø315, Ø630 and 700 × 250 mm through wall B with a sound reduction index of $R_w = 46$ dB.
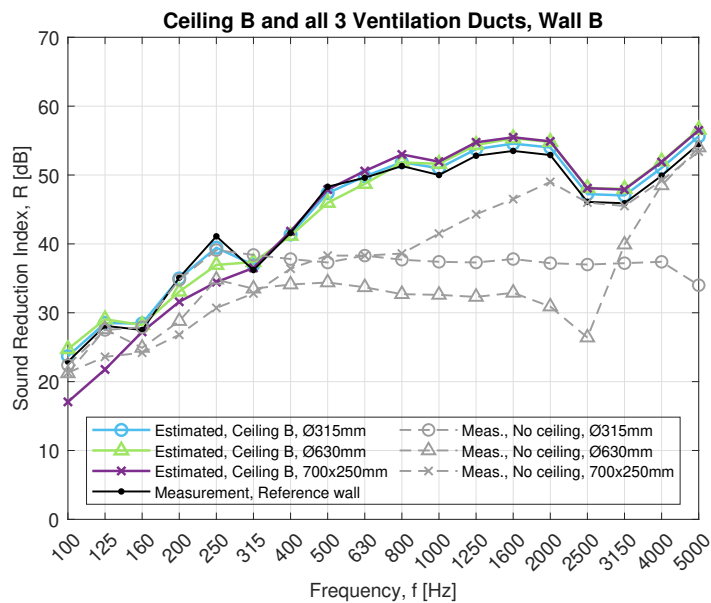

Figure C7: Estimated theory with a suspended absorbent ceiling, Ceiling B, as acoustical treatment. Ventilation duct with dimensions of Ø315, Ø630 and 700 × 250 mm through wall B with a sound reduction index of $R_w = 46$ dB.

Table C1: Units for different variables.

Variable	Unit, SI
a	m
b	m
c_0, c_L	m/s
d	m
L	m
$M_{\text{duct}}, M_{\text{wall}}$	m^2
P	m
q_{wrap}	kg/m^2
S, S_{wall}	m^2

Table C2: Calculated frequency values depending on the size and shape of the ventilation duct.

Variable	Value
$f_{1,315}$	638 Hz
$f_{1,630}$	319 Hz
$f_{1,700}$	245 Hz
$f_{e,315}$	336 Hz
$f_{e,630}$	168 Hz
$f_{R,315}$	5108 Hz
$f_{R,630}$	2554 Hz
$f_{L,700}$	1465 Hz

D   Appendix for Chapter 5

Table D1: Estimations and values for the standard deviations (SD) in Figure 5.27.

f [Hz]	Estimation	+1SD spread	-1SD spread	+1SD method	-1SD method	+1SD tot	-1SD tot
50	0.4	1.3	-0.5	0.7	0.1	1.3	-0.5
63	0.4	1.2	-0.3	0.6	0.2	1.2	-0.4
80	0.3	1.0	-0.5	0.5	0.1	1.1	-0.5
100	-0.1	0.7	-0.9	0.2	-0.4	0.7	-0.9
125	0.3	0.9	-0.3	0.5	0.1	0.9	-0.3
160	0.3	0.7	-0.1	0.4	0.2	0.7	-0.2
200	0.2	0.6	-0.2	0.3	0.1	0.6	-0.2
250	0.6	1.1	0.0	0.7	0.4	1.1	0.0
315	0.5	1.0	-0.1	0.6	0.4	1.0	-0.1
400	0.4	0.9	0.0	0.5	0.3	0.9	-0.1
500	0.6	1.0	0.2	0.6	0.5	1.0	0.2
630	0.6	1.0	0.2	0.7	0.5	1.0	0.2
800	0.6	1.1	0.0	0.6	0.5	1.1	0.0
1000	0.5	1.1	-0.1	0.6	0.4	1.2	-0.1
1250	0.5	1.1	-0.1	0.7	0.3	1.2	-0.1
1600	0.6	1.3	-0.1	0.8	0.4	1.3	-0.1
2000	0.8	1.4	0.2	0.9	0.7	1.5	0.2
2500	0.9	1.6	0.3	1.0	0.8	1.6	0.3
3150	0.8	1.6	0.1	1.0	0.6	1.6	0.1
4000	0.5	1.2	-0.1	0.7	0.4	1.2	-0.1
5000	0.4	1.0	-0.1	0.6	0.3	1.0	-0.1

Table D2: Estimations of the decrease in sound insulation per story lower down the building with various effects of flanking. Values from Figure 5.28.

f [Hz]	Low effect of flanking	Normal effect of flanking	High effect of flanking
50	0.0	0.4	1.3
63	0.0	0.4	1.2
80	0.0	0.3	1.1
100	0.0	0.0	0.7
125	0.0	0.3	0.9
160	0.0	0.3	0.7
200	0.0	0.2	0.6
250	0.0	0.6	1.1
315	0.0	0.5	1.0
400	0.0	0.4	0.9
500	0.2	0.6	1.0
630	0.2	0.6	1.0
800	0.0	0.6	1.1
1000	0.0	0.5	1.2
1250	0.0	0.5	1.2
1600	0.0	0.6	1.3
2000	0.2	0.8	1.5
2500	0.3	0.9	1.6
3150	0.1	0.8	1.6
4000	0.0	0.5	1.2
5000	0.0	0.4	1.0

E Appendix for Chapter 7

Frequency Hz	T-junction dB	X-junction dB
50	-0.0	1.6
63	-1.8	1.6
80	-0.1	0.3
100	1.0	0.4
125	0.3	1.3
160	1.3	0.5
200	2.6	0.0
250	2.2	0.8
315	2.8	0.9
400	2.9	0.7
500	3.5	1.1
630	1.6	0.7
800	3.9	0.9
1000	3.9	1.3
1250	4.4	1.1
1600	3.9	1.3
2000	3.3	1.1
2500	2.5	1.6
3150	2.3	1.5
4000	2.6	1.3
5000	2.2	0.8

(a) Data for the black curves shown in Figure 7.8, with the load correlation factor.

Frequency Hz	T-junction dB	X-junction dB
50	0.0	1.6
63	-1.3	1.4
80	-0.0	0.2
100	0.7	0.3
125	0.2	1.1
160	1.0	0.6
200	1.9	-0.2
250	1.6	0.6
315	2.1	0.7
400	2.1	0.6
500	2.6	1.0
630	1.2	0.8
800	2.8	1.1
1000	2.9	1.5
1250	3.3	1.3
1600	2.9	1.3
2000	2.4	1.2
2500	1.8	1.7
3150	1.7	1.7
4000	1.9	1.5
5000	1.6	1.0

(b) Data for the black curves shown in Figure 7.11, with the story correlation factor.

Figure E1: Data for the mean predicted values in Figure 7.8 and Figure 7.11.
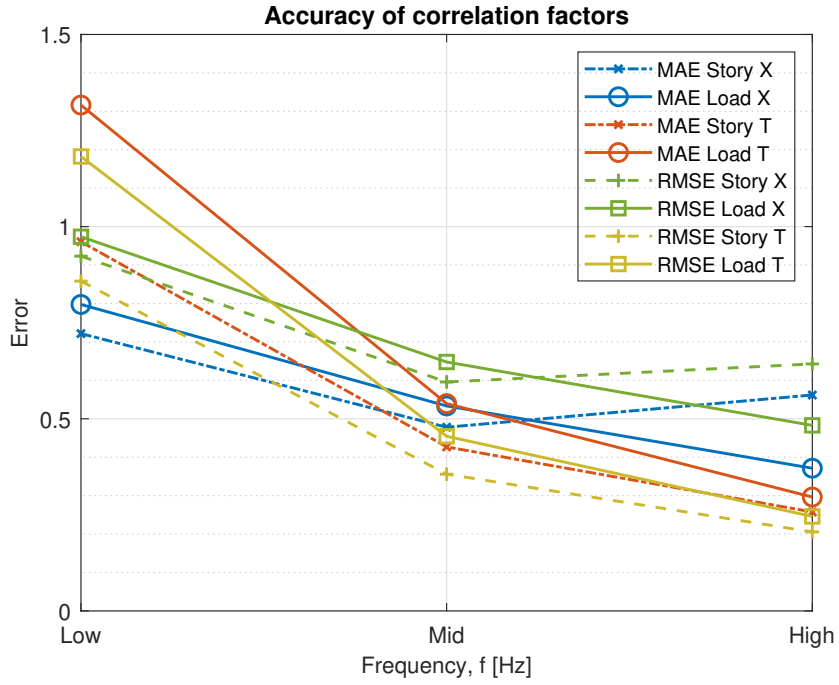
Figure E2: Statistical analysis of the correlation with load and number of stories for both X-junctions and T-junctions. Both RMSE and MAE are evaluated for the Wall–Wall path.

Table E1: Data for the resilient interlayers used in measured vertical junctions for the different projects between CLT elements. Project A uses a mixed cellular polyether urethane; projects B and C use a mixed cellular polyurethane.

Project and Wall Type	Stories	Thickness	Static E-Modulus	Dynamic E-Modulus
Project A, int. wall 1	5–6	6 mm	1.64 N/mm² [1]	3.63 N/mm² [1]
Project A, int. wall 1	9–10	6 mm	0.453 N/mm² [1]	1.06 N/mm² [1]
Project A, int. wall 2	5–6	6 mm	8.16 N/mm² [1]	21.5 N/mm² [1]
Project A, int. wall 2	9–10	6 mm	0.931 N/mm² [1]	2.27 N/mm² [1]
Project A, facade	5–6	6 mm	4.57 N/mm² [1]	10.4 N/mm² [1]
Project A, facade	9–10	6 mm	0.861 N/mm² [1]	1.86 N/mm² [1]
Project B, int. wall	2–3	25 mm	7.23 N/mm² [2]	11.08 N/mm² [1]
Project B, int. wall	5–6	25 mm	0.83 N/mm² [2]	1.52 N/mm² [1]
Project C, facade	1–2	12 mm	3.36 N/mm² [2]	5.42 N/mm² [1]
Project C, facade	3–4	12 mm	0.83 N/mm² [2]	1.52 N/mm² [1]
Project D, int. wall	2–3	-[3]	-[3]	-[3]
Project D, int. wall	5–6	-[3]	-[3]	-[3]

[1] Test method according to DIN 53513. [2] Calculated by the manufacturer as the first derivative of the static load deflection curve. [3] No resilient interlayers were used in the vertical junctions.

Table E2: Estimations of the decrease in vibration reduction index per story for the wall-wall path, an for X- and T-junctions, plus and minus one standard deviation of the measurement method (SD) from Figure 7.19.

f [Hz]	X	X + 1SD	X - 1SD	T	T + 1SD	T - 1SD
50	1.6	1.9	1.3	0.0	0.3	0.0
63	1.4	1.6	1.3	0.0	0.0	0.0
80	0.2	0.4	0.0	0.0	0.1	0.0
100	0.3	0.5	0.1	0.7	0.9	0.5
125	1.1	1.3	1.0	0.2	0.4	0.1
160	0.6	0.9	0.2	1.0	1.3	0.6
200	0.0	0.1	0.0	1.9	2.2	1.5
250	0.6	0.9	0.3	1.6	2.0	1.3
315	0.7	1.0	0.5	2.1	2.3	1.8
400	0.6	0.7	0.4	2.1	2.3	2.0
500	1.0	1.3	0.7	2.6	2.9	2.3
630	0.9	1.2	0.5	1.2	1.6	0.8
800	1.1	1.2	1.0	2.8	2.9	2.7
1000	1.5	1.9	1.0	2.9	3.3	2.5
1250	1.3	1.5	1.1	3.3	3.5	3.1
1600	1.3	1.7	0.9	2.9	3.3	2.5
2000	1.2	1.7	0.8	2.4	2.9	2.0
2500	1.7	2.3	1.1	1.8	2.4	1.2
3150	1.7	2.3	1.1	1.7	2.3	1.1
4000	1.6	2.4	0.7	1.9	2.8	1.1
5000	1.0	1.9	0.2	1.6	2.5	0.7

Table E3: Estimations of the decrease in vibration reduction index per story for the wall-floor path, plus and minus one standard deviation of the measurement method (SD) from Figure 7.20.

f [Hz]	Estimation	Estimation + 1SD	Estimation - 1SD
50	1.7	2.0	1.4
63	1.2	1.4	1.1
80	0.4	0.6	0.2
100	0.2	0.4	0.0
125	0.4	0.6	0.3
160	0.0	0.1	0.0
200	0.1	0.5	0.0
250	0.1	0.4	0.0
315	0.5	0.7	0.3
400	0.5	0.7	0.4
500	0.7	1.0	0.4
630	0.2	0.6	0.0
800	0.3	0.4	0.2
1000	0.6	1.0	0.2
1250	0.9	1.1	0.7
1600	0.9	1.3	0.5
2000	0.9	1.4	0.5
2500	0.7	1.3	0.1
3150	1.0	1.6	0.4
4000	0.9	1.8	0.0
5000	0.6	1.5	0.0

Table E4: Estimations of the decrease in vibration reduction index per story for the wall-ceiling path, plus and minus one standard deviation of the measurement method (SD) from Figure 7.21.

f [Hz]	Estimation	Estimation + 1SD	Estimation - 1SD
50	0.0	0.3	0.0
63	0.7	0.8	0.5
80	0.3	0.5	0.1
100	0.2	0.4	0.0
125	0.3	0.5	0.2
160	0.1	0.4	0.0
200	0.3	0.7	0.0
250	0.7	1.1	0.4
315	0.6	0.8	0.3
400	0.6	0.8	0.4
500	0.4	0.7	0.1
630	0.4	0.8	0.0
800	0.6	0.7	0.5
1000	0.9	1.3	0.5
1250	1.2	1.4	1.0
1600	1.1	1.4	0.7
2000	0.7	1.2	0.3
2500	1.1	1.8	0.5
3150	0.9	1.5	0.3
4000	0.8	1.7	0.0
5000	0.6	1.5	0.0